

Electronic Thesis and Dissertation Repository

9-5-2014 12:00 AM

The Development of Metal-Organic Compounds for Use as Molecular Imaging Agents

Emily J. Simpson, *The University of Western Ontario*

Supervisor: Dr. Leonard Luyt, *The University of Western Ontario*

A thesis submitted in partial fulfillment of the requirements for the Doctor of Philosophy degree in Chemistry

© Emily J. Simpson 2014

Follow this and additional works at: <https://ir.lib.uwo.ca/etd>

 Part of the [Organic Chemistry Commons](#), and the [Radiochemistry Commons](#)

Recommended Citation

Simpson, Emily J., "The Development of Metal-Organic Compounds for Use as Molecular Imaging Agents" (2014). *Electronic Thesis and Dissertation Repository*. 2417.
<https://ir.lib.uwo.ca/etd/2417>

This Dissertation/Thesis is brought to you for free and open access by Scholarship@Western. It has been accepted for inclusion in Electronic Thesis and Dissertation Repository by an authorized administrator of Scholarship@Western. For more information, please contact wlsadmin@uwo.ca.

THE DEVELOPMENT OF METAL-ORGANIC COMPOUNDS FOR USE AS
MOLECULAR IMAGING AGENTS

Integrated Article

by

Emily J. Simpson

Graduate Program in Chemistry

A thesis submitted in partial fulfillment
of the requirements for the degree of
Doctor of Philosophy

The School of Graduate and Postdoctoral Studies
The University of Western Ontario
London, Ontario, Canada

© Emily J. Simpson 2014

Abstract

Molecular imaging probes allow for the non-invasive diagnosis of many diseases through the use of a targeting entity for site specific delivery, as well as a signal for external visualization of probe accumulation in the body. This thesis will focus on the development of new approaches to synthesize targeting peptides and chelators for radionuclide incorporation towards the design of novel molecular imaging probes.

Histidine is a tridentate chelator that can be attached in a pendant fashion to a biomolecule in order to coordinate technetium-99m. Once coordinated, it forms a neutral complex that is capable of forming diastereomers with inverted stereochemistry at the alpha amine of the histidine. This is demonstrated through the synthesis and characterization, with LC-MS and 2D NMR spectroscopy, of four different histidine chelators that upon rhenium coordination form two products.

Copper-catalyzed azide-alkyne cycloaddition, or “click”, reactions form a 1,2,3-triazole that can be used to cyclize peptides, as well as coordinate $[^{99m}\text{Tc/Re}(\text{CO})_3]^+$. Clickable peptides can be developed combining these two concepts, such that a chelation site is created as a result of peptide cyclization in order to facilitate incorporation of $[^{99m}\text{Tc/Re}(\text{CO})_3]^+$ within the peptide. In order to do this, azide and alkyne modified amino acids can be incorporated into peptide sequences and reacted to form a triazole containing chelation sphere while simultaneously cyclizing the peptide.

Simultaneous peptide cyclization and $[^{99m}\text{Tc/Re}(\text{CO})_3]^+$ coordination was also performed with pentapeptides of the form Ac-HAAAH-OH. This was done in a [2+1] fashion using the imidazole of the N-terminal histidine and the imidazole and carboxylic acid of the C-

terminal histidine. Peptide coordination was verified through LC-MS, while computational studies as well as 2D and VT NMR spectroscopy allowed for the determination of the mode of coordination.

Finally, water soluble gold nanoparticles were conjugated with bombesin, a peptide known to target gastrin-releasing peptide receptors that are overexpressed in prostate cancer. This was done through the use of click chemistry to attach an azide modified bombesin to alkyne modified gold nanoparticles. Through transmission electron microscopy studies, these targeted nanoparticles showed specific uptake in prostate cancer cells, demonstrating their utility for targeting prostate cancer for both diagnostic and therapeutic purposes.

Keywords

Radiopharmaceuticals, Molecular imaging probes, Rhenium, Technetium-99m, Click chemistry, Peptide cyclization, Histidine, Gold nanoparticles

Co-Authorship Statement

Project conceptualization and manuscript editing was provided by Dr. Len Luyt.

The work presented in Chapter 2 was performed by the thesis author. Dr. Jen Hickey assisted with experimental design and editing. The cyclic RGD data included in the manuscript introduction was investigated by Mr. Dan Breadner.

Chapter 3 was first investigated by Mr. Brian Ngo and Ms. Barbara Wang, graduate and undergraduate students, respectively, in Dr. Len Luyt's lab. Preliminary work providing evidence that these pentapeptides would coordinate rhenium was presented at the 95th Canadian Chemistry Conference and Exhibition, as well as the 20th International Symposium on Radiopharmaceutical Sciences. The choice of which pentapeptide to carry forward was based on several pentapeptides that were synthesized and evaluated by both Brian and Barbara. However, experimental work and results obtained were all performed by the thesis author, with none of the preliminary work being incorporated into the chapter. As well, Dr. Jinqiang Hou provided all computational work.

Chapter 5 was completed in collaboration with the laboratory of Dr. Mark Workentin. The thesis author was responsible for the design and synthesis of the bombesin peptide derivative. The development and characterization of the gold nanoparticles and bioconjugation of bombesin to the nanoparticle was performed by Mr. Pierangelo Gobbo of Dr. Mark Workentin's lab. All cell culture and *in vitro* experimentation was performed by Ms. Fernanda Bononi of Dr. Len Luyt's lab. TEM sample preparation, image acquisition and analysis was carried out by the thesis author.

Acknowledgments

I would first like to thank my supervisor, Len Luyt, for hiring me 6 years ago when I was just a lowly undergrad who knew nothing about molecular imaging. Thank you for putting up with me, and taking me to so many amazing conferences!

To Jen Hickey for taking me under your wing. Thanks for all your help, but most of all for being a great friend! And to Carlie Charlton, thanks for being a great friend and letting me vent to you. But mostly, thanks for making the lab fun!

To all the Luyt lab members past and present for all your help and support over the years. You've made the last 6 years enjoyable!

To my parents for all your love and support, and for always being proud of me no matter what. I really appreciate everything you do for me!

And finally, Tyler, for always believing in me more than I believed in myself. Thank you for always being patient with me and not only celebrating my accomplishments, but also dealing with my breakdowns. I wouldn't be here without you!

Table of Contents

Certificate of Examination	ii
Abstract	iii
Co-Authorship Statement.....	v
Acknowledgments.....	vi
Table of Contents	vii
List of Tables	xi
List of Figures	xii
List of Schemes.....	xv
List of Appendices	xvii
List of Abbreviations	xviii
Chapter 1	1
1 Introduction	1
1.1 Molecular Imaging.....	1
1.2 Molecular Imaging Probes	1
1.2.1 Targeting Entity	2
1.2.2 Imaging Entity	6
1.3 Radiopharmaceuticals	7
1.4 Technetium-99m.....	8
1.5 Rhenium Analogues.....	10
1.6 Technetium-99m Radiopharmaceuticals	11
1.7 Emission and Computed Tomography.....	16
1.8 Positron Emission Tomography.....	17
1.9 Single Photon Emission Computed Tomography.....	19

1.10 Click Chemistry.....	22
1.10.1 Copper-Catalyzed Azide-Alkyne Cycloaddition	23
1.10.2 Strain-Promoted Azide-Alkyne Cycloaddition.....	25
1.11 Gold Nanoparticles for Diagnosis and Therapy	26
1.12 Peptide Receptor Binding.....	28
1.13 Summary	30
1.14 References	31
Chapter 2	38
2 Investigation of Isomer Formation Upon Coordination of Bifunctional Histidine Analogues with [^{99m} Tc/Re(CO) ₃] ⁺	38
2.1 Introduction.....	38
2.2 Results and Discussion	40
2.2.1 N ^α -benzyl-L-histidine	41
2.2.2 Stability Studies	44
2.2.3 Technetium-99m Labelling of N ^α -benzyl-L-histidine	45
2.2.4 Histidine Linkage Isomers	46
2.2.5 Methylation of N ^α -benzyl-L-histidine	47
2.2.6 N ^α -Histidinyl-acetyl-phenylalanine-OMe.....	49
2.3 Conclusions.....	52
2.4 Experimental.....	53
2.5 References.....	63
Chapter 3	66
3 Click to Cyclize and Chelate.....	66
3.1 Introduction.....	66
3.2 Results & Discussion	70
3.2.1 Clickable Peptide Design.....	70

3.2.2	First Clickable Peptide System	71
3.2.3	Second Clickable Peptide System.....	77
3.2.4	Third Clickable Peptide System.....	82
3.3	Conclusions.....	84
3.4	Experimental.....	85
3.5	References.....	93
Chapter 4	96
4	Cyclized Pentapeptides as [2+1] Chelation Systems for $^{99m}\text{Tc}/\text{Re}(\text{CO})_3^+$	96
4.1	Introduction.....	96
4.2	Results & Discussion	98
4.2.1	Peptide Synthesis	99
4.2.2	Radiolabelling.....	100
4.2.3	NMR Spectroscopy Studies	101
4.2.4	^1H NMR Spectroscopic Analysis.....	101
4.2.5	[2+1] Coordination	104
4.2.6	Variable Temperature ^1H NMR Spectroscopy	105
4.2.7	Computational Studies.....	107
4.3	Conclusions.....	110
4.4	Experimental.....	111
4.5	References.....	115
Chapter 5	119
5	Bombesin Functionalized Water-Soluble Gold Nanoparticles for Prostate Cancer Targeting	119
5.1	Introduction.....	119
5.2	Results & Discussion	122
5.2.1	Peptide Synthesis	122

5.2.2	Model <i>I</i> -SPAAC Reaction	123
5.2.3	Functionalization of Gold Nanoparticles	124
5.2.4	Transmission Electron Microscopy	126
5.3	Conclusions.....	130
5.4	Experimental.....	130
5.5	References.....	137
Chapter 6	141
6	Conclusions.....	141
6.1	References.....	146
Appendix A	: Characterization of Select Compounds.....	148
Appendix B	: Letter of Permission	180
Curriculum Vitae	181

List of Tables

Table 4.1: The $\Delta\delta/\Delta T$ values obtained from the VT ^1H NMR analysis for each amide proton in peptide 4.2	106
---	-----

List of Figures

Figure 1.1: Schematic of a molecular imaging probe	2
Figure 1.2: Solid-phase peptide synthesis cycle ¹⁴	6
Figure 1.3: Decay scheme of ⁹⁹ Mo to ⁹⁹ Ru.....	9
Figure 1.4: Schematic of a ⁹⁹ Mo/ ^{99m} Tc generator ²⁴	10
Figure 1.5: Schematic of a ^{99m} Tc(I)/Re(I) tricarbonyl core with a tridentate chelator ³⁴ ...	12
Figure 1.6: Schematic of pendant and integrated technetium-99m peptide-based radiopharmaceutical designs	14
Figure 1.7: a) PET scanner, ⁶⁷ and b) schematic of a PET scanner and positron annihilation ⁶⁸	18
Figure 1.8: CT, PET and fused PET/CT images of a ¹⁸ F sodium fluoride bone scan of a mouse ⁶⁹	19
Figure 1.9: a) SPECT scanner, ⁷⁰ and b) schematic of a SPECT scanner ⁶⁸	20
Figure 1.10: CT, SPECT and fused SPECT/CT images of a ^{99m} Tc-MDP bone scan of a mouse ⁷¹	21
Figure 1.11: Schematic of the Huisgen azide-alkyne cycloaddition.....	22
Figure 1.12: Schematic showing similarities between peptide bonds and 1, 4-disubstituted 1,2,3-triazoles (adapted from reference 82).....	25
Figure 1.13: Copper-catalyzed versus strain-promoted azide-alkyne cycloadditions	25
Figure 1.14: Schematic displaying the multivalency of gold nanoparticles (adapted from reference 102)	27
Figure 1.15: Internalization of a GRPR agonist into a cell (adapted from reference 107)	30
Figure 2.1: Cyclic RGD peptide system containing an N ^α -substituted histidine chelator	39
Figure 2.2: Simplified histidine chelation models used for investigation of diastereomer formation.....	41
Figure 2.3: Analytical HPLC trace, UV absorbance detected from 210-800 nm (RP-C ₁₈ 4.6 x 250 mm, 5 μm), of a) the mixture of isomers of 2.1, and b) the purified major isomer 2.1a.....	42

Figure 2.4: Methylene region of the ^1H NMR (400 MHz, MeOH-d ₄) of a) the uncoordinated product 2.6, b) the coordinated mixture of 2.1, and c) the pure major isomer 2.1a.....	43
Figure 2.5: NOESY spectrum (400 MHz, MeOH-d ₄) of the pure major isomer of 2.1 showing correlation between the proton on carbon A and the amine proton (solid circle) and the lack of correlation between protons on carbons A and C (dashed circle).....	44
Figure 2.6: Stereochemistry of the major isomer 2.1a as determined by gCOSY and NOESY experiments and interconversion of the major isomer 2.1a to the minor isomer 2.1b.....	45
Figure 2.7: Analytical HPLC gamma trace (C ₁₈ 4.6 x 150 mm, 5 μm) of $^{99\text{m}}\text{Tc}$ labelled 2.7.....	46
Figure 2.8: Methylene region of ^1H NMR (400 MHz, MeOH-d ₄) of 2.3. Isomers can still be seen even when the secondary amine is methylated; however, one isomer is much more predominant	49
Figure 2.9: ROESY spectrum (600 MHz, DMF-d ₇) of the pure major isomer of 2.4 showing correlation between the protons on carbon A and the amine proton (solid circle) and the lack of correlation between protons on carbons A and C (dashed circle).....	52
Figure 2.10: Stereochemistry of the diastereomers of 2.1, 2.3 and 2.4	53
Figure 3.1: Design of the three different clickable peptide systems described in this chapter, where M = Re or $^{99\text{m}}\text{Tc}$	71
Figure 3.2: Methylene region of the ^1H NMR spectra for 3.4 and 3.5 showing the shift in peaks and change in coupling pattern indicating rhenium coordination.....	74
Figure 3.3: HPLC traces showing the progression of synthesis of peptide 3.9	76
Figure 3.4: MALDI-MS of final clicked peptide 3.10 showing the desired coordinated mass and rhenium-185/187 signature	77
Figure 3.5: Methylene region of the ^1H NMR spectra for 3.14 and 3.15 showing the shift in peaks indicating rhenium coordination.....	79
Figure 4.1: Proposed structure of the coordinated pentapeptide resulting in a cyclic, neutral peptide-metal complex.....	99
Figure 4.2: UHPLC analysis showing correlation between a) UV chromatogram of rhenium coordinated peptide 4.2, and b) gamma trace of Tc-99m labelled peptide 4.3	101
Figure 4.3: 1D ^1H NMR of the aromatic region of a) linear peptide 4.1 and b) coordinated peptide 4.2, as well as the methylene region of c) linear peptide 4.1 and d) coordinated peptide 4.2 in DMSO-d ₆ at 600 MHz.....	102

Figure 4.4: TOCSY NMR spectra of coordinated peptide 4.2 in DMSO-d6 at 600 MHz, showing identification of a) alanine (A ₁ -A ₃) CH and CH ₃ , and b) histidine (H ₁ and H ₂) CH and CH ₂ protons	103
Figure 4.5: TOCSY NMR spectrum of coordinated peptide 4.2 in DMSO-d6 at 600 MHz, showing identification of alanine (A ₁ -A ₃) and histidine (H ₁ and H ₂) amide protons, as well as the much larger upfield shift of the H ₁ amide and CH protons compared to that of H ₂ (grey circles)	104
Figure 4.6: VT ¹ H NMR of coordinated peptide 4.2 in DMSO-d6 at 5°C intervals from 25-60°C at 600 MHz	106
Figure 4.7: Four possible isomers of the proposed structure for cyclized peptide 4.2, where 4.2a and 4.2b are diastereomers, and 4.2c and 4.2d are conformational isomers of 4.2a and 4.2b, respectively.....	107
Figure 4.8: Lowest energy isomer (4.2a) of the proposed structure of cyclized peptide 4.2 showing intramolecular hydrogen bonding interactions.....	108
Figure 4.9: Four possible isomers of the new proposed structure for cyclized peptide 4.2, where 4.2e and 4.2f are diastereomers, and 4.2g and 4.2h are conformational isomers of 4.2e and 4.2f, respectively	109
Figure 4.10: Lowest energy isomer (4.2e) of the new proposed structure of cyclized peptide 4.2 showing intramolecular hydrogen bonding interactions	110
Figure 4.11: Structures of the two lowest energy isomers of Re(CO) ₃ -Ac-HAAAHOH (4.2), with 4.2e being the most likely isomer based on VT NMR spectroscopy and computational studies.....	111
Figure 5.1: Structure of natural bombesin, truncated pan-bombesin, [D-Phe6, β-Ala11, Phe13, Nle14]bombesin-(6-14) and the azide functionalized pan-bombesin peptide 5.1	122
Figure 5.2: IR spectra of a) Bombesin-AuNPs (5.4), b) Bombesin-azide (5.1) and c) DBCO-AuNPs (5.3).....	125
Figure 5.3: TEM images at 60 kV of AuNPs (indicated by black arrows) in PC-3 cells. A) Cell incubated with targeted AuNPs conjugated with bombesin at a magnification of 19000 and B) 64000; C) blocking study cell at a magnification of 19000 and D) 64000; E) control cell at a magnification of 19000 and F) 64000	128

List of Schemes

Scheme 2.1: Synthesis and coordination of chelator 2.6	42
Scheme 2.2: Coordination of 2.8 with $[\text{Re}(\text{CO})_3]^+$ to form 2.2, a modification of 2.1 with a trityl protected imidazole to demonstrate that the isomers are formed at the secondary amine, as opposed to linkage isomers of the imidazole.....	47
Scheme 2.3: Synthesis of methylated complex 2.3.....	48
Scheme 2.4: Synthesis of dipeptide complex 2.4	50
Scheme 3.1: Synthesis of clickable chelator 3.3 for first clickable peptide system	72
Scheme 3.2: Synthesis of model chelator 3.5 for first clickable peptide system.....	72
Scheme 3.3: Synthesis of azide functionalized lysine 3.6	75
Scheme 3.4: Synthesis of first clickable peptide system with chelator 3.3	76
Scheme 3.5: Synthesis of clickable chelator 3.12.....	78
Scheme 3.6: Synthesis of model chelator 3.15 for the second clickable peptide system .	78
Scheme 3.7: Synthesis of second clickable peptide system with chelator 3.12.....	80
Scheme 3.8: Proposed synthesis of third clickable peptide system	83
Scheme 3.9: Attempted and proposed synthesis of alkyne modified lysine.....	83
Scheme 4.1: Coordination of pentapeptide 4.1 with $[\text{Re}(\text{CO})_3]^+$ or $[\text{}^{99\text{m}}\text{Tc}(\text{CO})_3]^+$, resulting in cyclic peptides 4.2 and 4.3.....	100
Scheme 5.1: Model <i>I</i> -SPAAC reaction of DBCO and bombesin azide peptide 5.1	123
Scheme 5.2: <i>I</i> -SPAAC reaction between DBCO functionalized AuNPs and bombesin azide peptide 5.1	124

List of Appendices

Appendix A : Characterization of Select Compounds.....	148
Appendix B : Letter of Permission	180

List of Abbreviations

Ar	aromatic
Ac	acetyl
ACN	acetonitrile
AuNP	gold nanoparticle
Boc	<i>tert</i> -butoxycarbonyl
Bq	Becquerel
Ci	Curie
CT	computed tomography
CuAAC	copper-catalyzed azide-alkyne cycloaddition
DBCO	dibenzocyclooctyne
DBU	1,8-diazabicycloundec-7-ene
DCC	dicyclohexylcarbodiimide
DCM	dichloromethane
DFT	density functional theory
DIC	<i>N,N</i> -diisopropylcarbodiimide
DIPEA	<i>N,N</i> -diisopropylethylamine
DMF	<i>N,N</i> -dimethylformamide
DMSO	dimethylsulfoxide
EDC	1-ethyl-3-(3-dimethylaminopropyl) carbodiimide
EDTA	ethylenediaminetetraacetic acid
EI	electron impact
EPR	enhanced permeability and retention
ESI	electrospray ionization
EtOH	ethanol
Fmoc	9-fluorenylmethoxycarbonyl
gCOSY	gradient Correlation Spectroscopy
GPCR	G protein-coupled receptor
GRP	gastrin-releasing peptide

GRP-R	gastrin-releasing peptide receptor
HBTU	<i>O</i> -Benzotriazole- <i>N,N,N',N'</i> -tetramethyl-uronium-hexafluoro-phosphate
HCTU	2-(6-chloro-1H-benzotriazole-1-yl)-1,1,3,3-tetramethylaminium hexafluorophosphate
HPC	high-performance computing
HPLC	high-performance liquid chromatography
HRMS	high resolution mass spectrometry
IR	infrared
<i>I</i> -SPAAC	interfacial strain-promoted azide-alkyne cycloaddition
LC-MS	liquid chromatography-mass spectrometry
MBHA	4-methylbenzhydrylamine
MeOH	methanol
MRI	magnetic resonance imaging
MS	mass spectrometry
NaAsc	sodium ascorbate
NEt ₃	triethylamine
NIR	near infrared
Nle	norleucine
NMR	nuclear magnetic resonance
NOESY	Nuclear Overhauser Effect Spectroscopy
OAc	acetate
OTf	trifluoromethanesulfonate
PBS	phosphate buffer saline
PC-3	human prostate cancer cell line
PEG	polyethylene glycol
PET	positron emission tomography
PSA	prostate specific antigen
RES	reticuloendothelial system
RF	radio frequency
ROESY	Rotational Overhauser Effect Spectroscopy
RP	reverse phase

SPAAC	strain-promoted azide-alkyne cycloaddition
SPECT	single photon emission computed tomography
SPPS	solid-phase peptide synthesis
TBME	<i>tert</i> -butylmethylether
tBu	<i>tert</i> -butyl
t-BuOH	<i>tert</i> -butanol
TEM	transmission electron microscopy
TFA	trifluoroacetic acid
THF	tetrahydrofuran
TIPS	triisopropylsilane
TLC	thin layer chromatography
TOCSY	Total Correlation Spectroscopy
Trt	trityl
UHPLC	ultra high-performance liquid chromatography
VT	variable temperature

The abbreviations for the common amino acids are in accordance with the recommendations of the IUPAC-IUB Joint Commission on Biochemical Nomenclature.

Chapter 1

1 Introduction

1.1 Molecular Imaging

In the last few decades, molecular imaging has become an integral component in the non-invasive diagnosis of many diseases, allowing for the *in vivo* observation of biochemical processes at the molecular and cellular level.¹ This technique uses biomarkers to visualize, characterize and measure biological processes within a living system. An image is obtained through the external detection of the biomarker, which has been injected into a patient, through the use of sophisticated diagnostic imaging equipment. There are a wide variety of biomarkers available for imaging many different targets and pathways *in vivo*, based on their chemical and biological properties.

In this way, molecular imaging can be used to non-invasively image tumours, and other diseases, allowing for pre-symptomatic disease detection. Not only is it useful for early diagnosis, but it can also be used to estimate disease staging, allowing for more a more personalized treatment approach. Molecular imaging can also be applied to track the progression of response to determine whether the choice is effective, or if a new approach needs to be followed. In order to accomplish this, a strategy must be developed that can differentiate between diseased and normal tissues using a molecular imaging probe.

1.2 Molecular Imaging Probes

In the past, perfusion agents were common; however, these have a very low targeting efficiency.² Therefore, recent advances have been made in the area of targeted molecular imaging probes. These probes are developed to target biomolecules that are

overexpressed on malignant tissues yet absent, or present in much lower concentration, on non-malignant tissues. Imaging probes must be designed so that they can be used to target the desired receptor and allow for external detection. These probes are comprised of two different components (Figure 1.1); a targeting entity provides site specific delivery of the probe to the malignant tissue, and a labelling moiety permits external detection of the target. If designed properly, an imaging probe can target a receptor that is specifically over-expressed on the malignant tissue and accumulate in high target to non-target ratio, which can then be detected externally due to the presence of the label.

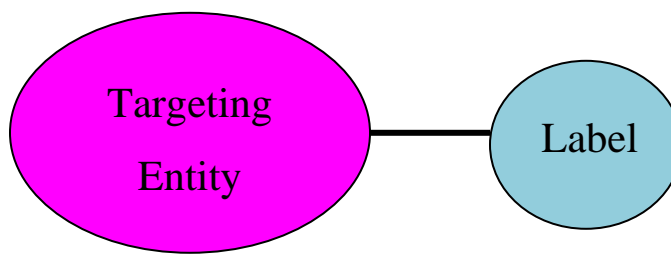


Figure 1.1: Schematic of a molecular imaging probe

1.2.1 Targeting Entity

The targeting entity component of an imaging probe must selectively bind to the tissue of interest in much higher concentration in the diseased state than the surrounding healthy tissue, in order to be effective. If this is the case, a high target to non-target ratio will be achieved, increasing the contrast in the image, as well as the precision and accuracy in diagnoses.³ The targeting entity can vary depending on the desired target, with the most common being small molecules, peptides and monoclonal antibodies. Peptides have many desirable characteristics required for use as targeting entities.⁴ As such, peptide-based probes can be designed for many biological targets and tend to have high uptake in target tissue while still maintaining rapid clearance from the blood and non-target tissue.

They also tend to have minimal side effects and low toxicity.⁵ In addition, they are easily synthesized and modified to enhance pharmacokinetic properties, and can be easily labelled with a wide range of isotopes, including radiometals, and optical agents, allowing for use with a variety of imaging modalities. Peptides also have a high enough molecular weight to allow for the addition of metal chelators, but still have low enough molecular weight for rapid clearance. In some cancers, endogenous peptide receptors tend to be over-expressed, making peptides ideal targeting molecules.⁵⁻⁷

However, peptides are not without their disadvantages. The main concern with peptides is their low biological half-life, which is often in the range of minutes as they quickly undergo enzymatic degradation *in vivo*. Linear peptides also have a very flexible backbone resulting in interactions with multiple receptors, decreasing their selectivity.⁸ As well, the addition of the imaging entity often decreases the binding affinity of the peptide for the receptor. Therefore, optimization is required before peptides can be used as targeting entities.

Peptidomimetics are molecules designed to mimic peptides *in vivo*. This generally entails altering the peptide backbone or incorporation of unnatural amino acids into the peptide sequence. This can decrease the rate of enzymatic degradation, greatly increasing the *in vivo* stability of the probes.^{9, 10} Cyclic peptides are also useful for this purpose as cyclization restricts the flexibility of the peptide backbone, minimizing receptor binding promiscuity, and occasionally enhancing the binding affinity of the probe. Octreotide, for example, is a synthetic eight amino acid peptidomimetic of somatostatin, a naturally occurring hormone that has a cyclic structure. The linear version of octreotide binds to the somatostatin receptor with a much lower affinity than the cyclic version, suggesting

that a specific conformation is required to achieve higher binding affinities.¹¹ Somatostatin has an *in vivo* half-life of only two to three minutes, whereas octreotide has a half-life of approximately one to two hours. This is most likely due to the substitution of natural L-tryptophan for unnatural D-tryptophan, allowing it to withstand enzymatic degradation.¹²

1.2.1.1 Solid-Phase Peptide Synthesis

Peptides can be synthesized either in solution or, more commonly, on a solid support. Solution phase peptide synthesis can be problematic, as dimerization and formation of other unwanted by-products requires purification steps after the addition of every amino acid. In the 1960s, solid-phase peptide synthesis (SPPS) was introduced by Merrifield.¹³ In SPPS the peptide is attached to a solid support, providing a pseudo-dilution effect, making the formation of dimers much less likely. As well, an excess of reagents can be used in order to drive the reaction to completion. This is possible as all excess reagents and any by-products are dissolved in the solvent and, thus, can be washed away while leaving the peptide chain on the resin, eliminating the need for tedious purification of intermediates. SPPS can also be performed either manually, or by an automated peptide synthesizer, making synthesis much more convenient.

To synthesize a peptide by SPPS, an amino acid is attached to an insoluble solid support resin bead, and the peptide is extended from the C-terminus to N-terminus. The first amino acid is loaded onto one of the functionalized chains attached to the polymer bead, and subsequent amino acids are coupled to form a peptide chain. The progress of the synthesis can be checked by cleaving small amounts of peptide from the resin and

checking by LC-MS. After the desired length is reached, the chain can then be cleaved from the resin to yield the linear peptide.

A common method to synthesize peptides by SPPS is the Fmoc (fluorenylmethoxycarbonyl) strategy. This strategy uses orthogonal protecting groups in order to keep the amino acid side-chains protected, while removing the N-terminal protecting group to attach the next amino acid to the chain. The peptide is generally attached to an acid sensitive resin, the amine group on the amino acid is protected by a base labile Fmoc group, and the side-chains are protected by acid labile protecting groups. In this way the Fmoc can be removed while leaving the side-chains protected, and the peptide on the resin. The peptide can then be removed from the resin by treatment with acid while simultaneously removing the side-chain protecting groups.

The resin bead is an insoluble polymer support and can contain varying functional groups. The choice of resin depends on the functional group desired on the C-terminus of the peptide once it is cleaved. For example, a Rink amide resin is functionalized with a free amine that attaches to the carboxyl group of the first amino acid, and forms an amide when it is cleaved with acid as opposed to a carboxylic acid as is seen when using Wang resin.

In SPPS, a protected amino acid is loaded onto an insoluble resin through standard coupling procedures to form a peptide bond. The N-terminal protecting group is then removed; in the case of Fmoc, piperidine is used. This is then followed by coupling of the next protected amino acid. This cycle is continued until the desired peptide length is

reached, at which point, the peptide can be cleaved from the resin and the protecting groups removed to give the desired peptide (Figure 1.2).

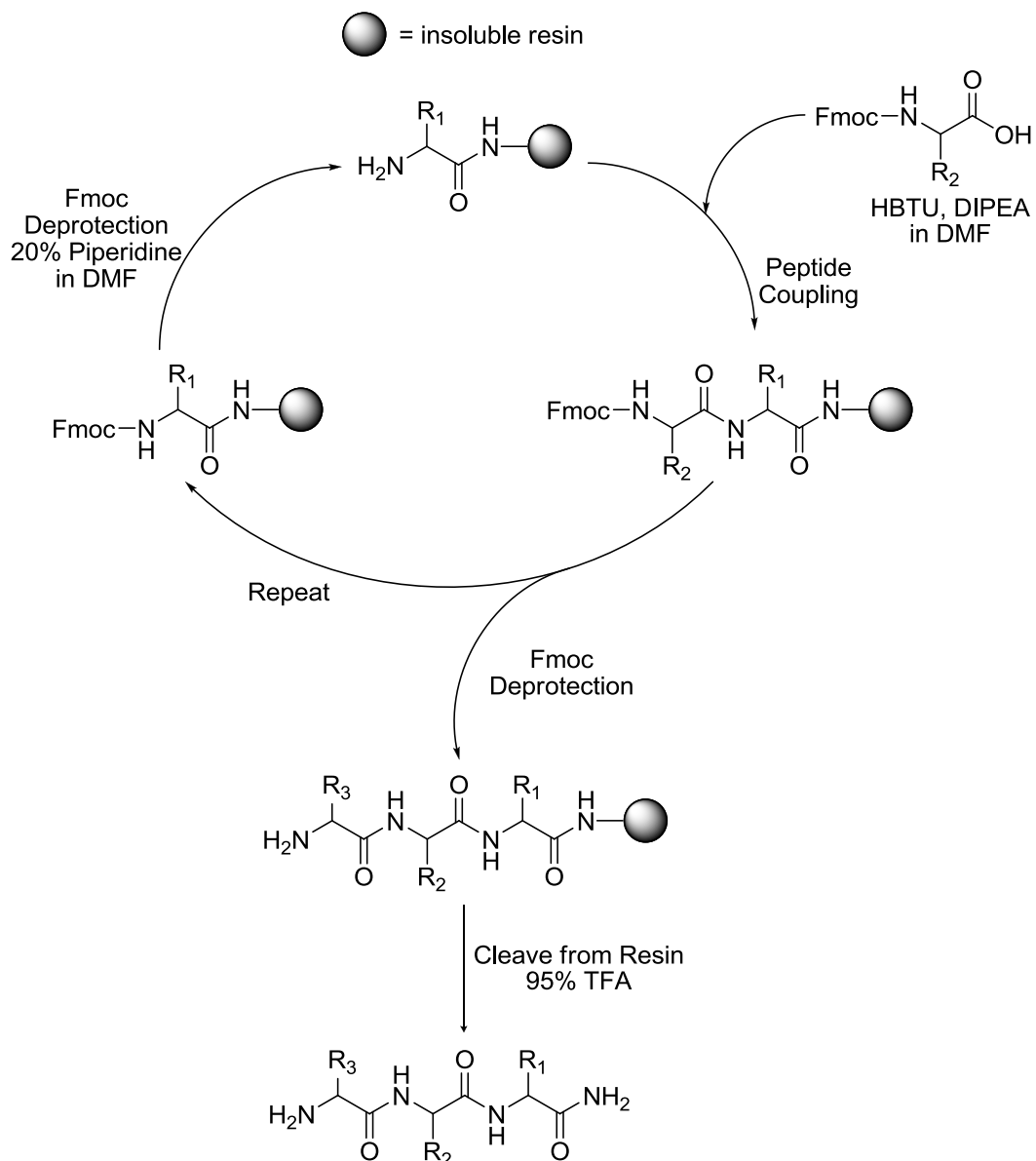


Figure 1.2: Fmoc-based solid-phase peptide synthesis cycle¹⁴

1.2.2 Imaging Entity

The imaging entity of a molecular imaging probe allows for the external detection of the localization of the probe. There are many types of imaging entities available with the

choice depending on the intended application as well as the desired imaging modality. Optical imaging requires addition of a fluorophore or bioluminescent enzyme to the targeting entity, and can be used for *in vitro* cell studies or *in vivo* applications.⁷ These include fluorescent probes that emit photons with 300-600 nm wavelengths. This wavelength cannot penetrate tissue without attenuation, and thus is generally used for *in vitro* cell studies.¹⁵ Near infrared (NIR) dyes can also be used with wavelengths ranging between 650-900 nm. These wavelengths are able to penetrate tissue and are suitable for *in vivo* applications.¹⁵ Many imaging modalities in nuclear medicine require the use of a radionuclide as an imaging entity for use in radiopharmaceuticals. The development and use of radiopharmaceuticals will be discussed in further detail in the following section.

1.3 Radiopharmaceuticals

A radiopharmaceutical is a perfusion agent or molecular imaging probe that is composed of a targeting entity labelled with a radionuclide for use in non-invasive diagnosis and treatment of many diseases, including cancer. In order to design a molecular imaging probe, a biologically active entity must be chosen based on its ability to accumulate at a specified target with a high target to non-target ratio. It is administered in trace quantities, as very little radiation is required; as a result it has no pharmacologic effect on the patient.¹⁶ Next, a suitable radionuclide must be attached to the targeting entity. The choice of radionuclide determines whether the radiopharmaceutical will be used for diagnostic or therapeutic purposes, however, approximately 95% of radiopharmaceuticals are used for diagnosis.¹⁷

For diagnosis, the radionuclide must emit a gamma-ray between 50 and 600 keV to allow for external detection.³ It must also have a short half-life so the radiation dose to the

patient remains low; ideally, only long enough to allow for radiosynthesis, purification, injection, biodistribution and imaging. Availability, ease of production and cost also play a major role in choice of a radionuclide. The radionuclide must also quickly and easily be incorporated into the biomolecule of choice through direct displacement and addition of a prosthetic group, or the use of a chelator. After addition of the radionuclide, the final radiopharmaceutical should still retain a high target to non-target ratio in order to be an effective diagnostic probe.^{3, 4}

Alpha (α) and beta (β^-) emitting radionuclides cause much more damage to surrounding tissue than γ -rays and thus should not be used for diagnostic purposes. While tissue is transparent to γ -rays, it is not transparent to α and β^- particles which have limited penetration depths of only a few μm , therefore they do not offer any diagnostic benefit. They can, however, be used for therapeutic purposes as they cause radiation damage to the targeted tissues.¹⁷

1.4 Technetium-99m

Technetium-99m ($^{99\text{m}}\text{Tc}$) is a manufactured element discovered by Perrier and Segré in 1937.¹⁸ In just over 75 years it has become the most common radionuclide used in diagnostic nuclear medicine, used in more than 80% of radiopharmaceuticals.¹⁹ It is an ideal radionuclide as it has a half-life of six hours which is long enough for labelling procedures as well as obtaining an image, but short enough that the dose of radiation to the patient remains very low.²⁰ As well, the gamma emission from the decay of $^{99\text{m}}\text{Tc}$ is 140 keV. This is energetic enough to pass through tissues, but not too high energy so as to give the patient a high dose of radiation. The decay occurs by release of a γ -ray

through an isomeric transition to technetium-99, which has a radioactive half-life of 2.12 times 10^5 years (Figure 1.3).

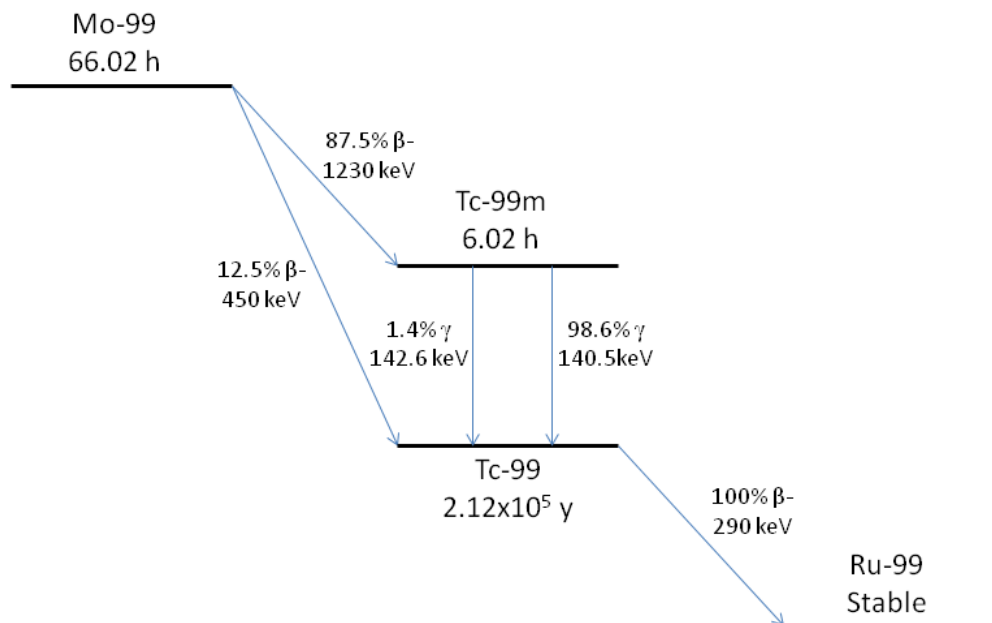


Figure 1.3: Decay scheme of ^{99}Mo to ^{99}Ru

In the 1950s, researchers at the Brookhaven National Laboratory developed the molybdenum-99/technetium-99m generator,²¹ which is currently how the majority of technetium-99m is obtained. The generators produce the $^{99\text{m}}\text{Tc}$ from ^{99}Mo at the location at which it is needed, thus decreasing the number of half lives the $^{99\text{m}}\text{Tc}$ undergoes before it is used in synthesis. The molybdenum-99 is produced in a nuclear reactor by the fission of uranium-235, and once purified can be loaded onto an alumina anion exchange column. The ^{99}Mo has a half-life of 66 hours, allowing it to decay to $^{99\text{m}}\text{Tc}$ (87.5%) and ^{99}Tc (12.5%) through β^- decay while still on the column.^{3, 22} The adsorbed $^{99\text{m}}\text{Tc}$ can then be eluted from the column using saline solution as sodium pertechnetate ($\text{Na}[^{99\text{m}}\text{TcO}_4^-]$) and collected in an evacuated sterilized vial (Figure 1.4). The majority of the $^{99\text{m}}\text{Tc}$

produced occurs in the first three parent half lives, therefore, the generator needs to be replaced approximately every week. Even with frequent replacement, the generator system allows the technetium-99m to be more readily available, and thus less expensive than many other diagnostically relevant radionuclides.²³

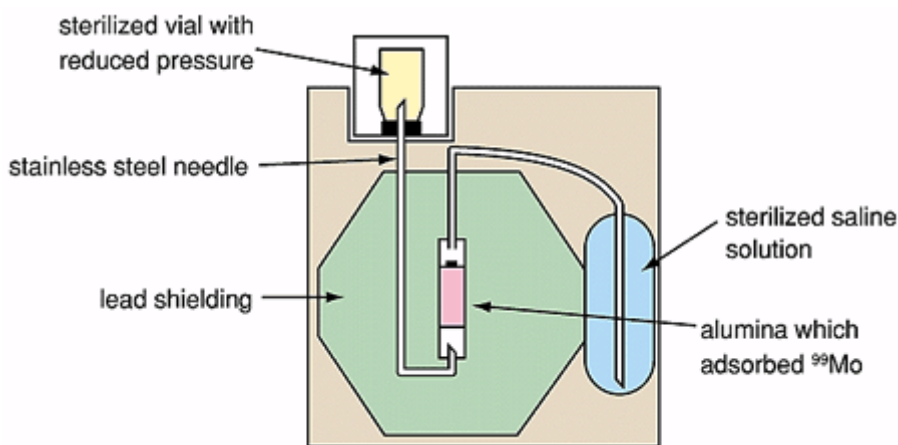


Figure 1.4: Schematic of a $^{99}\text{Mo}/^{99\text{m}}\text{Tc}$ generator²⁴

1.5 Rhenium Analogues

As technetium-99m is radioactive, only nanogram quantities can be used, making the use of standard spectroscopic methods for characterization impractical. A solution to this problem is to synthesize and characterize the desired compounds using a nonradioactive analogue that possesses the same properties as $^{99\text{m}}\text{Tc}$. This allows for larger quantities to be synthesized and characterized, before moving on to radioactive versions.

Rhenium is typically used in the place of technetium during the synthetic stages as it has similar chemical properties. It is in the same group as technetium, located one row below in the periodic table and exists as two stable isotopes, ^{185}Re (37.4%) and ^{187}Re (62.6%). The chemistry of technetium and rhenium is comparable, not only having the same size

and shape, but also formal charge and lipophilicity.^{6, 25} This makes the rhenium analogue nearly identical to the technetium-99m compound, allowing for larger quantities of the complex to be synthesized and characterized, prior to radiolabelling with technetium-99m, thus minimizing exposure to radioactive products. Rhenium can therefore be used as a non-radioactive substitute for technetium when designing compounds for use as imaging agents.

1.6 Technetium-99m Radiopharmaceuticals

Technetium exists in various oxidation states from 1- to 7+; however, no clinically relevant compounds have been prepared using the 0, 2+ or 6+ oxidation states.¹⁷ A variety of clinically relevant compounds have been formed using technetium in the 3+, 4+ and 7+ oxidation states, but the focus of research was previously on Tc(V).²⁶ This oxidation state was used with the $[\text{Tc}=\text{O}]^{3+}$ and $[\text{O}=\text{Tc}=\text{O}]^+$ cores to form square pyramidal or octahedral complexes, respectively, with various bi- or tetradentate ligand sets.²⁷

More recently, the Tc(I) oxidation state has been developed for use in radiopharmaceuticals and is found predominantly in octahedrally coordinated $^{99\text{m}}\text{Tc}/\text{Re}$ tricarbonyls.²⁸⁻³³ This has become the most promising technetium core as they are chemically inert and have a nearly spherical shape, making them very compact. The carbonyl ligands orient themselves in a facial arrangement, causing the trans ligands to become very labile, allowing for straightforward substitution by the chelator. These are generally used with tridentate chelators (Figure 1.5) as they tend to form a more stable complex that is protected against ligand attack or re-oxidation. As well, they tend to react

very fast, making them ideal for radiolabelling as the time required for synthesis can be decreased.^{19, 23}

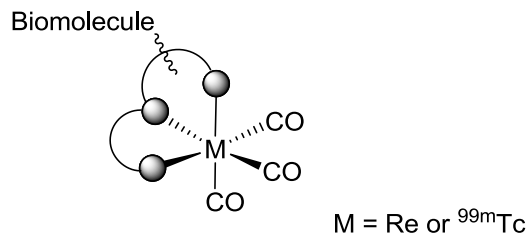


Figure 1.5: Schematic of a ^{99m}Tc(I)/Re(I) tricarbonyl core with a tridentate chelator³⁴

The [^{99m}Tc(CO)₃]⁺ precursor is easily synthesized as the tri-aqua complex in quantitative yields and excellent radiochemical purity by adding pertechnetate ([^{99m}TcO₄]⁻) eluted from a generator to commercially available Isolink kits.^{35, 36} These kits contain sodium tartrate, sodium tetraborate, sodium carbonate, and disodium boranocarbonate, which reduces the technetium in the pertechnetate from the +7 oxidation state to +1, and also acts as a carbonyl source.^{19, 23} This provides a quick synthetic procedure for the precursor, allowing for decreased synthesis times, and thus fewer elapsed half-lives. This Isolink kit, however, cannot be used to prepare [Re(CO)₃(H₂O)₃]⁺ as rhenium is slower to react and harder to reduce than technetium.²³

The [^{99m}Tc(CO)₃]⁺ core requires a ligand chelation system for biomolecule incorporation. Technetium is a group 7 transition metal, existing as d⁶ in its 1+ oxidation state. It has a low charge to ionic radius ratio, making it a soft metal. Although this means that it has a preference for soft π-acceptors, it can also bind hard σ-donors. This is due to the chemistry of the CO ligands. If there is an increase in CO π-backbonding, an electron deficient metal centre is produced, allowing for coordination of hard σ-donors. If there is

a stronger σ -donation from the CO to the metal, an increase in electron density on the metal occurs, resulting in coordination of soft π -acceptors. This allows the $[\text{}^{99\text{m}}\text{Tc}(\text{CO})_3]^+$ core to coordinate to a variety of donor and acceptor ligands.³⁷

The water molecules of the $[\text{}^{99\text{m}}\text{Tc}(\text{CO})_3(\text{H}_2\text{O})_3]^+$ core are facially coordinated and experience a strong trans influence from the facially coordinated carbonyl ligands. This effect causes the water molecules to be extremely labile, whereas the carbonyl ligands remain stable and cannot be substituted by incoming ligands.²³ This allows for easy substitution of the water molecules by chelators. Coordinating groups such as imidazoles, pyridines, pyrazoles, amides, carboxylic acids, thioethers, thiols and phosphines have been shown to coordinate well with the $[\text{}^{99\text{m}}\text{Tc}(\text{CO})_3]^+$ core.³⁷

Technetium-99m radiopharmaceuticals are generally composed of a biomolecule for targeting, the radiometal for external detection, and a chelator to attach the metal to the biomolecule. The metal complex can be added to a targeting peptide through two different approaches; pendant or integrated design (Figure 1.6). Pendant design is the classic approach where a bifunctional chelator is attached in a pendant fashion to the peptide through functionalization of either the side chain of an amino acid, such as lysine, or the carboxy or amine terminus of the peptide. A bifunctional chelator allows for attachment of the chelator to the biological entity while still allowing for coordination to the technetium core, placing the metal complex away from the biologically active site. The drawback to this approach is that adding a bulky chelator to the outside of the peptide is likely to affect the binding of the original peptide to the receptor. Therefore, further optimization with the attached metal complex must be performed.

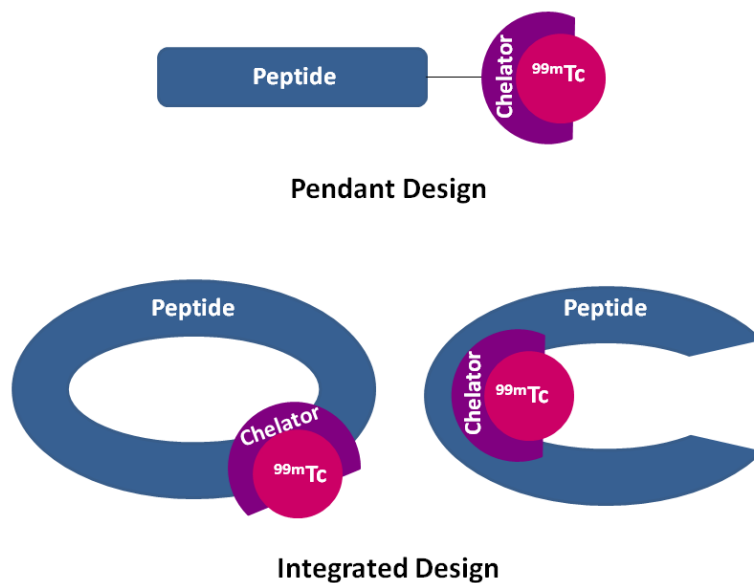


Figure 1.6: Schematic of pendant and integrated technetium-99m peptide-based radiopharmaceutical designs

An alternative approach is to form an integrated radiopharmaceutical where the metal is incorporated into the backbone of the peptide. This “hides” the metal in the molecule, minimizing interference with binding of the biomolecule to the receptor, and in some cases is an integral component in locking the peptide in its active form, making the metal imperative for biological activity. Integration can be achieved using cyclic peptides, or turn mimics, where the chelator can be incorporated into the turn region of the peptide, or a chelator can be formed as a result of peptide cyclization. This eliminates the need for addition of a bulky chelator, makes the complex more compact and decreases the molecular weight of the probe. The smaller size of integrated technetium complexes make them less likely to interfere with the binding of the probe to the target.³⁷ As well, lower molecular weight compounds are preferred as they more readily penetrate tumours and have faster clearance leading to higher tumour-to-background ratios.³⁸

Technetium-based radiopharmaceuticals have passed through three distinct generations, with the first two of these generations achieving clinical applications.³⁹ The first generation consists of perfusion agents, which do not contain a targeting entity. Due to their convenient synthesis and low cost, these first generation agents account for the majority of clinically used radiopharmaceuticals. Some of the first technetium-99m based radiopharmaceuticals were ^{99m}Tc-gluconates and ^{99m}Tc-glucoheptonates used for renal clearance studies.⁴⁰ While clinically relevant examples include: Tc-MIBI (Cardiolite[®]) for myocardial imaging;⁴¹ Tc-HMPAO (Ceretek[®]) for cerebral blood flow imaging;⁴² and Tc-MAG3 (Technescan[®]) for renal clearance studies.⁴³

Second generation technetium-based radiopharmaceuticals are target-specific, containing a targeting entity and a bifunctional chelator for technetium-99m. ^{99m}Tc labeled tropane systems target brain receptors and have been tested for diseases such as Alzheimer's, Parkinson disease and schizophrenia.⁴⁴⁻⁴⁶ A clinically tested example is ^{99m}Tc-TRODAT-1 which targets the dopamine receptor with high affinity.⁴⁷

The third generation models follow an integrated design, where the radiometal is essential for binding. These include rhenium and technetium labelled steroid analogues, first introduced by the Katzenellenbogen group.⁴⁸⁻⁵⁰ Although no third generation radiopharmaceuticals have reached the clinic, prostate specific membrane antigen (PSMA) targeting compounds using single amino acid chelate (SAAC) systems^{51, 52} for metal coordination are currently in Phase II clinical trials.

Peptide-based technetium-99m radiopharmaceuticals fall into the second and third generation models as they possess a targeting peptide. Some of the most common

peptides used in targeted technetium-99m based radiopharmaceuticals are: RGD analogues that target the $\alpha_v\beta_3$ integrin for imaging of angiogenesis;⁵³⁻⁵⁵ bombesin analogues targeting the gastrin-releasing peptide receptor;^{38, 56-59} somatostatin analogues targeting somatostatin-receptor-positive tumours;⁶⁰⁻⁶² neurotensin analogues for neuroendocrine tumour imaging;^{63, 64} and neuropeptide analogues for imaging a wide range of tumours.⁶⁵

1.7 Emission and Computed Tomography

Emission tomography is a form of functional medical imaging that measures γ -ray emission in order to form a three-dimensional image of physiological processes *in vivo*. There are two forms of emission tomography used for molecular imaging; positron emission tomography (PET) and single photon emission computed tomography (SPECT). Although their principles are very similar, their instrumentation, radiochemistry and emission are quite different.

In order to obtain an image, a radiotracer is injected into the patient and allowed to circulate through the body and accumulate in the tissue of interest. γ -rays are then emitted from the source and detected using a gamma camera. The gamma camera contains sodium iodide crystals doped with small amounts of thallium that emit a light photon once a γ -ray is detected. This light photon then strikes a photomultiplier tube causing a transformation to an electronic signal which is amplified by a preamplifier. This signal is converted to a digital signal to produce an image.¹⁷ The gamma camera is also equipped with a lead collimator which limits the field of view to decrease detection of scattered radiation from γ -rays emitted from areas of the body other than the tissue of interest, thus increasing the sensitivity of the instrument.³

Emission tomography can further be combined with computed tomography (CT) which uses an X-ray source and a parallel detector that rotate around the patient to acquire several two-dimensional X-rays from various angles to obtain three-dimensional anatomical images. Once fused, the objects seen in the functional SPECT or PET image can be given a relative position in the body using the anatomical CT image.

1.8 Positron Emission Tomography

Positron emission tomography (PET) is a highly sensitive, non-invasive form of molecular imaging that can construct a three-dimensional image through detection of injected tracers labelled with positron emitting radionuclides. These positron emitting radionuclides are generally short lived, with half-lives ranging from 10 minutes to 13 hours, although there are examples of longer lived PET radionuclides such as Zr-89 with an 80 hour half-life. As well, they can be either generator or cyclotron produced. In PET imaging, positron emission is indirectly measured through the production of γ -rays. A positron emitting radionuclide such as fluorine-18 decays to a neutron, releasing a positron and a neutrino in the process. Once the positron is emitted it travels a short distance (< 2 mm) where it annihilates with an electron from the surrounding tissue. This annihilation event causes two 511 keV photons to be emitted at a 180° angle.^{3, 66} These photons are then detected by a PET scanner (Figure 1.7a) containing a circular detector that can recreate the image based on the line of coincidence, displaying the biodistribution and accumulation of the tracer in the body (Figure 1.7b).

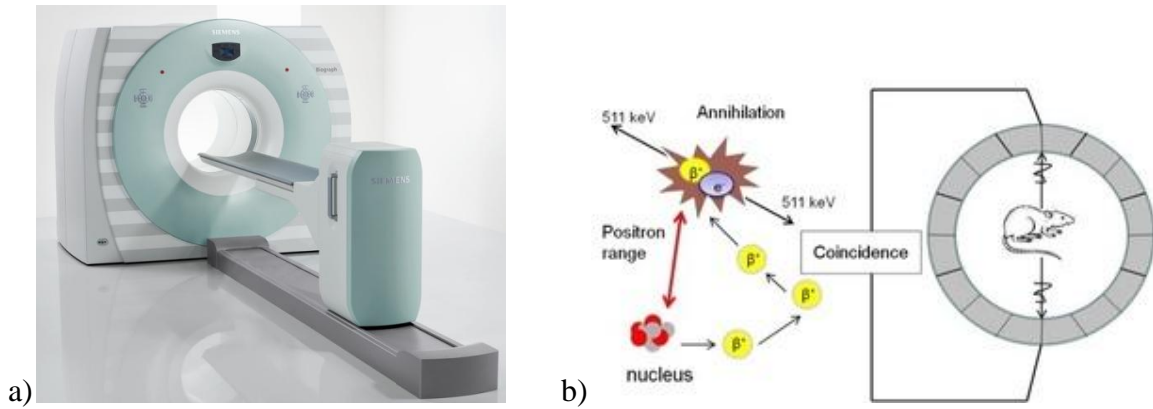


Figure 1.7: a) PET scanner,⁶⁷ and b) schematic of a PET scanner and positron annihilation⁶⁸

As stated above, a PET image can be combined with a CT image in order to combine both a functional and anatomical image. This also helps to increase the relatively poor resolution of PET imaging with the high resolution of CT imaging.³ These images can be taken consecutively; however, there is error in even fine movements of the patient over time from breathing or small movements. A PET/CT scanner has recently been developed that can obtain both a PET and CT image simultaneously, eliminating error from patient movement. In this way, the PET and CT images can be superposed to obtain an image giving a much better idea of the relative placement of the tumour in the body than a PET image alone. Figure 1.8 shows examples of a CT, PET and fused PET/CT images of a bone scan of a mouse. The CT image gives an anatomical image of the mouse whereas the PET image shows the accumulation of the probe in the mouse. Once fused, a more accurate representation of the location of the accumulation can be seen with higher accumulation of the radiotracer represented by the brighter red areas, showing the bone metastases.

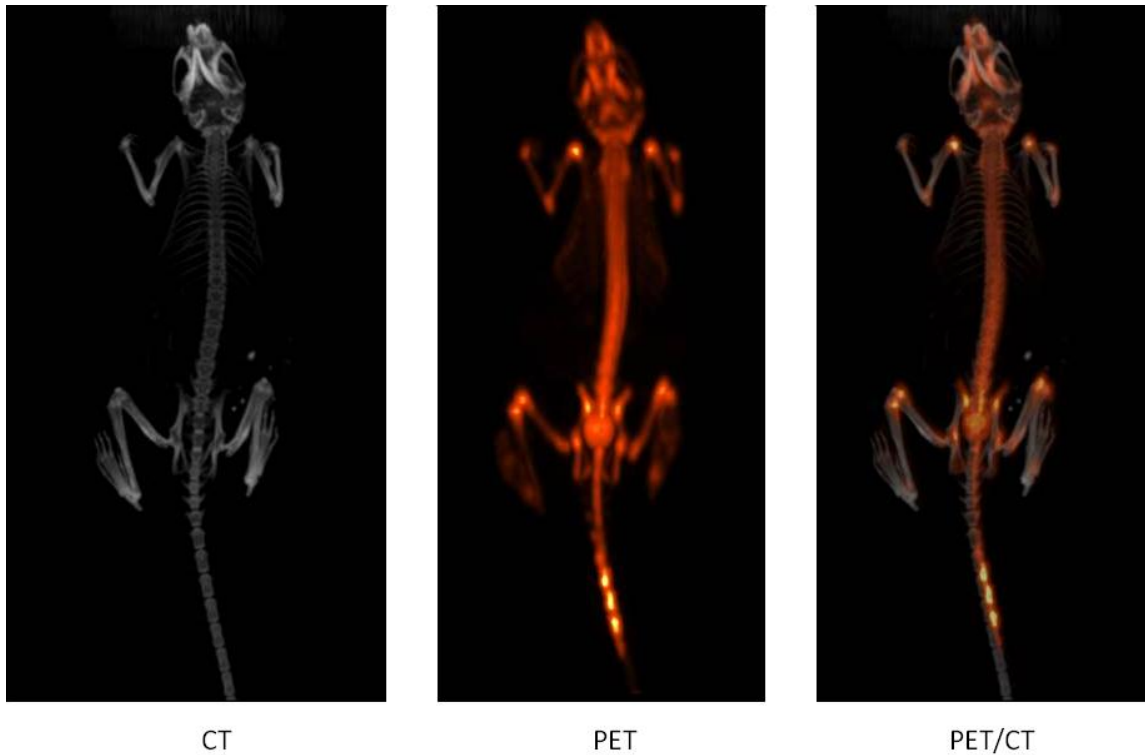


Figure 1.8: CT, PET and fused PET/CT images of a ^{18}F sodium fluoride bone scan of a mouse⁶⁹

1.9 Single Photon Emission Computed Tomography

Single photon emission computed tomography (SPECT) is the most widely used imaging modality in diagnostic nuclear medicine. It uses gamma-emitting radionuclides, such as technetium-99m, that have emission energies between 100 and 300 keV as they are energetic enough to pass through the body and be externally detected, but are not high enough energy to cause unnecessary harm to the patient.³ As is the case with PET isotopes, SPECT isotopes can be obtained from a cyclotron or a generator; however, they generally have much longer half-lives, ranging from 6 hours to 2.8 days, allowing for transportation of the isotopes from off-site cyclotron facilities, as well as more time for synthesis, administration and accumulation of the tracer prior to imaging.

SPECT imaging is very similar to PET imaging in that it uses γ -rays to construct three-dimensional functional images of radiotracer accumulation in the body. However, the radionuclides used are gamma-emitters; therefore, γ -ray emission is detected directly. As this is not a coincidence event, the photons are unidirectional. Therefore, a SPECT scanner (Figure 1.9a) has a gamma camera that rotates 180° or 360° around the patient, whereas the detector in a PET scanner remains stationary. The detector must rotate as γ -rays are emitted from the tumour from all angles, and in order to determine the location of the tracer accumulation and obtain a three-dimensional image, the detector must acquire multiple two-dimensional images at various angles around the patient (Figure 1.9b).

The unidirectional nature of the photons makes it much harder to determine the location of the γ -emission, making SPECT a lower resolution and less sensitive technique when compared to PET. However, SPECT is a much more cost effective method of imaging than PET as the majority of SPECT isotopes are generator produced and have much longer half-lives, making SPECT much more accessible than PET.

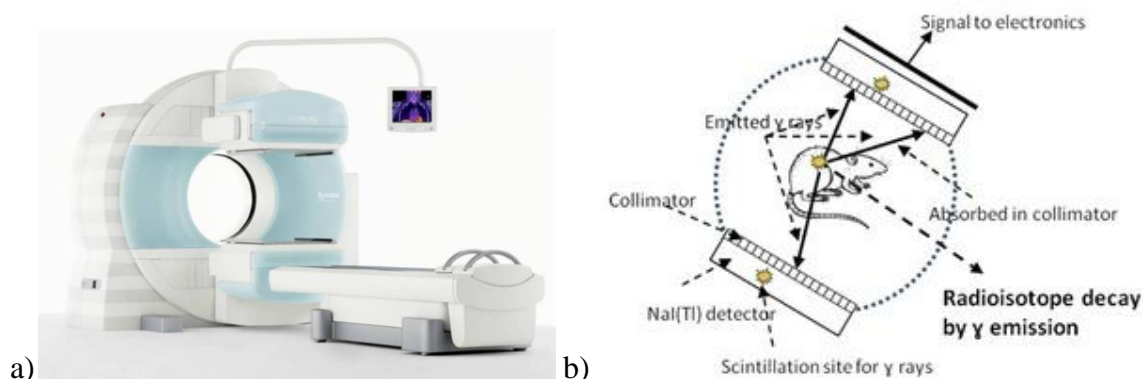


Figure 1.9: a) SPECT scanner,⁷⁰ and b) schematic of a SPECT scanner⁶⁸

As with PET, SPECT can also be combined with CT in order to give a higher resolution combined functional and anatomical image. Figure 1.10 shows the CT, SPECT and SPECT/CT images of a ^{99m}Tc -MDP (methylene diphosphonate) bone scan of a mouse. The CT image gives an anatomical reference for the SPECT image, which shows the uptake of the radiotracer in the mouse, with the brighter areas showing higher uptake in the bone metastases. The fused SPECT/CT image gives a better indication of the location of the tracer uptake, providing a higher resolution image.

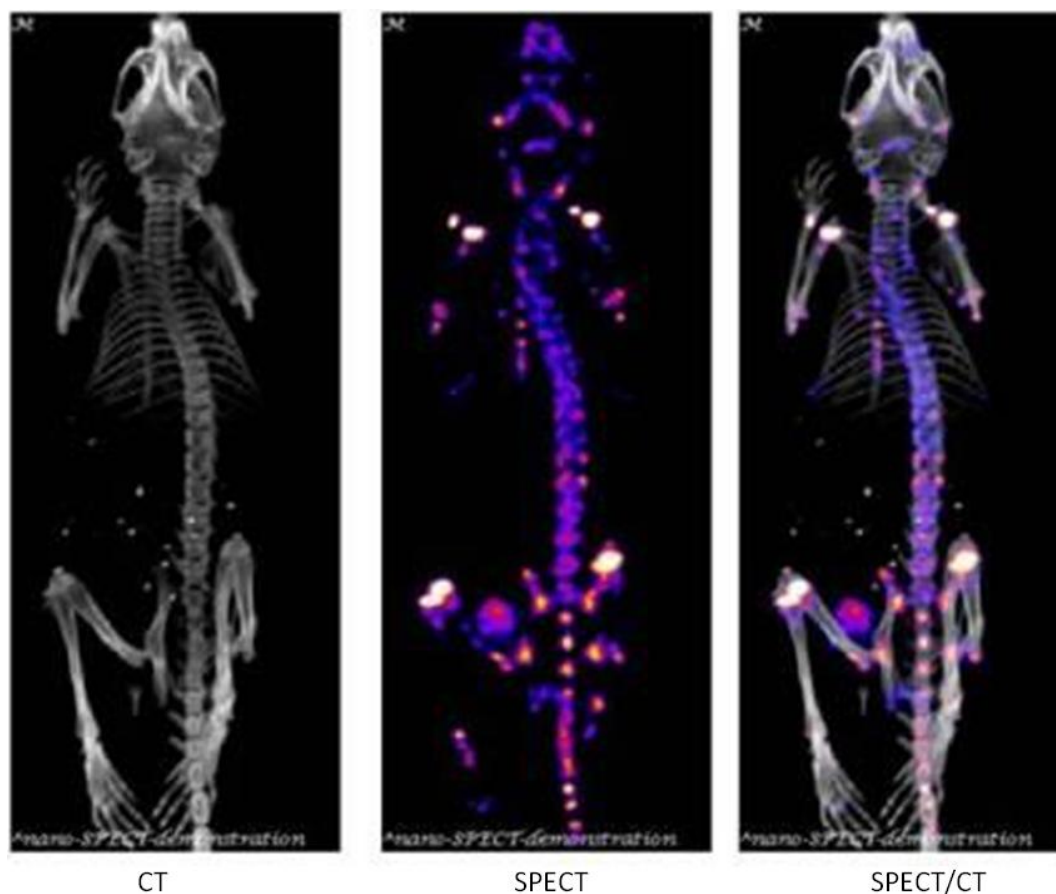


Figure 1.10: CT, SPECT and fused SPECT/CT images of a ^{99m}Tc -MDP bone scan of a mouse⁷¹

1.10 Click Chemistry

Click chemistry describes a variety of reactions that join small units together through heteroatoms quickly and reliably. The term “click chemistry” was first used by K. Barry Sharpless in 2001.⁷² There are many stipulations for reactions to be considered “click” reactions; these include being modular, wide in scope, high yielding, stereospecific and generating inoffensive byproducts. The reaction must also be simple, insensitive to oxygen and water, requiring only readily available starting materials, benign or easily removed solvents, and the product must be easily isolated.⁷² These conditions would allow for easy and reproducible reactions for joining two or more units together for a variety of purposes. These click reactions generally fall into one of four categories; cycloaddition reactions, nucleophilic ring-opening reactions, non-aldol carbonyl chemistry and addition to carbon-carbon multiple bonds.⁷³

The most common reaction that is associated with “click chemistry” is the azide-alkyne cycloaddition. This 1,3-dipolar cycloaddition reaction was first discovered by Rolf Huisgen in 1961⁷⁴ and was described by Sharpless as being the “cream of the crop” of click reactions.⁷² It irreversibly combines an internal, or more commonly a terminal alkyne and terminal azide to form both the 1,4- and 1,5-regioisomers of the 1,2,3-triazole, and was traditionally performed using high temperatures and long reaction times (Figure 1.11).

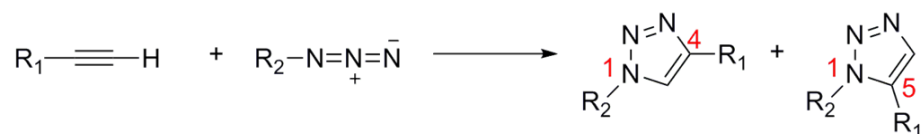


Figure 1.11: Schematic of the Huisgen azide-alkyne cycloaddition

1.10.1 Copper-Catalyzed Azide-Alkyne Cycloaddition

In 2001, forty years after its initial discovery, it was discovered that a copper(I) catalyst could be used to preferentially form the 1,4- regioisomer much (up to 10^7 times) faster and under much milder conditions.⁷⁵ This was further improved independently by both the Meldal and Sharpless groups in 2002.^{76, 77} This regioselective reaction using a copper catalyst has become known as the copper-catalyzed azide-alkyne cycloaddition (CuAAC) and is generally the reaction that is referred to as “click chemistry”.

As opposed to the thermal reaction introduced by Huisgen, which can take up to several days at very high temperatures, the copper catalyzed version can go to completion in a matter of hours at room temperature. A copper(I) catalyst, such as a copper halide, is required for this reaction, however it is often oxidized to the Cu(II) salt and is thus useless for the reaction. Alternatively, an *in situ* reduction of Cu(II) salts, such as $\text{CuSO}_4 \cdot 5\text{H}_2\text{O}$, can be performed using sodium ascorbate. This can be done using as little as 0.1 eq of the Cu(II) salt and 0.2 eq sodium ascorbate. This way the sodium ascorbate can prevent the re-oxidation of Cu(I) to Cu(II). This reaction can also be done in aqueous solutions, allowing for the use of a benign solvent as stated in the requirements for a click reaction.

The CuAAC reaction is chemoselective, as alkynes and azides are relatively inert in the absence of proper catalysts or conditions.⁷⁸ Azides have incredible stability towards water, oxygen and most organic synthesis conditions.^{79, 80} Both alkynes and azides are very unreactive to general solid-phase peptide synthesis reaction conditions; they can also be incorporated into peptides without the concern of reacting with amino acid side chains, even when unprotected. Both alkynes and azides can be inserted into the peptide early in

the sequence and remain invisible throughout the synthesis.⁷⁷ The conditions for the click reaction are tolerated by many functional groups, allowing for an unprotected peptide to be clicked in solution if desired; however, it can also be performed on solid support as the reaction conditions have been shown to be compatible with solid-phase peptide synthesis, all amino acids and their protecting groups.⁷⁶ This reaction is also very high yielding and extremely robust, tolerating many reaction conditions that are generally of concern. It does not require inert atmospheric conditions, and can be performed in a variety of solvents including aqueous alcohols, as well as pure water. It also proceeds at pH values ranging from 4 to 12.⁷⁷

This robustness has led to the CuAAC finding much versatility in chemistry and biochemistry. It has found utility in many areas such as bioconjugation, dendrimer synthesis, combinatorial drug discovery, and peptidomimetics.⁸¹ The 1,4-disubstituted 1,2,3-triazole formed has been found to be a peptide bond isostere, mimicking the placement and electronic properties of the peptide bond (Figure 1.12).^{82, 83} It was found through triazole scans of a biologically relevant peptide that the binding affinity of the peptide for the target remained approximately the same and even displayed enhanced stability compared to the natural ligand.⁸⁴ Unlike peptide bonds, triazoles are not prone to hydrolysis, enzymatic degradation, or oxidation and reduction, making the azide-alkyne cycloaddition a very attractive method of functionalizing peptides, especially for *in vivo* purposes.

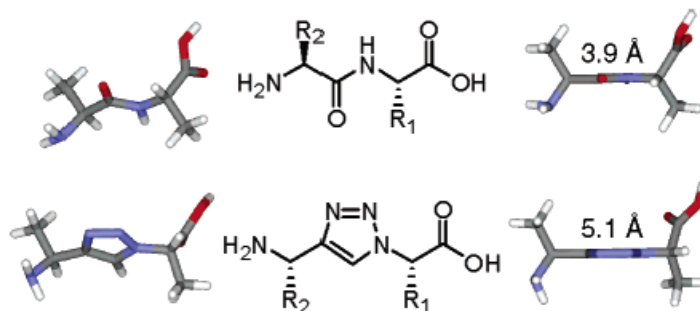


Figure 1.12: Schematic showing similarities between peptide bonds and 1, 4-disubstituted 1,2,3-triazoles (adapted from reference 82)

1.10.2 Strain-Promoted Azide-Alkyne Cycloaddition

A major issue with the CuAAC is the fact that copper is cytotoxic;⁸⁵ therefore, its utility for biological studies is limited. For this reason, the Bertozzi group developed the strain-promoted [3+2] azide-alkyne cycloaddition (SPAAC) in 2004.⁸⁶ This reaction has recently become quite popular as its lack of a copper catalyst makes it bioorthogonal and much more practical for *in vivo* studies. The “catalyst” for this reaction is the strain of the cyclic alkyne, generally a cyclooctyne as it is the smallest stable cycloalkyne. It goes to completion under physiological conditions in the absence of any other reagent or catalyst, and can be used to selectively modify biomolecules and living cells without any apparent physiological harm.⁸⁶ For this reason, SPAAC is becoming more widely used for biological applications than its copper catalyzed counterpart (Figure 1.13).

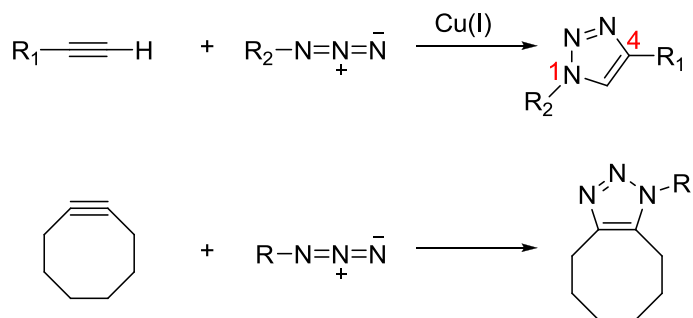


Figure 1.13: Copper-catalyzed versus strain-promoted azide-alkyne cycloadditions

The most exciting use of this reaction is the *in vivo* imaging of dynamic biological processes through “pretargeting”. This is accomplished by first targeting a receptor with either an alkyne or azide modified entity, such as a peptide or antibody. Once allowed to circulate and uptake is achieved, a fluorescently or radiolabelled alkyne or azide is injected and allowed to react *in vivo*.⁸⁷ This allows for the targeting entity to react with the receptor fully, and for the unreacted to be properly excreted from the body, increasing the target tissue to background ratio, resulting in high quality images of dynamic biological processes.

1.11 Gold Nanoparticles for Diagnosis and Therapy

Nanoparticles have recently been investigated for their use in cancer targeting. An ideal nanoparticle for this purpose is the gold nanoparticle (AuNP), as they are the most stable metal nanoparticles, they display low toxicity, are biocompatible and their surfaces are easily functionalized.⁸⁸⁻⁹² They also tend to be taken up in tumour cells due to the enhanced permeability and retention (EPR) effect they possess, with nanoparticles less than 100 nm having the ability to accumulate in malignant tissues.⁹³ This is due to blood vessel formation that occurs in response to tumours through angiogenesis, which tends to form irregular and more permeable vessels, allowing for “passive targeting” of the AuNPs; this uptake mechanism however, is non-specific. Specific uptake can be accomplished through the addition of a targeting entity, such as a peptide, antibody or small molecule to the nanoparticle. Specific uptake is more desirable, as it allows for accumulation of the nanoparticles in much higher concentration in the tissue of interest which is of use for both diagnostic and therapeutic purposes.

Gold nanoparticles show great potential for cancer targeting, as they are multifunctional. A polymer coating can be added to the outside of the nanoparticle for purposes such as increasing solubility. Targeting ligands can also be added, such as peptides, antibodies or small molecules to allow accumulation of the AuNP in the target of interest. In order to externally visualize the target, a PET isotope such as fluorine 18 can also be added for PET imaging, or an optical agent such as a dye can be added.⁹⁴⁻⁹⁷ The surface can also be functionalized with a drug in the form of a peptide or small molecule, as the targeting entity will allow for drug delivery to the target of interest.^{98, 99} Alternatively, a radioisotope could be attached for targeted radiotherapy.¹⁰⁰ Finally, a near infrared (NIR) laser or radio frequency (RF) radiation can be used for tumour ablation.¹⁰¹ The NIR laser or RF radiation cause the AuNP to heat, resulting in cell death. However, if the AuNPs are targeted, only the tumour cells should be affected. Therefore, nanoparticles can simultaneously be targeted while still allowing for imaging or therapy (Figure 1.14).

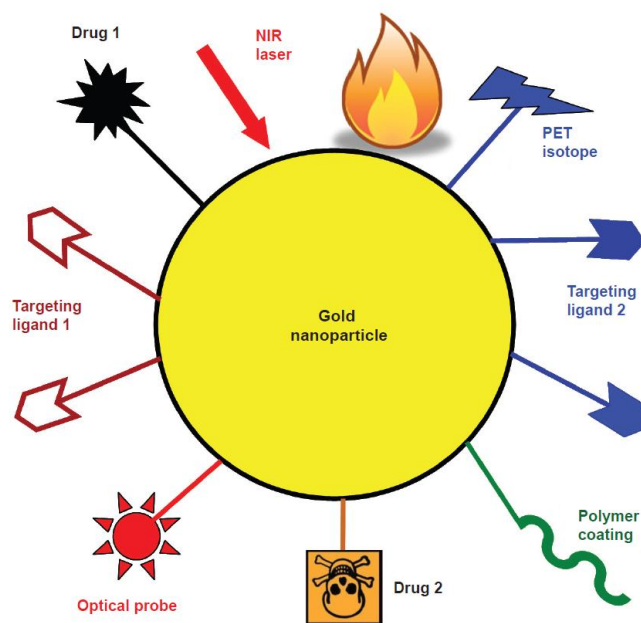


Figure 1.14: Schematic displaying the multivalency of gold nanoparticles (adapted from reference 102)

1.12 Peptide Receptor Binding

Receptors are proteins that are embedded either in the plasma membrane (cell surface receptors), cytoplasm (cytoplasmic receptors), or nucleus (nuclear receptors) of a cell. These receptors have endogenous ligands that bind in a “lock and key” fashion, triggering specific signaling pathways. Cells express many receptors; however each receptor-ligand interaction triggers its own biochemical pathway, regulating many cellular functions.

Approximately 40% of all prescription pharmaceuticals on the market target G-protein-coupled receptors (GPCR).¹⁰³ GPCRs represent a superfamily of cell surface receptors known as 7-transmembrane receptors, that are present on the surface of all cells.¹⁰⁴ They cross the cell membrane seven times and have both intracellular and extracellular domains. The transmembrane sections are hydrophobic and helical causing three extracellular loops and three intracellular loops, the N-terminus is extracellular, whereas the C-terminus is intracellular.¹⁰⁵ Although there are over 700 different GPCRs that react with many different ligands, only the extra- and intracellular domains differ, the overall structure of the transmembrane helices is highly conserved.¹⁰⁴ However, each different kind of ligand binds to the GPCR in a unique way, with peptides binding near the surface of the cell membrane, involving the top of the transmembrane helices, the extracellular loops and the N-terminal chain.^{8, 105} GPCRs represent the largest group of cell surface receptors on human cells and over half of these have roles in sensory events such as in olfaction, taste and vision.¹⁰⁴ They have also been found to have roles in many hereditary and somatic disorders and diseases, including cancer, infertility and HIV.¹⁰⁶

The gastrin-releasing peptide (GRP) receptor, part of the GPCR superfamily, is overexpressed in many forms of cancer including prostate cancer, breast cancer, renal cell

carcinoma, lung cancer, colon cancer, gastrinoma, endometrial cancer and gastrointestinal stromal tumours.¹⁰⁷ Its endogenous ligand is the gastrin-releasing peptide, which is a regulatory peptide responsible for regulating functions of the gastrointestinal and central nervous system.¹⁰⁷ It belongs to the subgroup known as bombesin-related peptides.

Bombesin is a 14 amino acid peptide isolated from the skin of the European fire-bellied toad *Bombina bombina*.¹⁰⁸ Bombesin has four known receptor subtypes; bombesin receptor subtype 1 (BB1), bombesin receptor subtype 2 (BB2), bombesin receptor subtype 3 (BB3) and bombesin receptor subtype 4 (BB4). The first three of which are found in humans, with BB3 being an orphan receptor with no known natural ligand, and BB4 being found only in amphibians.

Bombesin is a GRP receptor agonist.¹⁰⁹ Once the agonist interacts with the GRP receptor on the cell surface, the receptor-ligand complex gets internalized into the cell (Figure 1.15).¹¹⁰ This internalization is desirable over ligands that bind to the surface of the cell as it increases retention of the ligand in the target tissue.¹¹¹ Therefore, targeting tumours that overexpress GRP receptors, by designing GRP or bombesin-related peptides, have potential to be used clinically for both tumour diagnosis and therapy.

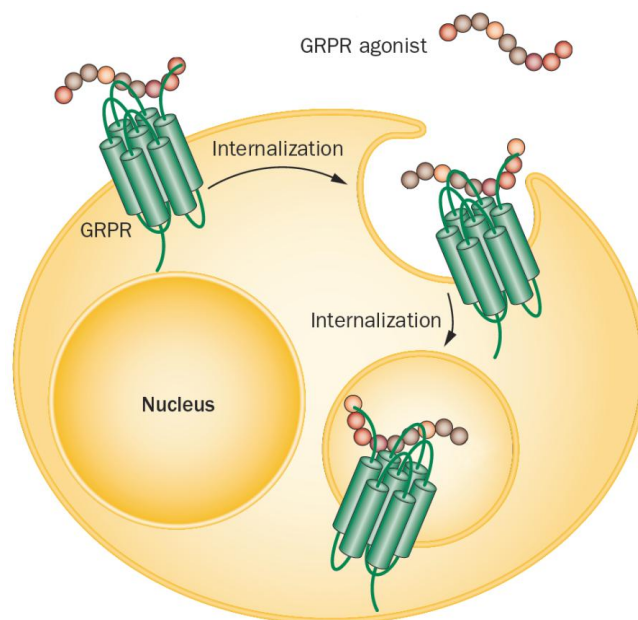


Figure 1.15: Internalization of a GRPR agonist into a cell (adapted from reference 107)

1.13 Summary

This thesis presents research on the design and synthesis of molecular imaging agents based on metal-organic compounds, specifically peptides with either technetium-99m for SPECT imaging, or gold nanoparticles for targeting prostate cancer. Chapter 2 discusses the implications of diastereomer formation when dealing with molecular imaging agents, through the coordination of various histidine compounds with $[^{99m}\text{Tc}/\text{Re}(\text{CO})_3]^+$. Chapters 3 and 4 describe synthesis of cyclic peptides for use as technetium-99m based molecular imaging agents. In Chapter 3, click chemistry is used to simultaneously cyclize and chelate peptides with $[^{99m}\text{Tc}/\text{Re}(\text{CO})_3]^+$, whereas a [2+1] chelation system involving pentapeptides containing terminal histidines is used in Chapter 4. Finally, Chapter 5 focuses on using bombesin to develop targeted water-soluble gold nanoparticles for prostate cancer targeting.

1.14 References

1. R. Weissleder and U. Mahmood, *Radiology*, 2001, 219, 316-333.
2. S. Lee, J. Xie and X. Chen, *Biochemistry*, 2010, 49, 1364-1376.
3. R. Chandra, *Nuclear Medicine Physics: The Basics*, Lippincott Williams Wilkins, Philadelphia, 7th edn., 2012.
4. S. M. Okarvi, *Med. Res. Rev.*, 2004, 24, 357-397.
5. J. C. Reubi, *Endocr. Rev.*, 2003, 24, 389-427.
6. S. Banerjee, M. R. Ambikalmajan Pillai and N. Ramamoorthy, *Semin. Nucl. Med.*, 2001, 31, 260-277.
7. S. Lee, J. Xie and X. Chen, *Chem. Rev.*, 2010, 110, 3087-3111.
8. G. R. Marshall, *Peptide Science*, 2001, 60, 246-277.
9. V. J. Hruby, *Biopolymers*, 1993, 33, 1073-1082.
10. V. J. Hruby, *Drug Discov. Today*, 1997, 2, 165-167.
11. Y. C. Patel, *Somatostatin*, Springer-Verlag: Berlin, New York, 1992.
12. M. D. Katz and B. L. Erstad, *Clin. Pharm.*, 1989, 8, 255-273.
13. R. B. Merrifield, *J. Am. Chem. Soc.*, 1963, 85, 2149-2154.
14. C.-F. Cho, S. Shukla, E. J. Simpson, N. F. Steinmetz, L. G. Luyt and J. D. Lewis, in *Virus Hybrids as Nanomaterials*, 2014, vol. 1108, ch. 16, pp. 211-230.
15. H. Kobayashi, M. Ogawa, R. Alford, P. L. Choyke and Y. Urano, *Chem. Rev.*, 2009, 110, 2620-2640.
16. W. Wadsak and M. Mitterhauser, *Eur. J. Radiol.*, 2010, 73, 461-469.
17. G. B. Saha, *Fundamentals of Nuclear Pharmacy*, Springer New York, New York, 6th edn., 2010.
18. C. Perrier and E. Segre, *Nature*, 1937, 140, 193-194.
19. I. Zolle, *Technetium-99m Pharmaceuticals*, Springer, New York, USA, 2007.
20. S. Liu and D. S. Edwards, *Chem. Rev.*, 1999, 99, 2235-2268.
21. P. Richards, W. D. Tucker and S. C. Srivastava, *Int. J. Appl. Radiat. Isot.*, 1982, 33, 793-799.

22. S. R. Cherry, J. A. Sorenson and M. E. Phelps, *Physics in Nuclear Medicine*, Saunders/Elsevier Science, Philadelphia, 3rd edn., 2003.
23. R. Alberto, *Top. Curr. Chem*, 2005, 252, 1-44.
24. <http://www.frankswebpace.org.uk/ScienceAndMaths/physics/physicsGCE/D1-1.htm>.
25. E. Deutsch, K. Libson, J.-L. Vanderheyden, A. R. Ketring and H. R. Maxon, *International Journal of Radiation Applications and Instrumentation. Part B. Nuclear Medicine and Biology*, 1986, 13, 465-477.
26. R. J. Kowalsky and S. W. Falen, *Radiopharmaceuticals in Nuclear Pharmacy and Nuclear Medicine*, American Pharmacists Association, Washington, 3rd edn., 2011.
27. D. R. van Staveren, S. Mundwiler, U. Hoffmanns, J. K. Pak, B. Spingler, N. Metzler-Nolte and R. Alberto, *Org. Biomol. Chem.*, 2004, 2, 2593-2603.
28. A. G. Jones, M. J. Abrams, A. Davison, J. W. Brodack, A. K. Toothaker, S. J. Adelstein and A. I. Kassis, *Int. J. Nucl. Med. Biol.*, 1984, 11, 225-234.
29. R. Alberto, R. Schibli, P. A. Schubiger, U. Abram and T. A. Kaden, *Polyhedron*, 1996, 15, 1079-1089.
30. R. Alberto, R. Schibli, D. Angst, P. A. Schubiger, U. Abram, S. Abram and T. A. Kaden, *Transition Met. Chem. (London)*, 1997, 22, 597-601.
31. R. Alberto, R. Schibli, A. Egli, F. F. Knapp and P. A. Schubiger, *Radiochim. Acta*, 1997, 79, 99-103.
32. R. Schibli, R. Alberto, U. Abram, S. Abram, A. Egli, P. A. Schubiger and T. A. Kaden, *Inorg. Chem.*, 1998, 37, 3509-3516.
33. U. Abram, S. Abram, R. Schibli, R. Alberto and J. R. Dilworth, *Polyhedron*, 1998, 17, 1303-1309.
34. E. García-Garayoa, R. Schibli and P. A. Schubiger, *Nucl. Sci. Tech.*, 2007, 18, 88-100.
35. R. Alberto, R. Schibli, A. Egli, A. P. Schubiger, U. Abram and T. A. Kaden, *J. Am. Chem. Soc.*, 1998, 120, 7987-7988.
36. R. Alberto, K. Ortner, N. Wheatley, R. Schibli and A. P. Schubiger, *J. Am. Chem. Soc.*, 2001, 123, 3135-3136.
37. R. Schibli and A. Schubiger, *Eur. J. Nucl. Med.*, 2002, 29, 1529-1542.

38. R. La Bella, E. Garcia-Garayoa, M. Langer, P. Bläuenstein, A. G. Beck-Sickinger and P. August Schubiger, *Nucl. Med. Biol.*, 2002, 29, 553-560.
39. S. Jürgens, W. A. Herrmann and F. E. Kühn, *J. Organomet. Chem.*, 2014, 751, 83-89.
40. W. de Kieviet, *J. Nucl. Med.*, 1981, 22, 703-709.
41. E. Prats, F. Aisa, M. D. Abos, L. Villavieja, F. Garcia-Lopez, M. J. Asenjo, P. Razola and J. Banzo, *J. Nucl. Med.*, 1999, 40, 296-301.
42. P. G. Hammersley, V. R. McCready, J. Babich and G. Coghlan, *Eur. J. Nucl. Med.*, 1987, 13, 90-94.
43. J. P. O'Malley, H. A. Ziessman and N. Cahntarapitak, *Clin. Nucl. Med.*, 1993, 18, 22-29.
44. B. J. Cleynhens, T. J. de Groot, H. P. Vanbilloen, D. Kieffer, L. Mortelmans, G. M. Bormans and A. M. Verbruggen, *Bioorg. Med. Chem.*, 2005, 13, 1053-1058.
45. H. F. Kung, M.-P. Kung and S. R. Choi, *Semin. Nucl. Med.*, 2003, 33, 2-13.
46. R. K. Hom and J. A. Katzenellenbogen, *Nucl. Med. Biol.*, 1997, 24, 485-498.
47. H. F. Kung, M.-P. Kung, S.-P. Wey, K.-J. Lin and T.-C. Yen, *Nucl. Med. Biol.*, 2007, 34, 787-789.
48. D. Y. Chi and J. A. Katzenellenbogen, *J. Am. Chem. Soc.*, 1993, 115, 7045-7046.
49. R. K. Hom, D. Y. Chi and J. A. Katzenellenbogen, *J. Org. Chem.*, 1996, 61, 2624-2631.
50. J. P. DiZio, R. Fiaschi, A. Davison, A. G. Jones and J. A. Katzenellenbogen, *Bioconjug. Chem.*, 1991, 2, 353-366.
51. M. Bartholoma, J. Valliant, K. P. Maresca, J. Babich and J. Zubieta, *Chem. Commun.*, 2009, 5, 493-512.
52. K. P. Maresca, S. M. Hillier, G. Lu, J. C. Marquis, C. N. Zimmerman, W. C. Eckelman, J. L. Joyal and J. W. Babich, *Inorg. Chim. Acta*, 2012, 389, 168-175.
53. S. Alves, J. D. Correia, L. Gano, T. L. Rold, A. Prasanphanich, R. Haubner, M. Rupprich, R. Alberto, C. Decristoforo, I. Santos and C. J. Smith, *Bioconjug. Chem.*, 2007, 18, 530-537.
54. Z.-F. Su, G. Liu, S. Gupta, Z. Zhu, M. Rusckowski and D. J. Hnatowich, *Bioconjug. Chem.*, 2002, 13, 561-570.

55. C. Decristoforo, B. Faintuch-Linkowski, A. Rey, E. von Guggenberg, M. Rupprich, I. Hernandez-Gonzales, T. Rodrigo and R. Haubner, *Nucl. Med. Biol.*, 2006, 33, 945-952.
56. S. Alves, J. D. G. Correia, I. Santos, B. Veerendra, G. L. Sieckman, T. J. Hoffman, T. L. Rold, S. D. Figueroa, L. Retzloff, J. McCrate, A. Prasanphanich and C. J. Smith, *Nucl. Med. Biol.*, 2006, 33, 625-634.
57. S. Alves, A. Paulo, J. D. G. Correia, L. Gano, C. J. Smith, T. J. Hoffman and I. Santos, *Bioconjug. Chem.*, 2005, 16, 438-449.
58. C. J. Smith, W. A. Volkert and T. J. Hoffman, *Nucl. Med. Biol.*, 2005, 32, 733-740.
59. V. Sancho, A. Di Florio, T. W. Moody and R. T. Jensen, *Curr. Drug Deliv.*, 2011, 8, 79-134.
60. J. Du, J. Hiltunen, M. Marquez, S. Nilsson and A. R. Holmberg, *Appl. Radiat. Isot.*, 2001, 55, 181-187.
61. K. P. Maresca, J. C. Marquis, S. M. Hillier, G. Lu, F. J. Femia, C. N. Zimmerman, W. C. Eckelman, J. L. Joyal and J. W. Babich, *Bioconjug. Chem.*, 2010, 21, 1032-1042.
62. C. Decristoforo and S. J. Mather, *Eur. J. Nucl. Med.*, 1999, 26, 869-876.
63. E. García-Garayoa, P. Bläuenstein, M. Bruehlmeier, A. Blanc, K. Iterbeke, P. Conrath, D. Tourwé and P. A. Schubiger, *J. Nucl. Med.*, 2002, 43, 374-383.
64. M. Bruehlmeier, E. G. Garayoa, A. Blanc, B. Holzer, S. Gergely, D. Tourwe, P. A. Schubiger and P. Blauenstein, *Nucl. Med. Biol.*, 2002, 29, 321-327.
65. M. Langer, R. La Bella, E. Garcia-Garayoa and A. G. Beck-Sickinger, *Bioconjug. Chem.*, 2001, 12, 1028-1034.
66. S. S. Gambhir, *Nat. Rev. Cancer*, 2002, 2, 683.
67. <http://www.healthcare.siemens.com/molecular-imaging/pet-ct/biograph-truepoint-petct>.
68. http://www.med.lu.se/bioimaging_center/modalities/pet_spect_ct/basic_principles.
69. <http://radiology.duke.edu/research/center/translational-petct-molecular-imaging-center/>.
70. <http://www.healthcare.siemens.com/molecular-imaging/spect-and-spect-ct/symbia-t>.
71. <http://www.umassmed.edu/saicf/petctimages/>.

72. H. C. Kolb, M. G. Finn and K. B. Sharpless, *Angew. Chem., Int. Ed.*, 2001, 40, 2004-2021.
73. H. C. Kolb and K. B. Sharpless, *Drug Discov. Today*, 2003, 8, 1128-1137.
74. R. Huisgen, *Proceedings of the Chemical Society*, 1961, 357-369.
75. C. Tornøe and M. Meldal, *Peptides-American Symposium*, 2001, 17, 263-264.
76. C. W. Tornøe, C. Christensen and M. Meldal, *J. Org. Chem.*, 2002, 67, 3057-3064.
77. V. V. Rostovtsev, L. G. Green, V. V. Fokin and K. B. Sharpless, *Angew. Chem., Int. Ed.*, 2002, 41, 2596-2599.
78. Y. L. Angell and K. Burgess, *Chem. Soc. Rev.*, 2007, 36, 1674-1689.
79. E. Saxon and C. R. Bertozzi, *Science*, 2000, 287, 2007-2010.
80. K. L. Kiick, E. Saxon, D. A. Tirrell and C. R. Bertozzi, *Proc. Natl. Acad. Sci. U. S. A.*, 2002, 99, 19-24.
81. M. Meldal and C. W. Tornøe, *Chem. Rev.*, 2008, 108, 2952-3015.
82. V. D. Bock, R. Perciaccante, T. P. Jansen, H. Hiemstra and J. H. van Maarseveen, *Org. Lett.*, 2006, 8, 919-922.
83. V. D. Bock, D. Speijer, H. Hiemstra and J. H. van Maarseveen, *Org. Biomol. Chem.*, 2007, 5, 971-975.
84. I. E. Valverde, A. Bauman, C. A. Kluba, S. Vomstein, M. A. Walter and T. L. Mindt, *Angew. Chem., Int. Ed.*, 2013, 52, 8957-8960.
85. N. J. Agard, J. M. Baskin, J. A. Prescher, A. Lo and C. R. Bertozzi, *ACS Chem. Biol.*, 2006, 1, 644-648.
86. N. J. Agard, J. A. Prescher and C. R. Bertozzi, *J. Am. Chem. Soc.*, 2004, 126, 15046-15047.
87. S. T. Laughlin, J. M. Baskin, S. L. Amacher and C. R. Bertozzi, *Science*, 2008, 320, 664-667.
88. M. R. Papasani, G. Wang and R. A. Hill, *Nanomedicine : nanotechnology, biology, and medicine*, 2012, 8, 804-814.
89. S. Naahidi, M. Jafari, F. Edalat, K. Raymond, A. Khademhosseini and P. Chen, *J. Control. Release*, 2013, 166, 182-194.
90. N. L. Rosi and C. A. Mirkin, *Chem. Rev.*, 2005, 105, 1547-1562.

91. N. L. Rosi, D. A. Giljohann, C. S. Thaxton, A. K. R. Lytton-Jean, M. S. Han and C. A. Mirkin, *Science*, 2006, 312, 1027-1030.
92. I. H. El-Sayed, X. Huang and M. A. El-Sayed, *Nano Lett.*, 2005, 5, 829-834.
93. A. K. Iyer, G. Khaled, J. Fang and H. Maeda, *Drug Discov. Today*, 2006, 11, 812-818.
94. M. Manchester and P. Singh, *Adv. Drug Delivery. Rev.*, 2006, 58, 1505-1522.
95. F. M. Brunel, J. D. Lewis, G. Destito, N. F. Steinmetz, M. Manchester, H. Stuhlmann and P. E. Dawson, *Nano Lett.*, 2010, 10, 1093-1097.
96. X. Montet, M. Funovics, K. Montet-Abou, R. Weissleder and L. Josephson, *J. Med. Chem.*, 2006, 49, 6087-6093.
97. J. Cheon and J.-H. Lee, *Acc. Chem. Res.*, 2008, 41, 1630-1640.
98. S. K. Libutti, G. F. Paciotti, A. A. Byrnes, H. R. Alexander, Jr., W. E. Gannon, M. Walker, G. D. Seidel, N. Yuldasheva and L. Tamarkin, *Clin. Cancer Res.*, 2010, 16, 6139-6149.
99. D. F. Emerich and C. G. Thanos, *J. Drug Target.*, 2007, 15, 163-183.
100. L. Zhang, H. Chen, L. Wang, T. Liu, J. Yeh, G. Lu, L. Yang and H. Mao, *Nanotechnol. Sci. Appl.*, 2010, 3, 159-170.
101. E. S. Glazer, C. Zhu, K. L. Massey, C. S. Thompson, W. D. Kaluarachchi, A. N. Hamir and S. A. Curley, *Clin. Cancer Res.*, 2010, 16, 5712-5721.
102. W. Cai, T. Gao, H. Hong and J. Sun, *Nanotechnol. Sci. Appl.*, 2008, 1, 17-32.
103. D. Filmore, *Modern Drug Discovery*, 2004, 7, 24-28.
104. J. D. A. Tyndall, B. Pfeiffer, G. Abbenante and D. P. Fairlie, *Chem. Rev.*, 2005, 105, 793-826.
105. G. L. Patrick, *An Introduction to Medicinal Chemistry*, Oxford University Press Inc., New York, 3rd edn., 2006.
106. T. H. Ji, M. Grossmann and I. Ji, *J. Biol. Chem.*, 1998, 273, 17299-17302.
107. R. Mansi, A. Fleischmann, H. R. Macke and J. C. Reubi, *Nat. Rev. Urol.*, 2013, 10, 235-244.
108. A. Anastasi, V. Erspamer and M. Bucci, *Experientia*, 1971, 27, 166-167.
109. J. C. Reubi and H. R. Maecke, *J. Nucl. Med.*, 2008, 49, 1735-1738.

110. R. V. Benya, Z. Fathi, T. Kusui, T. Pradhan, J. F. Battey and R. T. Jensen, *Mol. Pharmacol.*, 1994, 46, 235-245.
111. E. García Garayoa, D. Rüegg, P. Bläuenstein, M. Zwimpfer, I. U. Khan, V. Maes, A. Blanc, A. G. Beck-Sickinger, D. A. Tourwé and P. A. Schubiger, *Nucl. Med. Biol.*, 2007, 34, 17-28.

Chapter 2

2 Investigation of Isomer Formation Upon Coordination of Bifunctional Histidine Analogues with [$^{99m}\text{Tc}/\text{Re}(\text{CO})_3$] $^{+*}$

2.1 Introduction

A common radionuclide used in diagnostic nuclear medicine is technetium-99m; it is incorporated in more than 80% of radiopharmaceuticals today.¹ Previously, the majority of technetium was utilized in the +5 oxidation state for targeted agents. The $[\text{Tc}=\text{O}]^{3+}$ core forms complexes with square pyramidal geometry upon treatment with various tetradentate ligand sets.²⁻⁵ However, the presence of an unprotected side adjacent to the oxo ligand left these complexes open to protonation, which could lead to decomposition.⁶ The use of technetium in the +1 oxidation state was pioneered by Davison and Jones,⁷ and was developed for use in targeted radiopharmaceuticals by Alberto.⁸⁻¹² These octahedral Re/Tc tricarbonyl complexes, when coordinated with a tridentate chelator, are completely protected against ligand attack.⁶ Another advantage to this core is its small size and lipophilicity, which allows for easy incorporation into the ligand structure, therefore having little effect on biological activity.^{6, 13} These octahedral complexes are generally used with tridentate chelators as they tend to form a more stable complex and have a higher in vivo stability than bidentate chelators.¹⁴ As well, they tend to react very fast, making them ideal for radiolabelling as the time required for synthesis can be decreased.¹⁴

* A version of this chapter has been published. Simpson, E.J.; Hickey, J.L.; Breadner, D.; Luyt, L.G. Dalton Trans., **2012**, 41, 2950-2958. - Reproduced by permission of The Royal Society of Chemistry.

N^{α} -substituted histidine is a tridentate chelator capable of coordinating $\text{Re}/^{99\text{m}}\text{Tc}$ tricarbonyl.¹⁵⁻¹⁷ Histidine, as a chelator, forms complexes with many desirable properties, such as high biological stability and specific activity, as well as the ability to coordinate rapidly and quantitatively at low concentrations.^{2, 18, 19} This chelator has found use in the labelling of many different biomolecules including neurotensin analogues, which target pancreatic carcinoma;^{15, 16} bombesin analogues, which target gastrin-releasing peptide receptors;²⁰ and cyclic RGD peptide systems, which target the $\alpha_v\beta_3$ integrin, over-expressed in angiogenic vessels and malignant tumours.²¹

Once histidine is coordinated to the Re/Tc core, a neutral metal complex is created, which has the potential to produce diastereomers. The issue of isomer formation has previously been reported for Re/Tc chelators containing various amine-based ligand sets.²²⁻²⁴ However, diastereomer formation for biomolecules containing the N^{α} -substituted histidine chelator has not been described. Work has been done in our lab with a cyclic RGD peptide system containing an N^{α} -substituted histidine chelator (Figure 2.1). When coordinated with Re/Tc tricarbonyl, it was found that two products were formed. These products had the same molecular weight and, therefore, were thought to be isomers at the alpha amine of the histidine.

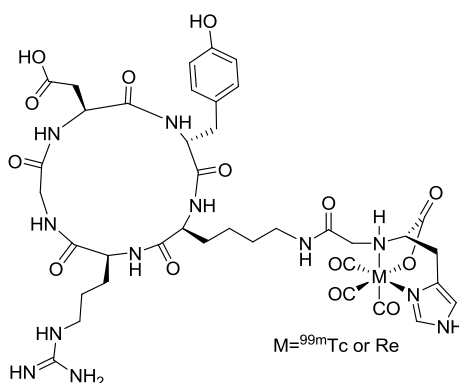


Figure 2.1: Cyclic RGD peptide system containing an N^{α} -substituted histidine chelator

Diastereomer formation is a significant concern in drug development as the presence of an unwanted isomer can cause side effects, toxicity and result in differing pharmacokinetic properties from that of the desired isomer. For this reason, there often is increased scrutiny during regulatory approval for drugs containing diastereomers. For example, the Food and Drug Administration (FDA) in the United States has indicated that, “diastereomers therefore should, with the rare exception of cases where in vivo interconversion occurs, be treated as separate drugs and developed accordingly”.²⁵

There are examples reported of N^τ-derivatized histidine,^{19, 26} as well as the related 1,2,3-triazole analogues,^{26, 27} which avoid isomer formation by leaving the N^α position as a primary amine. As such, these metal complexes show promise for radiopharmaceutical development. However, as the issue of diastereomer formation for N^α-substituted histidine complexes has not been previously addressed in the literature, the focus of this paper is the investigation of the existence and nature of the products formed upon coordination of this chelator with the [M(CO)₃]⁺ core. This was done through coordination of simplified chelation models with rhenium followed by thorough analysis by NMR spectroscopy, allowing for determination of the stereochemistry of the resultant diastereomers.

2.2 Results and Discussion

Four different histidine chelators (Figure 2.2) were synthesized and characterized both prior to and following coordination with rhenium tricarbonyl in order to determine the nature of the isomers being formed. The first was a small molecule histidine chelator synthesized by reductive amination, **2.1**. This chelator was then modified with a protected imidazole **2.2** in order to eliminate the possibility that the observed isomers were pros-

tele (π - τ) linkage isomers of the imidazole ring. The third chelator developed was a derivative of **2.1** with the alpha amine on the histidine methylated, **2.3**, in order to determine the role of the secondary amine in isomer formation. Finally, a modified dipeptide **2.4** was also synthesized by solution-phase techniques, in order to compare the role of histidine in isomer formation between the small molecule chelators and those within a peptide-like system.

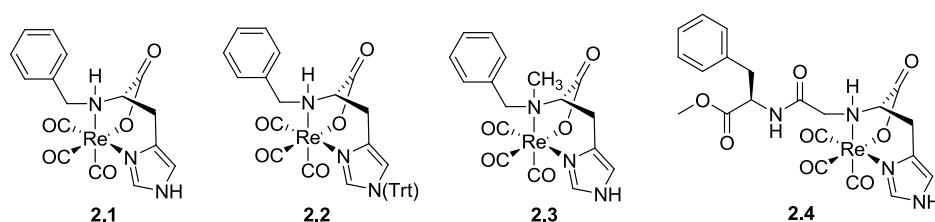
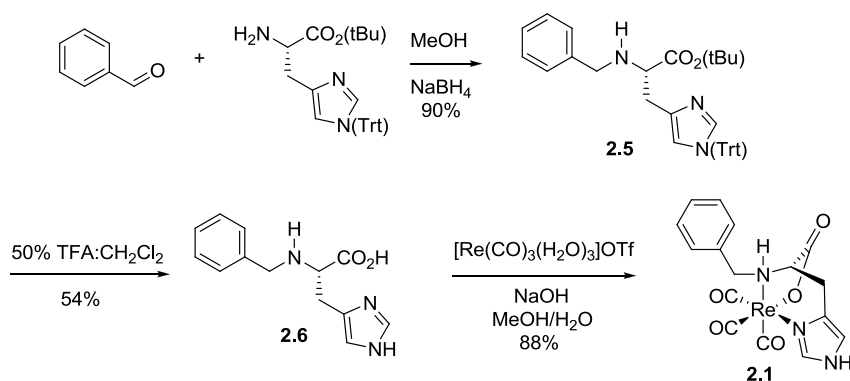


Figure 2.2: Simplified histidine chelation models used for investigation of diastereomer formation

2.2.1 N^{α} -benzyl-L-histidine

As a model system, a small molecule chelator consisting of a benzylated histidine was prepared. This was done by reductive amination of H-His(Trt)-O(tBu) and benzaldehyde with sodium borohydride to form chelator **2.6** (Scheme 2.1).²⁸ Chelator **2.6** could then be coordinated with $[\text{Re}(\text{CO})_3(\text{H}_2\text{O})_3]\text{OTf}$ ²⁹ in the presence of sodium hydroxide and methanol. This formed the final coordinated product **2.1**, which precipitated out of solution and was easily recovered by centrifugation.



Scheme 2.1: Synthesis and coordination of chelator **2.6**

Analytical LC-MS showed that two products were formed in approximately a 2:1 ratio upon coordination (Figure 2.3a). These products were believed to be diastereomers at the alpha amine of the histidine, as both products had the theoretical coordinated mass of 515.9/517.9 m/z (NaC₁₆H₁₄O₅N₃^{185/187}Re) displaying the characteristic rhenium 185/187 isotopic signature. The major isomer was isolated (Figure 2.3b) by recrystallization in acetonitrile, allowing for further experimentation.

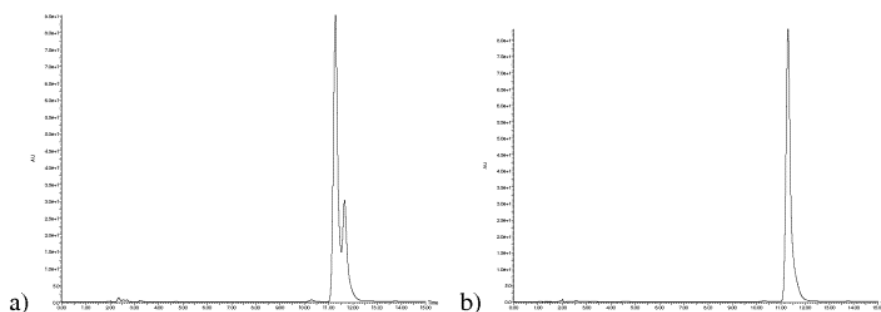


Figure 2.3: Analytical HPLC trace, UV absorbance detected from 210-800 nm (RP-C₁₈ 4.6 x 250 mm, 5 μm), of a) the mixture of isomers of **2.1**, and b) the purified major isomer **2.1a**

¹H NMR spectra of the purified product before and after coordination (Figure 2.4) was used to confirm the presence of isomers. When comparing the two NMR spectra, it was quite evident that [Re(CO)₃]⁺ incorporation was successful as a large change in the

splitting and chemical shift of the methylene protons was observed. Figure 2.4b shows that, upon coordination of $[\text{Re}(\text{CO})_3]^+$, all peaks were doubled, which indicated that there were two diastereomers formed.

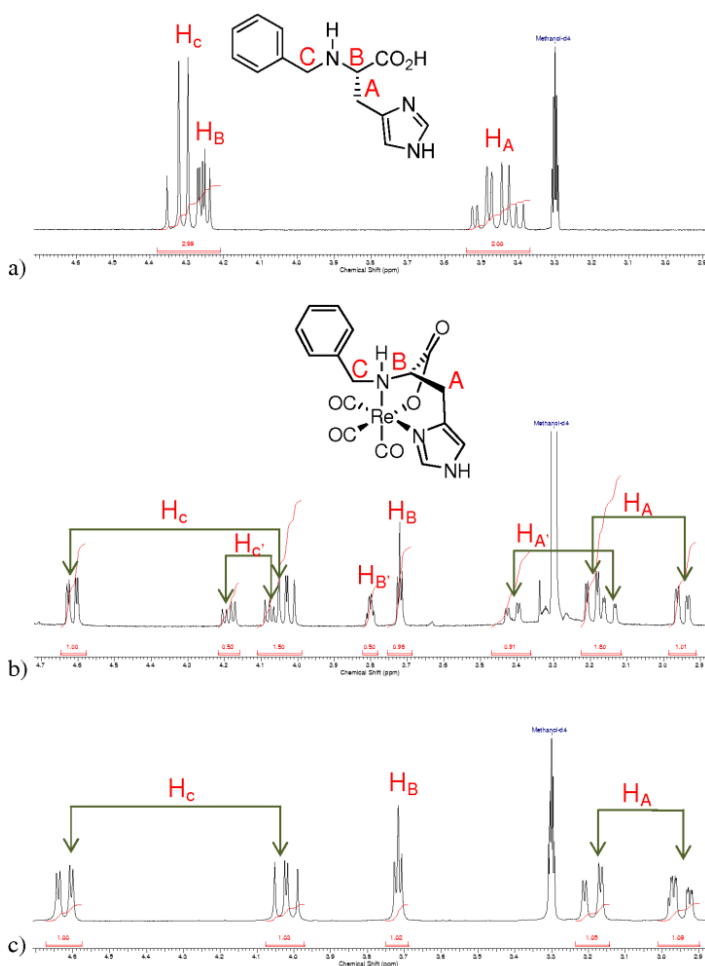


Figure 2.4: Methylene region of the ^1H NMR (400 MHz, MeOH-d_4) of a) the uncoordinated product **2.6**, b) the coordinated mixture of **2.1**, and c) the pure major isomer **2.1a**

The major isomer was successfully isolated from the mixture and ^1H (Figure 2.4c), ^{13}C , gCOSY, and NOESY NMR studies were performed. Through the NOESY experiment (Figure 2.5), the structure of the major isomer was determined based on the through-space correlations of the protons. Of particular interest was the interaction of the protons

on carbon C as well as the amine proton with the protons on carbon A. There is a correlation that can be seen between the amine proton and the A proton (solid circle on Figure 2.5), while no correlation is seen between the C protons and the A protons (dashed circle on Figure 2.5). This leads to the conclusion that the major isomer has the stereochemistry indicated as **2.1a** (Figure 2.6).

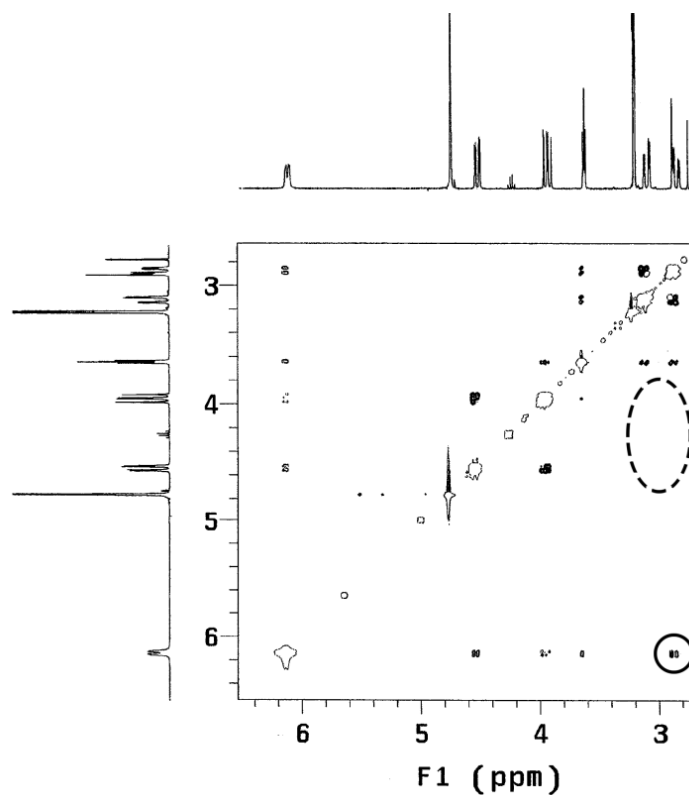


Figure 2.5: NOESY spectrum (400 MHz, MeOH-d₄) of the pure major isomer of **2.1** showing correlation between the proton on carbon A and the amine proton (solid circle) and the lack of correlation between protons on carbons A and C (dashed circle)

2.2.2 Stability Studies

In order to determine the stability of the complex, the purified major isomer **2.1a** was dissolved in MeOH under either neutral, acidic (0.1 M HCl) or basic (0.1 M NaOH) conditions and monitored by HPLC to see if the isomers interconvert in solution (Figure 2.6).

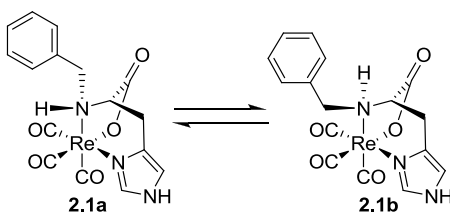


Figure 2.6: Stereochemistry of the major isomer **2.1a** as determined by gCOSY and NOESY experiments and interconversion of the major isomer **2.1a** to the minor isomer **2.1b**

In neutral solution no interconversion between isomers was detected at room temperature after 48 h. However, upon heating to approximately 35°C for 24 h, the isomers interconverted to their former ratio of approximately 2:1. Under acidic conditions (0.1 M HCl) there was no interconversion detected after 48 h. Upon heating, **2.1a** decomposed, rather than interconverting to the minor isomer. When **2.1a** was put into 0.1 M NaOH it immediately interconverted to the previous ratio. This ratio remained unchanged after stirring at room temperature for 48 h, followed by heating for 48 h. Since the interconversion occurred under both neutral and basic conditions, it can be concluded that the isomer formation is not due to epimerization at the alpha carbon upon addition of base during metal coordination.

2.2.3 Technetium-99m Labelling of N^α-benzyl-L-histidine

The small molecule chelator **2.6** was labelled with technetium-99m to give **2.7** (Figure 2.7). Addition of pertechnetate to a commercially available Isolink kit³⁰ formed the [^{99m}Tc(CO)₃(H₂O)₃]⁺ starting material. This reduced Tc-99m was then added to a solution of **2.6** to form the radiolabelled histidine derivative **2.7**. The analytical HPLC gamma trace revealed two peaks at the same retention time as the rhenium analogue; these two

peaks also appear in the same ratio as seen when **2.6** is coordinated with rhenium (Figure 2.7).

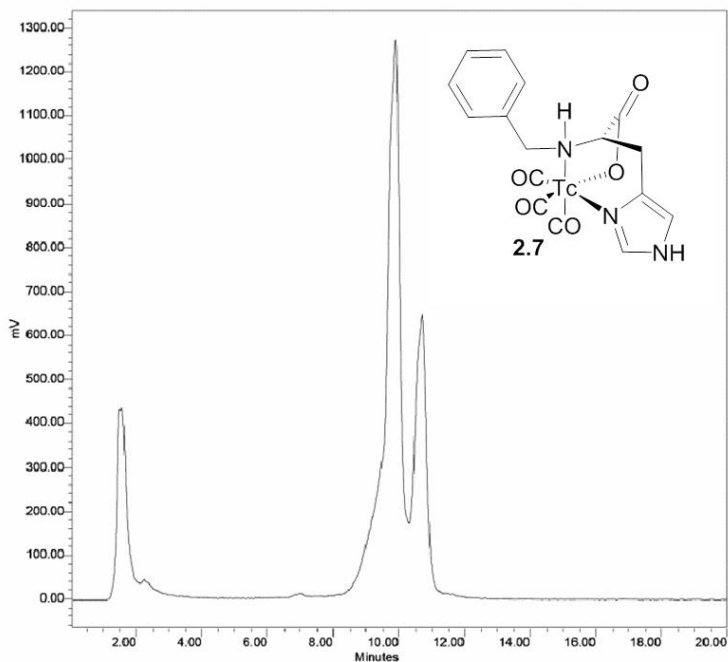


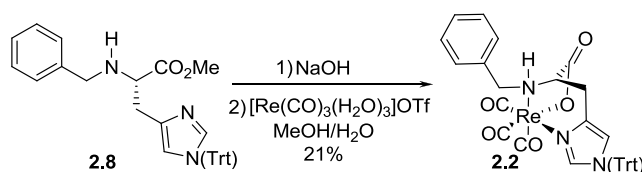
Figure 2.7: Analytical HPLC gamma trace (C_{18} 4.6 x 150 mm, 5 μ m) of ^{99m}Tc labelled **2.7**

From this, it could be seen that **2.6** was successfully labelled with $[\text{}^{99m}\text{Tc}(\text{CO})_3]^+$ and formed a mixture of two isomers in a similar fashion to that seen upon rhenium coordination.

2.2.4 Histidine Linkage Isomers

It was recently reported in the literature that histidine can form pro-s-tele (π - τ) linkage isomers with palladium and ruthenium, in a square planar arrangement, where the coordination can be to either of the imidazole N-atoms on the histidine.^{31, 32} In order to ensure that the observed isomers were, in fact isomers at the secondary amine, a protected version of **2.6** was synthesized (Scheme 2.2). It was prepared in the same manner as **2.6**,

with the exception that the histidine contained a methyl ester instead of a tert-butyl ester, which is an orthogonal protecting group to the trityl group present on the imidazole. This allowed for selective deprotection of the methyl ester prior to coordination, while leaving the trityl group intact. This experimental design would eliminate the possibility that the observed isomers were pro-tele (π - τ) linkage isomers, given that only the unprotected imidazole nitrogen is able to coordinate to the rhenium.



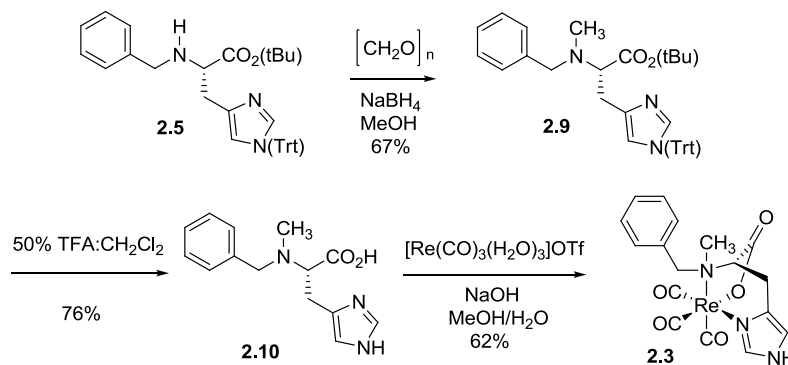
Scheme 2.2: Coordination of **2.8** with $[\text{Re}(\text{CO})_3]^+$ to form **2.2**, a modification of **2.1** with a trityl protected imidazole to demonstrate that the isomers are formed at the secondary amine, as opposed to linkage isomers of the imidazole

Chelator **2.8** was synthesized by the same method as was previously used for **2.5**, with the only difference being the protecting group on the histidine. Once purified by preparative TLC, a one-pot deprotection and subsequent coordination using $[\text{Re}(\text{CO})_3(\text{H}_2\text{O})_3]\text{OTf}$ was performed in a mixture of methanol and water at reflux. Analysis by LC-MS again showed two peaks, both with the same mass of 759.2/761.2 m/z, which matches the theoretical mass ($\text{NaC}_{35}\text{H}_{28}\text{N}_3\text{O}_5^{185/187}\text{Re}$) of complex **2.2**. As the imidazole was still trityl protected, this shows that the two products formed upon coordination are not linkage isomers of the histidine.

2.2.5 Methylation of N^α -benzyl-L-histidine

In order to determine the role of the secondary amine in the formation of diastereomers, another chelation model, where **2.6** is methylated at the alpha amine, was developed. This chelator was prepared starting from **2.5** (Scheme 2.3). Through treatment with

paraformaldehyde, the alpha amine of the histidine was methylated, giving **2.9**. Following TFA deprotection and rhenium coordination, the desired complex **2.3** was obtained in a 62% yield.



Scheme 2.3: Synthesis of methylated complex **2.3**

Through LC-MS analysis of **2.3**, two products were observed to have formed, as was seen with **2.1**. Although the peaks were not fully resolved, it could be seen that both products had the same molecular weight and rhenium signature. However, it appeared as though one diastereomer was much more predominant than in the non-methylated version **2.1**. This was most easily seen in the ^1H NMR of the mixture of isomers, where, by integration, there was approximately a 5:1 ratio (Figure 2.8). Although separation of the isomers was not possible, further characterization including gCOSY and NOESY spectra were performed on the mixture (see Appendix A). The NOESY spectrum confirmed the identical major isomer that was formed previously for **2.1**, as determined by the lack of a through-space correlation between the protons on carbons A and C. From this, it can be seen that the same diastereomers are still formed when the alpha amine is methylated. Therefore, isomer formation is not due to the fact that the amine in **2.1** is secondary. This

also leads to the possibility of controlling isomer formation through substitution at the amine in order to obtain a predominant product.

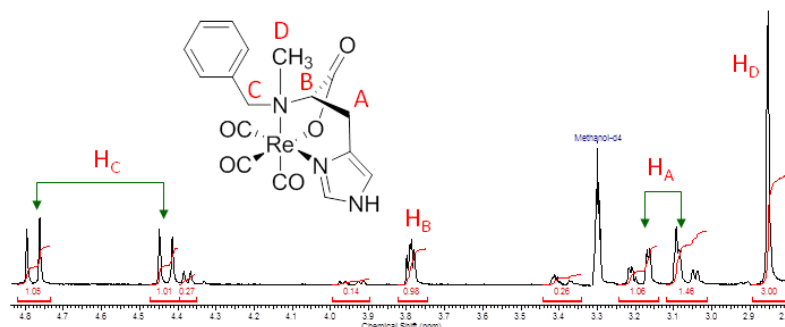
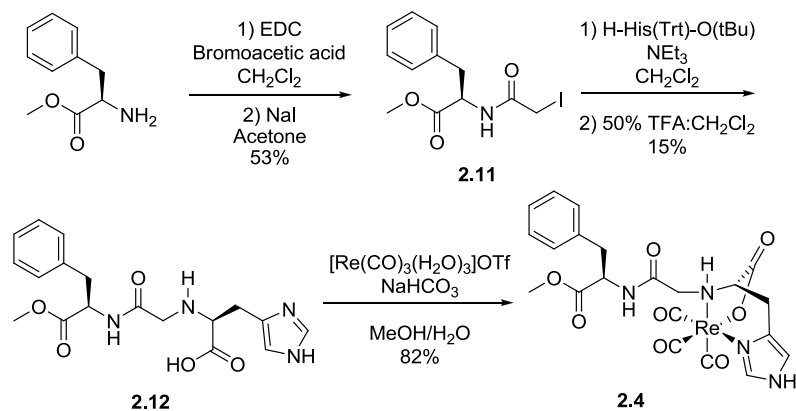


Figure 2.8: Methylene region of ^1H NMR (400 MHz, MeOH- d_4) of **2.3**. Isomers can still be seen even when the secondary amine is methylated; however, one isomer is much more predominant

The histidine chelator is generally reported in the literature as forming a single product upon coordination. As the retention times of the isomers of **2.1** and **2.3** are so close by LC-MS, two peaks could only be seen when using certain HPLC columns, whereas for others only one peak could be seen. The column and size of molecule used when studying this chelation system are potential reasons as to why a single product is commonly reported for the histidine chelator when conjugated to a biomolecule.¹⁷

2.2.6 N^α -Histidinyl-acetyl-phenylalanine-OMe

In order to compare the formation of coordination isomers between a small molecule chelator and a peptide-like chelator, a modified dipeptide was prepared by solution-phase synthesis (Scheme 2.4).



Scheme 2.4: Synthesis of dipeptide complex **2.4**

A methyl ester protected phenylalanine was used as the first amino acid in this dipeptide. The coupling of the phenylalanine to bromoacetic acid was attempted using three different coupling reagents: (i) diisopropylcarbodiimide (DIC), (ii) 1-ethyl-3-(3-dimethylaminopropyl) carbodiimide (EDC), and (iii) dicyclohexylcarbodiimide (DCC). It was found that coupling using DIC gave a mixture of the bromide and chloride analogues, with the bromide being the major component; while coupling with EDC gave the same mixture, but with the chloride analogue being the major component. Coupling using DCC gave approximately a 50:50 mixture of the two. The mixture prepared using DIC could not be purified to eliminate the diisopropyl urea side product, and DCC was not ideal to work with. For these reasons, EDC was chosen as the preferred coupling reagent for the reaction. After purification of the bromide-chloride substituted mixture, a Finkelstein reaction was performed to exchange the mixture of chloride and bromide leaving groups for iodine to make **2.11**. The iodo derivative then underwent a substitution reaction with H-His(Trt)-O(tBu) as in the synthesis of **2.5**, followed by TFA treatment to afford trityl deprotection. With the methyl ester protecting group still intact, **2.12** was then purified by preparative HPLC.

Given that the dipeptide contains a base-labile methyl ester protecting group, the coordination could not be done under the same conditions as was used for **2.1** and **2.3**. Therefore, coordination was performed by substituting NaHCO_3 for NaOH (Scheme 4). The rhenium product **2.4** precipitated out of solution and was collected by centrifugation. By LC-MS it was clear that two products were again formed upon coordination, each with the same mass ($\text{C}_{21}\text{H}_{22}\text{N}_4\text{O}_8$ $^{185/187}\text{Re}$, 644.1/646.1 m/z) and the expected isotopic rhenium signature. The isomers were separated by preparative HPLC, and NMR studies including ^1H , gCOSY and ROESY spectra were performed. Through the ROESY spectrum (Figure 2.9), the same through-space correlation between the protons on carbon A and the amine proton could be seen. As well, there was a lack of correlation between the protons on carbons A and C. Therefore, it can be seen that diastereomers also form in a peptide-like system with the same predominant isomer as in **2.1** and **2.3**.

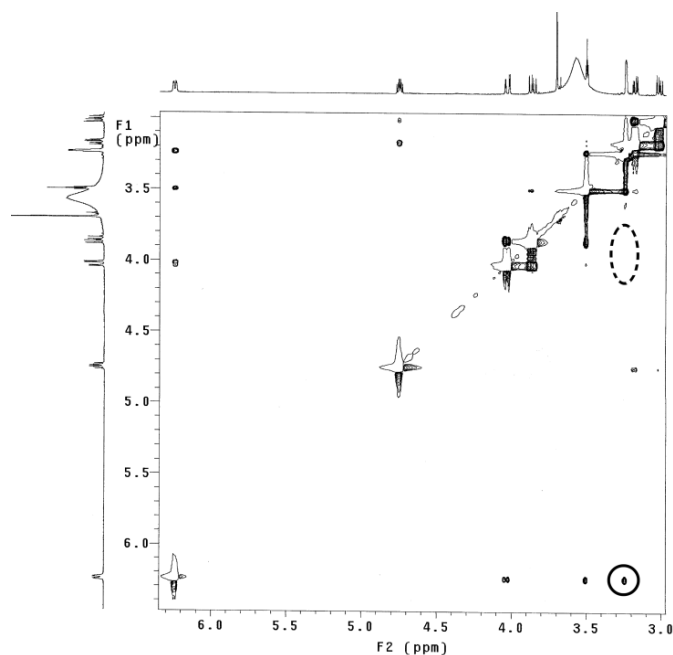


Figure 2.9: ROESY spectrum (600 MHz, DMF-d7) of the pure major isomer of **2.4** showing correlation between the protons on carbon A and the amine proton (solid circle) and the lack of correlation between protons on carbons A and C (dashed circle)

2.3 Conclusions

Histidine is well suited as a chelator for the radiolabelling of peptides by coordination of rhenium or technetium-99m. It can be used in histidine tags, which consist of repeating linear sequences of histidine attached to the end of a protein in order to incorporate technetium.³³⁻³⁹ However, a new challenge has been presented when using histidine as a tridentate chelator as multiple products are formed upon metal complexation. Two products can be seen in both small molecule and peptide-like systems. Through protecting group manipulation, it was determined that the isomers were not linkage isomers of the imidazole, but rather isomers at the alpha amine. When the secondary amine is methylated, the isomers are still present, yet the ratio is more favoured towards one isomer than in the non-methylated version. From gCOSY, NOESY and ROESY experiments, the stereochemistry of the major and minor isomers of **2.1**, **2.3** and **2.4** were determined (Figure 2.10).

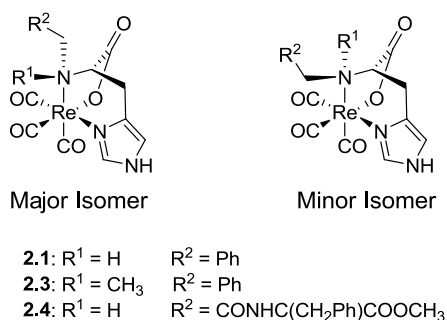


Figure 2.10: Stereochemistry of the diastereomers of **2.1**, **2.3** and **2.4**

The formation of diastereomers in any radiopharmaceutical is a major concern as regulatory approval of drugs is more difficult when isomers are involved. Therefore, it is critical that the formation of diastereomers be addressed when dealing with this chelation system for the coordination of $[^{99m}\text{Tc}/\text{Re}(\text{CO})_3]^+$.

2.4 Experimental

Materials and Methods

All chemicals were purchased from Sigma-Aldrich, Novabiochem, Peptides International and Chem-Impex and were used without further purification unless indicated. Isolink kits were a generous gift from Mallinckrodt Medical. Dry CH_2Cl_2 was prepared by distillation from CaH under argon. For LC-MS, a Waters, Inc. system was used, consisting of a Waters 2998 Photodiode Array Detector and a Waters 2767 Sample Manager. For analytical LC-MS studies, a Sunfire RP-C18 4.6 x 250 mm, 5 μm column and a Waters Symmetry RP-C18 4.6 x 150 mm, 5 μm column were used. For preparative LC-MS work, a Sunfire RP-C18 19 x 150 mm, 5 μm column was used. In both cases, absorbance was detected at wavelengths of 220 nm and 254 nm. A gradient solvent system consisting of CH_3CN + 0.1% of TFA (solvent A) and H_2O + 0.1% of TFA (solvent B) was used. Silicycle Silica Gel 60 (230-400 mesh) was used for flash column chromatography purification. EMD Silica Gel 60 F₂₅₄ plates were used for analytical TLC, and EMD Silica Gel 60 F₂₅₄, 2 mm glass plates were used for preparative TLC. Varian Mercury 400 and Varian INOVA 400 and 600 NMR spectrometers were used for ^1H , ^{13}C , gCOSY, NOESY and ROESY NMR studies. Chemical shifts are reported in parts per million (ppm) relative to TMS (0.00 ppm). For electron impact (EI) mass spectra a Finnigan MAT 8400 mass spectrometer was used and for electro-spray ionization (ESI) mass spectra a Micromass Quattro Micro API mass spectrometer was used.

N^α-benzyl-L-histidine(Trt)-O(tBu) (2.5)

The HCl salt of H-His(Trt)-O(tBu) was extracted using 0.1 M Na_2CO_3 aqueous solution and CH_2Cl_2 to give the neutral histidine (1.23 g, 2.71 mmol), which was subsequently

dissolved in 20 mL methanol followed by the addition of 1.05 equivalents of benzaldehyde (287 μ L, 2.85 mmol). This mixture was stirred at room temperature and reaction completion was followed by TLC. Formation of the imine was complete after 2 h, at which point 1.05 equivalents NaBH_4 (108 mg, 2.85 mmol) was added. This was allowed to stir at room temperature for 18 h. The methanol was removed with a rotary evaporator and the resulting oil was extracted from water with CH_2Cl_2 and then washed with de-ionized water (3 x 5 mL). The organic layers were filtered through cotton, and the solvent was removed on a rotary evaporator. This resulted in a 90% yield of **2.5** (1.33 g, 2.44 mmol). HRMS: m/z calculated for $\text{C}_{36}\text{H}_{38}\text{N}_3\text{O}_2$, 544.2964; observed $[\text{M}+\text{H}]^+$ 544.2965. ^1H -NMR Spectrum (400 MHz, CDCl_3 , δ): 7.35 (1H, d, imidazole, $^4J_{\text{H-H}} = 1.4$ Hz), 7.11-7.31 (20H, m, ar) 6.65 (1H, d, imidazole, $^4J_{\text{H-H}} = 1.2$ Hz), 3.83 (1H, d, PhCH_2N , $^2J_{\text{H-H}} = 12.9$ Hz), 3.65 (1H, d, PhCH_2N , $^3J_{\text{H-H}} = 12.9$ Hz), 3.50 (1H, dd, $\text{NCHCO}_2(\text{CH}_3)_3$, $^5J_{\text{H-H}} = 1.4$ Hz, $^2J_{\text{H-H}} = 5.9$ Hz), 2.97 (1H, dd, NHCHCH_2 , $^3J_{\text{H-H}} = 5.7$ Hz, $^2J_{\text{H-H}} = 14.5$ Hz), 2.83 (1H, dd, NHCHCH_2 , $^3J_{\text{H-H}} = 7.2$ Hz, $^2J_{\text{H-H}} = 14.5$ Hz), 1.41 (9H, s, $\text{CO}_2\text{C}(\text{CH}_3)_3$). ^{13}C -NMR Spectrum (100 MHz, CDCl_3 , δ): 173.6 ($\text{CHC}(\text{O})\text{O}$), 142.4 (ar), 140.1 (ar), 138.2 (imidazole), 137.4 (ar), 129.7 (ar), 128.1 (ar), 128.1 (ar), 127.9 (ar), 127.8 (ar), 126.7 (ar), 119.2 (imidazole), 80.6 (NCPH_3), 75.0 ($\text{CO}_2\text{C}(\text{CH}_3)_3$), 61.1 ($\text{NCHCO}_2(\text{CH}_3)_3$), 51.8 (PhCH_2N), 32.2 (NHCHCH_2), 28.0 ($\text{CO}_2\text{C}(\text{CH}_3)_3$).

N^{α} -benzyl-L-histidine (2.6)

Purified **2.5** (1.33 g, 2.44 mmol), was then deprotected in CH_2Cl_2 (6 mL) with trifluoroacetic acid (TFA) (6 mL). Two equivalents of triethylsilane (866 μ L, 5.42 mmol) was added as a scavenger for the trityl protecting group. This was stirred at room temperature for 4 h. The solution was then concentrated on a rotary evaporator and the

trityl by-product was removed by filtration. No further purification was necessary. This resulted in 323 mg (54%) of **2.6**. HRMS: m/z calculated for $C_{13}H_{16}O_2N_3$, 246.1243; observed $[M+H]^+$ 246.1247. 1H -NMR Spectrum (400 MHz, MeOH- d_4 , δ): 8.83 (1H, s, imidazole), 7.43-7.53 (6H, m, ar and imidazole) 4.24-4.35 (3H, m, Ph $\underline{CH_2}N$ and N $\underline{CHCO_2H}$), 3.50 (1H, dd, NHCH $\underline{CH_2}$, $^3J_{H-H} = 5.5$ Hz, $^2J_{H-H} = 15.6$ Hz), 3.42 (1H, dd, NHCH $\underline{CH_2}$, $^3J_{H-H} = 7.8$ Hz, $^2J_{H-H} = 15.6$ Hz). ^{13}C -NMR Spectrum (100 MHz, MeOH- d_4 , δ): 171.1 (CH $\underline{C(O)O}$), 135.3 (ar), 132.5 (imidazole), 131.2 (ar), 130.7 (ar), 130.2 (ar), 119.0 (ar), 111.4 (imidazole), 60.8 (N $\underline{CHCO_2H}$), 51.7 (Ph $\underline{CH_2}N$), 26.3 (NHCH $\underline{CH_2}$).

Rhenium(I) tricarbonyl- N^a -benzyl-L-histidine (**2.1**)

Chelator **2.6** (323 mg, 1.31 mmol) was coordinated with 1.2 equivalents of $[Re(CO)_3(H_2O)_3]OTf$ (15.7 mL of a 0.1 M solution, 1.57 mmol) and 5 equivalents of NaOH (1.31 mL of a 5 M solution, 6.55 mmol) in a solution of methanol (3 mL) and water (6 mL). This solution was stirred at 80°C for 2 h and was then centrifuged in order to separate the precipitated product. The crude solid was washed with water several times followed by centrifugation, resulting in 600 mg (88%) of **2.1**. HRMS: m/z calculated for $NaC_{16}H_{14}O_5N_3^{185/187}Re$, 536.0361/538.0389; observed $[M+Na]^+$ 536.0385/538.0333. 1H -NMR Spectrum of **2.1a** and **2.1b** (denoted by ') (600 MHz, MeOH- d_4 , δ): 8.06 (1H, s, ReN \underline{CHNH}), 8.05 (0.5H, s, ReN \underline{CHNH}'), 7.34-7.47 (5H, m, ar), 7.10 (0.5H, s, ReN \underline{CHNHCH}), 7.00 (1H, s, ReN \underline{CHNHCH}), 6.74 (0.5H, d, Ph $\underline{CH_2NH}$ ', $^3J_{H-H} = 4.4$ Hz), 6.22 (1H, dd, Ph $\underline{CH_2NH}$, $^3J_{H-H} = 3.1$ Hz, $^3J_{H-H} = 10.5$ Hz), 4.62 (1H, dd, Ph $\underline{CH_2}NH$, $^3J_{H-H} = 4.0$ Hz, $^2J_{H-H} = 14.5$ Hz), 4.19 (0.5H, dd, Ph $\underline{CH_2}NH'$, $^3J_{H-H} = 6.6$ Hz, $^2J_{H-H} = 14.1$ Hz), 4.08 (0.5H, dd, Ph $\underline{CH_2}NH'$, $^3J_{H-H} = 7.9$ Hz, $^2J_{H-H} = 14.1$ Hz), 4.03 (1H, dd, Ph $\underline{CH_2}NH$, $^3J_{H-H} = 11.0$ Hz, $^2J_{H-H} = 14.1$ Hz), 3.80 (0.5H, dd, NHCH $\underline{CH_2}$ ', $^3J_{H-H} = 4.4$ Hz,

$^3J_{\text{H-H}} = 7.9$ Hz), 3.72 (1H, dd, NHCHCH_2 , $^3J_{\text{H-H}} = 4.0$ Hz), 3.42 (0.5H, dd, NHCHCH_2 , $^3J_{\text{H-H}} = 4.8$ Hz, $^2J_{\text{H-H}} = 18.5$ Hz), 3.21 (1H, dd, NHCHCH_2 , $^3J_{\text{H-H}} = 3.5$ Hz, $^2J_{\text{H-H}} = 17.1$ Hz), 3.16 (0.5H, dd, NHCHCH_2 , $^3J_{\text{H-H}} = 2.6$ Hz, $^2J_{\text{H-H}} = 18.0$ Hz), 2.96 (1H, dd, NHCHCH_2 , $^3J_{\text{H-H}} = 4.0$ Hz, $^2J_{\text{H-H}} = 17.1$ Hz). $^{13}\text{C-NMR}$ Spectrum of **2.1a** (100 MHz, MeOH-d₄, δ): 184.0 ($\text{CHC}(\text{O})\text{O}$), 141.3 (ar), 137.6 (imidazole), 135.0 (ar), 130.3 (ar), 130.1 (ar), 129.6 (ar), 116.7 (imidazole), 64.1 (NCHCO_2), 58.5 (PhCH_2N), 28.8 (NHCHCH_2).

$^{99\text{m}}$ Tcnetium(I) tricarbonyl- N^{α} -benzyl-L-histidine (2.7)

To an Isolink kit containing sodium tartrate, sodium tetraborate, sodium carbonate, and sodium boranocarbonate, 13.71 mCi (0.5 mL) of [$^{99\text{m}}\text{Tc}$]-pertechnetate was added and the syringe rinsed with 0.5 mL water. This was stirred at 75°C for 30 min, then 0.7 mg of **2.6** was dissolved in 0.5 mL of the solution and stirred at 90°C for 1 h. HPLC analysis showed retention time of 9.8 min and 10.8 min for **2.7** at a linear gradient of 20-40% solvent A in B for 15 min. HPLC analysis of **2.1a** showed retention time of 10.8 min for the same gradient system.

N^{α} -benzyl-L-histidine(Trt)-OMe (2.8)

H-His(Trt)-OMeHCl was neutralized by stirring at room temperature in CH_2Cl_2 along with 1 eq NEt_3 for approximately 20 min. This was then extracted with water and the organic layers were concentrated and dried under vacuum to yield 144 mg of neutralized starting material. The same synthetic procedure was used as with **2.6**; however, a preparative TLC plate was run as a final purification step in a solution of 95% CH_2Cl_2 , 4% MeOH, and 1% NEt_3 . This yielded 47 mg (27%) of **2.8**. ESI+ MS: m/z calculated for

$C_{33}H_{33}N_3O_2$, 503.3; observed $[M+H]^+$ 503.9 1H -NMR Spectrum (400 MHz, $CDCl_3$, δ): 7.31 (1H, s, imidazole), 7.04-7.26 (20H, m, ar), 6.52 (1H, s, imidazole), 3.78 (1H, d, $Ph\text{CH}_2NH$, $^2J_{H-H} = 13.3$ Hz), 3.56-3.62 (5H, m, $Ph\text{CH}_2NH$, $NH\text{CHCO}_2Me$, and CO_2Me), 2.88 (2H, dd, $NHCH\text{CH}_2$, $^3J_{H-H} = 5.9$ Hz).

Rhenium(I) tricarbonyl- N^a -benzyl-L-histidine(Trt) (2.2)

The methyl ester protected **2.8** (47 mg, 0.094 mmol) was dissolved in MeOH (6 mL) and H_2O (3 mL) and added 5 eq (94 μL of a 5 M solution, 0.47 mmol) of NaOH, this was stirred at room temperature for 1 hour. To this solution was added 1.2 eq of $[Re(CO)_3(H_2O)_3]OTf$ (1.13 mL of a 0.1 M solution, 0.11 mmol) and the mixture was stirred at reflux for 2 hours. The solution was then lyophilized to yield a white powder. After dissolving the powder in acetonitrile, the product precipitated out of solution with the addition of water. After centrifugation, the liquid was decanted off and the remaining solid was washed with water, giving 15 mg (21%) of **2.2**. HRMS: m/z calculated for $NaC_{35}H_{28}N_3O_5$ $^{185/187}Re$, 778.1457/780.1485; observed $[M+Na]^+$ 778.1475/780.1521. 1H -NMR Spectrum of isomers of **2.2** (minor isomer denoted by ') (400 MHz, $CDCl_3$, δ): 7.60 (1.5H, s, imidazole and imidazole'), 6.95-7.27 (27H, m, ar), 4.48 (1H, d, $Ph\text{CH}_2NH$, $^2J_{H-H} = 14.1$ Hz), 4.16 (0.4H, d, $Ph\text{CH}_2NH'$, $^2J_{H-H} = 13.3$ Hz), 3.94 (1H, d, $Ph\text{CH}_2NH$, $^2J_{H-H} = 14.1$ Hz), 3.84 (0.4H, d, $Ph\text{CH}_2NH'$, $^2J_{H-H} = 13.3$ Hz), 3.69 (1.3H, m, $NH\text{CHC}(O)$), 3.32 (0.4H, dd, $NHCH\text{CH}_2$, $^3J_{H-H} = 3.5$ Hz, $^2J_{H-H} = 18.0$ Hz), 3.16 (1H, dd, $NHCH\text{CH}_2$, $^3J_{H-H} = 3.9$ Hz, $^2J_{H-H} = 18.4$ Hz), 3.02 (0.4H, dd, $NHCH\text{CH}_2'$, $^3J_{H-H} = 3.9$ Hz, $^2J_{H-H} = 10.6$ Hz), 2.60 (1H, dd, $NHCH\text{CH}_2$, $^3J_{H-H} = 3.9$ Hz, $^2J_{H-H} = 18.0$ Hz)

N^α-benzyl(methyl)-L-histidine(Trt)-O(tBu) (2.9)

The HCl salt of H-His(Trt)-O(tBu) was extracted using 0.1 M Na₂CO₃ aqueous solution and CH₂Cl₂ to give the neutral histidine. The neutral histidine (935 mg, 2.06 mmol) was dissolved in 20 mL methanol to which 1.05 equivalents of benzaldehyde (219 μL, 2.17 mmol) was added. This was stirred at room temperature and the reaction progress was followed by TLC. The reaction was complete after 2 h, at which point 1.05 equivalents NaBH₄ (82 mg, 2.17 mmol) was added. This was allowed to stir at room temperature for 18 h followed by the addition of one equivalent of powder paraformaldehyde (185 mg, 2.06 mmol). Upon complete dissolution (approximately 18 h), 1.05 equivalents of NaBH₄ (82 mg, 2.17 mmol) was added. After allowing to react overnight, the solution was concentrated with a rotary evaporator and the resulting oil was extracted from water with CH₂Cl₂ and then washed with de-ionized water (3 x 5 mL). The organic layers were filtered through cotton, and concentrated on a rotary evaporator. The resulting product was purified using flash column chromatography with an eluent of 98:1:1 CH₂Cl₂:MeOH:NEt₃, resulting in a 67% yield of **2.9** (772 mg, 1.38 mmol). HRMS: m/z calculated for C₃₇H₃₉N₃O₂, 557.3042; observed [M+H]⁺ 557.3032. ¹H-NMR Spectrum (400 MHz, CHCl₃, δ): 7.15-7.40 (21H, m, imidazole and ar), 6.67 (1H, d, imidazole, ⁵J_{H-H} = 1.2 Hz), 3.81 (1H, d, PhCH₂N, ²J_{H-H} = 13.7 Hz), 3.71 (1H, d, N(CH₃)CHCO₂(CH₃)₃, ²J_{H-H} = 7.2 Hz), 3.67 (1H, d, PhCH₂N, ³J_{H-H} = 13.7 Hz), 3.09 (1H, dd, N(CH₃)CHCH₂, ³J_{H-H} = 8.0 Hz, ²J_{H-H} = 14.7 Hz), 2.93 (1H, dd, N(CH₃)CHCH₂, ³J_{H-H} = 7.0 Hz, ²J_{H-H} = 14.7 Hz), 2.28 (3H, s, CH₂N(CH₃)CH), 1.47 (9H, s, CO₂C(CH₃)₃).

N^α-benzyl(methyl)-L-histidine (2.10)

Chelator **2.9** (772 mg, 1.38 mmol) was then deprotected with CH₂Cl₂ (6 mL) and TFA (6 mL). Two equivalents of triethylsilane (446 μL, 2.76 mmol) were added as a scavenger for the trityl group. After stirring for 4 hours at room temperature, the solution was concentrated on a rotary evaporator, at which point the oil was dissolved in acetonitrile. With the addition of water the trityl by-product precipitated out of solution and was filtered off and the filtrate was lyophilized to give the final product. No further purification was necessary. This resulted in 272 mg (76%) of **2.10**. HRMS: m/z calculated for C₁₄H₁₇N₃O₂, 259.1321; observed [M+H]⁺ 259.1329. ¹H-NMR Spectrum (400 MHz, MeOH-d₄, δ): 8.85 (1H, s, imidazole), 7.07-7.55 (6H, m, NCH₂Ph and imidazole), 4.52 (1H, d, NCH₂Ph, ²J_{H-H} = 12.7 Hz), 4.40 (2H, m, NCH₂Ph and NCHCO₂H), 3.61 (1H, dd, NCHCH₂, ³J_{H-H} = 3.7 Hz, ²J_{H-H} = 14.9 Hz), 3.51 (1H, dd, NCHCH₂, ³J_{H-H} = 9.8 Hz, ²J_{H-H} = 14.9 Hz), 2.92 (3H, s, PhCH₂N(CH₃)).

Rhenium(I) tricarbonyl-N^α-benzyl(methyl)-L-histidine (2.3)

The histidine chelator **2.10** (272 mg, 1.05 mmol) was coordinated with 1.2 equivalents of [Re(CO)₃(H₂O)₃]OTf (12.6 mL of a 0.1 M solution, 1.26 mmol) and 5 equivalents of NaOH (1.05 mL of a 5 M solution, 5.25 mmol) in a solution of methanol (3 mL) and water (6 mL). This was stirred at 80°C for 2 h. The coordinated product precipitated and was collected by centrifugation and washed with water. This resulted in 342 mg (62%) of **2.3**. HRMS: m/z calculated for NaC₁₇H₁₆O₅N₃^{185/187}Re, 550.0518/552.0546; observed [M+Na]⁺ 550.0524/552.0539. ¹H-NMR Spectrum of isomers of **2.3** (minor isomer denoted by ') (400 MHz, MeOH-d₄, δ): 8.14 (0.2H, s, imidazole'), 8.11 (1H, s, imidazole), 7.39-7.50 (5H, m, ar), 7.18 (0.2H, s, imidazole'), 7.05 (1H, s, imidazole),

4.78 (1H, d, PhCH₂N(Me), ²J_{H-H} = 13.5 Hz), 4.43 (1H, d, PhCH₂N(Me), ²J_{H-H} = 13.5 Hz), 4.38 (0.2H, d, PhCH₂N(Me)', ²J_{H-H} = 7.0 Hz), 3.94 (0.2H, dd, N(Me)CHCH₂', ³J_{H-H} = 4.9 Hz, ²J_{H-H} = 15.6 Hz), 3.79 (1H, dd, N(Me)CHCH₂, ³J_{H-H} = 3.3 Hz, ³J_{H-H} = 4.9 Hz), 3.38 (0.2H, dd, N(Me)CHCH₂', ³J_{H-H} = 4.7 Hz, ²J_{H-H} = 18.6 Hz), 3.18 (1H, dd, N(Me)CHCH₂, ³J_{H-H} = 3.1 Hz, ²J_{H-H} = 18.8 Hz), 3.07 (1H, dd, N(Me)CHCH₂, ³J_{H-H} = 4.8 Hz, ²J_{H-H} = 18.6 Hz), 2.85 (3H, s, N(Me)CHCH₂). ¹³C-NMR Spectrum (100 MHz, MeOH-d₄, δ): 183.7 (CHC(O)O), 141.5 (ar), 133.9 (imidazole), 133.5 (ar), 132.0 (ar), 130.4 (ar), 129.7 (ar), 116.6 (imidazole), 73.1 (NCHCO₂), 63.3 (PhCH₂N), 45.7 (PhCH₂N(CH₃)), 26.1 (NHCHCH₂).

N-iodocarbonyl-O-methyl phenylalanine (**2.11**)

H-Phe-OMe·HCl (520 mg, 2.41 mmol) was neutralized by stirring in CH₂Cl₂ with 1 equivalent of triethylamine (336 μL, 2.41 mmol) at room temperature for approximately 30 min. 1.1 eq of bromoacetic acid (37 mg, 2.65 mmol) was then pre-activated with 1.1 eq of EDC (411 mg, 2.65 mmol) in CH₂Cl₂ for approximately 5 min. This solution was added to the reaction mixture and allowed to stir at room temperature overnight. The crude solution was concentrated on a rotary evaporator. This was then purified using flash column chromatography using an eluent system of 99% CH₂Cl₂ and 1% MeOH. The column yielded 330 mg of crude **2.11**. This was dissolved in acetone and 1.1 eq of NaI (213 mg, 1.41 mmol) was added. The solution was refluxed overnight. The solid NaCl could then be filtered off, and the resulting filtrate concentrated on a rotary evaporator and dried under high vacuum, to yield 236 mg (0.68 mmol, 53%) of **2.11**. HRMS: m/z calculated for C₁₂H₁₄INO₃, 347.0018; observed [M+H]⁺, 347.0022. ¹H-NMR Spectrum (400 MHz, MeOH-d₄, δ): 7.20-7.29 (5H, m, CHCH₂Ph), 4.63 (1H, dd,

PhCH₂CH, ³J_{H-H} = 5.5 Hz, ³J_{H-H} = 8.6 Hz), 3.69 (5H, m, OCH₃ and C(O)CH₂I), 3.14 (1H, dd, PhCH₂CH, ³J_{H-H} = 5.5 Hz, ²J_{H-H} = 14.1 Hz), 2.97 (1H, dd, PhCH₂CH, ³J_{H-H} = 8.6 Hz, ²J_{H-H} = 14.1 Hz).

N^α-histidinyl-acetyl-phenylalanine (2.12)

From the previous step, **2.11** (236 mg, 0.68 mmol) was used without further purification. To this, 1.1 eq of neutralized H-His(Trt)-O(tBu) (341 mg, 0.75 mmol) was added in CH₂Cl₂ and refluxed for 48 h. The solution was then concentrated on a rotary evaporator and dried on high vacuum, which yielded 529 mg of the crude protected **2.12**. The crude material was then purified by flash column chromatography using an eluent system of 92% CH₂Cl₂, 7% MeOH and 1% NEt₃. This yielded 250 mg (0.37 mmol, 55%) of pure trityl protected **2.12**. The trityl containing **2.12** (220 mg, 0.33 mmol) was then deprotected using a 50:50 mixture of CH₂Cl₂ and TFA and 1 eq (52.2 μL, 0.33 mmol) of triethylsilane. This was stirred at room temperature for approximately 4 h, at which point it could be concentrated on a rotary evaporator by azeotropeing with excess CH₂Cl₂. It was dried on high vacuum to yield 19 mg (0.05 mmol, 15%) of **2.12**. HRMS: m/z calculated for C₁₈H₂₃N₄O₅, 375.1668; observed [M+H]⁺ 375.1671. ¹H-NMR Spectrum (400 MHz, MeOH-d₄, δ): 8.84 (1H, s, imidazole), 7.42 (1H, s, imidazole), 7.18-7.29 (5H, m, ar), 4.76 (1H, dd, NCHCO₂H, ³J_{H-H} = 5.1 Hz, ³J_{H-H} = 8.6 Hz), 4.05 (1H, dd, PhCH₂CH, ³J_{H-H} = 5.9 Hz), 3.92 (1H, d, PhCH₂CH, ²J_{H-H} = 16.0 Hz), 3.80 (1H, d, PhCH₂CH, ²J_{H-H} = 16.0 Hz), 3.70 (3H, s, MeOC(O)), 3.35 (2H, d, C(O)CH₂NH, ²J_{H-H} = 6.3 Hz), 3.18 (1H, dd, CO₂HCHCH₂, ³J_{H-H} = 5.1 Hz, ²J_{H-H} = 13.7 Hz), 2.98 (1H, dd, CO₂HCHCH₂, ³J_{H-H} = 8.6 Hz, ²J_{H-H} = 13.7 Hz).

Rhenium(I) tricarbonyl-N^α-histidinyl-acetyl-phenylalanine (2.4)

The purified **2.12** (19 mg, 0.05 mmol) was coordinated with 1.2 equivalents of [Re(CO)₃(H₂O)₃]OTf (600 μL of a 0.1 M solution, 0.06 mmol) and 5 equivalents of NaHCO₃ (21 mg, 0.25 mmol) in a mixture of methanol (3 mL) and water (6 mL). This was stirred at 80°C for 2 h. The precipitate was collected by centrifugation and washed with water. This resulted in 26 mg (82%) of **2.4**. HRMS: m/z calculated for C₂₁H₂₂N₄O₈^{185/187}Re, 643.0968/645.0995; observed [M+H]⁺ 643.1015/645.0984. ¹H-NMR Spectrum (600 MHz, DMF-d₇, δ): 8.82 (1H, d, MeOC(O)CHNH, ³J_{H-H} = 8.2 Hz), 8.27 (1H, t, imidazole, ⁴J_{H-H} = 1.2 Hz), 7.24-7.35 (5H, m, ar), 7.21 (1H, d, imidazole, ⁴J_{H-H} = 1.2 Hz), 6.23 (1H, dd, C(O)CH₂NHRe, ³J_{H-H} = 2.9 Hz, ³J_{H-H} = 10.5 Hz), 4.74 (1H, m, MeOC(O)CHNH), 4.01 (1H, dd, C(O)CH₂NHRe, ³J_{H-H} = 3.5 Hz, ²J_{H-H} = 15.8 Hz), 3.86 (1H, dd, C(O)CH₂NHRe, ³J_{H-H} = 10.5 Hz, ²J_{H-H} = 15.8 Hz), 3.69 (3H, s, MeOC(O)), 3.49 (1H, t, NHCH(O)CH₂, ³J_{H-H} = 4.1 Hz), 3.23 (2H, d, NHCH(O)CH₂, ³J_{H-H} = 2.3 Hz), 3.16 (1H, dd, PhCH₂CH, ³J_{H-H} = 5.9 Hz, ²J_{H-H} = 14.1 Hz), 3.01 (1H, dd, PhCH₂CH, ³J_{H-H} = 9.4 Hz, ²J_{H-H} = 14.1 Hz).

2.5 References

1. S. Liu and S. Chakraborty, *Dalton Trans.*, 2011, 40, 6077-6086.
2. D. R. van Staveren, S. Mundwiler, U. Hoffmanns, J. K. Pak, B. Spingler, N. Metzler-Nolte and R. Alberto, *Org. Biomol. Chem.*, 2004, 2, 2593-2603.
3. L. G. Luyt, H. A. Jenkins and D. H. Hunter, *Bioconjug. Chem.*, 1999, 10, 470-479.
4. D. H. Hunter and L. G. Luyt, *Bioconjug. Chem.*, 2000, 11, 175-181.
5. D. H. Hunter and L. G. Luyt, *J. Label. Compd. Radiopharm.*, 2000, 43, 403-412.
6. R. Schibli and A. Schubiger, *Eur. J. Nucl. Med.*, 2002, 29, 1529-1542.

7. A. G. Jones, M. J. Abrams, A. Davison, J. W. Brodack, A. K. Toothaker, S. J. Adelstein and A. I. Kassis, *Int. J. Nucl. Med. Biol.*, 1984, 11, 225-234.
8. R. Alberto, R. Schibli, P. A. Schubiger, U. Abram and T. A. Kaden, *Polyhedron*, 1996, 15, 1079-1089.
9. R. Alberto, R. Schibli, D. Angst, P. A. Schubiger, U. Abram, S. Abram and T. A. Kaden, *Transition Met. Chem. (London)*, 1997, 22, 597-601.
10. R. Alberto, R. Schibli, A. Egli, F. F. Knapp and P. A. Schubiger, *Radiochim. Acta*, 1997, 79, 99-103.
11. R. Schibli, R. Alberto, U. Abram, S. Abram, A. Egli, P. A. Schubiger and T. A. Kaden, *Inorg. Chem.*, 1998, 37, 3509-3516.
12. U. Abram, S. Abram, R. Schibli, R. Alberto and J. R. Dilworth, *Polyhedron*, 1998, 17, 1303-1309.
13. D. Rosita, M. A. DeWit and L. G. Luyt, *J. Med. Chem.*, 2009, 52, 2196-2203.
14. R. Alberto, *Top. Curr. Chem*, 2005, 252, 1-44.
15. V. Maes and D. Tourwé, *Int. J. Peptide Res. Therapeut.*, 2006, 12, 197-202.
16. V. Maes, E. Garcia-Garayoa, P. Bläuenstein and D. Tourwé, *J. Med. Chem.*, 2006, 49, 1833-1836.
17. R. Schibli, R. La Bella, R. Alberto, E. Garcia-Garayoa, K. Ortner, U. Abram and P. A. Schubiger, *Bioconjug. Chem.*, 2000, 11, 345-351.
18. A. Egli, R. Alberto, L. Tannahill, R. Schibli, U. Abram, A. Schaffland, R. Waibel, D. Tourwe, L. Jeannin, K. Iterbeke and P. A. Schubiger, *J. Nucl. Med.*, 1999, 40, 1913-1917.
19. J. K. Pak, P. Benny, B. Spingler, K. Ortner and R. Alberto, *Chem.--Eur. J.*, 2003, 9, 2053-2061.
20. C. Schweinsberg, V. Maes, L. Brans, P. Bläuenstein, D. A. Tourwé, P. A. Schubiger, R. Schibli and E. G. Garayoa, *Bioconjug. Chem.*, 2008, 19, 2432-2439.
21. X. Chen, R. Park, A. H. Shahinian, J. R. Bading and P. S. Conti, *Nucl. Med. Biol.*, 2004, 31, 11-19.
22. M. Lipowska, R. Cini, G. Tamasi, X. Xu, A. T. Taylor and L. G. Marzilli, *Inorg. Chem.*, 2004, 43, 7774-7783.
23. A. M. Christoforou, P. A. Marzilli, F. R. Fronczek and L. G. Marzilli, *Inorg. Chem.*, 2007, 46, 11173-11182.

24. T. Perera, P. A. Marzilli, F. R. Fronczek and L. G. Marzilli, *Inorg. Chem.*, 2010, 49, 2123-2131.
25. *Chirality*, 1992, 4, 338-340.
26. T. L. Mindt, C. Müller, M. Melis, M. de Jong and R. Schibli, *Bioconjug. Chem.*, 2008, 19, 1689-1695.
27. T. L. Mindt, H. Struthers, L. Brans, T. Anguelov, C. Schweinsberg, V. Maes, D. Tourwé and R. Schibli, *J. Am. Chem. Soc.*, 2006, 128, 15096-15097.
28. K. N. White and J. P. Konopelski, *Org. Lett.*, 2005, 7, 4111-4112.
29. S. P. Schmidt, J. Nitschke, W. C. Trogler, S. I. Hockett and R. J. Angelici, *Inorg. Synth.*, 1989, 26, 113-117.
30. R. Alberto, K. Ortner, N. Wheatley, R. Schibli and A. P. Schubiger, *J. Am. Chem. Soc.*, 2001, 123, 3135-3136.
31. H. N. Hoang, G. K. Bryant, M. J. Kelso, R. L. Beyer, T. G. Appleton and D. P. Fairlie, *Inorg. Chem.*, 2008, 47, 9439-9449.
32. M. T. Ma, H. N. Hoang, C. C. G. Scully, T. G. Appleton and D. P. Fairlie, *J. Am. Chem. Soc.*, 2009, 131, 4505-4512.
33. R. Waibel, R. Alberto, J. Willuda, R. Finnern, R. Schibli, A. Stichelberger, A. Egli, U. Abram, J.-P. Mach, A. Plückthun and P. A. Schubiger, *Nat. Biotech.*, 1999, 17, 897-901.
34. J. Willuda, A. Honegger, R. Waibel, P. A. Schubiger, R. Stahel, U. Zangemeister-Wittke and A. Plückthun, *Cancer Res.*, 1999, 59, 5758-5767.
35. J. Willuda, S. Kubetzko, R. Waibel, P. A. Schubiger, U. Zangemeister-Wittke and A. Plückthun, *J. Biol. Chem.*, 2001, 276, 14385-14392.
36. R. Tavaré, J. Williams, K. Howland, P. J. Blower and G. E. D. Mullen, *J. Inorg. Biochem.*, 2012, 114, 24-27.
37. A. Badar, J. Williams, R. de Rosales, R. Tavaré, F. Kampmeier, P. Blower and G. Mullen, *EJNMMI Research*, 2014, 4, 14.
38. R. Tavaré, R. Torres Martin De Rosales, P. J. Blower and G. E. D. Mullen, *Bioconjug. Chem.*, 2009, 20, 2071-2081.
39. Y. Yang, T. Neef, C. Mittelholzer, E. Garcia Garayoa, P. Blauenstein, R. Schibli, U. Aebi and P. Burkhard, *J. Nanobiotechnol.*, 2013, 11, 36.

Chapter 3

3 Click to Cyclize and Chelate

3.1 Introduction

Novel molecular imaging probes for use in the non-invasive diagnosis of many diseases have become essential tools in diagnostic nuclear medicine. Numerous radionuclides possess suitable characteristics for imaging purposes, the choice of which depends not only on the desired imaging modality, biomolecule used and need for quantitation, but also on the cost and availability. Technetium-99m not only has ideal decay characteristics for SPECT (single photon emission computed tomography) imaging ($T_{1/2} = 6\text{h}$, 140 keV γ -radiation), it can also be obtained from an on-site generator, making it both cost effective and readily available.¹ As such, it is currently incorporated in more than 80% of radiopharmaceuticals, making it the most common radionuclide used in diagnostic nuclear medicine.²

Technetium-99m in the +1 oxidation state was discovered in 1984³ and began being used for development of radiopharmaceuticals in 1996.⁴⁻⁸ This oxidation state became even more popular with the discovery of the commercially available Isolink kit,^{9,10} making the synthesis of the $[\text{}^{99\text{m}}\text{Tc}(\text{CO})_3(\text{H}_2\text{O})_3]^+$ precursor straightforward with quantitative yields and excellent radiochemical purity. These metal complexes prefer an octahedral coordination which protects them from ligand attack, giving them a high *in vivo* stability.^{1,11} The facial geometry of the carbonyls allow for easy substitution of the trans water molecules with the tridentate chelator. Tridentate chelation systems are ideal as they tend to form more stable complexes with faster reaction times when compared to

bidentate chelators.¹ The technetium tricarbonyl core is also very small and lipophilic, allowing it to be easily incorporated into the ligand structure.^{11, 12}

Rhenium and technetium-99m tricarbonyl can be incorporated into biologically relevant peptides through the use of a bifunctional chelator. As the name suggests, this chelator is able to chelate the metal while still maintaining a point of attachment to the biomolecule. One such bifunctional chelator is histidine, which can coordinate $[^{99m}\text{Tc/Re}(\text{CO})_3]^+$ through the imidazole-N1.^{13, 14} However, in order to make histidine a tridentate bifunctional chelator, it must be functionalized at either the imidazole-N3 or the alpha amine. As such, these chelators involve multistep syntheses requiring protecting groups and purification steps.¹⁵

Copper-catalyzed azide-alkyne cycloaddition (CuAAC) reactions, more commonly referred to as “click chemistry”, have received much attention since their discovery in 2001.^{16, 17} This reaction uses a copper(I) catalyst to form a 1,4-disubstituted 1,2,3-triazole from a terminal azide and a terminal alkyne. These reactions have many applications including bioconjugation, dendrimer synthesis, combinatorial drug discovery, and of particular interest in this chapter, peptidomimetics.¹⁸

In 2006, the group of Roger Schibli introduced the concept of “click-to-chelate”.¹⁹ They discovered that the triazole formed from the click reaction has very similar chelation properties to histidine functionalized at the imidazole-N3 and could therefore be substituted in a ligand system while still maintaining the $[^{99m}\text{Tc/Re}(\text{CO})_3]^+$ chelation. Click-to-chelate reactions proceed in a single step without the need for protecting groups or purification of intermediates, making it a much easier method to form a bifunctional

chelator. The presence of the opposing clickable entity on the peptide of interest allows for this reaction to simultaneously form a chelation site for Re/Tc tricarbonyl as a result of triazole formation, and to also form a stable attachment of the chelator to the peptide through the click reaction.¹⁹⁻²²

Bifunctional chelators attach the metal complex to the biomolecule in a pendant fashion. The addition of pendant metal complex moieties to targeting peptides has been shown to reduce binding affinities, increase clearance time and receptor promiscuity which generally results in lower signal-to-noise ratios and poorer image resolution and quality.^{23, 24} Another method to incorporate a radionuclide into a biomolecule is through an integrated approach. This method involves incorporating the radiometal into the peptide backbone, thus “hiding” the metal in the biologically active region of the peptide. This maintains the binding affinity of the peptide prior to coordination.²⁵ One such arrangement involves incorporation of the chelation site, and thus the metal, into the backbone of a peptide. Linear peptides, however, are inherently flexible and do not always have the proper conformation for interaction with receptors. Cyclic peptides, on the other hand, offer the advantage of locking the peptide structure in a more rigid conformation, which promotes and maintains the proper geometry for binding. Metal complexes incorporated into the backbones of cyclic peptides not only decrease the molecular weight of the compound due to the lack of a bulky chelator attached in a pendant fashion, but could also help constrain the peptide, increasing the target affinity.

In general, cyclic peptides are difficult to synthesize; synthesis typically involves high dilutions and results in very low yields.²⁶ One method to cyclize peptides is via peptide bond formation. However, if the peptide is small, the ring strain of the transition state can

occasionally be too high to overcome and the cyclization fails. In 2006 Bock et al. used the CuAAC reaction to cyclize a tetrapeptide tyrosinase inhibitor.²⁷ Previous attempts to cyclize the peptide using standard peptide coupling conditions were unsuccessful. The 1,4-disubstituted 1,2,3-triazole formed by the CuAAC reaction has been found to be a peptide bond mimic, having similar size, planarity, hydrogen bonding capabilities and dipole moment.^{27, 28} Therefore, the peptide was modified with an alkyne at the C-terminus and an azide at the N-terminus and successful cyclization through triazole formation using the CuAAC reaction was reported. Therefore, the CuAAC reaction appears to be an effective method of forming similar small cyclic peptides.

This chapter describes progress towards using CuAAC to create a metal chelation site as a result of peptide cyclization in order to facilitate incorporation of $[^{99m}\text{Tc}/\text{Re}(\text{CO})_3]^+$ within the peptide, while at the same time locking the conformation of the peptidomimetic. In order for this cyclization to occur, an azide modified amino acid and alkyne modified amino acid must be placed at both the C-terminus and N-terminus of the peptide sequence. These two functionalities can then be reacted to form a triazole while simultaneously cyclizing the peptide. This triazole can then act as part of a chelation site by coordinating to the metal through the N3 atom. Although this cycloaddition reaction has been previously reported to both cyclize a peptide as well as form a chelation site for $[^{99m}\text{Tc}/\text{Re}(\text{CO})_3]^+$, this will be the first example of both of these operations being done simultaneously in order to incorporate a metal within the peptide structure, allowing for a new method for integrating rhenium and technetium-99m tricarbonyl into a peptide structure.

3.2 Results & Discussion

3.2.1 Clickable Peptide Design

The design of "click-to-chelate" cyclic peptides requires many considerations. First, the peptide needs an alkyne at one terminus of the peptide and an azide at the other so that peptide cyclization occurs upon formation of the triazole. Second, since this triazole is to be used to coordinate the metal, two other metal chelating moieties must be designed into the peptide structure such that, following cyclization, they are both within suitable accessible geometries to participate in tridentate chelation of the metal with the triazole, as a tridentate chelator is preferred for both technetium-99m and rhenium tricarbonyl coordination. Though there are many possible N and O metal coordinating functional groups, these geometric restrictions severely limit the number of suitable functional groups available for proper design. An example of a suitable N-based donating group is an amine, either terminal or part of the peptide chain; and an example of an O-based donor is the carboxylic acid from the C-terminus of the peptide. The third chelating group could be added to the peptide prior to, or following cyclization; such as another carboxylic acid or pyridine functionality. The following sections will describe the design and synthesis of three different clickable peptide systems, which can be seen in Figure 3.1, and their chelators.

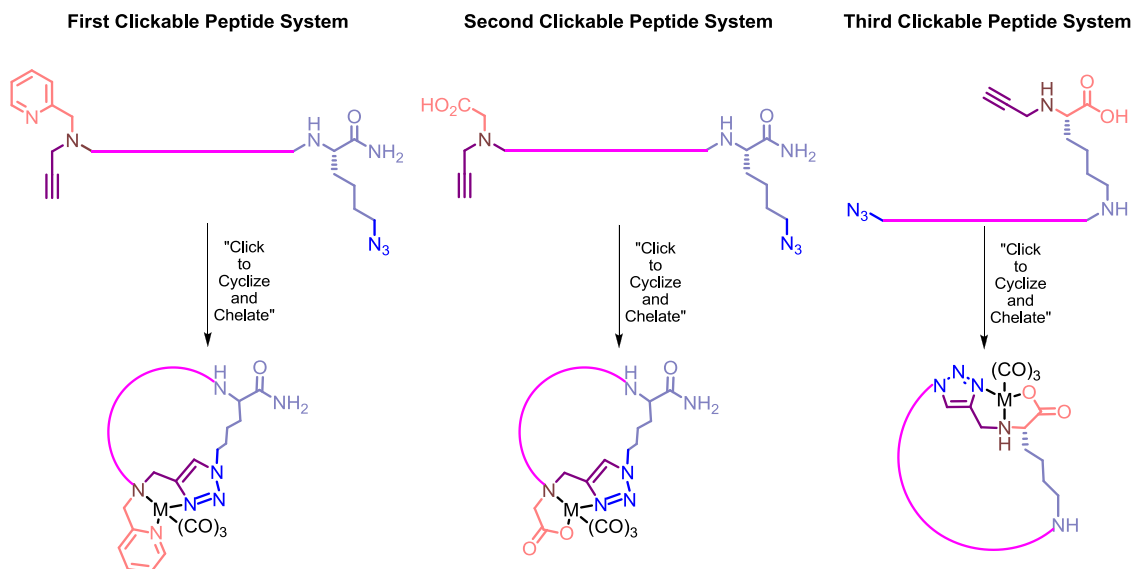
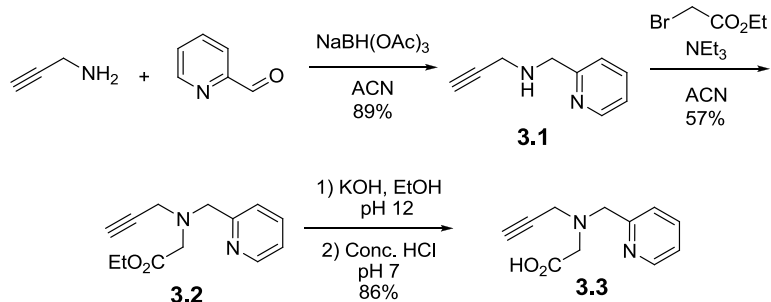


Figure 3.1: Design of the three different clickable peptide systems described in this chapter, where $M = \text{Re}$ or $^{99\text{m}}\text{Tc}$

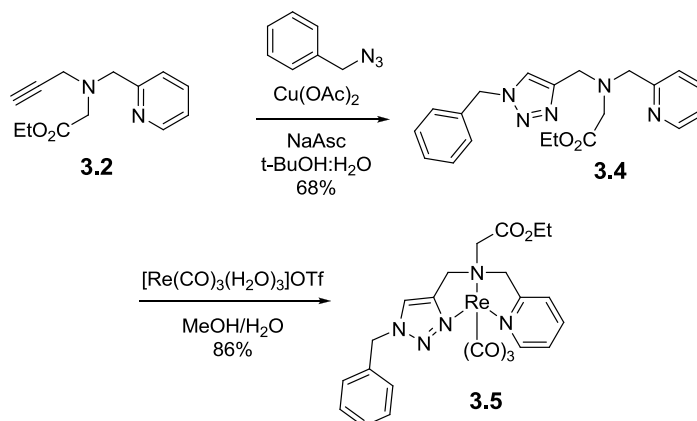
3.2.2 First Clickable Peptide System

In order to create a chelation site upon cyclization, the first "click-to-chelate" cyclic peptide design was based on a novel synthetic amino acid containing an alkyne and another coordinating group attached to the N-terminus of the peptide. The alkyne amino acid chosen for the first peptide system was one that contained a pyridine group. This synthetic amino acid was synthesized by reductive amination of propargylamine and 2-pyridinecarboxaldehyde, followed by addition of ethyl bromoacetate to the secondary amine. The ethyl ester was then deprotected with KOH to give the desired alkyne functionalized amino acid **3.3**, which could be added to the N-terminus of the clickable peptide (Scheme 3.1).



Scheme 3.1: Synthesis of clickable chelator **3.3** for first clickable peptide system

In order to determine if the chosen chelator would coordinate $[\text{Re}(\text{CO})_3]^+$, a model chelation system was synthesized by clicking the protected alkyne **3.2** with benzyl azide to form the triazole as the third coordination site (Scheme 3.2). This was then coordinated with $[\text{Re}(\text{CO})_3(\text{H}_2\text{O})_3]\text{OTf}$ that was synthesized by literature procedure.^{29, 30}



Scheme 3.2: Synthesis of model chelator **3.5** for first clickable peptide system

This chelation system has recently been synthesized in the literature by a different synthetic approach with a free carboxylic acid.³¹ When coordinated with $[\text{Re}(\text{CO})_3]^+$ there is a pH dependence for whether the carboxylic acid or the triazole are coordinated to the metal. If the $\text{pH} > 9$, the carboxylic acid is coordinated, and if the $\text{pH} < 4$, the triazole is coordinated. However, the carboxylic acid in **3.5** was protected with an ethyl ester so that

it could not coordinate to the metal. In the first attempt to synthesize **3.5**, NaHCO₃ was used as a base, however this caused deprotection of the ethyl ester, therefore creating the potential for the carboxylic acid to coordinate instead of the triazole. In this case, two products were seen by LC-MS analysis with the deprotected coordinated mass and rhenium isotopic signature, demonstrating that the coordination in **3.5** was occurring by both chelation methods. Since this system will be attached to the cyclic peptide through formation of a peptide bond between the deprotected carboxylic acid and the amine of the N-terminal amino acid, prior to both the click and coordination reactions, this pH dependence of coordination should not be an issue.

When **3.5** was synthesized in the absence of base only one peak was observed by LC-MS analysis which showed the coordinated mass and rhenium-185/187 signature of the protected ester. Further evidence of successful rhenium coordination was obtained using NMR spectroscopy. Comparing the methylene regions of the ¹H NMR spectra of the clicked chelators prior to (**3.4**) and following (**3.5**) rhenium coordination, a shift in all the peaks other than those of the ethyl ester was observed, as well as a change in the proton coupling pattern (Figure 3.2). These data, combined with the desired mass and rhenium isotopic signature, demonstrated that the chelator was coordinated with [Re(CO)₃]⁺. Successful chelation of rhenium by the small molecule design indicated that this particular chelation system was able to coordinate [Re(CO)₃]⁺ and thus could be used in the clickable peptide.

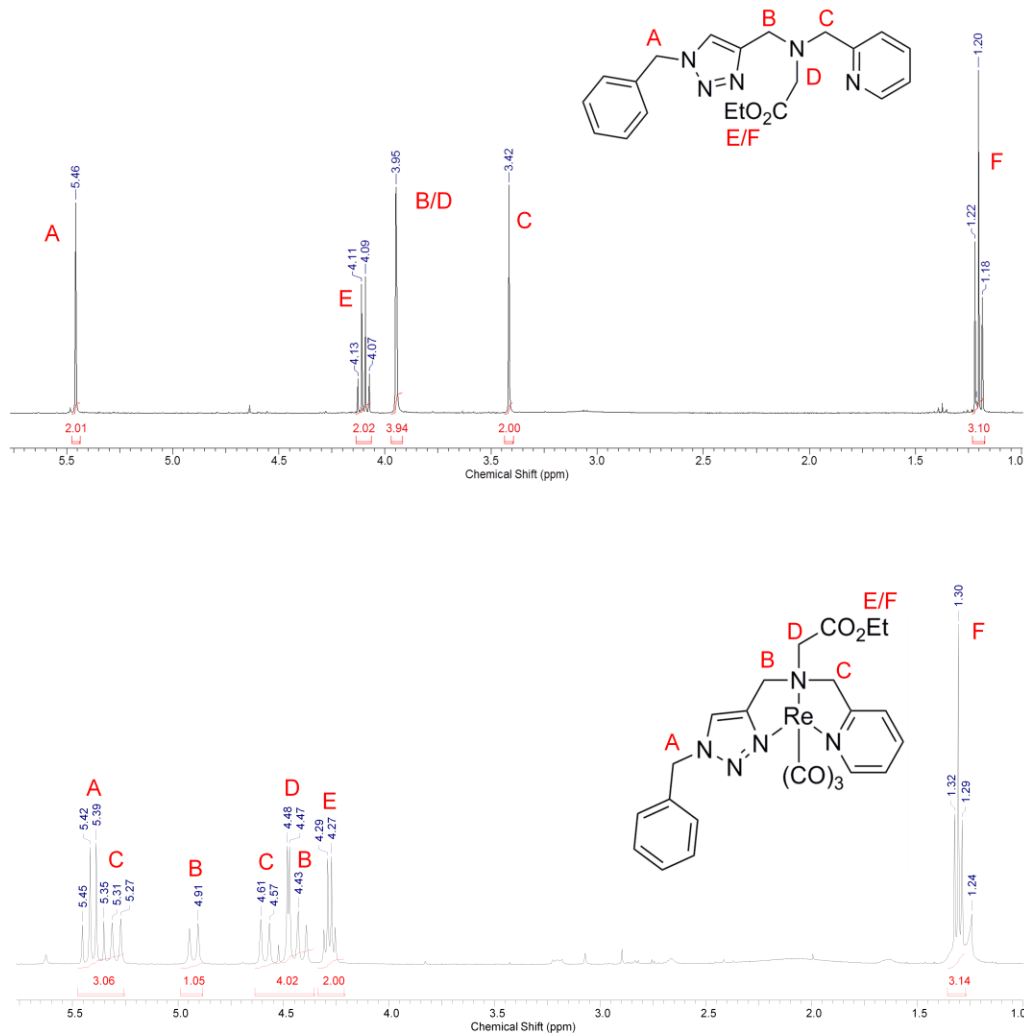
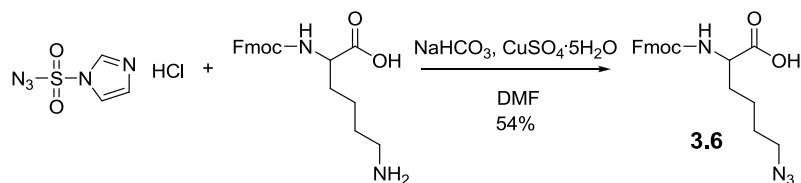


Figure 3.2: Methylene region of the ¹H NMR spectra for **3.4** and **3.5** showing the shift in peaks and change in coupling pattern indicating rhenium coordination

An azide modified amino acid also needed to be synthesized in order to add the azide functionality to the C-terminus of the peptide. The best choice of amino acid to do this is lysine, where the amine on the side-chain can be easily converted to an azide (Scheme 3.3). Azidation of the free side chain amine was accomplished using a diazotransfer reagent, imidazole-1-sulfonyl azide, that was first synthesized by a known literature procedure.³² A diazotransfer reaction could then take place with Fmoc-Lys-OH to substitute the side chain amine for an azide.

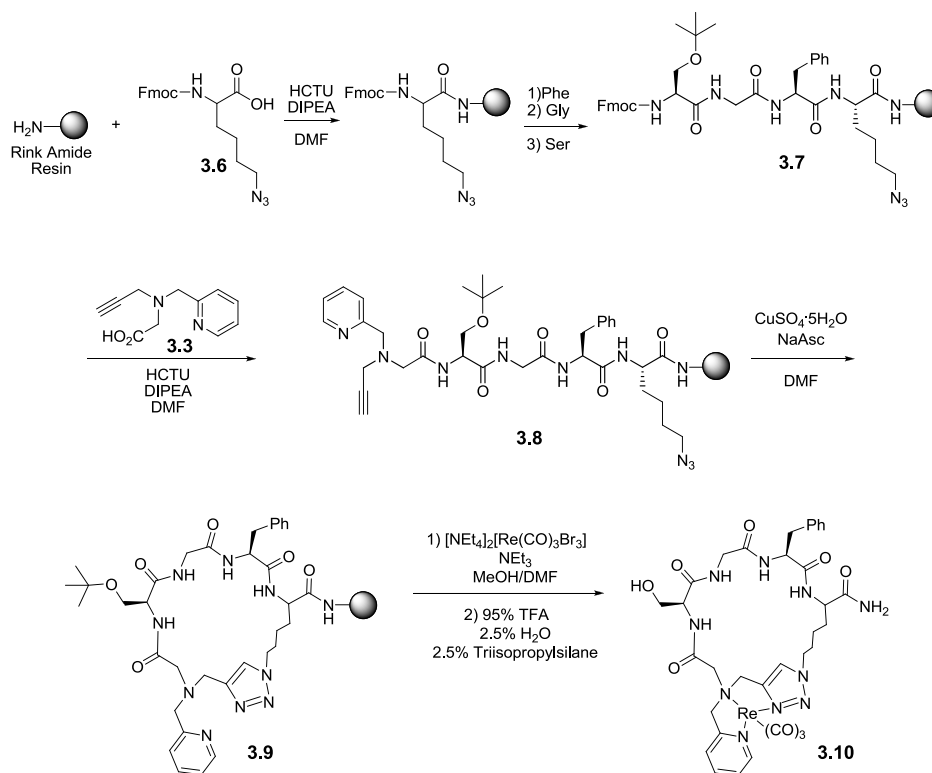


Scheme 3.3: Synthesis of azide functionalized lysine **3.6**

A clickable peptide was then synthesized through standard Fmoc solid-phase peptide synthesis using rink amide MBHA (4-methylbenzhydrylamine) resin to give an amide at the N-terminus. The azide functionality was added at the C-terminus through addition of the lysine azide **3.6**. The peptide was extended by adding phenylalanine, glycine and t-butyl protected serine. Finally the alkyne functionality was added through coupling of previously synthesized alkyne amino acid **3.3**. This was then clicked on resin in order to cyclize the peptide, creating a chelation sphere identical to that of the model chelator **3.5**. Addition of the rhenium core was performed using $[\text{NEt}_4]_2[\text{Re}(\text{CO})_3\text{Br}_3]$,³³ as coordination was to be completed on resin to give the final cyclized coordinated peptide **3.10** (Scheme 3.4).

A small amount of the peptide was cleaved from the resin and analyzed by LC-MS after each step of the reaction. When peptide **3.7** was cleaved from resin it showed a single peak by LC-MS as well as the desired mass. Once alkyne **3.3** was added to the chain to give peptide **3.8**, and the peptide cleaved from the resin, there was a single peak and a shift in retention time by HPLC; however, no peaks corresponding to the expected mass were observed. This lack of signal corresponding to the correct peptide masses continued after the click reaction to give peptide **3.9**; however, once cleaved from resin, again a single peak and a shift in retention time could be seen by HPLC (Figure 3.3). The lack of

a mass spectral signal corresponding to the products was thought to be due to the lack of an ionizable functional group on the peptide, which is discussed in the following section.



Scheme 3.4: Synthesis of first clickable peptide system with chelator **3.3**

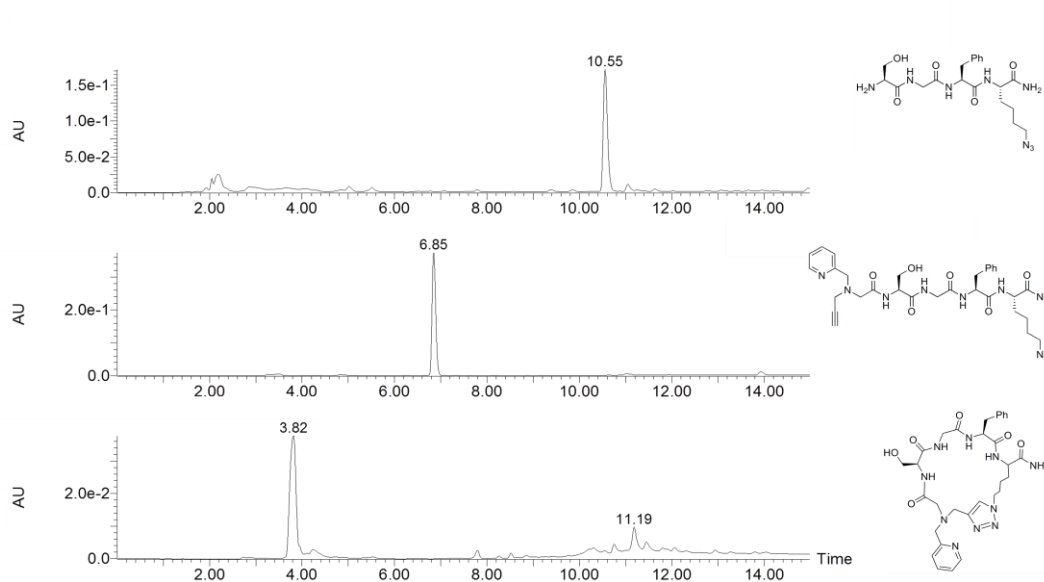


Figure 3.3: HPLC traces showing the progression of synthesis of peptide **3.9**

This trend also continued with the coordination reaction with $[\text{Re}(\text{CO})_3]^+$ to give peptide **3.10**. However, when a MALDI-MS was obtained of peptide **3.10**, the desired coordinated mass could be seen (Figure 3.4). As well, rhenium gives an isotopic signature for its two naturally occurring isotopes 185 (37.4%) and 187 (62.6%). In this MALDI-MS this approximately 2:1 isotopic signature was observed, giving promising preliminary results that this clickable peptide system was coordinating rhenium.

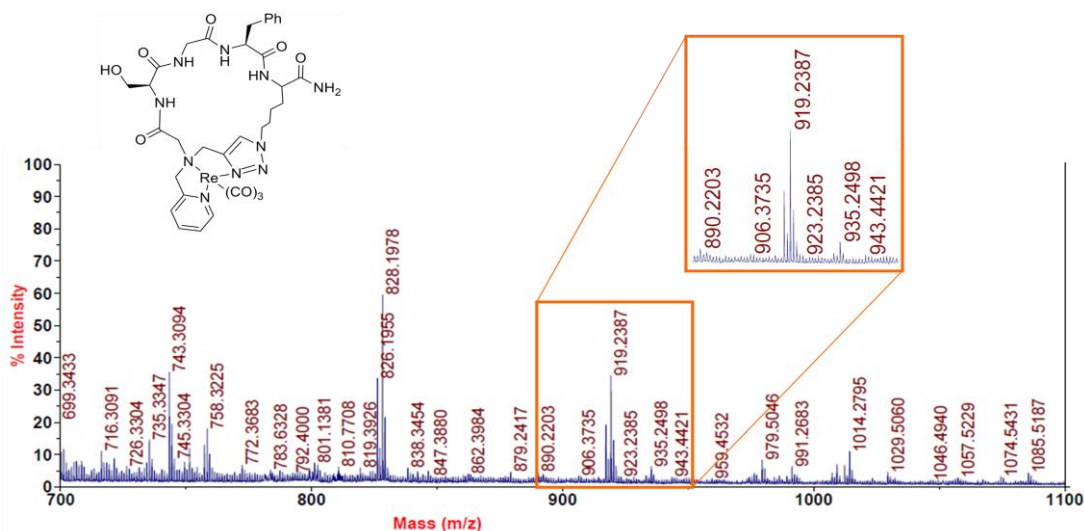


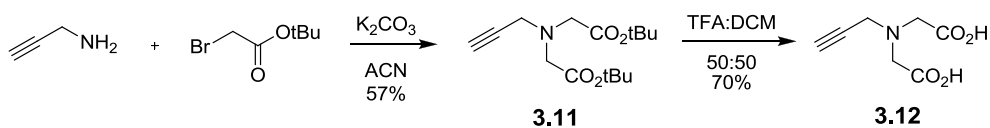
Figure 3.4: MALDI-MS of final clicked peptide **3.10** showing the desired coordinated mass and rhenium-185/187 signature

This peptide was re-synthesized several times by both solid and solution phase techniques in order to fully characterize each intermediate. However, this synthesis was not reproducible, and complete characterization was unsuccessful.

3.2.3 Second Clickable Peptide System

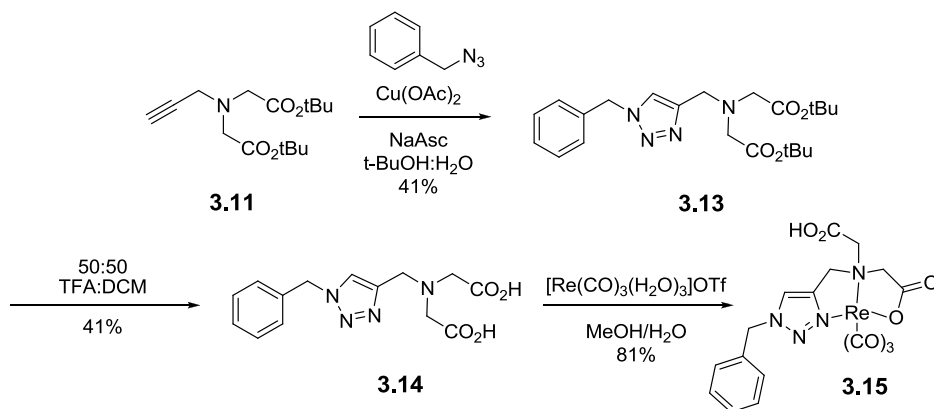
As synthesis of the first clickable peptide system became problematic with the addition of alkyne **3.3**, a second alkyne-containing synthetic amino acid chelator was designed in order to avoid the mass spectrometry problems. This second chelator was designed with a carboxylic acid as the extra coordinating group in place of pyridine in order to determine

if the issues with mass spectral analysis were due to the structure of the previous chelator. A similar synthetic route to the first artificial amino acid was followed to create the second with a substitution of the propargylamine with *tert*-butyl bromoacetate, followed by deprotection using trifluoroacetic acid (TFA) (Scheme 3.5).



Scheme 3.5: Synthesis of clickable chelator **3.12**

This chelator then underwent a click reaction, as before, with benzyl azide to create a small molecule system that contained the tridentate chelator in order to test the chelation sphere prior to incorporation into the peptide (Scheme 3.6). The issue of pH dependence for the coordination as discussed above³¹ is present for this chelation system as there are two free carboxylic acids. However, attachment to the peptide will occur prior to metal chelation, leaving only one free carboxylic acid for chelation, thus eliminating the potential problem of pH dependence as both the carboxylic acid and triazole are expected to coordinate the metal.



Scheme 3.6: Synthesis of model chelator **3.15** for the second clickable peptide system

Coordination of **3.14** with $[\text{Re}(\text{CO})_3(\text{H}_2\text{O})_3]\text{OTf}$ was initially performed in the presence of NaOH and **3.15** showed two products both by NMR spectroscopy and LC-MS analysis, each product having the expected coordinated mass and rhenium signatures. When this system was coordinated in the absence of base, only one product was seen. Comparison of the ^1H NMR spectra prior to (**3.14**) and following (**3.15**) coordination showed a shift in the peaks in the methylene region as well as a change in the proton coupling patterns (Figure 3.5). Additionally, the protons on carbon C and E in **3.15** have independent shifts as opposed to having identical shifts as seen in **3.14**. LC-MS studies also showed a single peak with the desired coordinated mass and $^{185/187}\text{Re}$ signature, indicating it was coordinating with $[\text{Re}(\text{CO})_3]^+$. It could therefore be concluded that this chelator was able to coordinate $[\text{Re}(\text{CO})_3]^+$, and thus was a suitable chelator for use in the clickable peptide.

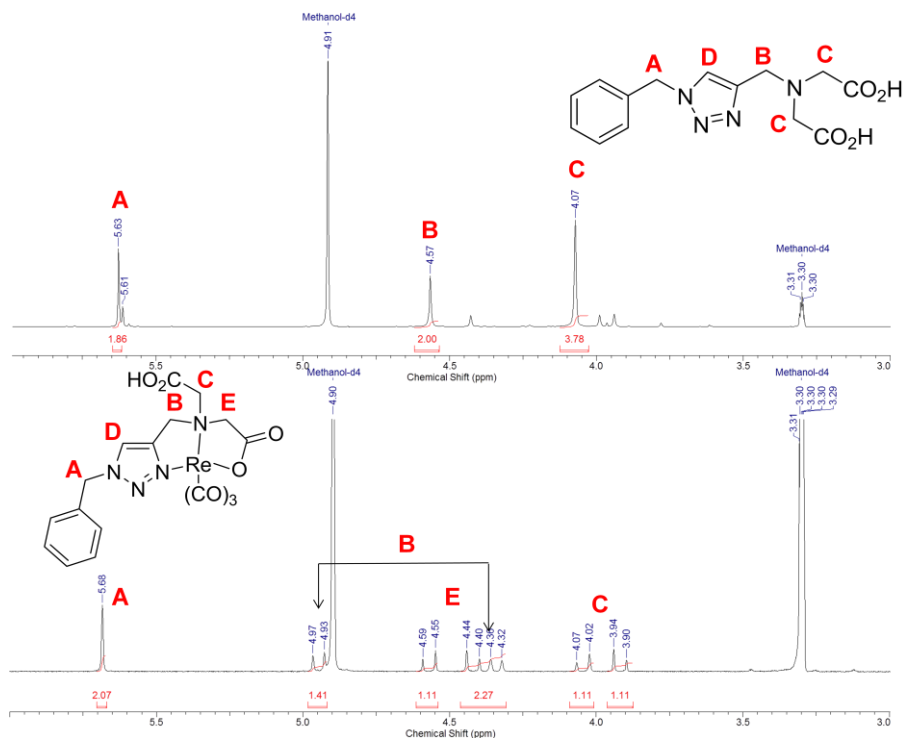
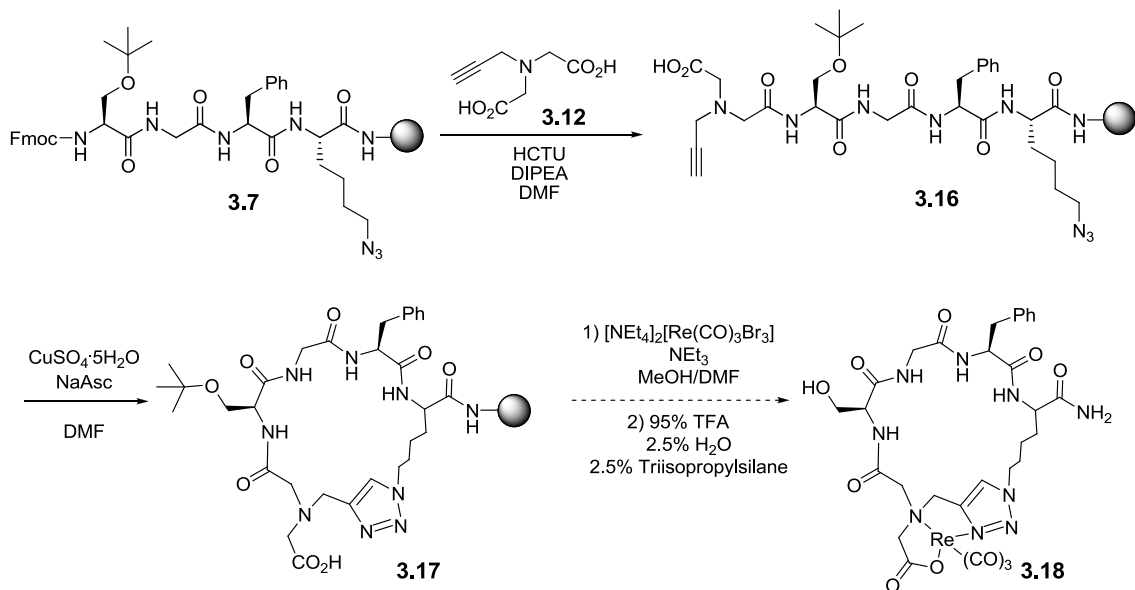


Figure 3.5: Methylene region of the ^1H NMR spectra for **3.14** and **3.15** showing the shift in peaks indicating rhenium coordination

With the suitability of the second chelation system demonstrated, the second artificial amino acid could then be incorporated onto peptide **3.7** using standard peptide coupling procedures (Scheme 3.7). Unlike the first synthetic alkyne amino acid coupled peptide **3.8**, the mass of peptide **3.16** could be seen in the mass spectrum, showing that chelator **3.12** was successfully added to the peptide. However, by LC-MS analysis there were many other peaks in addition to the product peak. When the click reaction was attempted on-resin almost no product and no starting material was observed. Therefore, peptide **3.16** was re-synthesized and cleaved from the resin using TFA prior to the click reaction of the alkyne and azide. It was then purified by preparative LC-MS before moving on to solution phase click cyclization.



Scheme 3.7: Synthesis of second clickable peptide system with chelator **3.12**

The cyclization of peptide **3.16** was attempted in solution in two different ways. It was first attempted using $\text{Cu}(\text{OAc})_2$ and NaAsc in a 50:50 mixture of water and *t*-BuOH. Only starting material was present after 3 days at room temperature. This was still the case after 2 days at 50°C . After 1 night at reflux there was no remaining starting material

as indicated by LC-MS analysis, but the chromatogram had many peaks, including two very small peaks with the mass of peptide **3.17**. Due to the number of peaks with similar retention times, this was not able to be purified.

Another cyclization method was attempted using DBU (1,8-diazabicycloundec-7-ene) and CuBr in toluene, refluxing overnight. By LC-MS analysis no product or starting material was observed. As the product was polar it could not be eluted on silica TLC (thin layer chromatography) plates and could therefore not be purified by column chromatography. As the cyclic peptide could not be isolated, coordination of this system was not attempted.

It was speculated that perhaps the problems with obtaining a mass spectrum were due to the peptide not being properly ionized in the mass spectrometer due to lack of protonation sites in the peptide system and including a protonation site in the cyclic peptide would permit detection by HPLC-ESI-MS. Therefore, two additional cyclic peptides were synthesized that included an ionizable arginine in the peptide at the N-terminus before either synthetic amino acids **3.3** or **3.12** were coupled to the peptide. This, however, did not seem to help, and only caused the formation of more by-products prior to addition of the chelator.

In order to ensure issues were not arising due to the fact that the azide functionality was too close to the resin, to add space between the azide and the resin an additional two peptides were synthesized that included an alanine added to the C-terminus before adding the azide modified lysine. This peptide was then coupled with both chelators **3.3** and

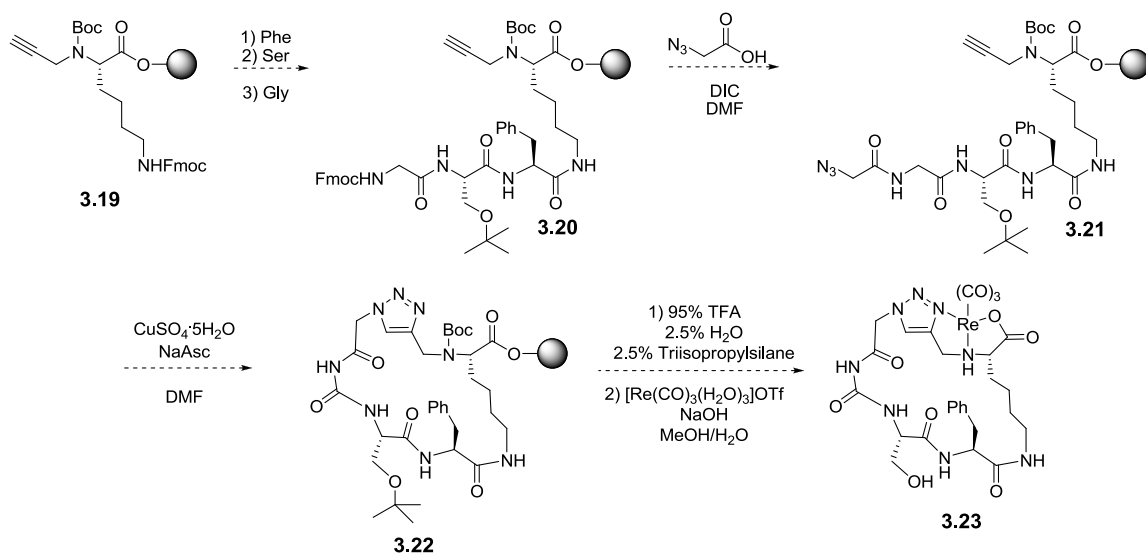
3.12. However, the addition of an alanine spacer did not appear to make any difference for either chelation sphere.

3.2.4 Third Clickable Peptide System

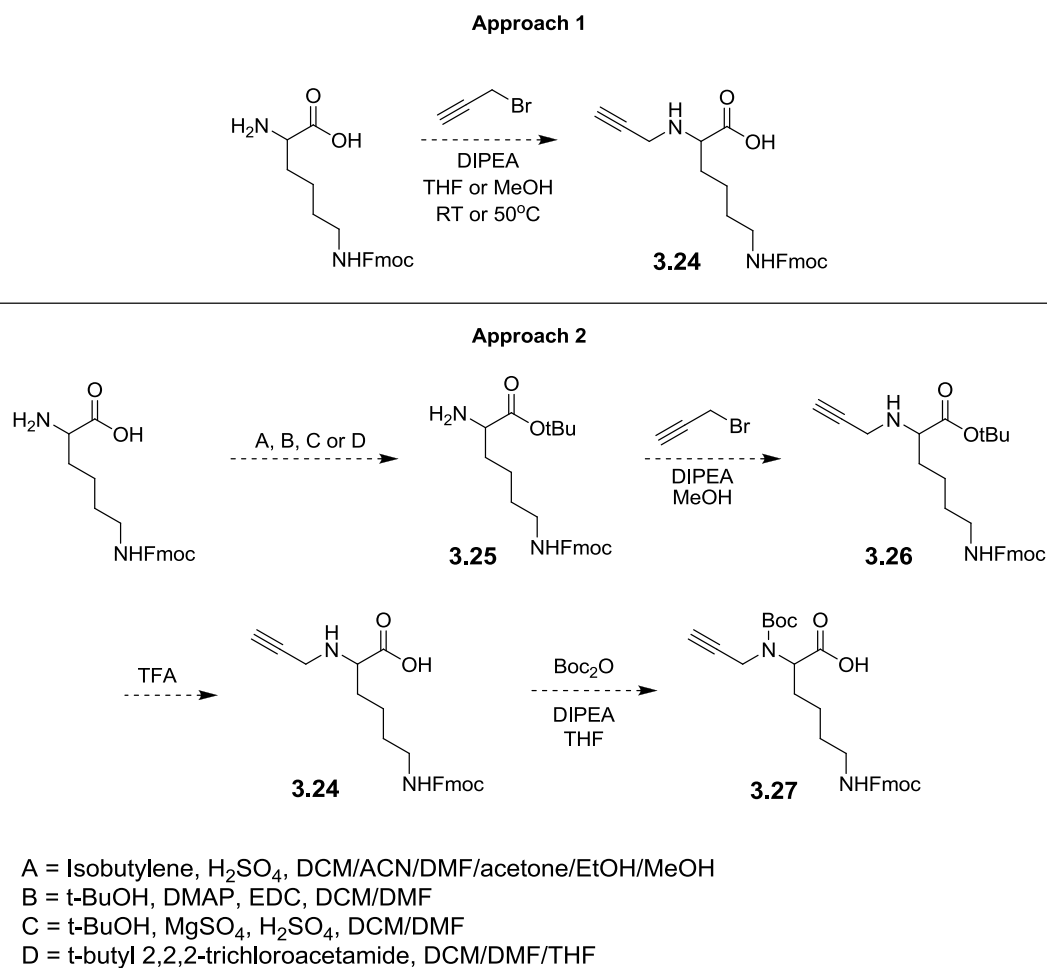
Given that the two previous clickable peptide systems did not appear to be capable of forming a cyclized and coordinated peptide, a new system needed to be developed with an entirely different approach. In order to make the peptide unique compared to the prior designs, the alkyne and azide were inverted, putting the alkyne at the C-terminus and the azide at the N-terminus.

In this new approach, a lysine could be loaded onto the resin, and the peptide extended from the ϵ -amine. As opposed to having the alkyne on the side chain of an amino acid in the chain, the alkyne could be attached to the α -amine of the lysine. This would not only provide a new approach, but also allow for the newly formed secondary amine of the lysine to act as a coordinating group for the rhenium as the triazole will be formed adjacent to it. If synthesized on Wang resin, a carboxylic acid will be formed on the C-terminus of the peptide upon cleavage from the resin resulting in a third coordination site for rhenium, forming a tridentate chelator upon cyclization (Scheme 3.8).

For this approach to work, an alkyne modified lysine would have to be developed (Scheme 3.9). In addition, the alpha-amine of the lysine is required as a coordinating group, and thus needs to exist as a secondary amine as opposed to an amide. Therefore, an alkyne would be added to the alpha-amine of lysine. This would allow for the modified amino acid to still attach to the resin through the carboxylic acid, while leaving the side chain amine intact for peptide chain growth.



Scheme 3.8: Proposed synthesis of third clickable peptide system



Scheme 3.9: Attempted and proposed synthesis of alkyne modified lysine

Multiple attempts were made to synthesize this alkyne modified lysine. An attempt was initially made to add propargyl bromide to H-Lys(Fmoc)-OH with the carboxylic acid unprotected (**3.24**), see Scheme 3.9 approach 1. However, this did not appear to be successful as multiple by-products were formed. Therefore, the carboxylic acid had to first be protected with a *tert*-butyl group that could be selectively removed prior to coupling onto the peptide. As can be seen in Scheme 3.9 approach 2, four different sets of reagents, each performed multiple times with varying equivalents and reaction times, were attempted to synthesize starting material **3.25**. However, this could not be accomplished, making continuation of the proposed synthetic approach for the third clickable peptide system in Scheme 3.8 impossible.

3.3 Conclusions

Three different clickable peptide systems were developed, each with their own unique chelation system. Synthesis of an azide modified lysine to add the azide functionality to the peptides was successful, as were two “click-to-chelate” alkyne modified chelators. Their ability to coordinate rhenium(I) tricarbonyl was verified by model click and subsequent chelation reactions. Synthesis of the first clickable peptide system had promising preliminary results, but did not appear to be reproducible and full characterization of the system was not possible. Incorporation of the second chelator into the second clickable peptide system was slightly more promising than the first; however the subsequent click and chelation reactions were unsuccessful. Therefore, a new approach of inverting the functionalities in the clickable peptide was attempted. However, this pathway was unsuccessful as the alkyne modified lysine starting material could not be prepared.

This project has been ongoing for a number of years and much effort has been put forward to synthesize and characterize these clickable peptides. As well, many different pathways have been proposed and attempted with minimal progress due to unforeseen synthetic and characterization difficulties. Therefore, while the proposal of simultaneously combining the ability of click chemistry to both cyclize a peptide and form a chelator for $[^{99m}\text{Tc}/\text{Re}(\text{CO})_3]^+$ appears elegant conceptually, it has proven to be synthetically problematic and was therefore abandoned.

3.4 Experimental

Materials and Methods

All chemicals were purchased from Sigma-Aldrich, Novabiochem, Aapptec, Peptides International and Chem-Impex and were used without further purification unless indicated. For HPLC-MS, a Waters, Inc. system was used, consisting of a Waters 2998 Photodiode Array Detector and a Waters 2767 Sample Manager. For analytical HPLC-MS studies, a Waters Atlantis RP-C18 4.6 x 150 mm, 5 μm column was used. For preparative HPLC-MS work, a Waters Atlantis RP-C18 19 x 150 mm, 5 μm column was used. In both cases, absorbance was detected at wavelengths of 220 nm and 254 nm. A gradient solvent system consisting of $\text{CH}_3\text{CN} + 0.1\%$ TFA (solvent A) and $\text{H}_2\text{O} + 0.1\%$ TFA (solvent B) was used. For analytical UHPLC-MS studies, a Waters, Inc. Acquity UPLC H-Class system was used, combined with a Xevo QToF. For analytical UHPLC studies, a Waters Acquity UPLC BEH C18 2.1 x 50 mm, 1.7 μm column was used. A gradient solvent system consisting of $\text{CH}_3\text{CN} + 0.1\%$ formic acid (solvent C) and $\text{H}_2\text{O} + 0.1\%$ formic acid (solvent D) was used. A Biotage Isolera One flash chromatography system was used for flash column chromatography purification. Silicycle Silica Gel 60

(230–400 mesh) was used for column chromatography purification and EMD Silica Gel 60 F254 plates were used for analytical TLC. Varian INOVA 400 and 600 NMR spectrometers were used for NMR studies. Chemical shifts are reported in parts per million (ppm) relative to TMS (0.00 ppm). For electron impact (EI) mass spectra a Finnigan MAT 8400 mass spectrometer was used and for electro-spray ionization (ESI) mass spectra a Micromass Quattro Micro API mass spectrometer was used.

General Peptide Synthesis

Fully protected resin-bound peptides were synthesized manually by Fmoc solid-phase peptide synthesis using Rink amide MBHA resin (loading 0.34 mmol/g) and all *N*-Fmoc amino acids. The resin-bound peptide was treated with 20% piperidine in *N,N*-dimethylformamide (DMF) for 5 and 15 minutes to remove the Fmoc protecting group, followed by washes with both DMF and dichloromethane (DCM) after each addition. All natural Fmoc amino acids were coupled twice using 3 eq. of Fmoc amino acid, 3 eq. 2-(6-chloro-1H-benzotriazole-1-yl)-1,1,3,3-tetramethylaminium hexafluorophosphate (HCTU) and 6 eq. *N,N*-diisopropylethylamine (DIPEA) in DMF for 30 min and 1 h. Modified amino acids were coupled under the same conditions, but were left to couple overnight. Once the linear sequence was complete a small amount of peptide could be deprotected and cleaved from the resin by treatment with TFA containing water (2.5% v/v) and triisopropylsilane (2.5% v/v) as scavengers for 2 h, and its identity and purity verified by LC-MS analysis.

If the next step was to be performed on-resin, the peptide was left on the resin. However, if the next step required solution phase synthesis, the peptide was deprotected and

cleaved from the resin by treatment with TFA containing water (2.5% v/v) and triisopropylsilane (2.5% v/v) as scavengers, shaking for 4 h. The peptide could then be precipitated from the TFA solution using cold *tert*-butyl methyl ether (TBME) and collected by centrifugation and decantation. The resulting peptide was dissolved in water and lyophilized to obtain the crude peptide which could then be purified by preparative LC-MS.

N-propargyl-pyridine-2-methylamine (3.1)

To 5 mL of acetonitrile (ACN) under argon was added 1.1 eq. propargylamine (71 μ L, 1.1 mmol) and 1 eq. 2-pyridine carboxaldehyde (95 μ L, 1.0 mmol). After stirring for 5 min, 1.6 eq. sodium triacetoxyborohydride (339 mg, 1.6 mmol) was added and was left to stir under argon overnight. The reaction was quenched with 5 M NaOH and the solvent removed by rotary evaporation. The remaining aqueous solution was made basic by adding 5 M NaOH and extracted with dichloromethane to give an 89% crude yield of **3.1** (130 mg, 0.9 mmol). ESI MS: m/z calculated for $C_9H_{11}N_2$, 147.09; observed $[M+H]^+$ 147.01. 1H -NMR Spectrum (400 MHz, $CDCl_3$, δ): 8.44 (1H, d, ar, $^3J_{H-H} = 4.3$ Hz), 7.53 (1H, ddd, ar, $^3J_{H-H} = 7.8$ Hz, $^3J_{H-H} = 7.8$ Hz, $^4J_{H-H} = 1.9$ Hz), 7.22 (1H, d, ar, $^3J_{H-H} = 7.8$ Hz), 7.06-7.03 (1H, m, ar), 3.89 (2H, s, $NHCH_2pyr$), 3.37 (2H, d, $CHCCH_2NH$, $^4J_{H-H} = 2.3$ Hz), 2.43 (1H, broad s, $CHCCH_2NH$), 2.16 (1H, dd, $CHCCH_2NH$, $^4J_{H-H} = 2.3$ Hz). ^{13}C -NMR spectrum (100 MHz, $CDCl_3$, δ): 158.58 (ar), 149.29 (ar), 136.47 (ar), 122.44 (ar), 122.09 (ar), 81.37 ($HCCCH_2$), 71.90 ($HCCCH_2$), 53.36 ($NHCH_2Pyr$), 37.59 ($HCCCH_2$).

Ethyl-propargyl-pyridine-2-methylamino-acetate (3.2)

To 10 mL ACN was added 1 eq. **3.1** (45 mg, 0.3 mmol), 1.5 eq. triethylamine (64 μ L, 0.5 mmol) and 1.2 eq. ethylbromoacetate (51 μ L, 0.5 mmol). The reaction was stirred overnight at 50°C. The ACN was removed by evaporation and the resulting oil extracted using DCM and NaHCO₃. This was then purified by column chromatography using a solvent system of 25% ethyl acetate and 75% hexanes, resulting in a 57% yield of **3.2** (41 mg, 0.2 mmol). HR-EI-MS: m/z calculated for C₁₃H₁₆N₂O₂, 232.1212; observed [M+H]⁺ 232.1284. ¹H-NMR Spectrum (400 MHz, CDCl₃, δ): 8.55 (1H, d, ar, ³J_{H-H} = 4.3 Hz), 7.74 (1H, ddd, ar, ³J_{H-H} = 7.8 Hz, ³J_{H-H} = 7.8 Hz, ⁴J_{H-H} = 1.6 Hz), 7.62 (1H, d, ar, ³J_{H-H} = 7.8 Hz), 7.25-7.22 (1H, m, ar), 4.16 (2H, q, NCH₂C(O)OCH₂CH₃, ³J_{H-H} = 7.0 Hz), 3.98 (2H, s, NCH₂C(O)OCH₂CH₃), 3.55 (2H, d, CHCCH₂N, ⁴J_{H-H} = 2.3 Hz), 3.48 (2H, s, NCH₂pyr), 2.26 (1H, dd, CHCCH₂N, ⁴J_{H-H} = 2.3 Hz, ⁴J_{H-H} = 2.3 Hz), 1.26 (3H, t, NCH₂C(O)OCH₂CH₃, ³J_{H-H} = 7.0 Hz). ¹³C-NMR spectrum (100 MHz, CDCl₃, δ): 170.6 (CH₂C(O)OCH₂CH₃), 158.2 (ar), 149.0 (ar), 136.6 (ar), 123.2 (ar), 122.2 (ar), 78.3 (HCCCH₂), 73.6 (HCCCH₂), 60.5 (CH₂C(O)OCH₂CH₃), 59.3 (NHCH₂Pyr), 54.2 (CH₂C(O)OCH₂CH₃), 42.8 (HCCCH₂), 14.1 (CH₂C(O)OCH₂CH₃).

Propargyl-pyridine-2-methylamino-acetic acid (3.3)

To 10 mL ethanol was added 1 eq. **3.2** (580 mg, 2.5 mmol) and 1.5 eq. KOH (210 mg, 3.8 mmol). This was stirred at 50°C for 2 h. The solvent was removed by evaporation and re-dissolved in water and was then neutralized using concentrated HCl. The aqueous solution was then frozen and lyophilized. Once dry, the powder was triterated with CHCl₃, resulting in an 86% yield of **3.3** (516 mg, 2.1 mmol). HR-EI-MS: m/z calculated

for $C_{11}H_{13}N_2O_2$, 205.0977; observed $[M+H]^+$ 205.0826. 1H -NMR Spectrum (600 MHz, $CDCl_3$, δ): 8.44 (1H, d, ar, $^3J_{H-H} = 4.7$ Hz), 7.49 (1H, dd, ar, $^3J_{H-H} = 7.6$ Hz, $^3J_{H-H} = 7.6$ Hz), 7.17 (1H, d, ar, $^3J_{H-H} = 7.6$ Hz), 7.01 (1H, dd, ar, $^3J_{H-H} = 7.0$ Hz, $^3J_{H-H} = 5.3$ Hz), 3.67 (2H, s, $NCH_2C(O)OH$), 3.23 (2H, s, $CHCCH_2N$), 3.11 (2H, s, NCH_2pyr), 2.12 (1H, s, $CHCCH_2N$).

1-(benzyl)triazole-pyridine-2-methylamino-acetate (3.4)

A 700 μ L solution of 1:1 t-BuOH and water was made and 1 eq. **3.2** (17 mg, 0.07 mmol) was dissolved to make a 0.1 M solution of **3.2**. To this solution, 1 eq. of benzyl azide (9 μ L, 0.07 mmol), 0.1 eq. $Cu(OAc)_2$ (1 mg, 0.007 mmol) and 0.2 eq. NaAsc (3 mg, 0.014 mmol) were added and allowed to stir at room temperature for 3 nights. The reaction mixture was extracted with ethyl acetate, and the resulting organic layer extracted with NaCl. The solvent was then removed with a rotary evaporator and dried under high vacuum, giving a crude yield of 68% for **3.4** (17 mg, 0.05 mmol). HR-EI-MS: m/z calculated for $C_{20}H_{23}N_5O_2$, 365.4289; observed $[M+H]^+$ 365.1838. 1H -NMR Spectrum (400 MHz, $CDCl_3$, δ): 8.48-8.46 (1H, m, ar), 7.66-7.62 (1H, m, ar), 7.53-7.51 (2H, m, ar), 7.35-7.29 (3H, m, ar), 7.24-7.20 (2H, m, ar), 7.16-7.13 (1H, m, ar), 5.49 (2H, s, $PhCH_2N$), 4.12 (2H, q, $NCH_2C(O)OCH_2CH_3$, $^3J_{H-H} = 7.0$ Hz), 3.98 (4H, m, $CCH_2NCH_2C(O)OCH_2CH_3$), 3.44 (2H, s, NCH_2pyr), 1.23 (3H, t, $NCH_2C(O)OCH_2CH_3$, $^3J_{H-H} = 7.0$ Hz). ^{13}C -NMR spectrum (100 MHz, $CDCl_3$, δ): 170.9 ($CH_2C(O)OCH_2CH_3$), 158.2 (ar), 148.2 (ar), 144.7 (ar), 137.3 (ar), 134.6 ($NCHC(N)CH_2$), 129.0 (ar), 128.6 (ar), 128.0 (ar), 123.7 (ar), 123.1 ($NCHC(N)CH_2$), 122.4 (ar), 60.5 ($CH_2C(O)OCH_2CH_3$), 58.8 ($NHCH_2Pyr$), 54.5 ($PhCH_2N$), 54.0 ($NCHC(N)CH_2$), 48.8 ($CH_2C(O)OCH_2CH_3$), 14.2 ($CH_2C(O)OCH_2CH_3$).

Rhenium(I) tricarbonyl-1-(benzyl)triazole-pyridine-2-methylamino-acetate (3.5)

In 1.5 mL MeOH and 3 mL water, 1 eq. **3.4** (17 mg, 0.05 mmol) was dissolved, and to this, 1.2 eq of a 0.1 M solution of $[\text{Re}(\text{CO})_3(\text{H}_2\text{O})_3]\text{OTf}$ (600 μL , 0.06 mmol) was added and stirred at 60°C for 1.5 h. The reaction mixture was lyophilized and washed with water resulting in an 86% yield of **3.5** (27 mg, 0.04mmol). HR-EI-MS: m/z calculated for $\text{C}_{23}\text{H}_{23}\text{N}_5\text{O}_5^{185/187}\text{Re}$, 634.1229/636.1257; observed $[\text{M}+\text{H}]^+$ 634.1220/636.1284. ^1H -NMR Spectrum (600 MHz, CDCl_3 , δ): 8.56 (1H, d, ar, $^3J_{\text{H-H}} = 5.3$ Hz), 7.93 (1H, s, triazole), 7.83 (1H, dd, ar, $^3J_{\text{H-H}} = 8.2$ Hz, $^3J_{\text{H-H}} = 7.6$ Hz), 7.63 (1H, d, ar, $^3J_{\text{H-H}} = 7.6$ Hz), 7.34-7.31 (3H, m, ar), 7.21-7.19 (2H, m, ar), 7.16 (1H, dd, ar, $^3J_{\text{H-H}} = 6.4$ Hz, $^3J_{\text{H-H}} = 7.0$ Hz), 5.40 (2H, dd, PhCH_2N , $^2J_{\text{H-H}} = 20.5$ Hz, $^4J_{\text{H-H}} = 14.6$ Hz), 5.28 (1H, d, NCH_2pyr , $^2J_{\text{H-H}} = 16.4$ Hz), 4.91 (1H, d, NCHCCH_2N , $^2J_{\text{H-H}} = 16.4$ Hz), 4.59 (1H, d, NCH_2pyr , $^2J_{\text{H-H}} = 16.4$ Hz), 4.48 (2H, dd, $\text{NCH}_2\text{C}(\text{O})\text{OCH}_2\text{CH}_3$, $^2J_{\text{H-H}} = 16.4$ Hz, $^4J_{\text{H-H}} = 9.4$ Hz), 4.42 (1H, d, NCHCCH_2N , $^2J_{\text{H-H}} = 16.4$ Hz), 4.28 (2H, q, $\text{NCH}_2\text{C}(\text{O})\text{OCH}_2\text{CH}_3$, $^3J_{\text{H-H}} = 7.0$ Hz), 1.30 (3H, t, $\text{NCH}_2\text{C}(\text{O})\text{OCH}_2\text{CH}_3$, $^3J_{\text{H-H}} = 7.0$ Hz).

Fmoc-Lys(N₃)-OH (3.6)

To 6 mL DMF 1 eq. Fmoc-Lys-OH·HCl (616 mg, 1.8 mmol), 1.2 eq. imidazole-1-sulfonyl azide·HCl (385 mg, 2.2 mmol), 3.7 eq. NaHCO_3 (473 mg, 6.7 mmol) and 0.01 eq. $\text{CuSO}_4 \cdot 5\text{H}_2\text{O}$ (4 mg, 0.02 mmol) were added and stirred at room temperature overnight. The reaction mixture was diluted with 75 mL H_2O and acidified from pH 7 to 4 with concentrated HCl. The aqueous solution was extracted with ethyl acetate, and the resulting organic layer extracted with NaCl. The organic layer was dried with MgSO_4 , filtered and the solvent removed with a rotary evaporator. The resulting oil was purified

by column chromatography removing the first impurity with 100% CHCl_3 and then flushing with 1% acetic acid in CHCl_3 to collect the product. This resulted in a 54% yield of **3.6** (380 mg, 1.0 mmol). ESI MS: m/z calculated for $\text{C}_{21}\text{H}_{23}\text{N}_4\text{O}_4$, 395.17; observed $[\text{M}+\text{H}]^+$ 395.15. $^1\text{H-NMR}$ Spectrum (400 MHz, CDCl_3 , δ): 7.75 (2H, d, ar, $^3J_{\text{H-H}} = 7.4$ Hz), 7.59 (2H, d, ar, $^3J_{\text{H-H}} = 7.4$ Hz), 7.39 (2H, dd, ar, $^3J_{\text{H-H}} = 7.4$ Hz, $^3J_{\text{H-H}} = 7.4$ Hz), 7.31 (2H, dd, ar, $^3J_{\text{H-H}} = 7.4$ Hz, $^3J_{\text{H-H}} = 7.4$ Hz), 4.42-4.35 (3H, m, CHCH_2O), 4.22 (1H, t, NHCHCO_2H , $^3J_{\text{H-H}} = 7.0$ Hz), 3.31-3.27 (2H, m, $\text{CH}(\text{CH}_2)_4\text{N}_3$), 2.13-2.00 (2H, m, $\text{CH}(\text{CH}_2)_4\text{N}_3$), 1.89-1.74 (2H, m, $\text{CH}(\text{CH}_2)_4\text{N}_3$), 1.62-1.37 (2H, m, $\text{CH}(\text{CH}_2)_4\text{N}_3$).

***tert*-butyl-propargyliminodiacetate (3.11)**

To 10 mL ACN, 1 eq. propargylamine (256 μL , 4.0 mmol), 1.2 eq. K_2CO_3 (662 mg, 4.8 mmol) and 2 eq. *t*-butyl bromoacetate (1.18 mL, 8 mmol) were added and the solution stirred at 90°C overnight. The solvent was removed with a rotary evaporator and the resulting oil re-dissolved in DCM and extracted with NaCl. The solvent was again removed by evaporation and dried on high vacuum. The crude product was purified on a silica pad, removing the first impurity with 100% DCM and then adding 10% MeOH in DCM to obtain product **3.11** in a 57% yield (647 mg, 2.3 mmol). ESI MS: m/z calculated for $\text{C}_{15}\text{H}_{26}\text{NO}_4$, 284.19; observed $[\text{M}+\text{H}]^+$ 284.15. $^1\text{H-NMR}$ Spectrum (400 MHz, CDCl_3 , δ): 3.64 (2H, d, CHCCH_2N , $^4J_{\text{H-H}} = 2.4$ Hz), 3.42 (4H, s, $\text{NCH}_2\text{C}(\text{O})\text{OC}(\text{CH}_3)_3$), 2.22 (1H, dd, CHCCH_2N , $^4J_{\text{H-H}} = 2.4$ Hz), 1.45 (18H, s, $\text{NCH}_2\text{C}(\text{O})\text{OC}(\text{CH}_3)_3$).

N-propargyliminodiacetic acid (3.12)

In 6 mL DCM and 6 mL TFA **3.11** (449 mg, 1.6 mmol) was dissolved and stirred at room temperature for 3.5 h. The reaction mixture was then azeotroped with DCM and the

solvent removed with a rotary evaporator and dried on high vacuum. This resulted in a 70% crude yield of **3.12** (450 mg, 1.1 mmol). ESI MS: m/z calculated for $C_7H_{10}NO_4$, 172.06; observed $[M+H]^+$ 172.09. 1H -NMR Spectrum (400 MHz, D_2O , δ): 4.25 (2H, d, $CHCCH_2N$, $^4J_{H-H} = 2.7$ Hz), 4.11 (4H, s, $NCH_2C(O)OH$), 3.10 (1H, dd, $CHCCH_2N$, $^4J_{H-H} = 2.7$ Hz).

1-(benzyl)triazole-propargyliminodiacetate (3.13)

A 7 mL solution of 1:1 t-BuOH and water was made and 1 eq. **3.11** (198 mg, 0.7 mmol) was dissolved to make a 0.1 M solution of **3.11**. To the reaction mixture, 1 eq. benzyl azide (87 μ L, 0.7 mmol), 0.1 eq. $Cu(OAc)_2$ (13 mg, 0.07 mmol) and 0.2 eq. NaAsc (28 mg, 0.14 mmol) was added and stirred at room temperature overnight. The reaction mixture was then extracted with ethyl acetate, and the resulting organic layer extracted with NaCl. The solvent was then removed by rotary evaporation and dried on high vacuum. The resulting oil was purified by flash column chromatography with a gradient solvent system of 6-50% ethyl acetate in hexanes. This resulted in a 41% yield of **13** (119 mg, 0.3 mmol). ESI MS: m/z calculated for $C_{22}H_{33}N_4O_4$, 417.25; observed $[M+H]^+$ 417.26. 1H -NMR Spectrum (400 MHz, $CDCl_3$, δ): 7.49 (1H, s, triazole), 7.33-7.20 (5H, m, ar), 5.45 (2H, s, $PhCH_2N$), 3.96 (2H, s, $NCHCCH_2N$), 3.38 (4H, s, $NCH_2C(O)OC(CH_3)_3$), 1.38 (18H, s, $NCH_2C(O)OC(CH_3)_3$).

1-(benzyl)triazole-propargyliminodiacetic acid (3.14)

In 7 mL DCM and 7 mL TFA **3.13** (119 mg, 0.29 mmol) was dissolved and stirred at room temperature for 3.5 h. The reaction mixture was then azeotroped with DCM and the solvent removed with a rotary evaporator and dried on high vacuum. The resulting oil

was purified by flash column chromatography with a gradient solvent system of 1-10% MeOH in DCM. This resulted in a 41% yield of **3.14** (37 mg, 0.12 mmol). ESI MS: m/z calculated for $C_{14}H_{17}N_4O_4$, 305.13; observed $[M+H]^+$ 305.12. 1H -NMR Spectrum (400 MHz, MeOH- d_4 , δ): 8.15 (1H, s, triazole), 7.37-7.33 (5H, m, ar), 5.63 (2H, s, $PhCH_2N$), 4.57 (2H, s, $NCHCCH_2N$), 4.07 (4H, s, $NCH_2C(O)OH$).

Rhenium(I) tricarbonyl-1-(benzyl)triazole-propargyliminodiacetic acid (**3.15**)

To 3 mL MeOH and 6 mL water, 1 eq. **3.14** (37 mg, 0.12 mmol) was added, along with 1 eq. of a 0.1 M solution of $[Re(CO)_3(H_2O)_3]OTf$ (1.2 mL, 0.12 mmol). The reaction mixture was then stirred at 60°C for 1 h, after which time it was frozen and lyophilized. The resulting powder was washed with water, resulting in an 81% yield of **3.15** (55 mg, 0.1 mmol). ESI MS: m/z calculated for $C_{21}H_{23}N_4O_4$, 573.06/575.06; observed $[M+H]^+$ 573.09/575.05. 1H -NMR Spectrum (400 MHz, MeOH- d_4 , δ): 8.12 (1H, s, triazole), 7.42-7.35 (5H, m, ar), 5.58 (2H, s, $PhCH_2N$), 4.94 (1H, d, $NCHCCH_2N$, $^3J_{H-H} = 15.6$ Hz), 4.56 (1H, d, $NCH_2C(O)ORe$, $^3J_{H-H} = 17.2$ Hz), 4.43 (1H, d, $NCH_2C(O)ORe$, $^3J_{H-H} = 17.2$ Hz), 4.35 (1H, d, $NCHCCH_2N$, $^3J_{H-H} = 15.6$ Hz), 4.04 (1H, d, $NCH_2C(O)OH$, $^3J_{H-H} = 17.2$ Hz), 3.93 (1H, d, $NCH_2C(O)OH$, $^3J_{H-H} = 17.2$ Hz).

3.5 References

1. R. Alberto, *Top. Curr. Chem*, 2005, 252, 1-44.
2. S. Liu and S. Chakraborty, *Dalton Trans.*, 2011, 40, 6077-6086.
3. A. G. Jones, M. J. Abrams, A. Davison, J. W. Brodack, A. K. Toothaker, S. J. Adelstein and A. I. Kassis, *Int. J. Nucl. Med. Biol.*, 1984, 11, 225-234.
4. R. Alberto, R. Schibli, P. A. Schubiger, U. Abram and T. A. Kaden, *Polyhedron*, 1996, 15, 1079-1089.

5. R. Alberto, R. Schibli, D. Angst, P. A. Schubiger, U. Abram, S. Abram and T. A. Kaden, *Transition Met. Chem. (London)*, 1997, 22, 597-601.
6. R. Alberto, R. Schibli, A. Egli, F. F. Knapp and P. A. Schubiger, *Radiochim. Acta*, 1997, 79, 99-103.
7. R. Schibli, R. Alberto, U. Abram, S. Abram, A. Egli, P. A. Schubiger and T. A. Kaden, *Inorg. Chem.*, 1998, 37, 3509-3516.
8. U. Abram, S. Abram, R. Schibli, R. Alberto and J. R. Dilworth, *Polyhedron*, 1998, 17, 1303-1309.
9. R. Alberto, R. Schibli, A. Egli, A. P. Schubiger, U. Abram and T. A. Kaden, *J. Am. Chem. Soc.*, 1998, 120, 7987-7988.
10. R. Alberto, K. Ortner, N. Wheatley, R. Schibli and A. P. Schubiger, *J. Am. Chem. Soc.*, 2001, 123, 3135-3136.
11. R. Schibli and A. Schubiger, *Eur. J. Nucl. Med. Mol. Imaging*, 2002, 29, 1529-1542.
12. D. Rosita, M. A. DeWit and L. G. Luyt, *J. Med. Chem.*, 2009, 52, 2196-2203.
13. E. J. Simpson, J. L. Hickey, D. Breadner and L. G. Luyt, *Dalton Trans.*, 2012, 41, 2950-2958.
14. J. K. Pak, P. Benny, B. Spingler, K. Ortner and R. Alberto, *Chemistry*, 2003, 9, 2053-2061.
15. D. R. van Staveren, S. Mundwiler, U. Hoffmanns, J. K. Pak, B. Spingler, N. Metzler-Nolte and R. Alberto, *Org. Biomol. Chem.*, 2004, 2, 2593-2603.
16. C. W. Tornøe, C. Christensen and M. Meldal, *J. Org. Chem.*, 2002, 67, 3057-3064.
17. V. V. Rostovtsev, L. G. Green, V. V. Fokin and K. B. Sharpless, *Angew. Chem., Int. Ed.*, 2002, 41, 2596-2599.
18. M. Meldal and C. W. Tornøe, *Chem. Rev.*, 2008, 108, 2952-3015.
19. T. L. Mindt, H. Struthers, L. Brans, T. Anguelov, C. Schweinsberg, V. Maes, D. Tourwé and R. Schibli, *J. Am. Chem. Soc.*, 2006, 128, 15096-15097.
20. H. Struthers, B. Spingler, T. L. Mindt and R. Schibli, *Chemistry*, 2008, 14, 6173-6183.
21. T. L. Mindt, C. Muller, M. Melis, M. de Jong and R. Schibli, *Bioconjug. Chem.*, 2008, 19, 1689-1695.

22. C. A. Kluba and T. L. Mindt, *Molecules*, 2013, 18, 3206-3226.
23. R. Schibli and A. Schubiger, *Eur. J. Nucl. Med.*, 2002, 29, 1529-1542.
24. R. La Bella, E. Garcia-Garayoa, M. Langer, P. Bläuenstein, A. G. Beck-Sickinger and P. August Schubiger, *Nucl. Med. Biol.*, 2002, 29, 553-560.
25. J. L. Hickey and L. G. Luyt, *Chem.--Eur. J.*, 2012, 18, 12999-13007.
26. E. Marsault and M. L. Peterson, *J. Med. Chem.*, 2011, 54, 1961-2004.
27. V. D. Bock, R. Perciaccante, T. P. Jansen, H. Hiemstra and J. H. van Maarseveen, *Org. Lett.*, 2006, 8, 919-922.
28. I. E. Valverde, A. Bauman, C. A. Kluba, S. Vomstein, M. A. Walter and T. L. Mindt, *Angew. Chem., Int. Ed.*, 2013, 52, 8957-8960.
29. H. He, M. Lipowska, X. Xu, A. T. Taylor, M. Carlone and L. G. Marzilli, *Inorg. Chem.*, 2005, 44, 5437-5446.
30. S. P. Schmidt, J. Nitschke, W. C. Trogler, S. I. Hockett and R. J. Angelici, *Inorg. Synth.*, 1989, 26, 113-117.
31. S. C. Bottorff, A. L. Moore, A. R. Wemple, D.-K. Bučar, L. R. MacGillivray and P. D. Benny, *Inorg. Chem.*, 2013, 52, 2939-2950.
32. E. D. Goddard-Borger and R. V. Stick, *Org. Lett.*, 2007, 9, 3797-3800.
33. R. Alberto, A. Egli, U. Abram, K. Hegetschweiler, V. Gramlich and P. A. Schubiger, *J. Chem. Soc., Dalton Trans.*, 1994, 2815-2820.

Chapter 4

4 Cyclized Pentapeptides as [2+1] Chelation Systems for $[\text{}^{99\text{m}}\text{Tc/Re}(\text{CO})_3]^+$

4.1 Introduction

Cyclic peptides are increasingly of interest in the development of pharmaceutical products due to their improved stability, conformational constraint providing enhanced target affinity and the potential for better mimicking protein:protein interactions as compared to small molecules. As opposed to inherently flexible linear peptides, cyclic peptides have a locked conformation and thus maintain a desirable secondary structure, resulting in a higher binding affinity.¹ As well, they are more resistant to enzymatic degradation, giving them a much longer *in vivo* half-life.² Another method of peptide cyclization is through metal binding using amino acid side chains that have been found to coordinate metals in metalloproteins.

Naturally occurring metalloproteins are known to bind a variety of metals through histidine residues, including copper in plastocyanin³ and hemocyanin,⁴ iron in hemoglobin,⁵ and zinc in thermolysin⁶ and zinc fingers.^{7, 8} In some cases this metal coordination through the histidine residues can influence the secondary structure of the protein. This can be seen with the native prion protein (PrP), which can selectively bind Cu^{2+} through four His residues.⁹ The binding mode of these four histidines with copper determines the secondary structure of the protein. Short protein fragments (<15 amino acids) however, are generally not thermodynamically stable enough to form helical turns in solution.^{10, 11} In order to induce a turn conformation in these short protein fragments, metal clips have been developed that can coordinate metals such as copper, palladium,

rhodium and ruthenium. These small peptide metal clips use two histidine residues separated by three amino acids, which stabilizes a short helical turn in aqueous solution.¹²⁻¹⁴

Histidine can also chelate $[\text{}^{99\text{m}}\text{Tc/Re}(\text{CO})_3]^+$ for use in molecular imaging probes as it displays high biological stability and specific activity, and is able to coordinate rapidly and quantitatively at low concentrations.¹⁵⁻¹⁷ N^α -substituted histidine has found use as a bifunctional chelator for labelling biologically relevant peptides as targeted molecular imaging probes.¹⁶⁻²² However, coordination using the secondary amine of this histidine analogue can form diastereomers.²³ To avoid isomer formation, histidine can also be used as a bidentate or monodentate chelator. Although it has been suggested that pro-tele (π - τ) linkage isomers of the histidine imidazole ring can form upon coordination with palladium,¹²⁻¹⁴ it has been shown that this is not the case when coordinating N^α -substituted histidine with $[\text{}^{99\text{m}}\text{Tc/Re}(\text{CO})_3]^+$.²³

Histidine has also been used in repeating linear sequences, known as histidine tags, to label proteins with Tc-99m.²⁴⁻³⁰ This process involves adding a sequence of histidines to the end of a protein in order to incorporate $[\text{}^{99\text{m}}\text{Tc}(\text{CO})_3]^+$ and effectively label the protein. The metal incorporation is due to the monodentate coordination with the imidazole of two different histidines in the sequence. While histidine has shown potential in both stabilizing turn conformations as well as coordination with technetium-99m, the ability of technetium coordination with histidine to form a cyclic structure for use in radiopharmaceuticals has not been investigated.

Pentapeptides of the form Ac-HXXXXH-OH have the potential to be cyclized with the two terminal histidines coordinating $[\text{}^{99\text{m}}\text{Tc/Re}(\text{CO})_3]^+$ in a [2+1] fashion using the imidazole of the N-terminal histidine, and the imidazole and carboxylic acid of the C-terminal histidine. Once a peptide is cyclized with technetium-99m, only the cyclic version will be biologically active and have a high binding affinity, whereas the more flexible linear peptide will not be able to bind as strongly to the target. Herein, we report on the ability of $[\text{}^{99\text{m}}\text{Tc/Re}(\text{CO})_3]^+$ to cyclize and coordinate a di-histidine containing pentapeptide of the form Ac-HAAAH-OH in a [2+1] fashion, and the method by which this coordination occurs, through NMR spectroscopy and computational studies.

4.2 Results & Discussion

In order to investigate the capability of $^{99\text{m}}\text{Tc/Re}$ tricarbonyl to form a metal clip, the pentapeptide Ac-HAAAH-OH was synthesized and characterized both prior to and following coordination with rhenium tricarbonyl. The peptide was designed to have two terminal histidines capable of coordinating rhenium or technetium, as well as three central alanine residues to aid in forming a turn in the peptide upon coordination, as alanine rich sequences have been shown to form stable α -helices in water.³¹ This would allow the peptide to coordinate the rhenium or technetium in a [2+1] fashion using the imidazole of the N-terminal histidine, and the imidazole and the carboxylic acid of the C-terminal histidine, resulting in a neutral peptide-metal complex.

It was predicted that, due to the findings in our previous exploration of histidine coordination with rhenium,²³ the imidazole-N1 of each histidine would preferentially coordinate to the rhenium. This coordination has also been proposed with histidine tags where Tc-99m coordinates to the peptide through the imidazole-N1 of the histidines.³²

This method of coordination was also hypothesized through computational studies suggesting that it is favourable for the $[\text{}^{99\text{m}}\text{Tc}(\text{CO})_3]^+$ to be coordinated with the imidazole-N1 of both His4 and His2 of a 5-His-tag.³³ This led to the proposed structure shown in Figure 4.1.

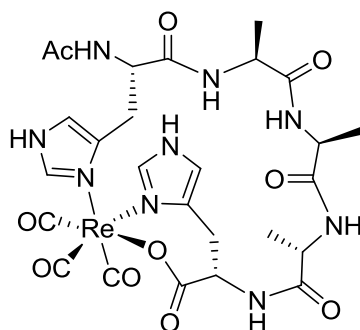
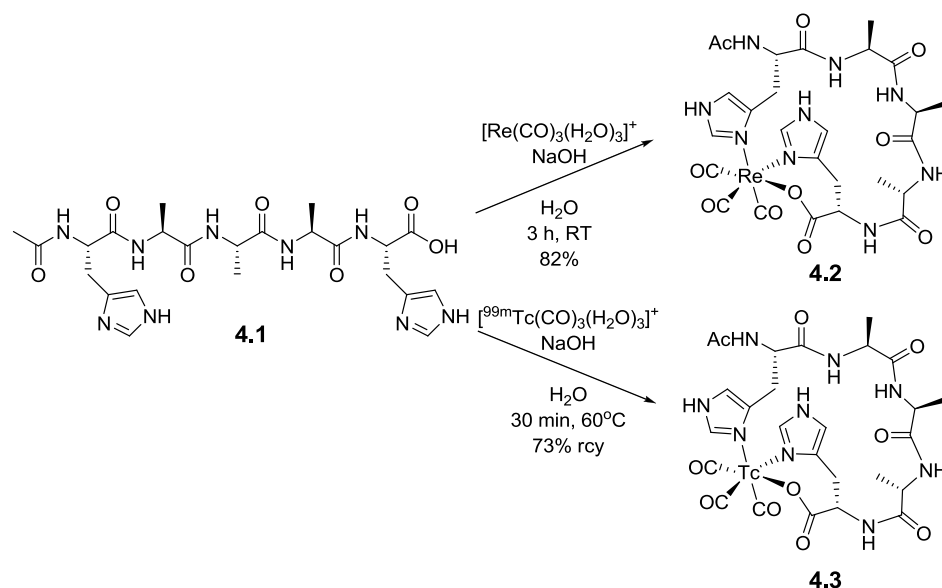


Figure 4.1: Proposed structure of the coordinated pentapeptide resulting in a cyclic, neutral peptide-metal complex

4.2.1 Peptide Synthesis

The acetylated pentapeptide Ac-HAAAHOH was assembled using standard 9-fluorenylmethoxycarbonyl (Fmoc) solid-phase peptide synthesis (SPPS)³⁴ on Wang resin pre-loaded with histidine. The peptide was synthesized and the N-terminal amine capped using 10% acetic anhydride in DMF. This peptide was then cleaved from the resin with trifluoroacetic acid (TFA) and precipitated using *tert*-butyl methyl ether (TBME). The peptide was then purified by preparative HPLC to give pure linear Ac-HAAAHOH (**4.1**). The peptide could then be cyclized and coordinated using $[\text{Re}(\text{CO})_3(\text{H}_2\text{O})_3]\text{OTf}$ ³⁵,³⁶ (Scheme 4.1). This was done by heating the peptide in a solution of water, NaOH and previously prepared $[\text{Re}(\text{CO})_3(\text{H}_2\text{O})_3]\text{OTf}$. Once coordinated, the peptide was purified by reverse-phase flash chromatography.



Scheme 4.1: Coordination of pentapeptide **4.1** with $[\text{Re}(\text{CO})_3]^+$ or $[\text{}^{99\text{m}}\text{Tc}(\text{CO})_3]^+$, resulting in cyclic peptides **4.2** and **4.3**

4.2.2 Radiolabelling

Peptide **4.1** was labelled with technetium-99m to give peptide **4.3** (Scheme 4.1). Addition of pertechnetate to a commercially available Isolink kit³⁷ formed the $[\text{}^{99\text{m}}\text{Tc}(\text{CO})_3(\text{H}_2\text{O})_3]^+$ starting material. The reduced Tc-99m was then added to a solution of **4.1** to form radiolabelled **4.3**. This was then purified using a Waters Sep-Pak C18 Plus Cartridge to give a decay corrected radiochemical yield of 73%. The success of the radiolabelling was confirmed by analytical UHPLC, where the retention time of the radiolabelled peptide **4.3** in the gamma trace correlated well with that of the rhenium coordinated peptide **4.2** in the UV chromatogram (Figure 4.2). From this, it could be seen that **4.1** was successfully labelled with $[\text{}^{99\text{m}}\text{Tc}(\text{CO})_3]^+$, forming peptide **4.3**.

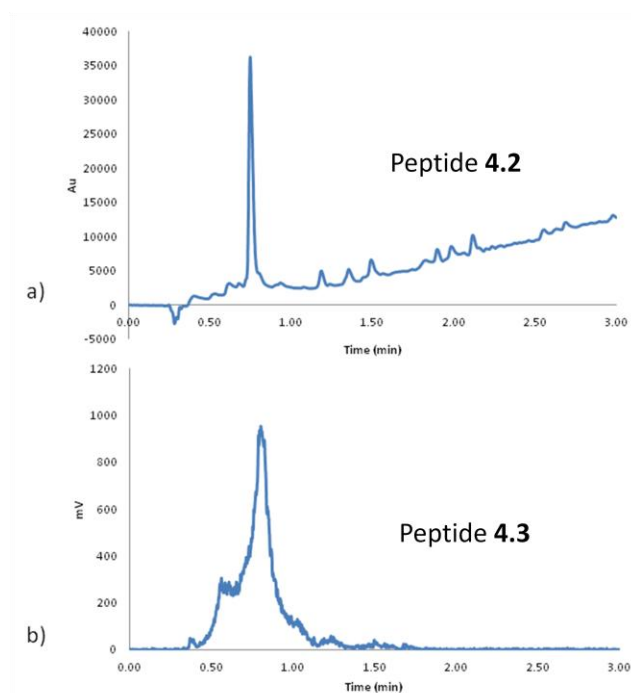


Figure 4.2: UHPLC analysis showing correlation between a) UV chromatogram of rhenium coordinated peptide **4.2**, and b) gamma trace of Tc-99m labelled peptide **4.3**

4.2.3 NMR Spectroscopy Studies

Through LC-MS studies, the purity and identity of the linear peptide **4.1** and coordinated peptide **4.2** were verified. However, further structural analysis through NMR spectroscopy was required. This was done using 1D ^1H NMR, 2D ^1H - ^1H NMR, as well as variable temperature (VT) NMR spectroscopy to determine if any hydrogen bonding existed in the coordinated species.

4.2.4 ^1H NMR Spectroscopic Analysis

Structure elucidation of both the linear (**4.1**) and the cyclized (**4.2**) peptides was accomplished through 1D ^1H , as well as 2D g-COSY and TOCSY NMR spectroscopy studies. Figure 4.3 shows the aromatic and methylene regions of the ^1H NMR for both the linear and coordinated peptides. When looking at the aromatic region (Figure 4.3a and b),

it can be seen that all four histidine imidazole protons shift significantly upfield in the coordinated peptide, as compared to the linear peptide. A considerable shift can also be seen for both the histidine and alanine amide protons. In the methylene region (Figure 4.3c and d), a dramatic shift can be seen in the histidine and alanine CH protons in the NMR spectrum of the coordinated peptide, when compared to that of the linear peptide.

The linear peptide displays pseudo-symmetry, causing several overlapping peaks in the ^1H NMR spectrum. However, once coordinated, a separation of peaks can be seen. This is evident in the methylene region for the histidine and alanine CH peaks, further verifying that the peptide is coordinated with rhenium. This overlapping of peaks can also be seen for the imidazole peaks in the linear peptide; however, once coordinated a unique chemical shift can be seen for all four imidazole protons. This indicates that both histidines are coordinated to the rhenium and that the peptide cyclizes as a result of coordination.

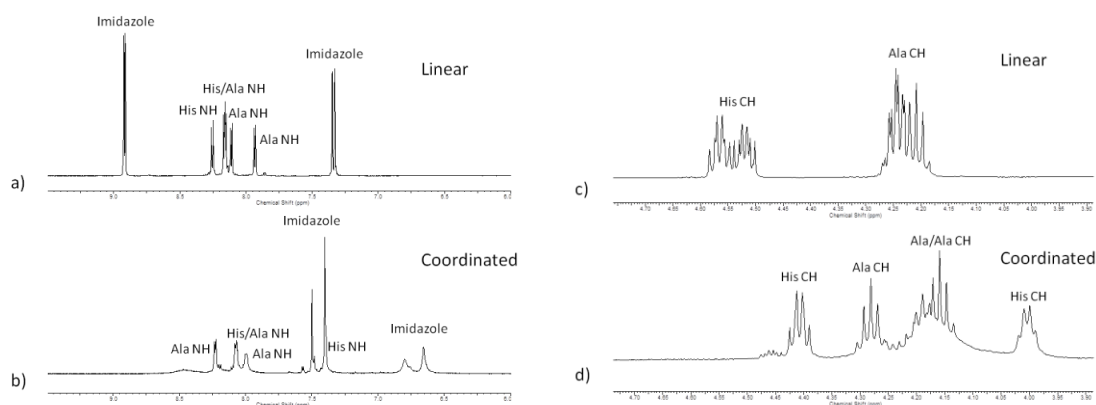


Figure 4.3: 1D ^1H NMR of the aromatic region of a) linear peptide **4.1** and b) coordinated peptide **4.2**, as well as the methylene region of c) linear peptide **4.1** and d) coordinated peptide **4.2** in DMSO- d_6 at 600 MHz

In order to identify individual amino acids and assign amide protons for variable temperature NMR, g-COSY and TOCSY experiments were also performed. Through the TOCSY NMR spectrum of the coordinated peptide **4.2**, it was possible to identify which peaks belonged to each amino acid. From the correlations of the alanine CH₃ to the CH peaks, it was possible to determine which CH peaks corresponded to alanine (A₁-A₃), and by default, which were histidine (H₁ and H₂) CH peaks (Figure 4.4a). The identity of the histidine CH peaks were further confirmed from the TOCSY correlations to the histidine CH₂ peaks (Figure 4.4b), allowing for assigning of individual histidines.

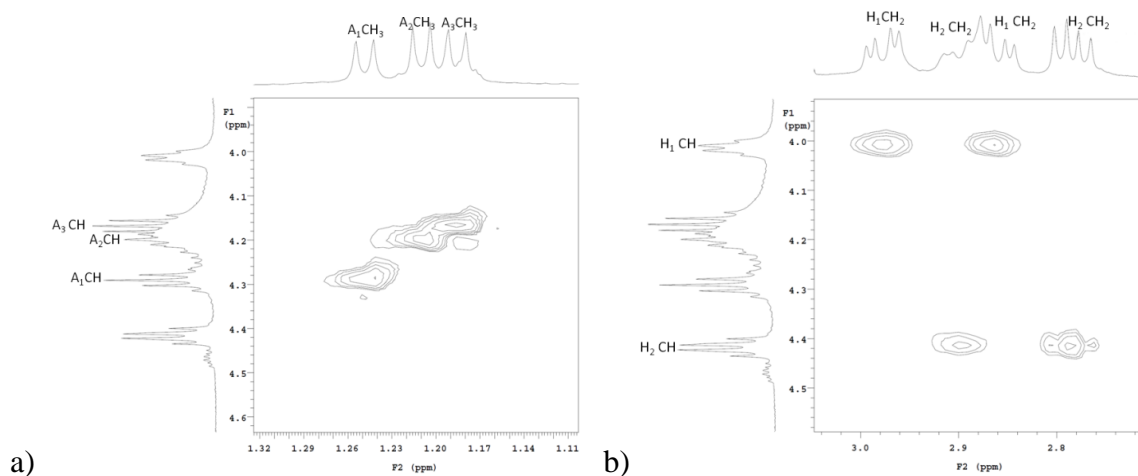


Figure 4.4: TOCSY NMR spectra of coordinated peptide **4.2** in DMSO-d₆ at 600 MHz, showing identification of a) alanine (A₁-A₃) CH and CH₃, and b) histidine (H₁ and H₂) CH and CH₂ protons

From the identified CH peaks, it was then possible to assign all amide protons to specific amino acids, as seen in Figure 4.5. With the identity of all the amide protons assigned, VT NMR could then be used to determine which of these amide protons participated in intramolecular hydrogen bonding. Further g-COSY and TOCSY spectra for both the linear and coordinated peptides can be seen in Appendix A.

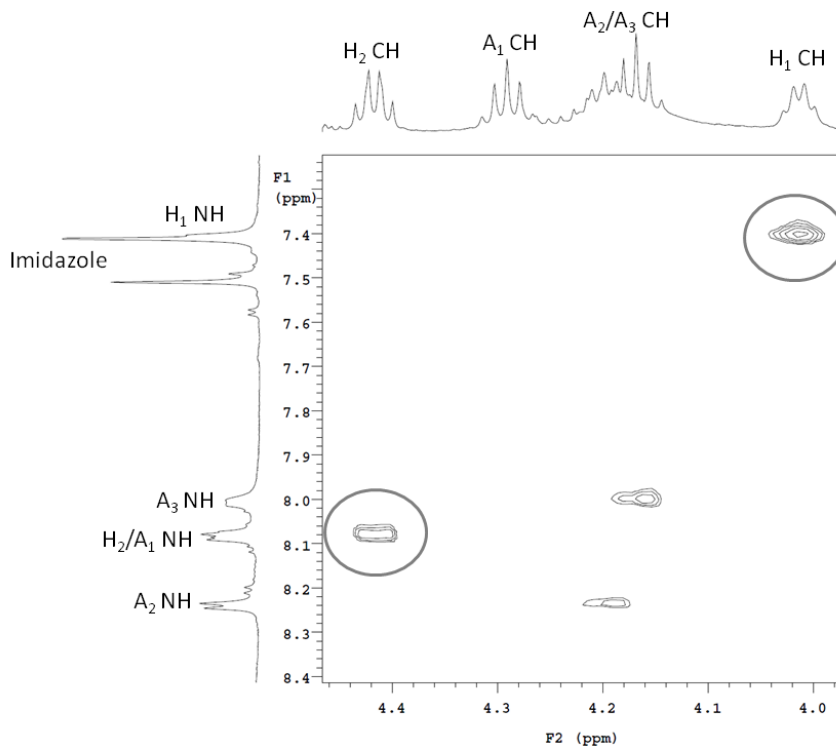


Figure 4.5: TOCSY NMR spectrum of coordinated peptide **4.2** in DMSO-d₆ at 600 MHz, showing identification of alanine (A₁-A₃) and histidine (H₁ and H₂) amide protons, as well as the much larger upfield shift of the H₁ amide and CH protons compared to that of H₂ (grey circles)

4.2.5 [2+1] Coordination

The ¹H NMR spectra shown in Figure 4.3, shows a much larger shift in both the amide and CH protons of one of the histidines. From the TOCSY NMR in Figure 4.5, it can be seen that the amide and CH protons that have a larger shift both correspond to the same histidine (H₁); whereas the amide and CH protons that have a smaller shift, both correspond to H₂. A study on the coordination of histidine with rhenium was previously published in our lab and in Chapter 2.²³ In Chapter 2, a benzylated histidine was coordinated with rhenium through the imidazole, the carboxylic acid, and the secondary amine of the histidine. When comparing the shifts seen upon coordination, the ¹H NMR spectrum in the current study shows nearly identical changes in shift in the CH proton of

H₁ to that seen in the previous study, while the CH proton of H₂ varies significantly from that seen previously, as described in Chapter 2.

Previously, the CH proton shifted from 4.25 ppm to 3.72 ppm upon coordination; a shift of 0.53 ppm. In the current study, the CH proton of H₁ shifts from 4.52 ppm to 4.00 ppm; a shift of 0.52 ppm. However, the CH proton of H₂ only shifts from 4.56 ppm to 4.41 ppm; a shift of 0.15 ppm. This comparison in shifts suggests that H₁ is the C-terminal histidine, and that it is coordinated to the rhenium through both the imidazole and the free carboxylic acid giving the desired [2+1] coordination of the peptide to rhenium.

4.2.6 Variable Temperature ¹H NMR Spectroscopy

Once the amide peaks were assigned to individual amino acids, it was possible to determine which of these displays intramolecular hydrogen bonding interactions. The most common method for identifying the presence of intramolecular hydrogen bonds in a peptide is through VT NMR spectroscopy.³⁸⁻⁴⁰ The chemical shifts of amide protons involved in intramolecular hydrogen bonding will not be as sensitive to changes in temperature as those that are not hydrogen bonded, or are intermolecularly hydrogen bonded to the surrounding solvent. Increasing temperature causes an upfield shift in amide protons; however, the shift is much less if the proton is hydrogen bonded. This can be tracked quantitatively by dividing the change in shift over the change in temperature ($\Delta\delta/\Delta T$), with $\Delta\delta/\Delta T$ values that are more positive than -4.6 ppb/K corresponding to protons that are involved in intramolecular hydrogen bonding.^{41, 42}

VT NMR spectroscopy studies were performed on the coordinated peptide **4.2** in dimethylsulfoxide-d₆ (DMSO-d₆) from 25-60°C at 5°C intervals. The series of ¹H NMR

spectra obtained can be seen in Figure 4.6. As the temperature is increased, a difference in the magnitude of the change in shift of each individual proton can be seen. When converted to a $\Delta\delta/\Delta T$ value (Table 4.1), it can be seen that both histidine amide protons as well as two of the three alanine amide protons seem to be intramolecularly hydrogen bonded.

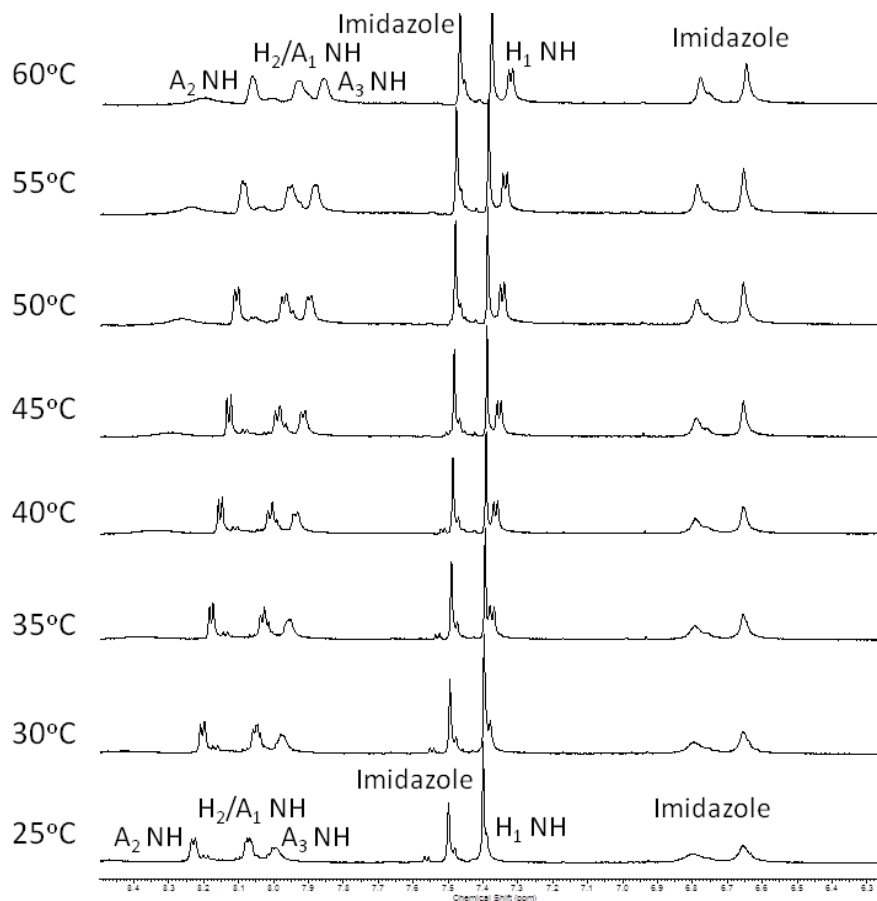


Figure 4.6: VT ^1H NMR of coordinated peptide **4.2** in DMSO- d_6 at 5°C intervals from 25 - 60°C at 600 MHz

Table 4.1: The $\Delta\delta/\Delta T$ values obtained from the VT ^1H NMR analysis for each amide proton in peptide **4.2**

$\Delta\delta/\Delta T$ (ppb/K)			
A_2 NH	H_2/A_1 NH	A_3 NH	H_1 NH
-4.6	-3.7	-3.7	-2.0

4.2.7 Computational Studies

In order to determine if the proposed structure in Figure 4.1 matched the results from the VT NMR spectra, computational studies were performed for the coordinated peptide. There is potential for the formation of four isomers upon coordination of the linear peptide **4.1** with $[\text{Re}(\text{CO})_3]^+$ (Figure 4.7). Two of these isomers are diastereomers (**4.2a** and **4.2b**), while **4.2c** and **4.2d** are conformational isomers of **4.2a** and **4.2b**, respectively, which exist due to the restricted rotation of the macrocycle. All isomers were optimized using density functional theory (DFT), employing the B3LYP functional.

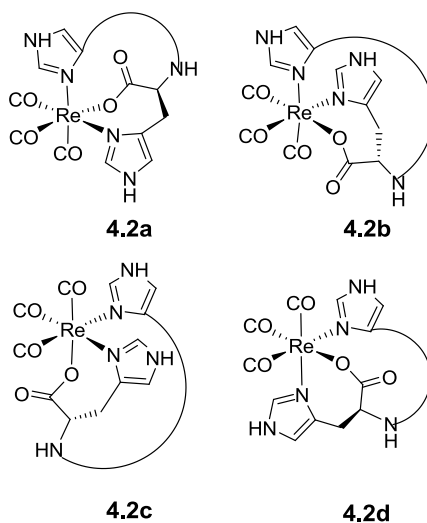


Figure 4.7: Four possible isomers of the proposed structure for cyclized peptide **4.2**, where **4.2a** and **4.2b** are diastereomers, and **4.2c** and **4.2d** are conformational isomers of **4.2a** and **4.2b**, respectively

In comparing to the VT NMR spectroscopy results, we were surprised to find that the lowest energy isomer (**4.2a**) revealed hydrogen bonding for only two of the alanine amides (Figure 4.8). This was not in concordance with what was seen for the VT NMR studies. The other three possible isomers (**4.2b-d** seen in Appendix A) also did not show

the expected hydrogen bonding. Therefore, the proposed structure based upon the expected N1 nitrogen coordination for both imidazole heterocycles did not appear to be in agreement with the computational results.

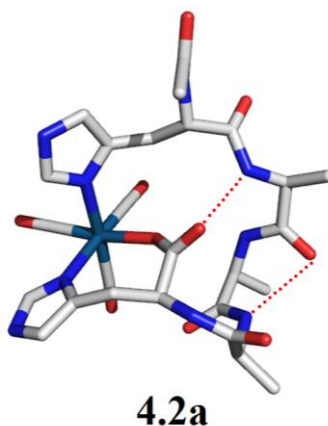


Figure 4.8: Lowest energy isomer (**4.2a**) of the proposed structure of cyclized peptide **4.2** showing intramolecular hydrogen bonding interactions

As was discussed previously in Chapter 2,²³ the C-terminal histidine can only coordinate to the rhenium through the imidazole-N1 when the carboxylic acid of the histidine is also coordinated to the rhenium in a bidentate fashion. Therefore, it is not possible for the C-terminal histidine to coordinate to the rhenium with the imidazole-N3. However, as was seen previously with this peptide when coordinated to palladium, linkage isomers of histidine can form when coordinated in a monodentate fashion where either the imidazole-N1 or N3 can coordinate.^{12, 13} Therefore, the N-terminal histidine should be able to coordinate rhenium with either the imidazole-N1 or N3 when coordinating in a monodentate fashion.

Therefore, calculations were performed on a new structure where the N-terminal histidine was coordinated to the rhenium through the imidazole-N3. This method of coordination

gives another four possible isomers (Figure 4.9) where **4.2e** and **4.2f** are diastereomers, and **4.2g** and **4.2h** are conformational isomers of **4.2e** and **4.2f**, respectively, resulting in a possibility of eight total isomers for the [2+1] coordination.

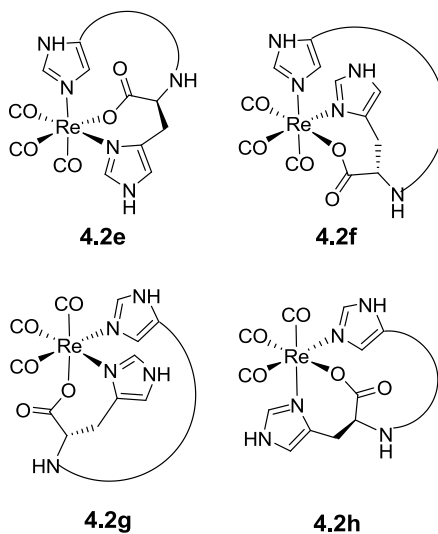


Figure 4.9: Four possible isomers of the new proposed structure for cyclized peptide **4.2**, where **4.2e** and **4.2f** are diastereomers, and **4.2g** and **4.2h** are conformational isomers of **4.2e** and **4.2f**, respectively

Although three of the isomers for this new proposed structure did not show any hydrogen bonding (**4.2f-h** seen in Appendix A), the lowest energy isomer (**4.2e**) (Figure 4.10) did show intramolecular hydrogen bonding for both histidine amides as well as two of the alanine amides, while one alanine amide did not display intramolecular hydrogen bonding. This matched perfectly with what was determined from the VT NMR studies. Therefore, it was concluded that this new proposed structure is the most likely method of coordination for the cyclized peptide **4.2**.

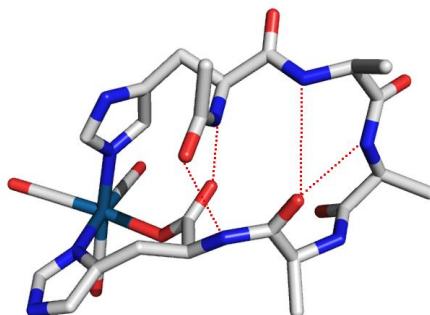
**4.2e**

Figure 4.10: Lowest energy isomer (**4.2e**) of the new proposed structure of cyclized peptide **4.2** showing intramolecular hydrogen bonding interactions

4.3 Conclusions

A peptide of the form Ac-HAAAH-OH was synthesized and coordinated with $[^{99m}\text{Tc}/\text{Re}(\text{CO})_3]^+$ in a [2+1] fashion using the imidazole of the N-terminal histidine and the imidazole and free carboxylic acid of the C-terminal histidine. The structure was evaluated through ^1H , g-COSY, and TOCSY NMR spectroscopy. These NMR spectra confirmed that both histidines were coordinated to the metal in a [2+1] fashion. VT NMR studies were completed to determine which amide protons displayed intramolecular hydrogen bonding interactions. Computational studies showed that none of the four possible isomers of the original proposed structure in Figure 4.1 matched the results from the VT NMR spectra. As a result, the proposed structure was altered such that the N-terminal histidine coordinated the metal instead through the imidazole-N3. This also gave four potential isomers, with the lowest energy isomer matching with the experimental data from the VT NMR. This led to the conclusion that structure **4.2e** seen in Figure 4.11 is the most likely structure of the cyclized peptide.

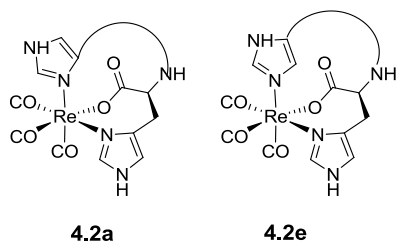


Figure 4.11: Structures of the two lowest energy isomers of $\text{Re}(\text{CO})_3\text{-Ac-HAAA-H-OH}$ (**4.2**), with **4.2e** being the most likely isomer based on VT NMR spectroscopy and computational studies

The results from the VT NMR spectra when combined with the computational studies gives a much better understanding of the coordination of histidine with $[\text{}^{99\text{m}}\text{Tc}/\text{Re}(\text{CO})_3]^+$. This discovery is important when coordinating histidine in a monodentate fashion, which is relevant not only for coordination of these [2+1] HXXXH peptide systems, but also when preparing His tags for radiolabelling proteins. This method of [2+1] coordination using terminal histidines provides a quick and easy way to simultaneously cyclize and coordinate biologically relevant peptides for use as molecular imaging probes.

4.4 Experimental

Materials & Methods

All chemicals were purchased from Sigma-Aldrich, Novabiochem, Aapptec, Peptides International and Chem-Impex and were used without further purification unless indicated. For LC-MS, a Waters, Inc. system was used, consisting of a Waters 2998 Photodiode Array Detector and a Waters 2767 Sample Manager. For analytical LC-MS studies, a Waters Atlantis RP-C18 4.6 x 150 mm, 5 μm column was used. For preparative LC-MS work, a Waters Atlantis RP-C18 19 x 150 mm, 5 μm column was used. In both cases, absorbance was detected at wavelengths of 220 nm and 254 nm. A gradient solvent

system consisting of CH₃CN + 0.1% TFA (solvent A) and H₂O + 0.1% TFA (solvent B) was used. For analytical UHPLC-MS studies, a Waters, Inc. Acquity UPLC H-Class system was used, combined with a Xevo QToF and a Bioscan Inc. FC-1000 Flow-Count Radio-HPLC Detector System. For analytical UHPLC studies, a Waters Acquity UPLC BEH C18 2.1 x 50 mm, 1.7 μm column was used. A gradient solvent system consisting of CH₃OH + 0.1% formic acid (solvent C) and H₂O + 0.1% formic acid (solvent D) was used. A Biotage Isolera One flash chromatography system was used for flash column chromatography purification fitted with a Snap 12 g reversed phase C-18 column. Analtech HPTLC-RP18F reversed phase plates were used for analytical TLC. Varian INOVA 600 NMR spectrometer was used for ¹H, g-COSY and TOCSY NMR studies. Chemical shifts are reported in parts per million (ppm) relative to TMS (0.00 ppm). For electron impact (EI) mass spectra a Finnigan MAT 8400 mass spectrometer was used and for electro-spray ionization (ESI) mass spectra a Micromass Quattro Micro API mass spectrometer was used.

Ac-HAAA-H-OH (4.1)

Pentapeptide **4.1** was synthesized on-resin using standard Fmoc solid-phase peptide chemistry by manual synthesis using Wang resin (0.5 mmol, loading 0.34 mmol/g) pre-loaded with Fmoc protected histidine. Removal of Fmoc was carried out using 20% piperidine in DMF for 5 and 15 minutes, each followed by rinses with dichloromethane (DCM) and *N,N*-dimethylformamide (DMF). Fmoc-Ala-OH was then coupled twice for 30 min and 1 h using 3 eq. of Fmoc amino acid, 3 eq. of 2-(6-chloro-1H-benzotriazole-1-yl)-1,1,3,3-tetramethylaminium hexafluorophosphate (HCTU) and 6 eq. of *N,N*-diisopropylethylamine (DIPEA) in 15 mL DMF. This was repeated 2 more times with

Fmoc-Ala-OH, followed by Fmoc-His(Trt)-OH. The peptide was then capped by treatment with 10% acetic anhydride in DMF twice for 15 min. Once complete, the peptide was deprotected and cleaved from the resin by treatment with TFA containing water (2.5% v/v) and triisopropylsilane (2.5% v/v) as scavengers for 4 h. The peptide was then precipitated from the cleavage solution by treatment with cold TBME followed by centrifugation and decanting of the ether. Purification was performed by preparative HPLC (linear gradient of 0-30% solvent A in B). The purity of the resultant peptide was determined to be 95% pure by analytical LC-MS (linear gradient of 5-40% solvent A in B). This resulted in a 56% yield of **4.1** (0.155 g, 0.28 mmol). HRMS: m/z calculated for $C_{23}H_{33}N_9O_7$, 548.2581; observed $[M+H]^+$ 548.2575. 1H -NMR Spectrum (600 MHz, DMSO- d_6 , δ): 8.92 (1H, d, imidazole, $^4J_{H-H} = 1.2$ Hz), 8.91 (1H, d, imidazole, $^4J_{H-H} = 1.2$ Hz), 8.25 (1H, d, NH of His, $^3J_{H-H} = 7.6$ Hz), 8.17 (1H, d, NH of His, $^3J_{H-H} = 8.2$ Hz), 8.16 (1H, d, NH of Ala, $^3J_{H-H} = 6.5$ Hz), 8.11 (1H, d, NH of Ala, $^3J_{H-H} = 7.0$ Hz), 7.93 (1H, d, NH of Ala, $^3J_{H-H} = 7.6$ Hz), 7.35 (1H, s, imidazole), 7.33 (1H, s, imidazole), 4.56 (1H, ddd, CH of His, $^3J_{H-H} = 8.2$ Hz, $^3J_{H-H} = 5.9$ Hz), 4.52 (1H, ddd, CH of His, $^3J_{H-H} = 8.2$ Hz, $^3J_{H-H} = 5.3$ Hz), 4.20-4.26 (3H, m, CH of Ala), 3.13 (1H, dd, CH_2 of His, $^2J_{H-H} = 15.8$ Hz, $^3J_{H-H} = 5.3$ Hz), 3.03 (1H, dd, CH_2 of His, $^2J_{H-H} = 15.3$ Hz, $^3J_{H-H} = 5.9$ Hz), 3.00 (1H, dd, CH_2 of His, $^2J_{H-H} = 15.3$ Hz, $^3J_{H-H} = 8.8$ Hz), 2.91 (1H, dd, CH_2 of His, $^2J_{H-H} = 15.3$ Hz, $^3J_{H-H} = 8.2$ Hz), 1.81 (3H, s, $CH_3C(O)NH$), 1.21 (3H, d, CH_3 of Ala, $^3J_{H-H} = 7.0$ Hz), 1.18 (3H, d, CH_3 of Ala, $^3J_{H-H} = 7.0$ Hz), 1.17 (3H, d, CH_3 of Ala, $^3J_{H-H} = 7.0$ Hz).

Re(CO)₃-Ac-HAAA-H-OH (4.2)

Purified linear peptide **4.1** (60 mg, 0.11 mmol) was coordinated with 0.9 equivalents of $[Re(CO)_3(H_2O)_3]OTf$ (990 μ L of a 0.1 M solution, 0.10 mmol), using 5 equivalents of

NaOH (109.5 μL of a 5 M solution, 0.55 mmol) in H_2O (6 mL). This was stirred at room temperature for 3 hours, followed by lyophilization. The crude coordinated peptide was purified by reverse-phase flash chromatography (linear gradient of 12 – 100% methanol in water). This resulted in an 82% yield of **4.2** (70 mg, 0.09 mmol). HRMS: m/z calculated for $\text{C}_{26}\text{H}_{33}\text{N}_9\text{O}_{10}^{185/187}\text{Re}$, 816.1880/818.1909; observed $[\text{M}+\text{H}]^+$ 816.1948/818.2047. $^1\text{H-NMR}$ Spectrum (600 MHz, DMSO-d_6 , δ): 8.22 (1H, d, NH of Ala, $^3J_{\text{H-H}} = 6.5$ Hz), 8.06-8.08 (2H, m, NH of His and Ala), 7.99-8.00 (1H, m, NH of Ala), 7.50 (1H, s, imidazole), 7.39-7.40 (2H, m, imidazole and NH of His), 6.80 (1H, s, imidazole), 6.66 (1H, s, imidazole), 4.40 (1H, dd, CH of His, $^3J_{\text{H-H}} = 7.6$ Hz, $^3J_{\text{H-H}} = 13.5$ Hz), 4.28 (1H, dq, CH of Ala, $^3J_{\text{H-H}} = 7.0$ Hz), 4.13-4.22 (2H, m CH of Ala), 4.00 (1H, dd, CH of His, $^3J_{\text{H-H}} = 5.9$ Hz, $^3J_{\text{H-H}} = 11.7$ Hz), 2.97 (1H, dd, CH_2 of His, $^2J_{\text{H-H}} = 14.7$ Hz, $^3J_{\text{H-H}} = 5.3$ Hz), 2.83-2.91 (2H, m, CH_2 of His), 2.77 (1H, dd, CH_2 of His, $^2J_{\text{H-H}} = 14.7$ Hz, $^3J_{\text{H-H}} = 7.6$ Hz), 1.81 (3H, s, $\text{CH}_3\text{C}(\text{O})\text{NH}$), 1.23 (3H, d, CH_3 of Ala, $^3J_{\text{H-H}} = 7.0$ Hz), 1.19 (3H, d, CH_3 of Ala, $^3J_{\text{H-H}} = 7.0$ Hz), 1.18 (3H, d, CH_3 of Ala, $^3J_{\text{H-H}} = 7.0$ Hz).

$^{99\text{m}}\text{Tc}(\text{CO})_3\text{-Ac-HAAA-H-OH}$ (4.3)

To an Isolink kit containing sodium tartrate, sodium tetraborate, sodium carbonate, and sodium boranocarbonate, 1361 MBq (1.0 mL) of [$^{99\text{m}}\text{Tc}$]-pertechnetate was added. This was stirred at 90°C . After 20 min, 120 μL of 1 M HCl was added and was allowed to stand for 5 min. 272 MBq (300 μL) was then added to **4.1** (0.5 mg, 0.9 μmol) to a total volume of 1 mL H_2O . To this, 10 eq NaOH (12 μL of a 5 M solution, 9 μmol) was added to a pH of 12, and stirred at 60°C for 30 min. UHPLC analysis showed retention time of 0.80 min for **4.3** at a linear gradient of 20-80% solvent C in D for 3 min. UHPLC analysis of **4.2** showed retention time of 0.75 min for the same gradient system. The labelled

peptide **4.3** was then purified using a Waters Sep-Pak Plus C18 Cartridge by eluting with 5 mL H₂O and 5 mL MeOH. This resulted in a 73% decay corrected radiochemical yield.

Computational Studies

All the structures were initially constructed by DS viewer 3.5. The structures were first optimized using semi-empirical PM6 method. Further optimizations of the structures were performed using density functional theory (DFT), employing the B3LYP functional. The LANL2DZ pseudopotential⁴³⁻⁴⁵ and the 6-31G(d) basis set were used to model rhenium and the remaining atoms, respectively. No geometry restraint was applied during all optimizations. The nature of the optimized structures and energy minima were defined by subsequent frequency calculations. All calculated structures were characterized as true minima (i.e., no imaginary frequencies). All the calculations were performed with Gaussian 09 (RevD.01)⁴⁶ on high-performance computing (HPC) facilities within the Compute Canada network.⁴⁷

4.5 References

1. E. Marsault and M. L. Peterson, *J. Med. Chem.*, 2011, 54, 1961-2004.
2. C. J. White and A. K. Yudin, *Nature Chem.*, 2011, 3, 509-524.
3. Y. Xue, M. Okvist, O. Hansson and S. Young, *Protein Sci.*, 1998, 7, 2099-2105.
4. K. A. Magnus, B. Hazes, H. Ton-That, C. Bonaventura, J. Bonaventura and W. G. Hol, *Proteins*, 1994, 19, 302-309.
5. M. F. Perutz, *Nature*, 1970, 228, 726-734.
6. D. R. Holland, A. C. Hausrath, D. Juers and B. W. Matthews, *Protein Sci.*, 1995, 4, 1955-1965.
7. H. A. Greisman and C. O. Pabo, *Science*, 1997, 275, 657-661.

8. B. A. Krizek, B. T. Amann, V. J. Kilfoil, D. L. Merkle and J. M. Berg, *J. Am. Chem. Soc.*, 1991, 113, 4518-4523.
9. G. Di Natale, K. Ösz, Z. Nagy, D. Sanna, G. Micera, G. Pappalardo, I. Sóvágó and E. Rizzarell, *Inorg. Chem.*, 2009, 48, 4239-4250.
10. B. H. Zimm and J. K. Bragg, *The Journal of Chemical Physics*, 1959, 31, 526-535.
11. J. M. Scholtz and R. L. Baldwin, *Annu. Rev. Biophys. Biomol. Struct.*, 1992, 21, 95-118.
12. M. T. Ma, H. N. Hoang, C. C. G. Scully, T. G. Appleton and D. P. Fairlie, *J. Am. Chem. Soc.*, 2009, 131, 4505-4512.
13. H. N. Hoang, G. K. Bryant, M. J. Kelso, R. L. Beyer, T. G. Appleton and D. P. Fairlie, *Inorg. Chem.*, 2008, 47, 9439-9449.
14. M. J. Kelso, H. N. Hoang, T. G. Appleton and D. P. Fairlie, *J. Am. Chem. Soc.*, 2000, 122, 10488-10489.
15. D. R. van Staveren, S. Mundwiler, U. Hoffmanns, J. K. Pak, B. Spingler, N. Metzler-Nolte and R. Alberto, *Org. Biomol. Chem.*, 2004, 2, 2593-2603.
16. A. Egli, R. Alberto, L. Tannahill, R. Schibli, U. Abram, A. Schaffland, R. Waibel, D. Tourwé, L. Jeannin, K. Iterbeke and P. A. Schubiger, *J. Nucl. Med.*, 1999, 40, 1913-1917.
17. J. K. Pak, P. Benny, B. Spingler, K. Ortner and R. Alberto, *Chem.--Eur. J.*, 2003, 9, 2053-2061.
18. V. Maes and D. Tourwé, *Int. J. Peptide Res. Therapeut.*, 2006, 12, 197-202.
19. V. Maes, E. Garcia-Garayoa, P. Bläuenstein and D. Tourwé, *J. Med. Chem.*, 2006, 49, 1833-1836.
20. R. Schibli, R. La Bella, R. Alberto, E. Garcia-Garayoa, K. Ortner, U. Abram and P. A. Schubiger, *Bioconjug. Chem.*, 2000, 11, 345-351.
21. C. Schweinsberg, V. Maes, L. Brans, P. Bläuenstein, D. A. Tourwé, P. A. Schubiger, R. Schibli and E. G. Garayoa, *Bioconjug. Chem.*, 2008, 19, 2432-2439.
22. X. Chen, R. Park, A. H. Shahinian, J. R. Bading and P. S. Conti, *Nucl. Med. Biol.*, 2004, 31, 11-19.
23. E. J. Simpson, J. L. Hickey, D. Breadner and L. G. Luyt, *Dalton Trans.*, 2012, 41, 2950-2958.

24. R. Waibel, R. Alberto, J. Willuda, R. Finnern, R. Schibli, A. Stichelberger, A. Egli, U. Abram, J.-P. Mach, A. Plückthun and P. A. Schubiger, *Nat. Biotech.*, 1999, 17, 897-901.
25. J. Willuda, A. Honegger, R. Waibel, P. A. Schubiger, R. Stahel, U. Zangemeister-Wittke and A. Plückthun, *Cancer Res.*, 1999, 59, 5758-5767.
26. J. Willuda, S. Kubetzko, R. Waibel, P. A. Schubiger, U. Zangemeister-Wittke and A. Plückthun, *J. Biol. Chem.*, 2001, 276, 14385-14392.
27. R. Tavaré, J. Williams, K. Howland, P. J. Blower and G. E. D. Mullen, *J. Inorg. Biochem.*, 2012, 114, 24-27.
28. A. Badar, J. Williams, R. de Rosales, R. Tavaré, F. Kampmeier, P. Blower and G. Mullen, *EJNMMI Research*, 2014, 4, 14.
29. R. Tavaré, R. Torres Martin De Rosales, P. J. Blower and G. E. D. Mullen, *Bioconjug. Chem.*, 2009, 20, 2071-2081.
30. Y. Yang, T. Neef, C. Mittelholzer, E. Garcia Garayoa, P. Blauenstein, R. Schibli, U. Aebi and P. Burkhard, *J. Nanobiotechnol.*, 2013, 11, 36.
31. S. Marqusee, V. H. Robbins and R. L. Baldwin, *Proc. Natl. Acad. Sci. U. S. A.*, 1989, 86, 5286-5290.
32. C. Hofström, M. Altai, H. Honarvar, J. Strand, J. Malmberg, S. J. Hosseinimehr, A. Orlova, T. Gräslund and V. Tolmachev, *J. Med. Chem.*, 2013, 56, 4966-4974.
33. R. Schibli and A. Schubiger, *Eur. J. Nucl. Med.*, 2002, 29, 1529-1542.
34. W. C. W. Chan, P. D., *Fmoc Solid Phase Peptide Synthesis: A Practical Approach*, Oxford University Press, New York, USA, 1 edn., 2000.
35. S. P. Schmidt, J. Nitschke, W. C. Trogler, S. I. Hockett and R. J. Angelici, *Inorg. Synth.*, 1989, 26, 113-117.
36. H. He, M. Lipowska, X. Xu, A. T. Taylor, M. Carlone and L. G. Marzilli, *Inorg. Chem.*, 2005, 44, 5437-5446.
37. R. Alberto, K. Ortner, N. Wheatley, R. Schibli and A. P. Schubiger, *J. Am. Chem. Soc.*, 2001, 123, 3135-3136.
38. H. Kessler, *Angew. Chem., Int. Ed.*, 1982, 21, 512-523.
39. N. Baxter and M. Williamson, *J. Biomol. NMR*, 1997, 9, 359-369.
40. S. H. Gellman, G. P. Dado, G. B. Liang and B. R. Adams, *J. Am. Chem. Soc.*, 1991, 113, 1164-1173.

41. T. Cierpicki and J. Otlewski, *J. Mol. Biol.*, 2000, 302, 1179-1192.
42. T. Cierpicki, I. Zhukov, R. A. Byrd and J. Otlewski, *J. Magn. Reson.*, 2002, 157, 178-180.
43. P. J. Hay and W. R. Wadt, *J. Chem. Phys.*, 1985, 82, 270-283.
44. W. R. Wadt and P. J. Hay, *J. Chem. Phys.*, 1985, 82, 284-298.
45. P. J. Hay and W. R. Wadt, *J. Chem. Phys.*, 1985, 82, 299-310.
46. Gaussian 09, Revision D.01, M. J. Frisch, G. W. Trucks, H. B. Schlegel, G. E. Scuseria, M. A. Robb, J. R. Cheeseman, G. Scalmani, V. Barone, B. Mennucci, G. A. Petersson, H. Nakatsuji, M. Caricato, X. Li, H. P. Hratchian, A. F. Izmaylov, J. Bloino, G. Zheng, J. L. Sonnenberg, M. Hada, M. Ehara, K. Toyota, R. Fukuda, J. Hasegawa, M. Ishida, T. Nakajima, Y. Honda, O. Kitao, H. Nakai, T. Vreven, J. A. Montgomery, Jr., J. E. Peralta, F. Ogliaro, M. Bearpark, J. J. Heyd, E. Brothers, K. N. Kudin, V. N. Staroverov, T. Keith, R. Kobayashi, J. Normand, K. Raghavachari, A. Rendell, J. C. Burant, S. S. Iyengar, J. Tomasi, M. Cossi, N. Rega, J. M. Millam, M. Klene, J. E. Knox, J. B. Cross, V. Bakken, C. Adamo, J. Jaramillo, R. Gomperts, R. E. Stratmann, O. Yazyev, A. J. Austin, R. Cammi, C. Pomelli, J. W. Ochterski, R. L. Martin, K. Morokuma, V. G. Zakrzewski, G. A. Voth, P. Salvador, J. J. Dannenberg, S. Dapprich, A. D. Daniels, O. Farkas, J. B. Foresman, J. V. Ortiz, J. Cioslowski, and D. J. Fox, Gaussian, Inc., Wallingford CT, 2013.
47. SHARCNET (www.sharcnet.ca) is a consortium of colleges, universities and research institutes operating a network of high-performance computer clusters across south western, central and northern Ontario.

Chapter 5

5 Bombesin Functionalized Water-Soluble Gold Nanoparticles for Prostate Cancer Targeting

5.1 Introduction

Prostate cancer is the most common cancer affecting Canadian men. It is estimated that 1 in 7 men will develop prostate cancer during their lifetime, and 1 in 28 will die from the disease.¹ If diagnosed early, the survival rate for prostate cancer is high, with the five year relative survival ratios in Canada being 96%.² Diagnosis of prostate cancer is difficult as symptoms are not always present in the early stages. Two common methods of diagnosis are the prostate specific antigen (PSA) test and the digital rectal exam. The accuracy of these invasive methods has recently been subject to debate.^{3, 4} Detection of cancer using molecular imaging offers a more accurate and non-invasive method of diagnosis by targeting receptors overexpressed on cancer cells. Prostate cancer imaging probes, for example, can target the overexpressed gastrin-releasing peptide receptor (GRP-R).^{5, 6} This targeting of overexpressed receptors can also be used for therapeutic purposes, as was shown by Plonowski et al., where a cytotoxic bombesin analogue was developed that targeted GRP-R and inhibited the growth of prostate cancer.⁷

Gold nanoparticles (AuNPs) have recently been used for applications in cancer targeting as they are the most stable metal nanoparticle, have low toxicity, are biocompatible, and their surface is easily functionalized.⁸⁻¹² The small size of AuNPs allows them to get close to a target; however, they are non-targeted. Tumour blood vessels formed through angiogenesis tend to be irregular and more permeable, allowing for “passive targeting” of AuNPs due to the enhanced permeability and retention (EPR) effect.¹³ Therefore, the

visualization and/or treatment of a desired target may be difficult with AuNPs as they can accumulate in various locations. For this reason, development of targeted AuNPs would be advantageous as they could accumulate in higher concentration in the tissue of interest, which could prove useful for both diagnostic and therapeutic purposes.

Nanoparticles show great potential for cancer targeting, as they are multifunctional. As a result, they can be used to attach not only a targeting entity to give the probe specificity, but also have the ability to attach an imaging moiety, allowing for external visualization;¹⁴⁻¹⁷ a druggable target for drug delivery;^{18, 19} or a radiotherapeutic isotope.²⁰ Therefore, nanoparticles can simultaneously be targeted using a peptide, antibody or small molecule, while still allowing for imaging or therapy through the attachment of a radioisotope, fluorescent dye or drug to the same nanoparticle. Targeted AuNPs can also be used to induce thermal ablation of tumours through irradiation with radio frequency (RF) radiation due to their inherent thermoablative properties.²¹

In a study by Morales-Avila et al., ^{99m}Tc labelled HYNIC-GGC was attached to gold nanoparticles, along with c[RGDfK(C)] to image tumour angiogenesis.²² Through *in vivo* mouse studies, they found that these nanoparticles showed increased tumour uptake when compared to ^{99m}Tc labelled HYNIC-c[RGDyK] which was not attached to the AuNPs. Therefore, attaching a known targeting peptide to gold nanoparticles can increase tumour uptake *in vivo*.

The AuNPs used in this study are spherical and small, approximately 3 nm.²³ Through PEGylation, these nanoparticles have been made water-soluble, making them suitable for biological studies. They are soluble not only in water, but also many other organic

solvents. These PEGylated AuNPs have been previously functionalized with a maleimide for use in Michael addition reactions.²⁴⁻²⁶ They have also been functionalized with an azide²⁷ or dibenzocyclooctyne (DBCO)²⁸ for use in interfacial strain-promoted azide-alkyne cycloaddition (*I*-SPAAC) reactions. In this study the AuNPs are functionalized with DBCO at the interface to be used in an *I*-SPAAC reaction with an azide functionalized peptide in order to make the AuNPs targeted. This method of bioconjugation gives the advantage of using a bioorthogonal “click” reaction that can be performed under copper free conditions, making it more suitable for biological studies than the copper-catalyzed azide-alkyne cycloaddition.

Targeting of AuNPs can be accomplished using a targeting entity, such as a peptide, antibody, or small molecule. One such peptide is bombesin, a tetradecapeptide isolated from the skin of the European fire-bellied toad, *Bombina bombina*.²⁹ It specifically targets cell surface gastrin-releasing peptide (GRP) receptors, which are overexpressed in prostate cancer cells,³⁰⁻³³ and has been shown to target prostate cancer when conjugated to nanoparticles.^{34, 35} There are four bombesin receptor subtypes that are known; BB1, BB2, BB3, and BB4. It was found that a truncated pan-bombesin, [D-Phe⁶, β-Ala¹¹, Phe¹³, Nle¹⁴]bombesin-(6-14) (Figure 5.1), successfully targets all four bombesin receptor subtypes with high affinity and specificity.³⁶⁻³⁸

Bombesin peptides have been shown to retain high affinity after extensive modifications to the N-terminus;^{30, 39-41} therefore, a PEG azide was added to the N-terminus of the pan-bombesin peptide not only to add the azide functionality, but to also provide distance between the targeting peptide and the nanoparticle. This allowed for attachment of the peptide to the DBCO functionalized AuNP through an *I*-SPAAC reaction. After

characterization through IR spectroscopy and ζ -potential analysis, these nanoparticles were then used for *in vitro* cell studies using a human prostate cancer cell line (PC-3) and the uptake visualized through transmission electron microscopy (TEM).

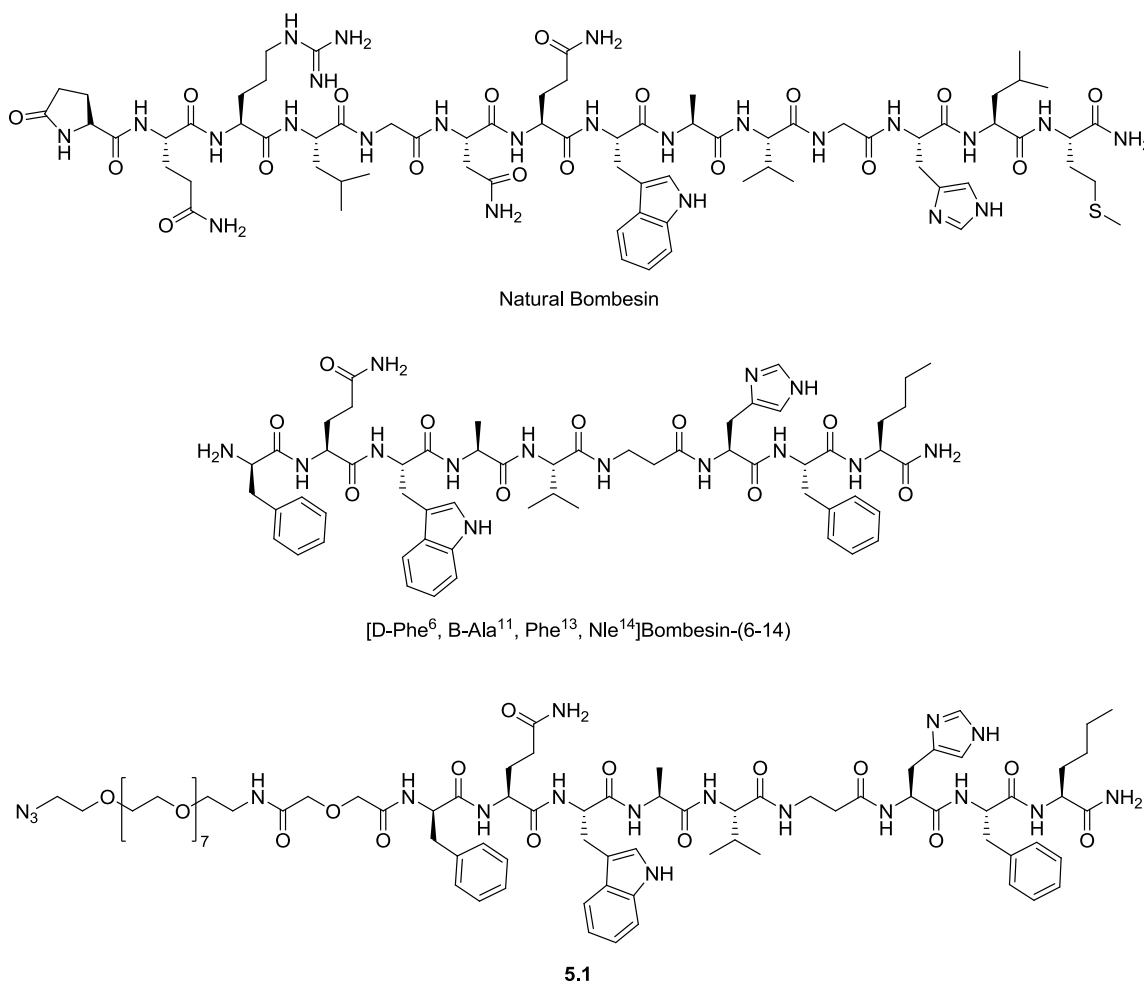


Figure 5.1: Structure of natural bombesin, truncated pan-bombesin, [D-Phe⁶, β -Ala¹¹, Phe¹³, Nle¹⁴]bombesin-(6-14) and the azide functionalized pan-bombesin peptide **5.1**

5.2 Results & Discussion

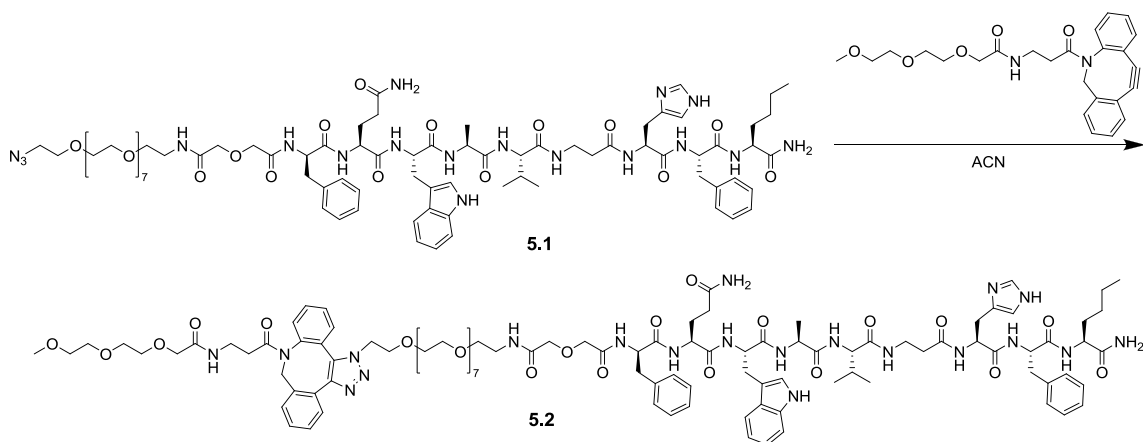
5.2.1 Peptide Synthesis

A pan-bombesin peptide, [D-Phe⁶, β -Ala¹¹, Phe¹³, Nle¹⁴]bombesin-(6-14), was synthesized by standard 9-fluorenylmethoxycarbonyl (Fmoc) solid-phase peptide

synthesis using rink amide 4-methylbenzhydrylamine (MBHA) resin. A PEG-azide was added to the N-terminus of the synthesized peptide through standard coupling methods in order to provide a point of attachment for the peptide to the DBCO functionalized AuNP through *I*-SPAAC (Figure 5.1). Once complete, the peptide was removed from the resin and purified by preparative HPLC-MS to give the desired azide modified pan-bombesin peptide **5.1**.

5.2.2 Model *I*-SPAAC Reaction

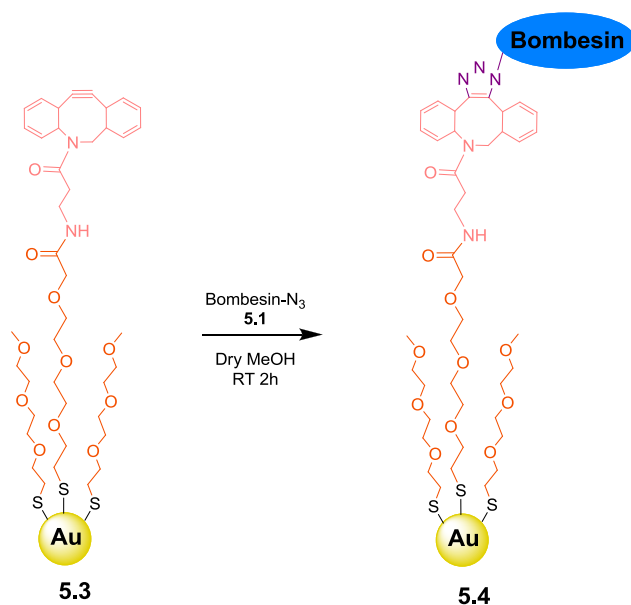
A model *I*-SPAAC reaction (Scheme 5.1) was performed using the bombesin azide peptide (**5.1**) and a PEGylated DBCO in acetonitrile. The reaction was followed by UHPLC-MS and was complete after 1 hour at room temperature, demonstrating the suitability of the synthesized peptide for an *I*-SPAAC reaction with the DBCO functionalized AuNP.



Scheme 5.1: Model *I*-SPAAC reaction of DBCO and bombesin azide peptide **5.1**

5.2.3 Functionalization of Gold Nanoparticles

The DBCO functionalized AuNPs were prepared according to previously published procedures.^{23, 28} The DBCO-AuNPs were then reacted with the bombesin azide peptide (**5.1**) in an *I*-SPAAC reaction (Scheme 5.2) giving a final yield of approximately 60% of reacted DBCO. This was slightly lower than the 70% yield seen with the Michael addition reaction of the maleimide-AuNPs,²⁴ and similar to the 60% yield seen with *I*-SPAAC reaction of the azide-AuNPs.²⁸ This relatively low yield is most likely due to the steric hindrance from the large size of the peptide and the small gold core diameter.



Scheme 5.2: *I*-SPAAC reaction between DBCO functionalized AuNPs and bombesin azide peptide **5.1**

The bombesin-AuNPs were characterized through IR spectroscopy and ζ -potential measurements. The IR spectrum of the bombesin-AuNPs (**5.4**) compared to that of bombesin-azide (**5.1**) and DBCO-AuNPs (**5.3**) (Figure 5.2) clearly shows the absence of the azide stretching mode at 2100 cm^{-1} , a marked increase of the N-H stretching at 3300

cm^{-1} and the appearance of a signal at 1624 cm^{-1} that corresponds to the amide bond stretch of the peptide which differs from the amide bond stretch of the DBCO-AuNPs, that instead falls at 1660 cm^{-1} . This indicates that the washing procedure used is effective in removing the unreacted peptide and that the peptide has been successfully conjugated to the AuNP surface.

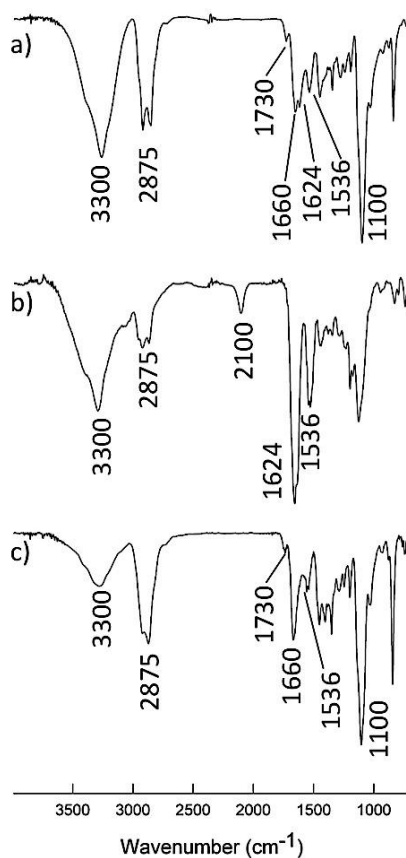


Figure 5.2: IR spectra of a) Bombesin-AuNPs (5.4), b) Bombesin-azide (5.1) and c) DBCO-AuNPs (5.3)

Finally, the success of the bioconjugation through the *I*-SPAAC reaction was confirmed by the change in the AuNPs surface charge. After the bioconjugation of the bombesin the ζ -potential of the AuNP shifts from -36.1 eV to -59.4 eV confirming the presence of the peptide on the AuNPs surface and showing an excellent stability of the AuNP-bioconjugate in an aqueous solution.

Toxicity of gold nanoparticles is size-dependent. It has been found that AuNPs between 1-2 nm are toxic, with nanoparticles that are either smaller or larger being non-toxic.^{42, 43} This is in part due to the fact that 1.4 nm AuNPs can fit into the major groove of DNA and coordinate irreversibly.⁴⁴ They also display reticuloendothelial system (RES) uptake, which causes accumulation in the liver, spleen, bone marrow, and other non-targeted areas. However, it was found that PEGylation of the nanoparticles can reduce this accumulation and increase circulation times as the nanoparticles become more hydrophilic and the surface energy is decreased, resulting in less aggregation of the nanoparticles.⁴⁵

This reduction in toxicity through PEGylation also applies to small gold nanoparticles. In a study by Gu, et al., it was shown through cell viability tests that PEGylated 3.7 nm AuNPs showed higher than 85% cell viability after incubation with a 10 μ M of the nanoparticles for 24 h, and 70% cell viability after 72 h.⁴⁶ A previous study was performed with the same 3 nm AuNPs used in the current study. The AuNPs were conjugated with a gadolinium(III) chelate for *in vivo* mouse studies using MRI.²⁴ In the study, 200 μ L of 10 mM Gd^{3+} -AuNPs were injected into the tail vein of a mouse. It was found that 24 h post-scan, the mouse showed no ill effects. Therefore, these small, PEGylated AuNPs do not appear to be toxic.

5.2.4 Transmission Electron Microscopy

In vitro cell studies were performed using PC-3 cells, a human prostate cancer cell line that is androgen independent and highly tumorigenic. This cell line was chosen as it expresses high levels of GRP receptors,⁴⁷ which is the desired target for the bombesin functionalized AuNPs. It has also been shown that there are 44, 000 bombesin receptor

sites on these cells.⁴⁸ The cells were incubated with the AuNPs in the following manner. The first was a targeting study involving cells incubated with a 1 mg/mL solution of bombesin conjugated AuNPs. A blocking study was also performed with cells that were incubated with a 50 μ g/mL solution of bombesin peptide for 2 hours followed by incubation with a 1 mg/mL solution of bombesin conjugated AuNPs. Finally, a control study using cells incubated with a 1 mg/mL solution of AuNPs was performed.

The cells were then embedded in epon-araldite plastic and cut into 70 nm slices using an Ultracut ultramicrotome. The slices were collected on copper grids and visualized by transmission electron microscopy (TEM) at 60 kV. This was done with the cells incubated with the targeted bombesin conjugated AuNPs, the cells blocked with peptide, and the control cells.

The targeted AuNPs showed considerable uptake, as would be expected given that they are designed to target the GRP receptors that are overexpressed on the PC-3 cells used. The pan-bombesin peptide used is a bombesin receptor agonist,⁴⁹ and once bound to the GRP receptors found on the surface of the PC-3 cells, the receptor-ligand complex can undergo internalization.⁵⁰ As opposed to compounds that remain on the cell surface, this internalization is ideal as it increases retention in the target tissue.⁵¹ This internalization can be seen in the TEM images of the targeted nanoparticles (Figure 5.3a and b).

The blocking study incubated the cells with bombesin for 2 h before adding the targeted bombesin-AuNPs. This study showed less uptake of the AuNPs than with the targeted nanoparticles (Figure 5.3c and d). While there was a reduction in cellular uptake, the

multi-valent targeting capability of the bombesin-AuNPs may render it difficult to adequately block the target receptor with mono-valent peptide ligand.

The control cells were incubated with only AuNPs, and thus are not targeted. As would be expected, these cells showed minimal uptake of the nanoparticles (Figure 5.3e and f). Figure 5.3 shows TEM images of each study, representative across all cells, where the AuNPs can be seen as small black dots indicated by the black arrows.

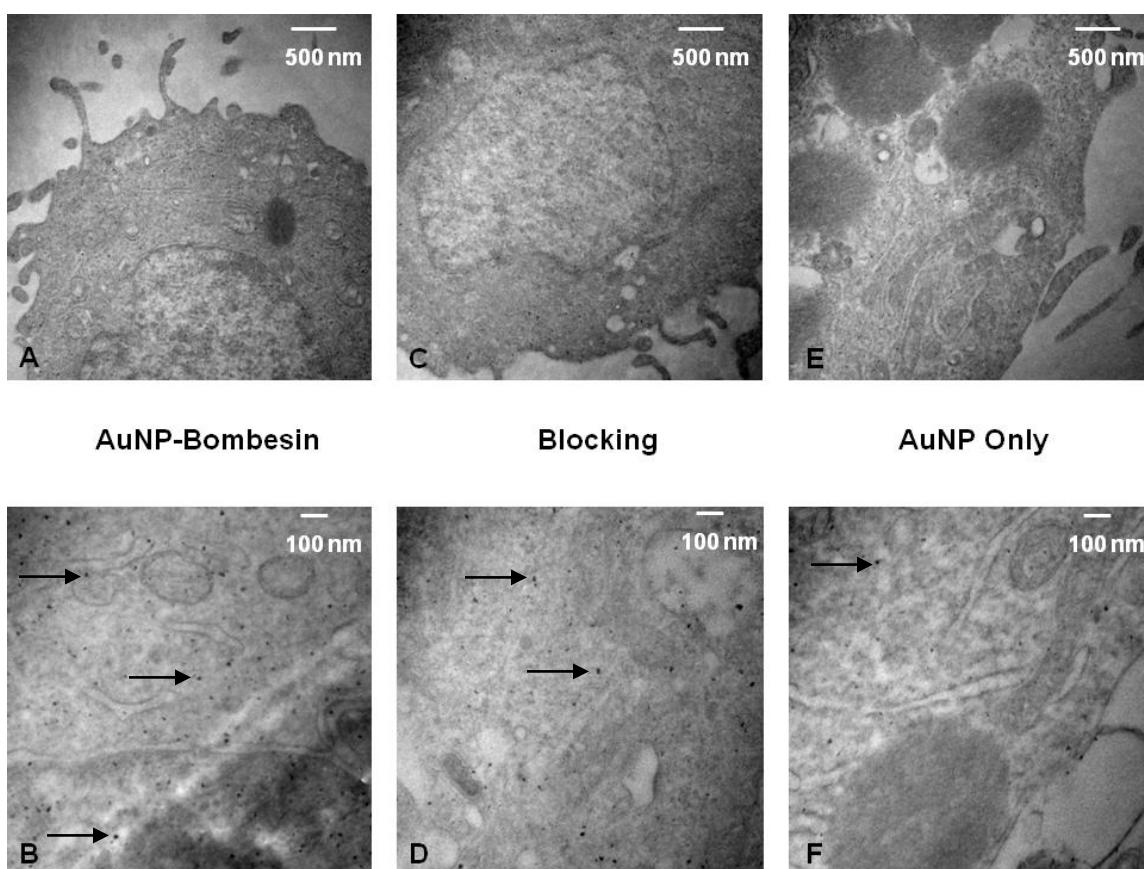


Figure 5.3: TEM images at 60 kV of AuNPs (indicated by black arrows) in PC-3 cells. A) Cell incubated with targeted AuNPs conjugated with bombesin at a magnification of 19000 and B) 64000; C) blocking study cell at a magnification of 19000 and D) 64000; E) control cell at a magnification of 19000 and F) 64000

Grid-based manual counting of the TEM images at a magnification of 64000 (Figure 5.3b, d and f) was performed in order to quantify the nanoparticle uptake. It was determined that the cells showed a ratio of approximately 2:4:7 nanoparticles for control:blocking:targeted, indicating that the targeted AuNPs displayed higher uptake than in either the blocking or control studies.

The AuNPs appeared to be dispersed fairly uniformly throughout the cell, with no accumulation around any particular organelle. It is also important to note that all studies showed no AuNPs around the cells; all AuNPs were either in the cells or in the vesicles surrounding the cells. This demonstrates that the targeted bombesin-AuNPs show specificity for the receptors present on the prostate cancer cells used, and thus have potential to be used to target prostate cancer for both diagnostic and therapeutic purposes. To our knowledge, this is the first example of visualizing *in vitro* cell uptake of bombesin conjugated AuNPs via TEM.

Bombesin has been conjugated to AuNPs for prostate cancer imaging in the past.^{42, 52-54} However, these previous examples were not PEGylated. This PEGylation not only lowers toxicity, but also increases the solubility of the AuNPs. Therefore, our bombesin functionalized AuNPs have solubility of >10 mg/mL in water, whereas the best solubility reported for bombesin functionalized AuNPs was <3 mg/mL in PBS buffer.⁵³ Solubility in water is a very important consideration when using nanoparticles for animal studies; therefore, these new water-soluble bombesin functionalized AuNPs are much more suitable for *in vivo* studies due to their increased solubility in water.

Peptides are most commonly conjugated to AuNP surface through a thiol, usually a cysteine⁴² or disulfide,⁵³ or an N-terminal primary amine such as through the ϵ -amine of a lysine.^{52, 54} A much more convenient way of functionalizing AuNPs is through the use of click chemistry, which is inherently quick, easy and reproducible. Our AuNPs are functionalized with DBCO, allowing for the use of *I*-SPAAC for conjugation of an azide modified peptide to the AuNP. Azide modification of peptides is easily accomplished through the addition of a commercially available PEG-azide. Using strain-promoted click chemistry has the added advantage of not requiring a copper catalyst to drive the reaction, further enhancing its compatibility for *in vivo* studies.

5.3 Conclusions

An azide modified pan-bombesin peptide was successfully synthesized and conjugated to DBCO functionalized AuNPs, creating targeted, water-soluble AuNPs. These were formed through *I*-SPAAC, providing a quick, easy and bioorthogonal method of conjugation of a peptide to AuNPs. The bioconjugation was confirmed through IR spectroscopy and ζ -potential measurements, showing that a stable bioconjugate was formed. Through *in vitro* TEM studies, it was shown that the targeted AuNPs were internalized by the PC-3 cells in much higher concentration than either the blocking or control studies. Bombesin has been shown to target the GRP receptors that are over-expressed on PC-3 cells, and through this study it has been shown that this is still the case when bombesin is conjugated to small, water-soluble AuNPs. This provides a new platform for the conjugation of bombesin to AuNPs while also allowing for addition of a radioisotope, dye or drug through *I*-SPAAC with free DBCO on the nanoparticles allowing them to be utilized for targeting prostate cancer for both diagnosis and therapy.

5.4 Experimental

Materials & Methods

All chemicals were purchased from Sigma-Aldrich, Caledon, Cambridge Isotope Laboratories, Commercial Alcohols, BDH, Spectra/Por, Novabiochem, Aapptec, Peptides International, Chem-Impex, Wisent Inc. and Life-technologies and were used without further purification unless indicated. For HPLC-MS, a Waters, Inc. system was used, consisting of a Waters 2998 Photodiode Array Detector and a Waters 2767 Sample Manager. For analytical HPLC-MS studies, a Sunfire RP-C18 4.6 x 250 mm, 5 μ m column was used. For preparative HPLC-MS work, a Sunfire RP-C18 19 x 150 mm, 5 μ m column was used. In both cases, absorbance was detected at wavelengths of 220 nm and 254 nm. A gradient solvent system consisting of CH₃CN + 0.1% of TFA (solvent A) and H₂O + 0.1% of TFA (solvent B) was used. For analytical UHPLC-MS studies, a Waters, Inc. Acquity UPLC H-Class system was used, combined with a Xevo QToF. For analytical UHPLC-MS studies, a Waters Acquity UPLC BEH C18 2.1 x 50 mm, 1.7 μ m column was used. A gradient solvent system consisting of CH₃CN + 0.1% formic acid (solvent C) and H₂O + 0.1% formic acid (solvent D) was used. An INOVA 400 NMR spectrometer was used for ¹H NMR studies. Chemical shifts are reported in parts per million (ppm) relative to TMS (0.00 ppm). For electro-spray ionization (ESI) mass spectra a Micromass Quattro Micro API mass spectrometer was used. For cell centrifugation, an IEC Centra CL2 was used. For TEM, an Ultracut Ultramicrotome was used for sample preparation, and a Phillips CM10 TEM with Digital Camera Output was used for imaging. Infrared spectra were recorded using a Bruker Vector33 spectrometer by making a thin film of sample onto a KBr disk. ζ -potential measurements were

performed using a Zetasizer Nano-ZS (Malvern Instrument). A solution of AuNPs in PBS pH 7.0 was prepared with concentration 0.5 mg ml^{-1} . 1 ml of this solution was inserted in a latex folded capillary cell equipped with electrodes and the ζ -potential was calculated by employing the Huckel approximation.

Bombesin-azide Peptide (5.1)

The peptide was synthesized on-resin using standard Fmoc solid-phase peptide chemistry by manual synthesis using Fmoc protected rink amide MBHA resin (0.5 mmol, loading 0.52 mmol/g). The Fmoc protecting group was removed by treatment with 20% piperidine in *N,N*-dimethylformamide (DMF) for 5 and 15 minutes, followed by rinses with dichloromethane (DCM) and DMF. Fmoc protected amino acids were then coupled from C-terminus to N-terminus for 1 h and 45 min using 3 eq. of Fmoc amino acid, 3 eq. of 2-(6-chloro-1H-benzotriazole-1-yl)-1,1,3,3-tetramethylaminium hexafluorophosphate (HCTU) and 6 eq. of *N,N*-diisopropylethylamine (DIPEA) in 5 mL DMF. Finally, a 550 MW N_3 -(PEG) $_7$ -COOH spacer was coupled overnight using 3 eq of the spacer, 3 eq HCTU and 6 eq DIPEA in 5 mL DMF. Once complete, the peptide was deprotected and cleaved from the resin by treatment with trifluoroacetic acid (TFA) containing water (2.5% v/v) and triisopropylsilane (2.5% v/v) as scavengers for 4 h. Purification was performed by preparative HPLC-MS (linear gradient of 30-70% solvent A in B). The purity of the resultant peptide was determined to be >99% by analytical UHPLC (linear gradient of 5-60% solvent A in B). This resulted in a 6% yield of bombesin peptide **5.1** (50 mg, 0.03 mmol). HRMS (ESI $^+$): m/z calculated for $\text{C}_{79}\text{H}_{116}\text{N}_{18}\text{O}_{21}$, 1653.8641 $[\text{M}+\text{H}]^+$; observed 1653.8644 $[\text{M}+\text{H}]^+$.

Model I-SPAAC reaction (5.2)

PEG-DBCO (3 mg, 0.007 mmol) was dissolved in 250 μ L of acetonitrile. Bombesin peptide **5.1** (12 mg, 0.007 mmol) was also dissolved in 250 μ L of acetonitrile and added to the DBCO solution. To this, another 500 μ L of acetonitrile was added. This was stirred at room temperature and followed by UHPLC (linear gradient of 20-80% solvent A in B). The reaction was complete after 1 h. MS (ESI+): m/z calculated for $C_{104}H_{145}N_{20}O_{26}$, 2090.06 $[M+H]^+$, 1045.54 $[M+2H]^{2+}$; observed 2090.08 $[M+H]^+$, 1045.53 $[M+2H]^{2+}$.

Triethylene Glycol Monomethyl Ether AuNP (Me-EG₃-AuNP)

Me-EG₃-AuNP were synthesized according to our previously established procedure.²³ Briefly, 19 mg of $HAuCl_4 \cdot 3H_2O$ (49 μ mol) were dissolved in 7.5 mL of dry MeOH and 1.25 ml of glacial acetic acid. To this mixture 26 mg of triethylene glycol monomethyl ether thiol (Me-EG₃-SH) (146 μ mol) were added. The solution was stirred vigorously for 1 hour. Under vigorous stirring 19 mg of $NaBH_4$ (490 μ mol) dissolved in 1.25 mL of nanopure water was added to the reaction mixture drop wise. After the first 3-4 drops the solution turned dark brown. The reaction was stirred overnight at room temperature and was then concentrated at rotavapor, 20 mL of brine were added and the nanoparticles were extracted with toluene. At the end of the process the water phase was colorless. The Me-EG₃-AuNP solution in toluene was transferred into a clean round bottom flask and the solvent was evaporated leaving a film of AuNPs that was washed with hexanes to remove the excess of Me-EG₃-SH. The nanoparticles were then re-dissolved in nanopure water and purified by dialysis overnight (MWCO 6000-8000 Da).

^1H NMR shows the presence of three broad peaks: one at 3.34 ppm that corresponds to the $-\text{CH}_3$ at the nanoparticle's interface, and one at 3.58 ppm and one at 3.66 ppm related to the protons of the ethylene glycol units.

HOOC-EG₄-AuNP

HOOC-EG₄-AuNPs were synthesized according to our previously established procedure.²⁸ Briefly, 74 mg of Me-EG₃-AuNP were dissolved in 5 mL of DCM in a 25 mL round bottom flask. To this mixture were added 11 mg of HOOC-EG₄-SH. The reaction was allowed to proceed for 30 minutes and the solvent was removed under vacuum. The AuNP film was washed with hexanes and isopropyl alcohol and then the HOOC-EG₄-AuNP were re-dissolved in milliQ water. The solvent was removed and the particles were washed and re-dissolved 2 more times. The removal of free thiols was monitored through ^1H NMR spectroscopy by the disappearance of sharp peaks. The ^1H NMR of the clean HOOC-EG₄-AuNPs shows the appearance of a small and broad peak at 4.11 ppm that corresponds to the two protons belonging to the carbon alpha of the carboxylic acid group in the carboxy-terminated ligands. These AuNPs contain the carboxylic group in concentration $0.46 \mu\text{mol mg}^{-1}$.

DBCO-AuNP (5.3)

DBCO-AuNPs were synthesized according to our previously established procedure.²⁸ Briefly, to a 25 mL round bottom flask were added 65 mg HOOC-EG₄-AuNPs (30 μmol of $-\text{COOH}$). The flask was purged with argon for 15 minutes and then 9 mL of dry DMF were added. After addition of the DMF, 16 μL (90 μmol) of DIPEA was added to the AuNP solution and the reaction was cooled down to 0°C on an ice bath. In a separate

flask, 23 mg (60 μmol) of O-Benzotriazole- N,N,N',N'-tetramethyl- uronium-hexafluoro-phosphate (HBTU) was placed under argon followed by addition of 5 mL of dry DMF. The HBTU solution was purged for 15 minutes and was then added to the AuNP solution and allowed to stir for 15 minutes at 0°C. In another flask, 17 mg (60 μmol) of DBCO-amine was placed under argon and dissolved in 3 mL of dry DMF. After 15 minutes of purging, the DBCO-amine solution was added to the AuNP reaction solution and the ice bath was removed. The reaction was allowed to proceed overnight under an inert atmosphere. The next day the reaction mixture was inserted into a dialysis bag (MWCO 6000-8000 Da) and dialyzed against DMF to remove the reaction byproducts. The DMF was changed every 2 hours twice. Finally the sample was dialyzed against water overnight. As previously reported, the DBCO-AuNPs prepared following this procedure were found to contain the DBCO in concentration 0.1 $\mu\text{mol mg}^{-1}$.

Bombesin-AuNP (5.4)

In a typical bioconjugation procedure 20 mg of DBCO-AuNP **5.3** (2 μmol of DBCO) were mixed with 10 mg of bombesin-azide **5.1** (6 μmol) in 5 mL of dry methanol. The reaction was allowed to proceed for 2 hours. After 2 hours the methanol was evaporated and bombesin-AuNP and excess bombesin-azide were re-dissolved in 4 mL of a 1:1 mixture MeOH/H₂O. The excess peptide was then removed by centrifugation (6000 rpm for 7.5 min) using Millipore centrifuge filters (MWCO 10000 Da). Bombesin-AuNP were never allowed to dry completely on the filter taking care that 500 μL of solvent was still present inside the filter after centrifugation. Bombesin-AuNP were washed 4 times and finally transferred into a vial. The solvent was completely evaporated, and the

bombesin-AuNPs were re-dissolved in MilliQ water to obtain a final concentration of 10 mg/mL. This solution was stored at 4°C.

In order to calculate the *I*-SPAAC reaction yield, the purification washes were then collected and the solvent was evaporated carefully. This resulted in 4.7 μmol of bombesin-azide being recovered, indicating that ~60% of the interfacial DBCO reacted with the peptide.

Cell Preparation

PC-3 cells were grown in T-75 flasks using Ham's F-12 media supplemented with 10% fetal bovine serum and were incubated with a 1 mg/mL solution of gold nanoparticles either with or without bombesin to a final concentration of 50 μg/mL, at 37° C for 24 hours. For blocking studies, bombesin was added to the cells to a final concentration of 50 μg/mL for 2 hours, before the addition of the bombesin-containing nanoparticles. After 24 hours, the cells were gently washed with phosphate buffer saline (PBS), gently lifted using a 0.05% Trypsin-EDTA solution and centrifuged at 1200 rpm for 5 minutes. The cell pellet was washed two times with PBS and fixed with a 2% glutaraldehyde in PBS solution overnight. Cells were then washed 3 times with PBS to remove the fixing agent, re-suspended in PBS and analyzed by transmission electron microscopy (TEM).

Transmission Electron Microscopy

Once the cells were fixed with a 2% glutaraldehyde in PBS solution, they were washed three times with PBS buffer and re-suspended in 2% OsO₄ for 1 h. They were then washed three times with double distilled water. Cells were set in a 1% agarose solution

that was then cut into small cubes and subjected to dehydration in acetone series; percent acetone in water: 20%, 50%, 70%, 90%, 95%, 100%, 100%, 100%. The cells were then embedded with a series of epon-araldite plastic in acetone; 50%, 66%, 100%, 100%. The samples were then set in a form using epon-araldite plastic. The moulds were then cut into 70 nm slices using an Ultracut ultramicrotome. The slices were collected on copper grids and visualized using a Phillips CM10 TEM at 60 kV.

5.5 References

1. <http://www.cancer.ca>.
2. L. F. Ellison, H. Bryant, G. Lockwood and L. Shack, *Health Rep.*, 2011, 22, 21-25.
3. R. K. Nam, A. Toi, L. H. Klotz, J. Trachtenberg, M. A. S. Jewett, S. Appu, D. A. Loblaw, L. Sugar, S. A. Narod and M. W. Kattan, *J. Clin. Oncol.*, 2007, 25, 3582-3588.
4. G. W. K. Chodak, P.; Schoenberg, H.W., *J. Urol.*, 1989, 141, 1136-1138.
5. O. Patel, A. Shulkes and G. S. Baldwin, *BBA – Rev. Cancer*, 2006, 1766, 23-41.
6. B. Sun, A. V. Schally and G. Halmos, *Regul. Pept.*, 2000, 90, 77-84.
7. A. Plonowski, A. Nagy, A. V. Schally, B. Sun, K. Groot and G. Halmos, *Int. J. Cancer*, 2000, 88, 652-657.
8. M. R. Papasani, G. Wang and R. A. Hill, *Nanomedicine : nanotechnology, biology, and medicine*, 2012, 8, 804-814.
9. S. Naahidi, M. Jafari, F. Edalat, K. Raymond, A. Khademhosseini and P. Chen, *J. Control. Release*, 2013, 166, 182-194.
10. N. L. Rosi and C. A. Mirkin, *Chem. Rev.*, 2005, 105, 1547-1562.
11. N. L. Rosi, D. A. Giljohann, C. S. Thaxton, A. K. R. Lytton-Jean, M. S. Han and C. A. Mirkin, *Science*, 2006, 312, 1027-1030.
12. I. H. El-Sayed, X. Huang and M. A. El-Sayed, *Nano Lett.*, 2005, 5, 829-834.
13. A. K. Iyer, G. Khaled, J. Fang and H. Maeda, *Drug Discov. Today*, 2006, 11, 812-818.

14. M. Manchester and P. Singh, *Adv. Drug Delivery. Rev.*, 2006, 58, 1505-1522.
15. F. M. Brunel, J. D. Lewis, G. Destito, N. F. Steinmetz, M. Manchester, H. Stuhlmann and P. E. Dawson, *Nano Lett.*, 2010, 10, 1093-1097.
16. X. Montet, M. Funovics, K. Montet-Abou, R. Weissleder and L. Josephson, *J. Med. Chem.*, 2006, 49, 6087-6093.
17. J. Cheon and J.-H. Lee, *Acc. Chem. Res.*, 2008, 41, 1630-1640.
18. S. K. Libutti, G. F. Paciotti, A. A. Byrnes, H. R. Alexander, Jr., W. E. Gannon, M. Walker, G. D. Seidel, N. Yuldasheva and L. Tamarkin, *Clin. Cancer Res.*, 2010, 16, 6139-6149.
19. D. F. Emerich and C. G. Thanos, *J. Drug Target.*, 2007, 15, 163-183.
20. L. Zhang, H. Chen, L. Wang, T. Liu, J. Yeh, G. Lu, L. Yang and H. Mao, *Nanotechnol. Sci. Appl.*, 2010, 3, 159-170.
21. E. S. Glazer, C. Zhu, K. L. Massey, C. S. Thompson, W. D. Kaluarachchi, A. N. Hamir and S. A. Curley, *Clin. Cancer Res.*, 2010, 16, 5712-5721.
22. E. Morales-Avila, G. Ferro-Flores, B. E. Ocampo-García, L. M. De León-Rodríguez, C. L. Santos-Cuevas, R. o. García-Becerra, L. A. Medina and L. Gómez-Oliván, *Bioconjug. Chem.*, 2011, 22, 913-922.
23. P. Gobbo and M. S. Workentin, *Langmuir*, 2012, 28, 12357-12363.
24. M. Milne, P. Gobbo, N. McVicar, R. Bartha, M. S. Workentin and R. H. E. Hudson, *J. Mater. Chem. B*, 2013, 1, 5628-5635.
25. P. Gobbo, M. C. Biesinger and M. S. Workentin, *Chem. Commun.*, 2013, 49, 2831-2833.
26. J. Zhu, C. Waengler, R. B. Lennox and R. Schirrmacher, *Langmuir*, 2012, 28, 5508-5512.
27. P. Gobbo, S. Novoa, M. C. Biesinger and M. S. Workentin, *Chem. Commun.*, 2013, 49, 3982-3984.
28. P. Gobbo, Z. Mossman, A. Nazemi, A. Niaux, M. C. Biesinger, E. R. Gillies and M. S. Workentin, *J. Mater. Chem. B*, 2014, 2, 1764-1769.
29. A. Anastasi, V. Erspamer and M. Bucci, *Experientia*, 1971, 27, 166-167.
30. R. La Bella, E. Garcia-Garayoa, M. Langer, P. Bläuenstein, A. G. Beck-Sickinger and P. August Schubiger, *Nucl. Med. Biol.*, 2002, 29, 553-560.

31. G. Ferro-Flores, C. A. de Murphy, J. Rodr`iguez-Corte`s, M. Pedraza-Lo`pez and M. a. T. Ram`rez-Iglesias, *Nucl. Med. Commun.*, 2006, 27, 371-376.
32. M. Visser, H. F. Bernard, J. L. Erion, M. A. Schmidt, A. Srinivasan, B. Waser, J. C. Reubi, E. P. Krenning and M. Jong, *Eur. J. Nucl. Med. Mol. Imaging*, 2007, 34, 1228-1238.
33. J. C. Reubi, *Endocr. Rev.*, 2003, 24, 389-427.
34. A. Martin, J. Hickey, A. Ablack, J. Lewis, L. Luyt and E. Gillies, *J. Nanopart. Res.*, 2010, 12, 1599-1608.
35. N. F. Steinmetz, A. L. Ablack, J. L. Hickey, J. Ablack, B. Manocha, J. S. Mymryk, L. G. Luyt and J. D. Lewis, *Small*, 2011, 7, 1664-1672.
36. S. A. Mantey, H. C. Weber, E. Sainz, M. Akeson, R. R. Ryan, T. K. Pradhan, R. P. Searles, E. R. Spindel, J. F. Battey, D. H. Coy and R. T. Jensen, *J. Biol. Chem.*, 1997, 272, 26062-26071.
37. J. C. Reubi, S. Wenger, J. Schmuckli-Maurer, J.-C. Schaer and M. Gugger, *Clin. Cancer Res.*, 2002, 8, 1139-1146.
38. T. K. Pradhan, T. Katsuno, J. E. Taylor, S. H. Kim, R. R. Ryan, S. A. Mantey, P. J. Donohue, H. C. Weber, E. Sainz, J. F. Battey, D. H. Coy and R. T. Jensen, *Eur. J. Pharmacol.*, 1998, 343, 275-287.
39. C. Van de Wiele, F. Dumont, R. Vanden Broecke, W. Oosterlinck, V. Cocquyt, R. Serreyn, S. Peers, J. Thornback, G. Slegers and R. A. Dierckx, *Eur. J. Nucl. Med.*, 2000, 27, 1694-1699.
40. K. E. Baidoo, K.-S. Lin, Y. Zhan, P. Finley, U. Scheffel and H. N. Wagner, *Bioconjug. Chem.*, 1998, 9, 218-225.
41. C. J. Smith, G. L. Sieckman, N. K. Owen, D. L. Hayes, D. G. Mazuru, R. Kannan, W. A. Volkert and T. J. Hoffman, *Cancer Res.*, 2003, 63, 4082-4088.
42. L. Hosta-Rigau, I. Olmedo, J. Arbiol, L. J. Cruz, M. J. Kogan and F. Albericio, *Bioconjug. Chem.*, 2010, 21, 1070-1078.
43. Y. Pan, S. Neuss, A. Leifert, M. Fischler, F. Wen, U. Simon, G. Schmid, W. Brandau and W. Jahnen-Dechent, *Small*, 2007, 3, 1941-1949.
44. M. Tsoli, H. Kuhn, W. Brandau, H. Esche and G. Schmid, *Small*, 2005, 1, 841-844.
45. J. V. Jokerst, T. Lobovkina, R. N. Zare and S. S. Gambhir, *Nanomed.*, 2011, 6, 715-728.

46. Y.-J. Gu, J. Cheng, C.-C. Lin, Y. W. Lam, S. H. Cheng and W.-T. Wong, *Toxicol. Appl. Pharmacol.*, 2009, 237, 196-204.
47. B. E. Rogers, H. M. Bigott, D. W. McCarthy, D. D. Manna, J. Kim, T. L. Sharp and M. J. Welch, *Bioconjug. Chem.*, 2003, 14, 756-763.
48. H. Reile, P. E. Armatis and A. V. Schally, *The Prostate*, 1994, 25, 29-38.
49. J. C. Reubi and H. R. Maecke, *J. Nucl. Med.*, 2008, 49, 1735-1738.
50. R. V. Benya, Z. Fathi, T. Kusui, T. Pradhan, J. F. Battey and R. T. Jensen, *Mol. Pharmacol.*, 1994, 46, 235-245.
51. E. García Garayoa, D. Rüegg, P. Bläuenstein, M. Zwimpfer, I. U. Khan, V. Maes, A. Blanc, A. G. Beck-Sickinger, D. A. Tourwé and P. A. Schubiger, *Nucl. Med. Biol.*, 2007, 34, 17-28.
52. B. Ocampo-García, G. Ferro-Flores, E. Morales-Avila and F. d. M. Ramírez, *Nucl. Med. Commun.*, 2011, 32, 1095-1104.
53. N. Chanda, V. Kattumuri, R. Shukla, A. Zambre, K. Katti, A. Upendran, R. R. Kulkarni, P. Kan, G. M. Fent, S. W. Casteel, C. J. Smith, E. Boote, J. D. Robertson, C. Cutler, J. R. Lever, K. V. Katti and R. Kannan, *Proc. Natl. Acad. Sci. U.S.A.*, 2010, 107, 8760-8765.
54. N. Jiménez-Mancilla, G. Ferro-Flores, C. Santos-Cuevas, B. Ocampo-García, M. Luna-Gutiérrez, E. Azorín-Vega, K. Isaac-Olivé, M. Camacho-López and E. Torres-García, *J. Label. Compd. Radiopharm.*, 2013, 56, 663-671.

Chapter 6

6 Conclusions

Molecular imaging has become a true multi-disciplinary approach for the non-invasive diagnosis of diseases; with biologists discovering biological targets, chemists developing imaging probes specific for the desired target, and physicists and engineers designing the instrumentation needed to image the probe accumulation in the body.¹ With contributions from so many fields, molecular imaging has quickly become an indispensable tool since its formalization only a few decades ago. As such, many critical advancements have been made in recent years, resulting in an increase in the number of PET and SPECT facilities for both clinical and research applications.² However, there is still a need to improve the current generation of radiopharmaceuticals. In order to meet this need, new approaches to radiopharmaceutical development are required. This includes improved design, synthesis and methods of incorporating radionuclides that are both quick and efficient with the hopes of creating radiopharmaceuticals that have increased *in vivo* stability and improved target affinities, resulting in increased target-to-background ratios and higher quality images.³

In designing pharmaceuticals, the issue of isomer formation is a major concern as each isomer formed can possess unique properties. This is also of concern when synthesizing imaging agents. In previous work in our lab with cyclic RGD peptides containing an N^α-substituted histidine chelator, it was discovered that isomers were formed as a result of rhenium(I) tricarbonyl coordination. This isomer formation was investigated through the synthesis and characterization of three small molecule and one peptide-like model

histidine chelators. The first small molecule consisted of a benzylated histidine that contained a secondary alpha amine as a model system. The second was a protected version of the first where the imidazole-N3 was protected to ensure histidine linkage isomers were not being observed. The third was a methylated version of the first making the alpha amine tertiary. The final model was a dipeptide to compare isomer formation between small molecules and peptides. Through ^1H and various 2D NMR spectroscopic techniques, it was determined that the isomers formed by the coordination of rhenium with histidine were diastereomers of the secondary alpha amine on the bifunctional histidine chelator and the structures of both the major and minor isomers for the model chelators were determined.

Isomers can be very problematic in radiopharmaceutical synthesis as they can lead to side-effects, toxicity and can possess different pharmacokinetic properties. Histidine is a very effective chelator for rhenium and technetium-99m tricarbonyl; as such, this study shows that awareness of isomer formation is critical for development of any radiopharmaceuticals containing this chelation system or a similar chelation system with a coordinating secondary amine.

Histidine can also function as a mono- or bidentate chelator for various metals, and has been found to be effective in stabilizing small peptide turns through this coordination.⁴⁻⁶

A pentapeptide of the sequence Ac-HAAAH-OH was designed such that the terminal histidines would be able to coordinate $[\text{}^{99}\text{Tc/Re}(\text{CO})_3]^+$ in a [2+1] fashion using the imidazole of the N-terminal histidine and the imidazole and carboxylic acid of the C-terminal histidine. This coordination would effectively cyclize the peptide, forming an integrated radiolabelled peptidomimetic. Through ^1H and 2D NMR spectroscopy of the

coordinated peptide it was determined that coordination of the metal was occurring in a [2+1] manner, and thus cyclizing the peptide in the process. The C-terminal histidine is functioning as a bidentate chelator and preferentially coordinates the metal through the imidazole-N1, as was seen in Chapter 2. However, the N-terminal histidine is a monodentate chelator with the potential to coordinate through either the imidazole-N1 or N3, leading to eight possible isomers of the cyclized coordinated peptide. Through the combination of 2D and VT NMR spectroscopy along with computational studies, the most probable structure of the cyclic peptide was determined.

This technique could be applied to the development of various biologically relevant cyclic peptides, such as RGD, to form integrated radiopharmaceuticals that become biologically active only upon incorporation of the metal. This technique can also be used to synthesize focused libraries of technetium-99m labelled cyclic pentapeptides in order to explore the surrounding chemical space.⁷ Development of these integrated molecular imaging probes that are biologically active only when cyclized with a metal hold much promise for the future of technetium-99m based radiopharmaceuticals as they allow for increased specificity of the probe for the target of interest, increased binding affinities, increased bioavailability and decreased receptor promiscuity.

Cyclic peptidomimetics were also developed which incorporated both an azide and alkyne functionality such that triazole formation through a click reaction would form not only a cyclic peptide, but would also result in a chelation site for rhenium/technetium-99m tricarbonyl. This follows an integrated design as the chelator, and thus the metal, is incorporated into the backbone of the cyclic peptide. Synthesis of this "click to cyclize and chelate" model was attempted through three different clickable peptide systems. The

first two systems contained an azide modified amino acid at the C-terminus of the peptide, and different alkyne modified amino acids at the N-terminus. It was demonstrated that both of these chelators were able to coordinate $[\text{Re}(\text{CO})_3]^+$ through the synthesis and characterization of model chelation systems. The third system had inverted functionality with a lysine, modified at the alpha amine with an alkyne, placed at the C-terminus. The peptide could then be extended from the side-chain amine of the lysine and an azide attached to the N-terminus. Once clicked, all the proposed systems had the potential to form a cyclic peptide and in the process, a chelator for rhenium/technetium-99m tricarbonyl. However, all attempts at synthesizing and characterizing these systems were unsuccessful.

Although the idea of click to cyclize and chelate was unsuccessful, click chemistry still has great potential for applications in radiopharmaceutical development due to its broad scope;⁸ especially in terms of click-to-chelate for labelling biomolecules with technetium-99m.⁹ This click-to-chelate approach can also be used to coordinate therapeutic isotopes of rhenium (186 and 188). This permits both diagnostic, when technetium-99m is coordinated, and therapeutic, by substituting for rhenium-186/188, applications with the same probe. Synthesis of imaging probes with different radionuclides for different imaging modalities from a single precursor using click reactions, allows for the comparison of different imaging probes and modalities.¹⁰ The development of multifunctional radiopharmaceuticals with click chemistry¹¹ demonstrates the potential use in theranostics, which combines therapeutic and diagnostic entities on the same probe, in the same dose. Click chemistry would allow both a diagnostic and a therapeutic entity to be “clicked” to a functionalized targeted probe

allowing for detection of probe localization while at the same time, providing the patient with a therapeutic dose.

A promising pathway for the development of theranostic probes is through the use of gold nanoparticles.¹² Their multifunctionality allows for the addition of a targeting entity while at the same time containing a diagnostic radionuclide, a therapeutic radioisotope, or both simultaneously. One method to attach different entities to these nanoparticles is with click chemistry as was described in Chapter 5. In this chapter, small, water-soluble gold nanoparticles were functionalized with a pan-bombesin ligand that has been shown to target gastrin-releasing peptide receptors that are overexpressed on prostate cancer (PC-3) cells. Bioconjugation was achieved with copper-free click chemistry to react an azide modified pan-bombesin with DBCO functionalized gold nanoparticles. These targeted AuNPs were incubated with PC-3 cells and the uptake visualized by TEM studies. Blocking studies where the AuNPs were first incubated with bombesin, as well as control studies where the cells were incubated only with AuNPs, were also performed and visualized by TEM. These images showed specific accumulation of the targeted nanoparticles in the PC-3 cells, demonstrating their potential for both diagnostic and therapeutic purposes.

Traditionally, conjugation of biomolecules with gold nanoparticles uses thiol-Au chemistry, which is sensitive to reducing conditions. Click-based bioconjugates have a much broader scope as they form a much more stable bioconjugate, thus expanding their potential applications.¹² This system holds the potential for attachment of other azide modified entities through click chemistry as the AuNPs are functionalized with DBCO. This would allow for attachment of multiple entities to the nanoparticles either

individually or simultaneously. If both a diagnostic label, such as technetium-99m or fluorine-18, is attached along with a therapeutic isotope, such as rhenium-186/188 or iodine-131, simultaneous imaging and therapy can be accomplished with the theranostic agent all in one dose.

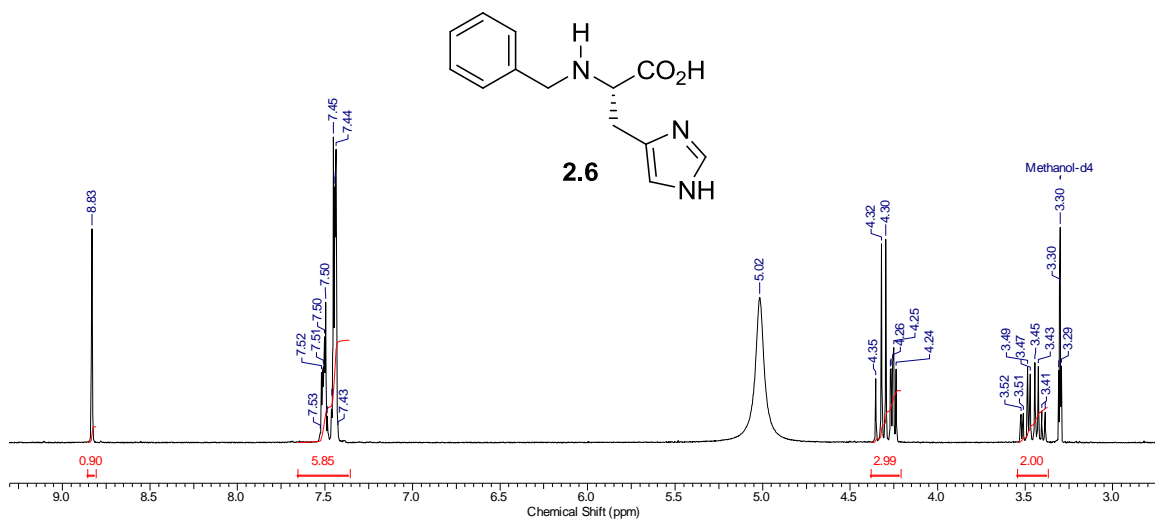
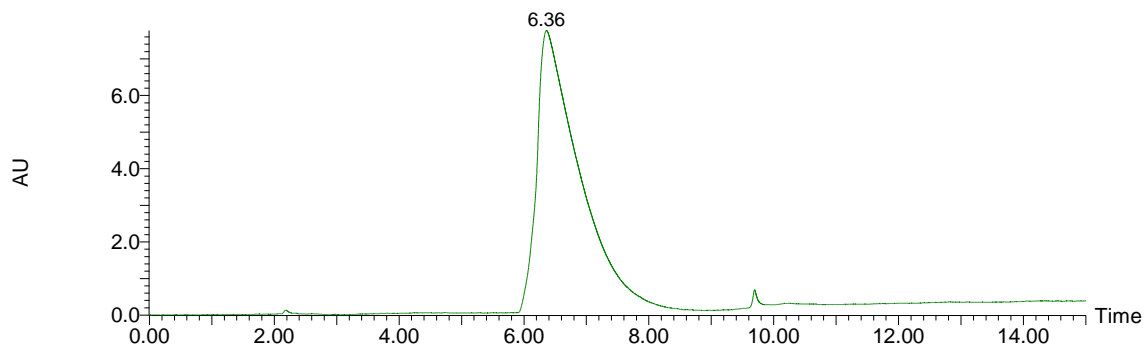
In conclusion, this thesis has developed several novel methods for the synthesis of molecular imaging agents. Molecular imaging and radiopharmaceutical development are essential and emerging fields. Advancement in identification, synthesis, and characterization of novel molecular imaging agents is critical for the creation of superior radiopharmaceuticals capable of producing higher resolution images allowing for earlier detection of disease on-set and better methods of tracking disease progression and treatment. Integrated technetium-99m based radiopharmaceuticals will aid in creating targeted imaging agents with low molecular weight and improved affinity due to the conformational constraint induced by metal incorporation.¹³ Gold nanoparticles offer additional multifunctionality as a distinct advantage over traditional methods of developing pharmaceuticals, with the ability to conjugate numerous diagnostic and therapeutically relevant entities on the same probe.¹⁴ The use of click chemistry in radiopharmaceutical design is still an emerging field, and as a result, there have been very few examples of marketed pharmaceuticals containing a 1,2,3-triazole. As such, an emergence of triazole containing imaging agents and therapeutics should be expected in the coming decades.^{15, 16}

6.1 References

1. P. J. Cassidy and G. K. Radda, *J. Royal Soc. Interface*, 2005, 2, 133-144.
2. S. L. Pimlott and A. Sutherland, *Chem. Soc. Rev.*, 2011, 40, 149-162.

3. R. Weissleder, *Science*, 2006, 312, 1168-1171.
4. M. T. Ma, H. N. Hoang, C. C. G. Scully, T. G. Appleton and D. P. Fairlie, *J. Am. Chem. Soc.*, 2009, 131, 4505-4512.
5. H. N. Hoang, G. K. Bryant, M. J. Kelso, R. L. Beyer, T. G. Appleton and D. P. Fairlie, *Inorg. Chem.*, 2008, 47, 9439-9449.
6. M. J. Kelso, H. N. Hoang, T. G. Appleton and D. P. Fairlie, *J. Am. Chem. Soc.*, 2000, 122, 10488-10489.
7. C. Lipinski and A. Hopkins, *Nature*, 2004, 432, 855-861.
8. H. C. Kolb and K. B. Sharpless, *Drug Discov. Today*, 2003, 8, 1128-1137.
9. C. A. Kluba and T. L. Mindt, *Molecules*, 2013, 18, 3206-3226.
10. T. L. Mindt, C. Müller, F. Stuker, J.-F. Salazar, A. Hohn, T. Mueggler, M. Rudin and R. Schibli, *Bioconjug. Chem.*, 2009, 20, 1940-1949.
11. T. L. Mindt, H. Struthers, B. Spingler, L. Brans, D. Tourwe, E. Garcia-Garayoa and R. Schibli, *Chem. Med. Chem.*, 2010, 5, 2026-2038.
12. J. Xie, S. Lee and X. Chen, *Adv. Drug Deliv. Rev.*, 2010, 62, 1064-1079.
13. J. L. Hickey and L. G. Luyt, *Chem.--Eur. J.*, 2012, 18, 12999-13007.
14. W. Cai, T. Gao, H. Hong and J. Sun, *Nanotechnol. Sci. Appl.*, 2008, 1, 17-32.
15. J. Hou, X. Liu, J. Shen, G. Zhao and P. G. Wang, *Expert Opin. Drug Discovery*, 2012, 7, 489-501.
16. P. Thirumurugan, D. Matosiuk and K. Jozwiak, *Chem. Rev.*, 2013, 113, 4905-4979.

Appendix A : Characterization of Select Compounds

N^α-benzyl-L-histidine (2.6)**Figure A1:** ¹H NMR (400 MHz, MeOH-d₄) of **2.6****Figure A2:** Analytical HPLC trace, UV absorbance detected from 210-800 nm (RP-C18 4.6 x 250 mm, 5 μm), of **2.6**

Rhenium(I) tricarbonyl-N^α-benzyl-L-histidine (2.1)

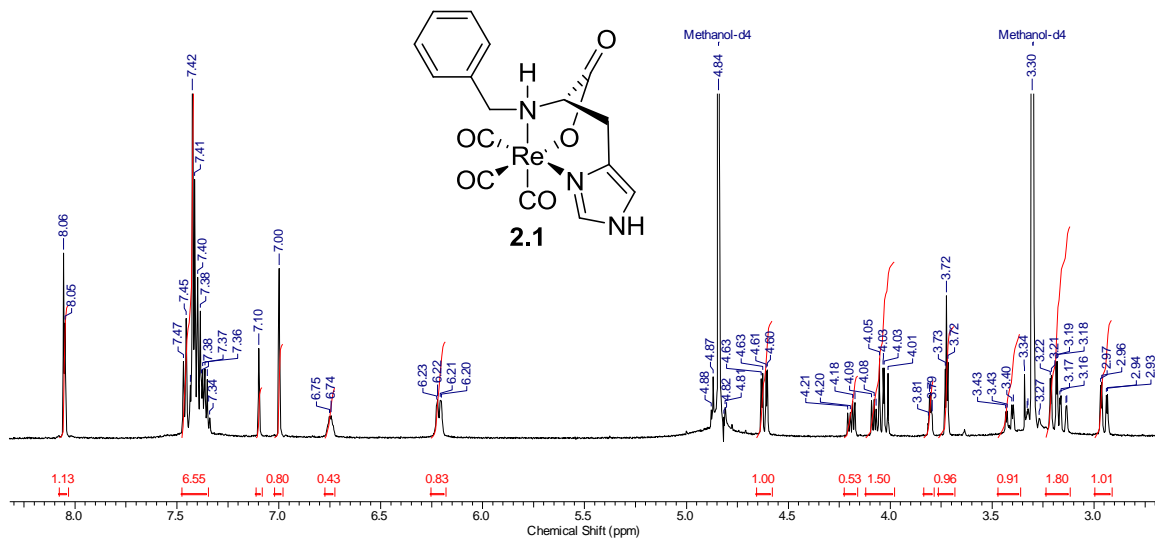


Figure A3: ¹H NMR (400 MHz, MeOH-d₄) of **2.1**

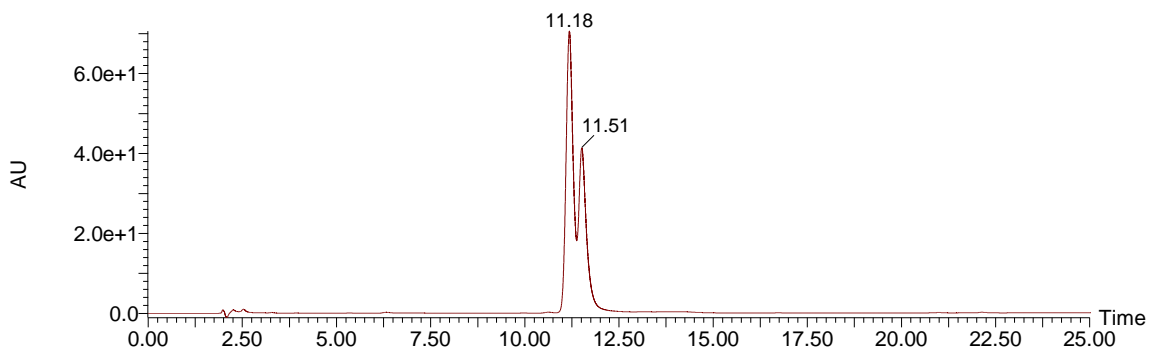


Figure A4: Analytical HPLC trace, UV absorbance detected from 210-800 nm (RP-C18 4.6 x 250 mm, 5 μm), of **2.1**

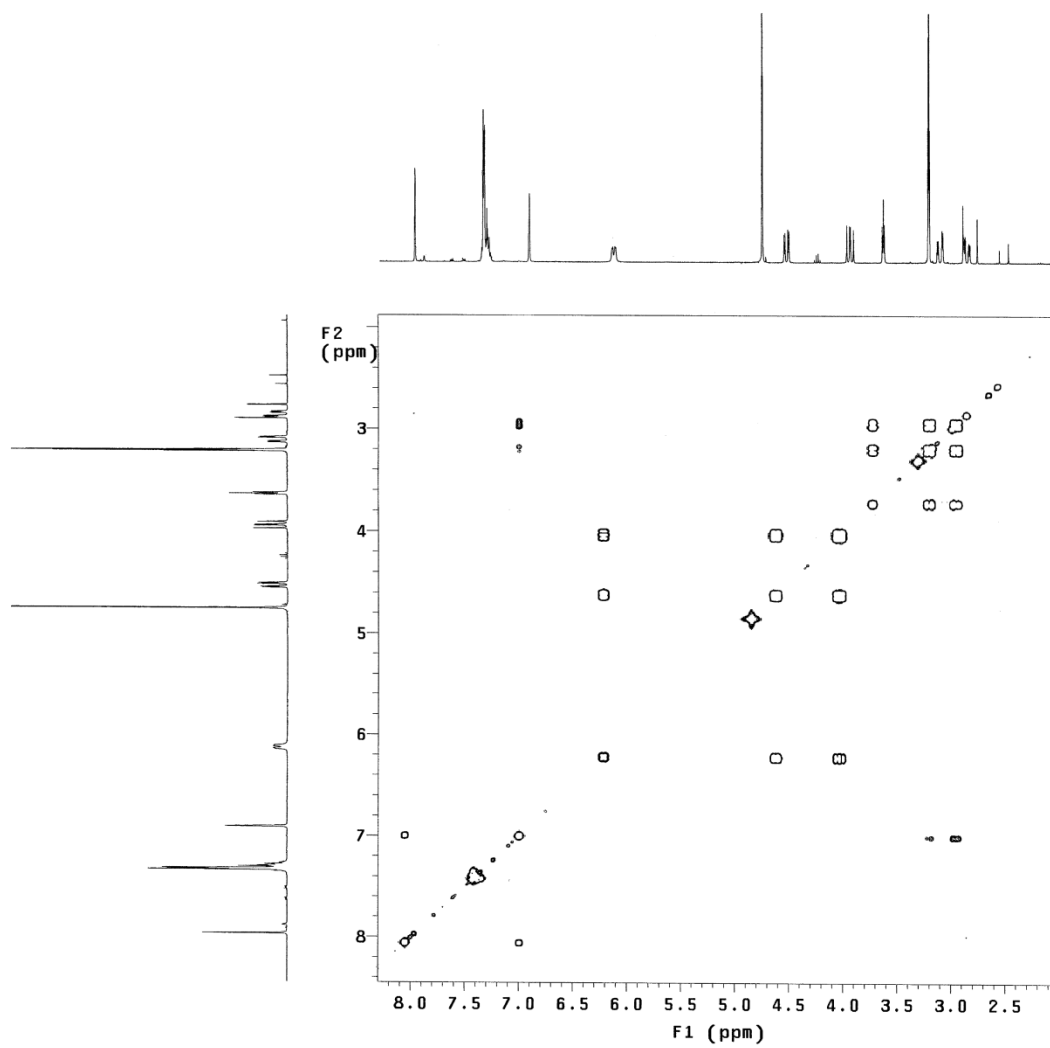
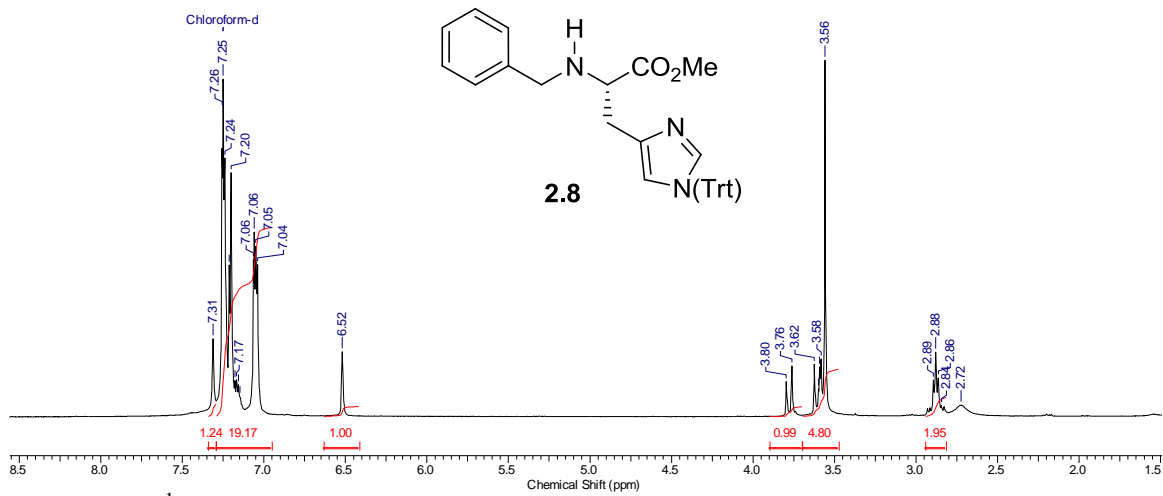


Figure A5: gCOSY spectrum (400 MHz, MeOH-d₄) of **2.1**

N^α-benzyl-L-histidine(Trt)-OMe (2.8)

Rhenium(I) tricarbonyl-N^α-benzyl-L-histidine(Trt) (**2.2**)

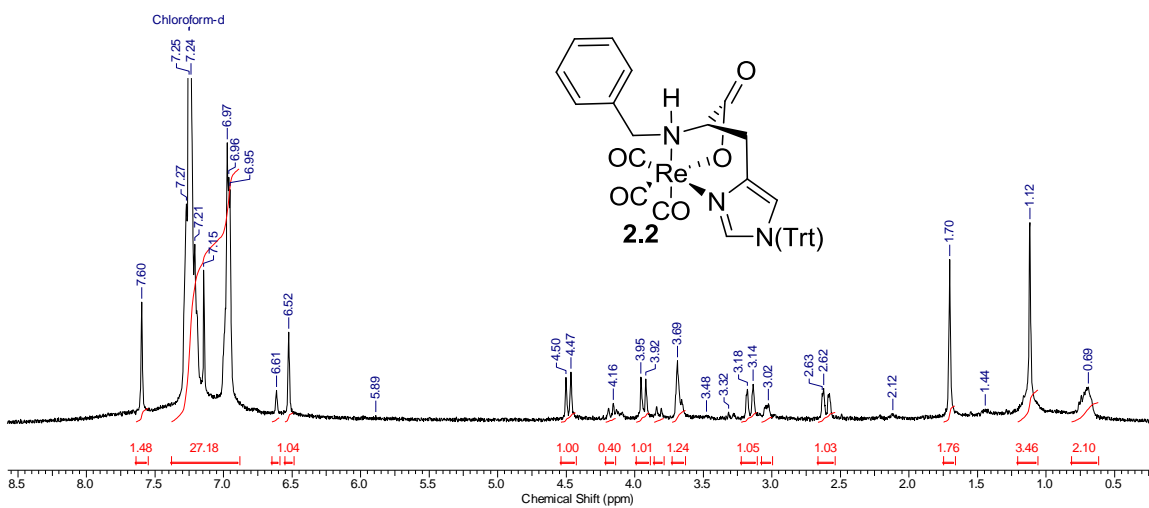


Figure A7: ¹H NMR (400 MHz, CDCl₃) of **2.2**

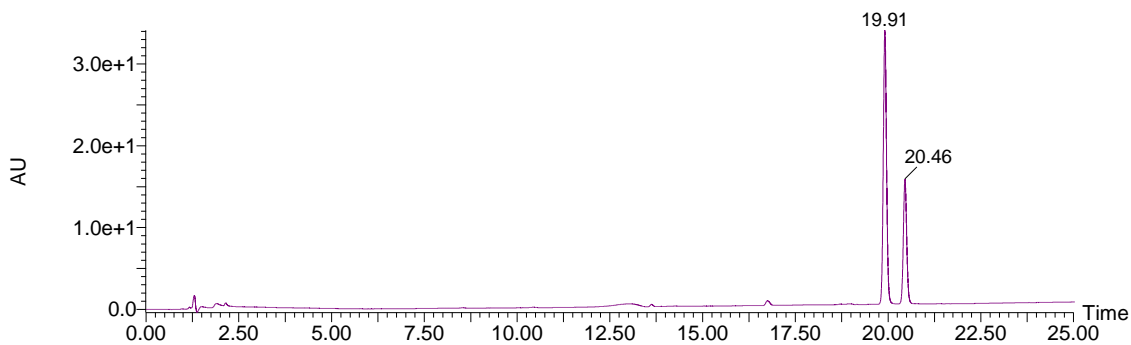
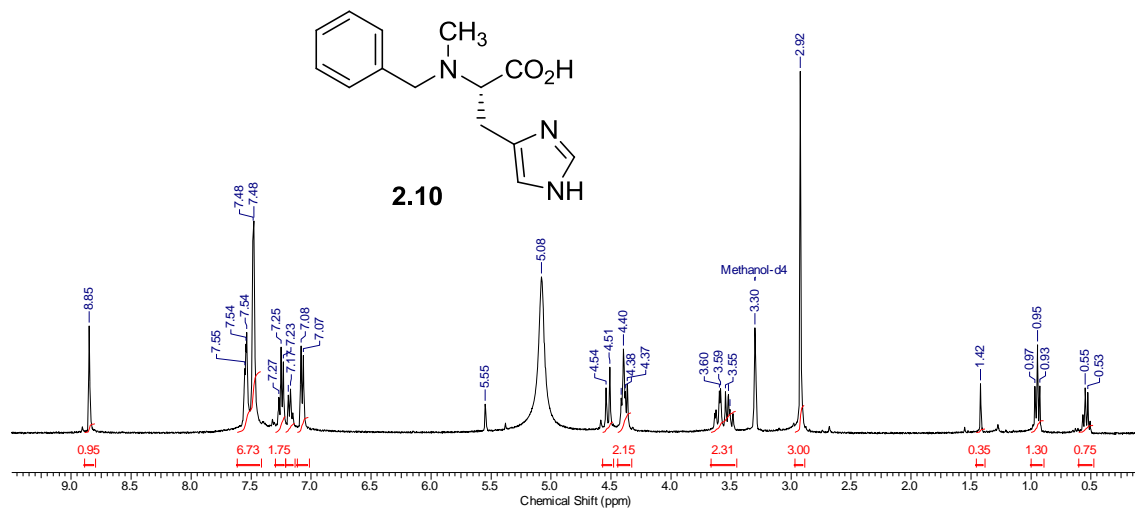
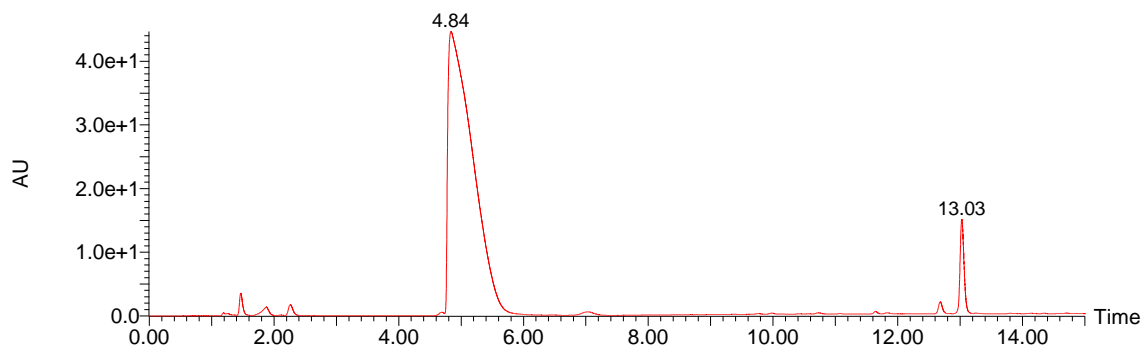


Figure A8: Analytical HPLC trace, UV absorbance detected from 210-800 nm (RP-C18 4.6 x 250 mm, 5 μm), of **2.2**

N^α-benzyl(methyl)-L-histidine (2.10)**Figure A9:** ¹H NMR (400 MHz, MeOH-d₄) of **2.10****Figure A10:** Analytical HPLC trace, UV absorbance detected from 210–800 nm (RP-C18 4.6 x 250 mm, 5 μm), of **2.10**

Rhenium(I) tricarbonyl-N^α-benzyl(methyl)-L-histidine (2.3)

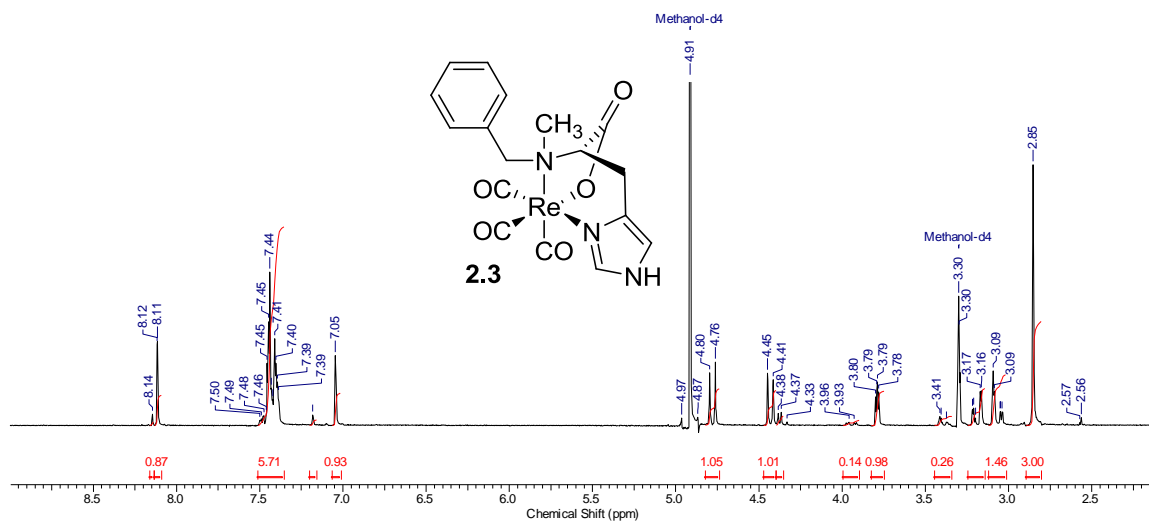


Figure A11: ¹H NMR (400 MHz, MeOH-d₄) of **2.3**

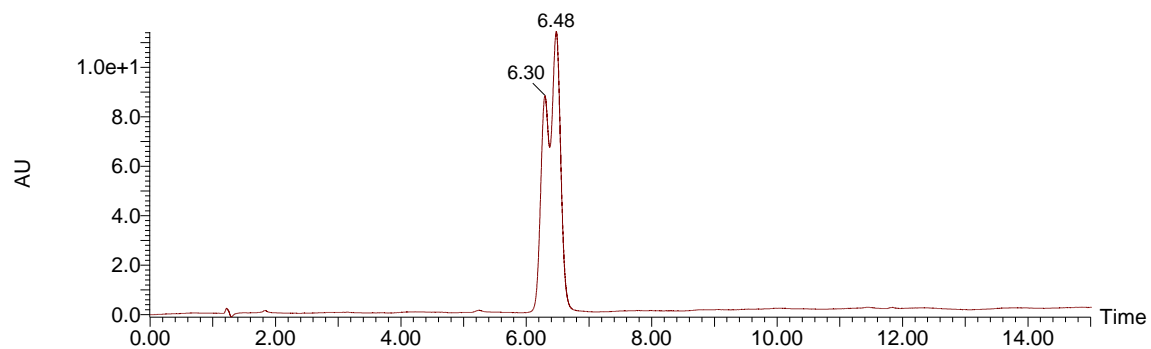


Figure A12: Analytical HPLC trace, UV absorbance detected from 210-800 nm (RP-C18 4.6 x 250 mm, 5 μm), of **2.3**

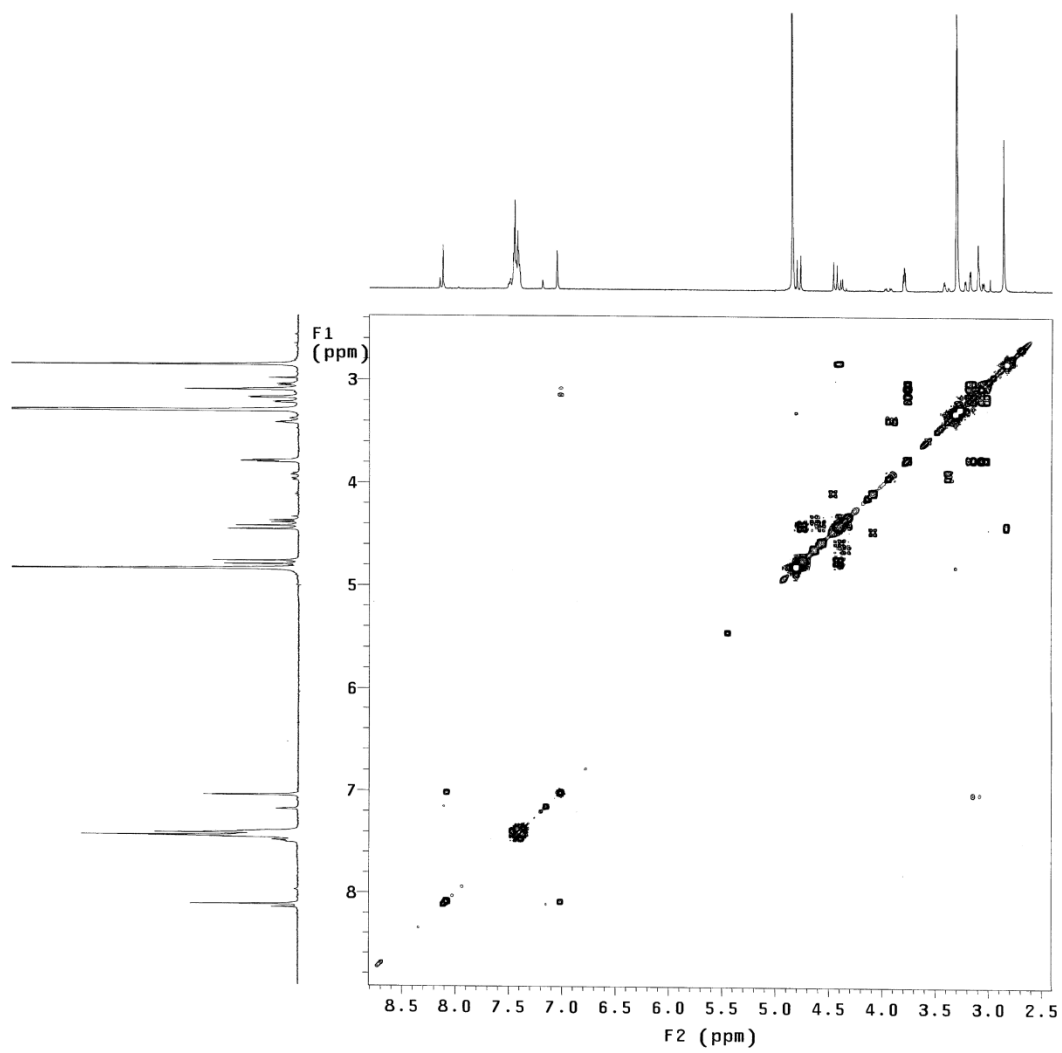


Figure A13: gCOSY spectrum (400 MHz, MeOH-d₄) of **2.3**

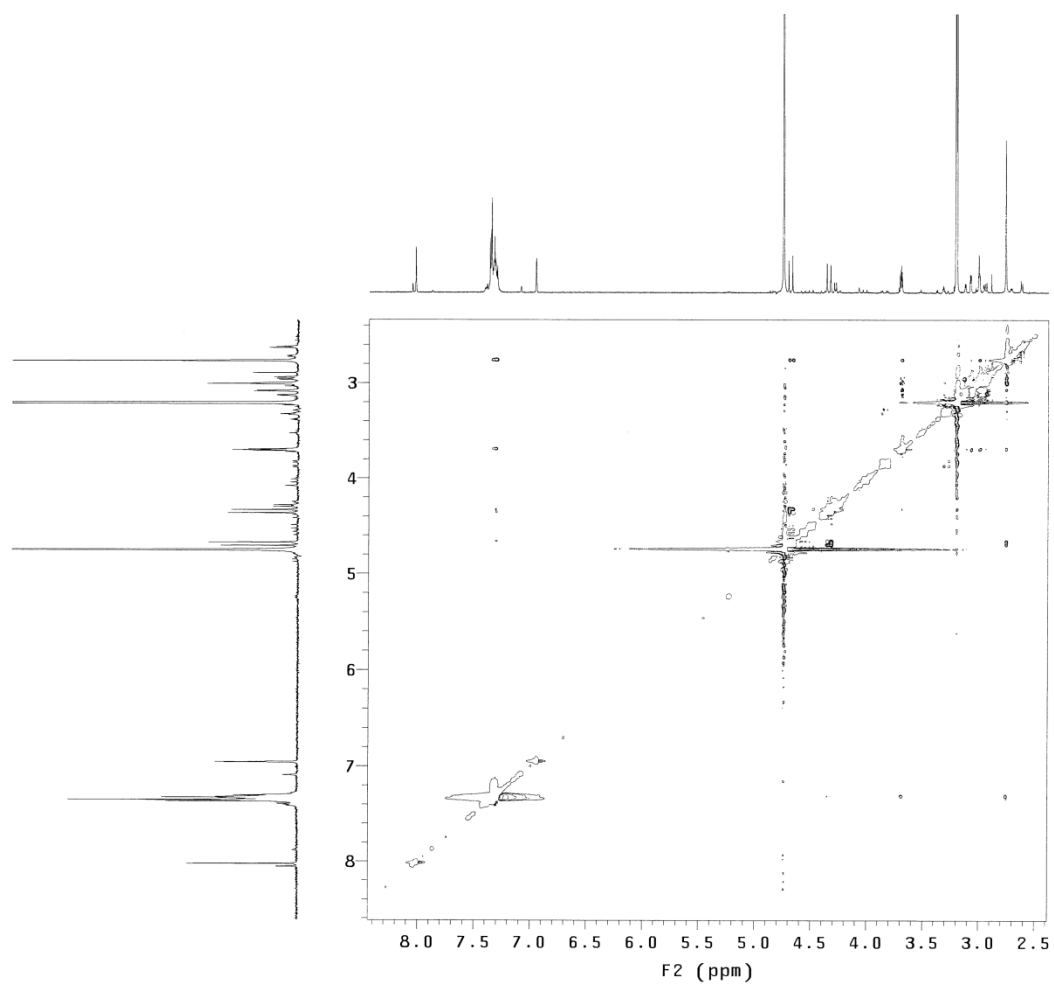
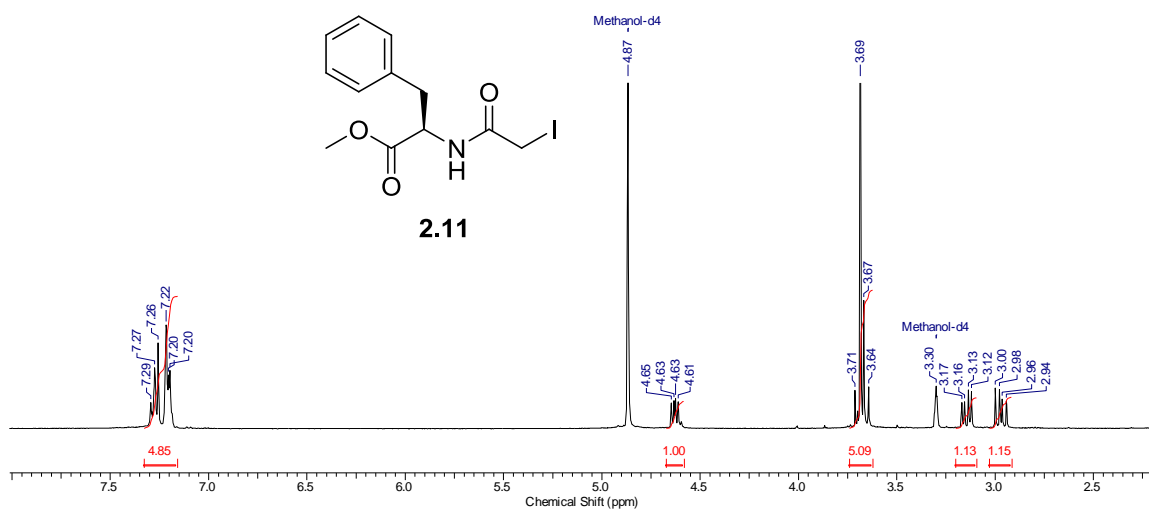
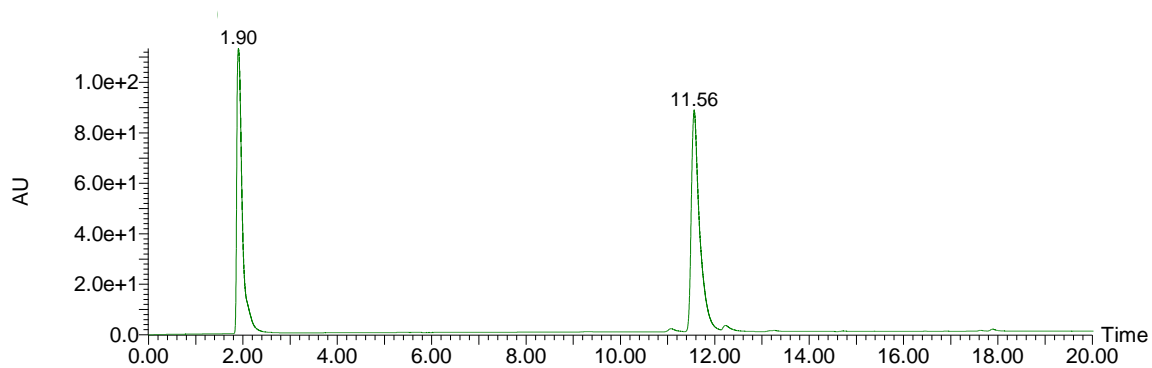
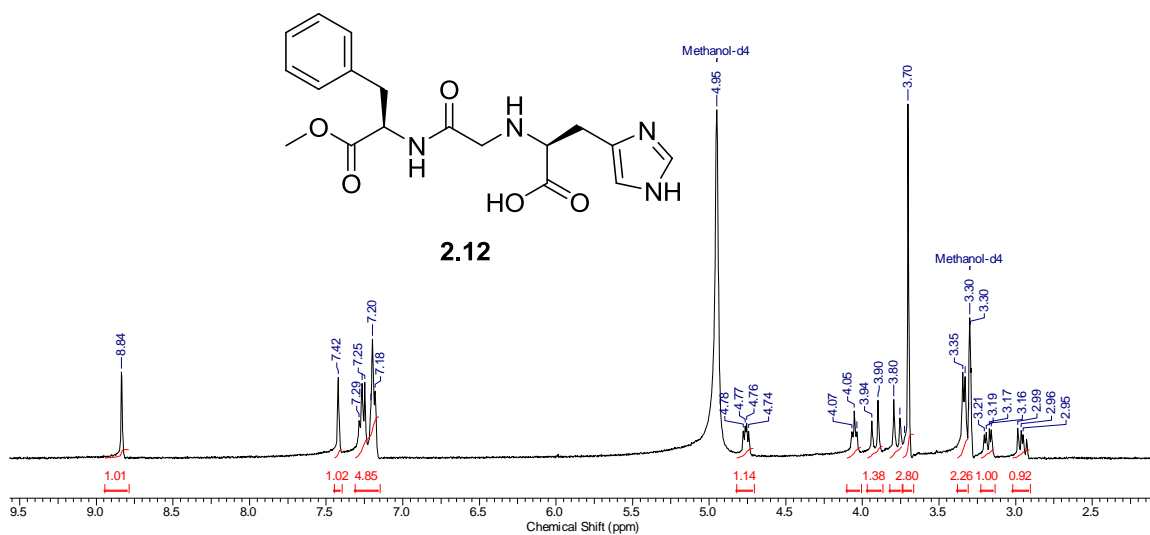
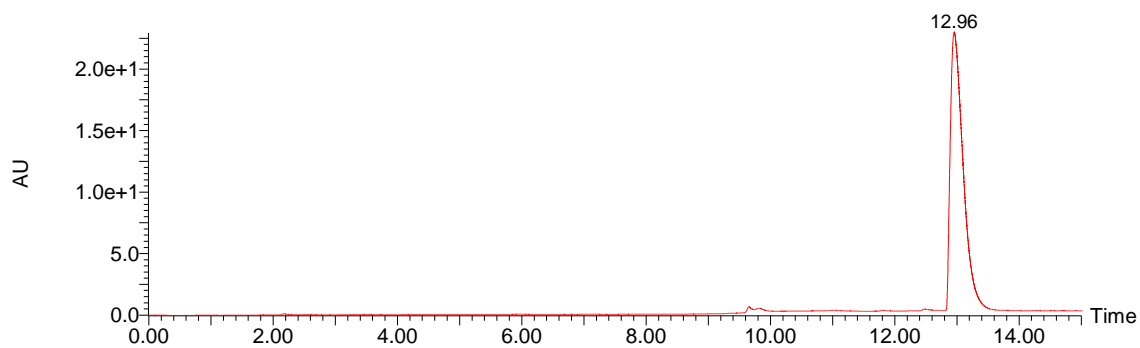


Figure A14: NOESY spectrum (400 MHz, MeOH-d₄) of **2.3**

N-iodocarbonyl-O-methyl phenylalanine (2.11)**Figure A15:** ^1H NMR (400 MHz, MeOH-d₄) of **2.11****Figure A16:** Analytical HPLC trace, UV absorbance detected from 210-800 nm (RP-C18 4.6 x 250 mm, 5 μm), of **2.11**

N^α-histidinyl-acetyl-phenylalanine (2.12)**Figure A17:** ¹H NMR (400 MHz, MeOH-d₄) of **2.12****Figure A18:** Analytical HPLC trace, UV absorbance detected from 210-800 nm (RP-C18 4.6 x 250 mm, 5 μm), of **2.12**

Rhenium(I) tricarbonyl-N^α-histidinyl-acetyl-phenylalanine (2.4)

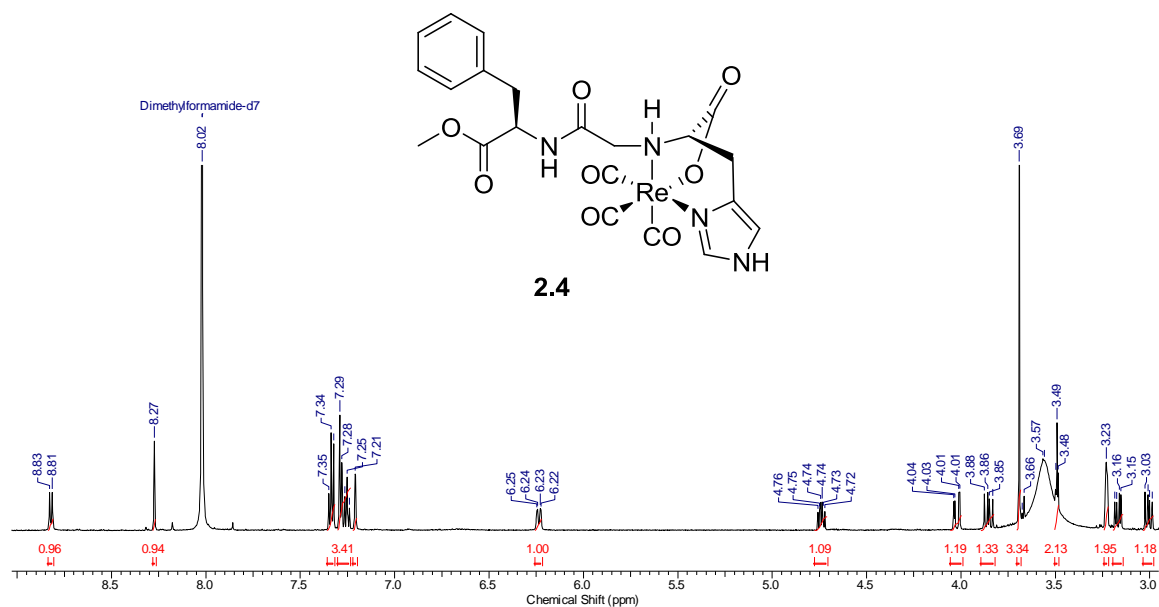


Figure A19: ¹H NMR (600 MHz, DMF-d7) of **2.4**

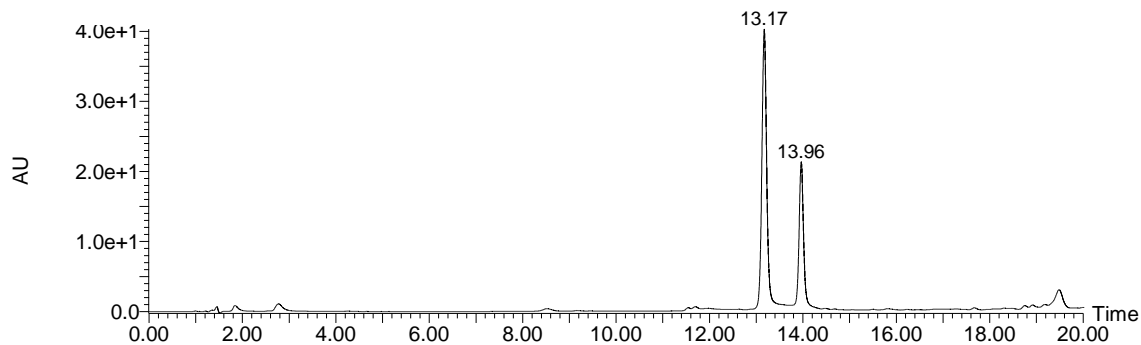


Figure A20: Analytical HPLC trace, UV absorbance detected from 210-800 nm (RP-C18 4.6 x 250 mm, 5 μm), of **2.4**

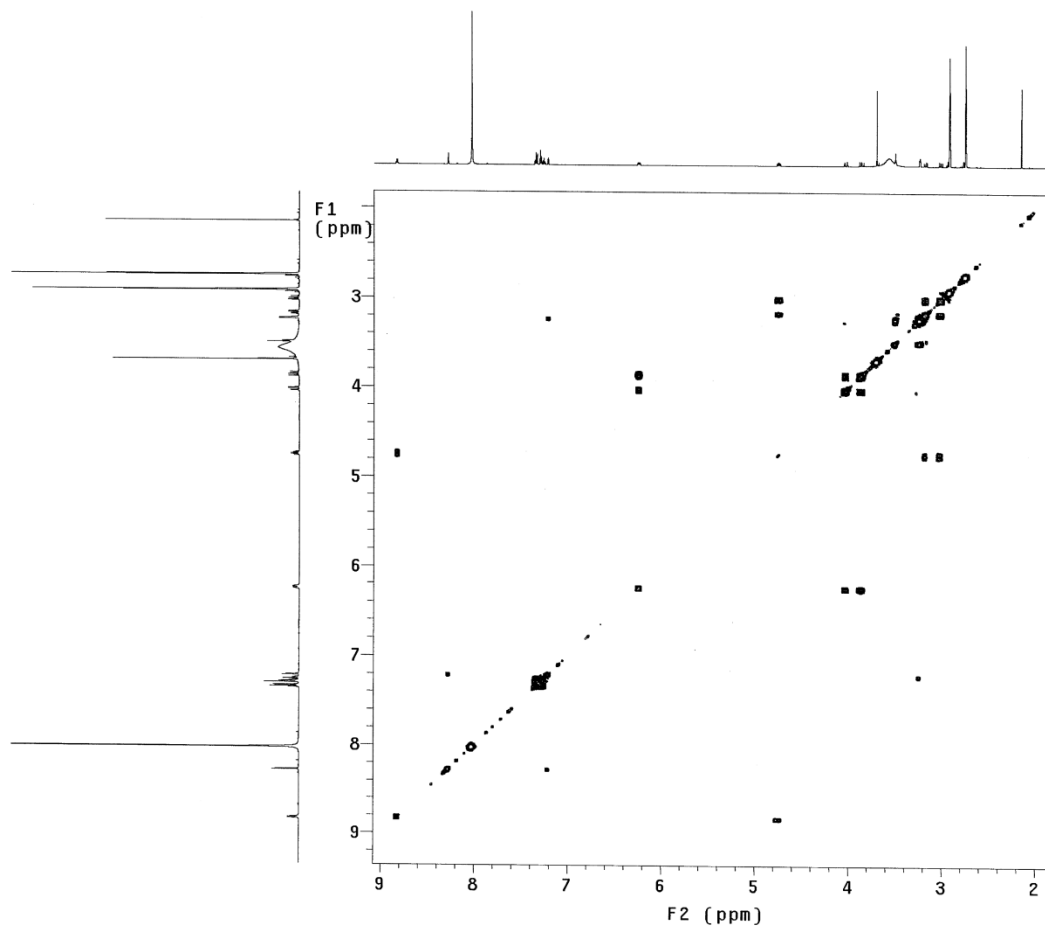
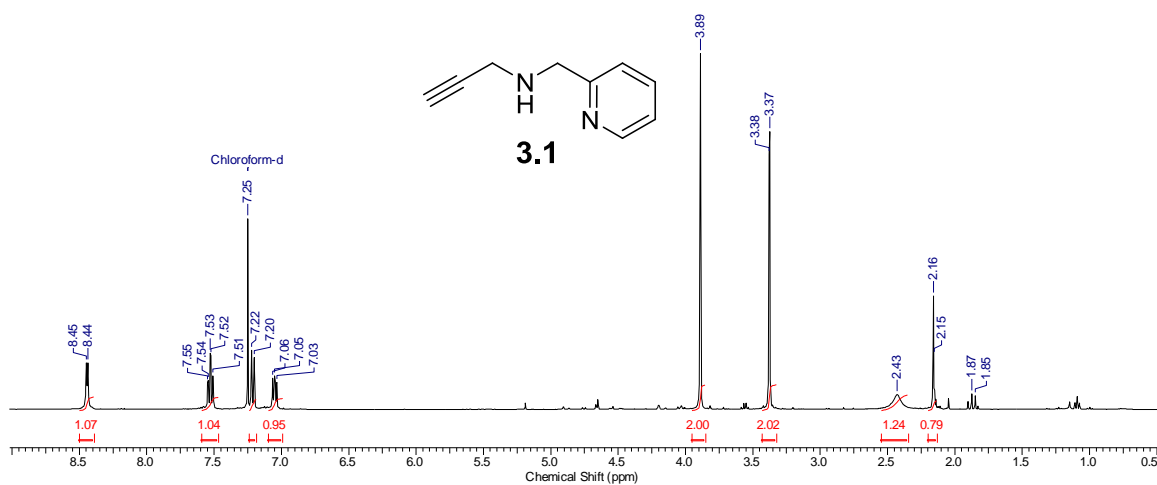
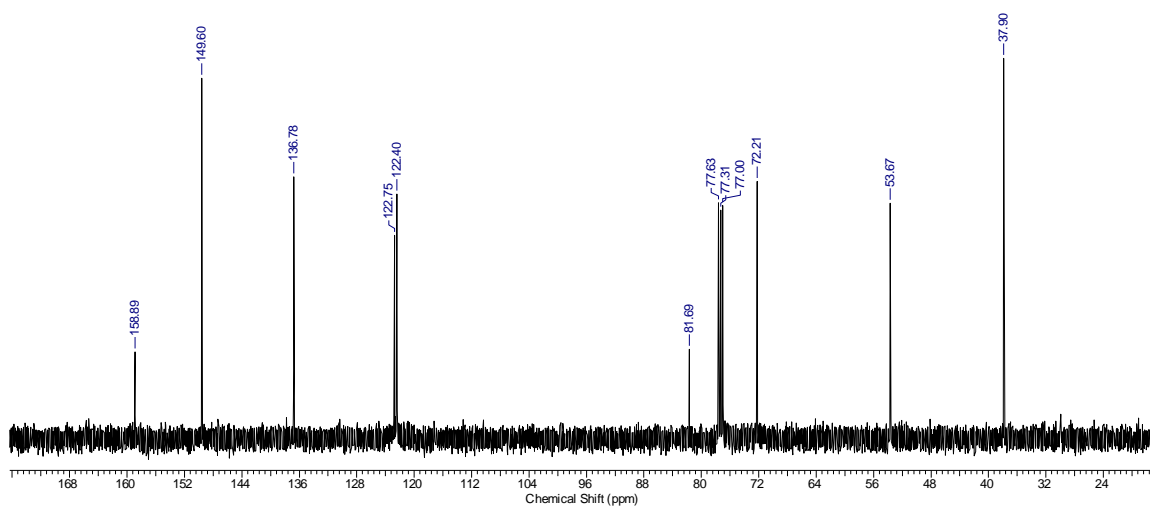
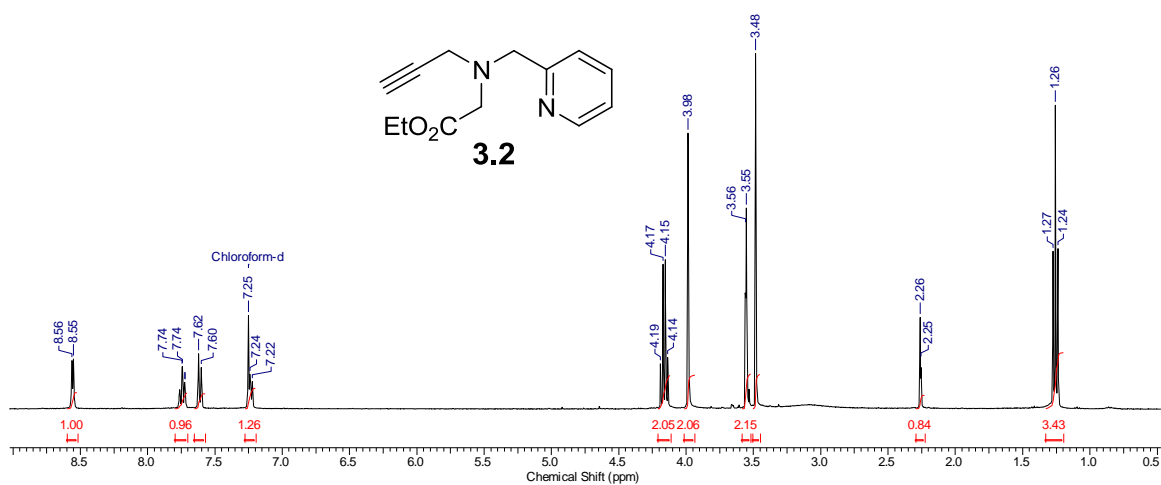
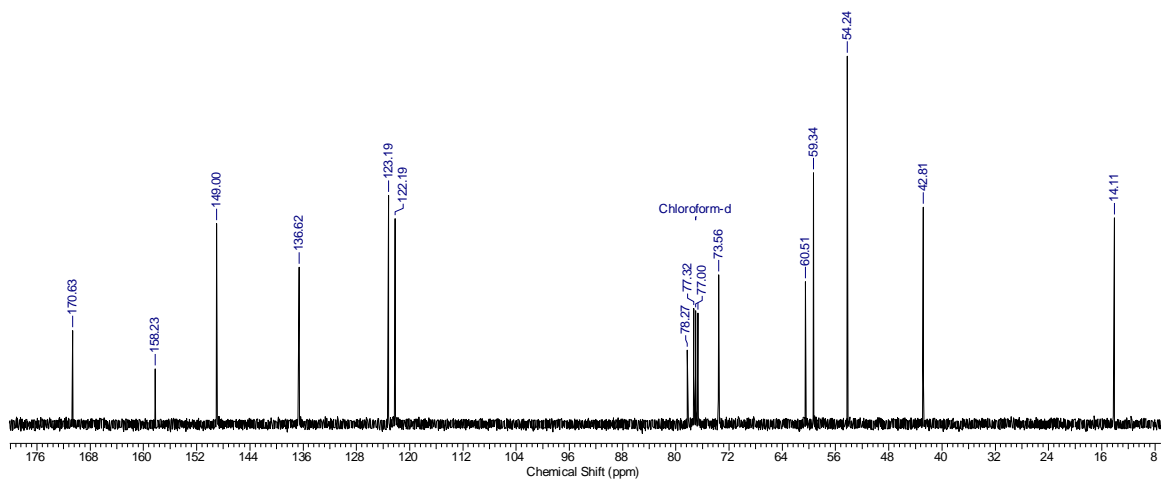
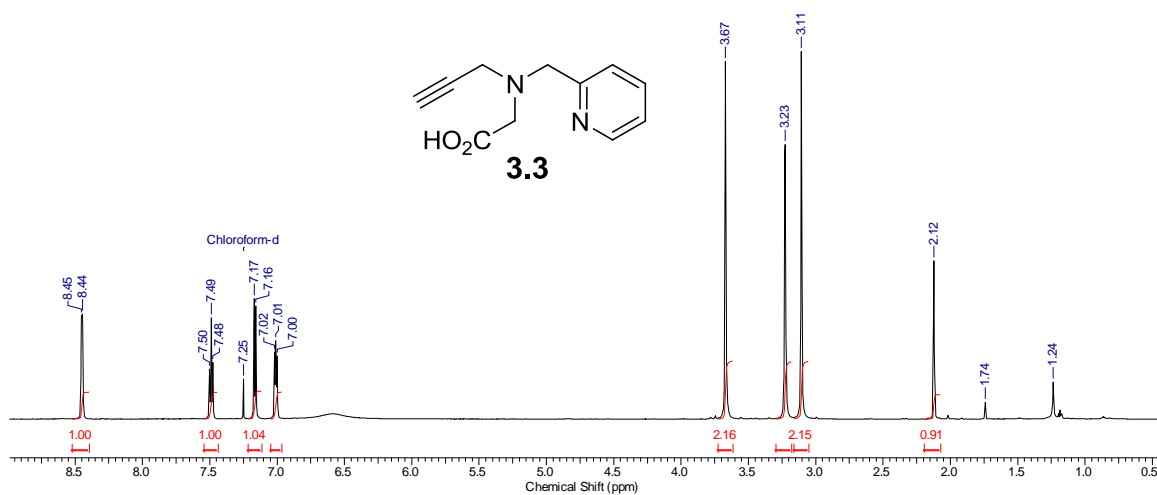
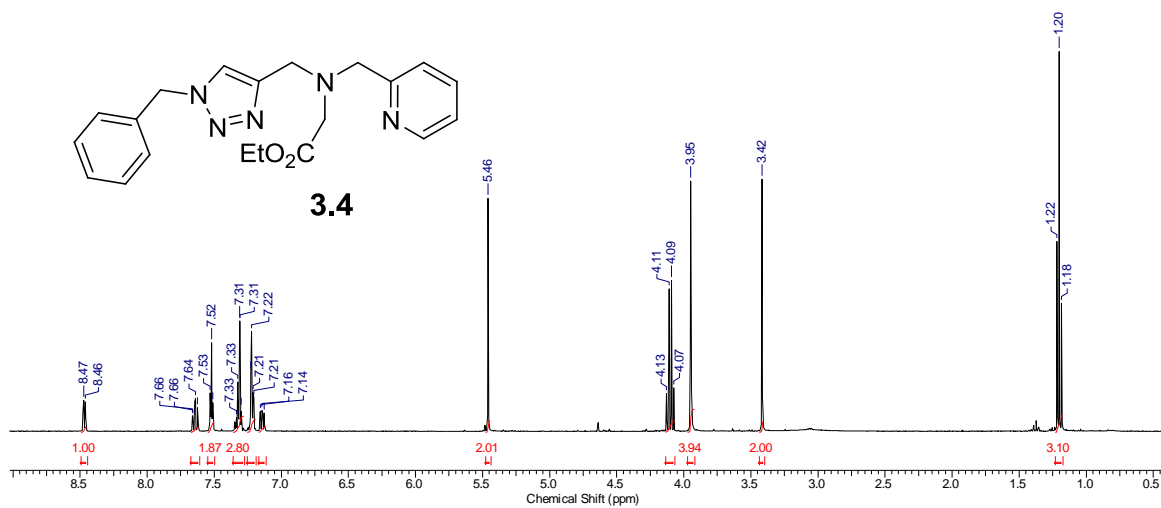
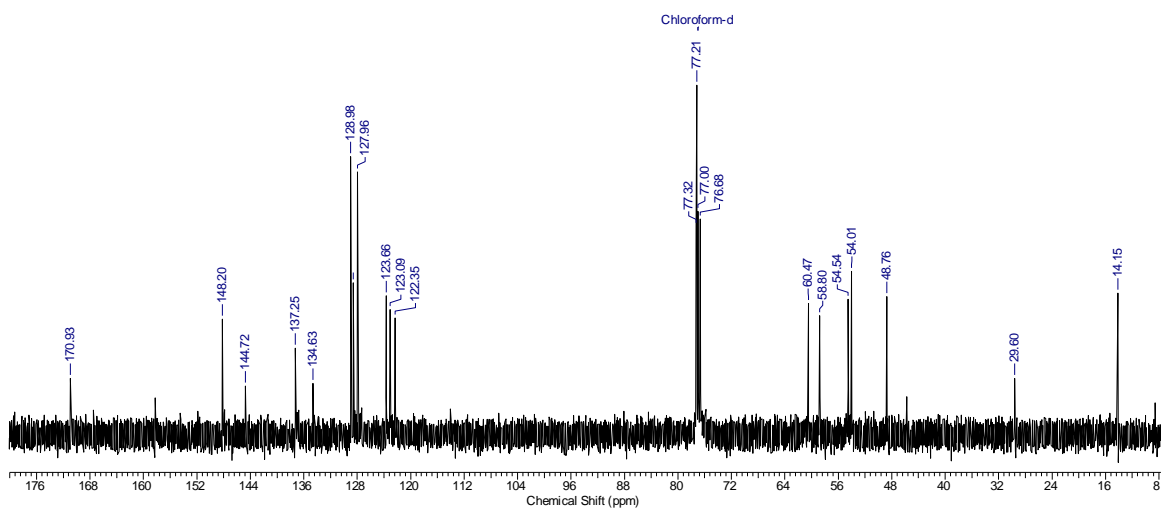


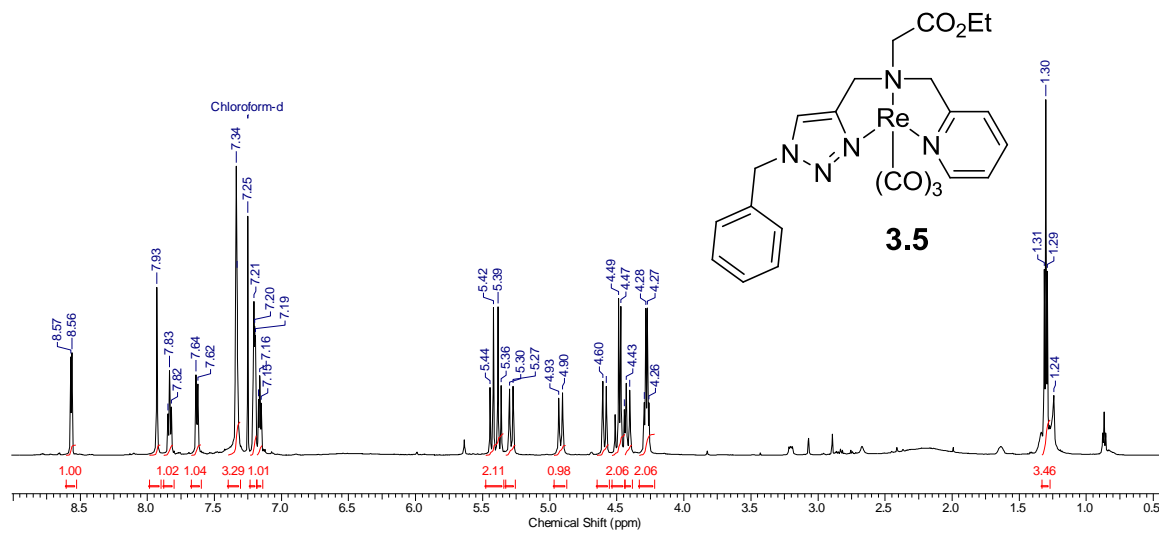
Figure A21: gCOSY spectrum (600 MHz, DMF-d₇) of **2.4**

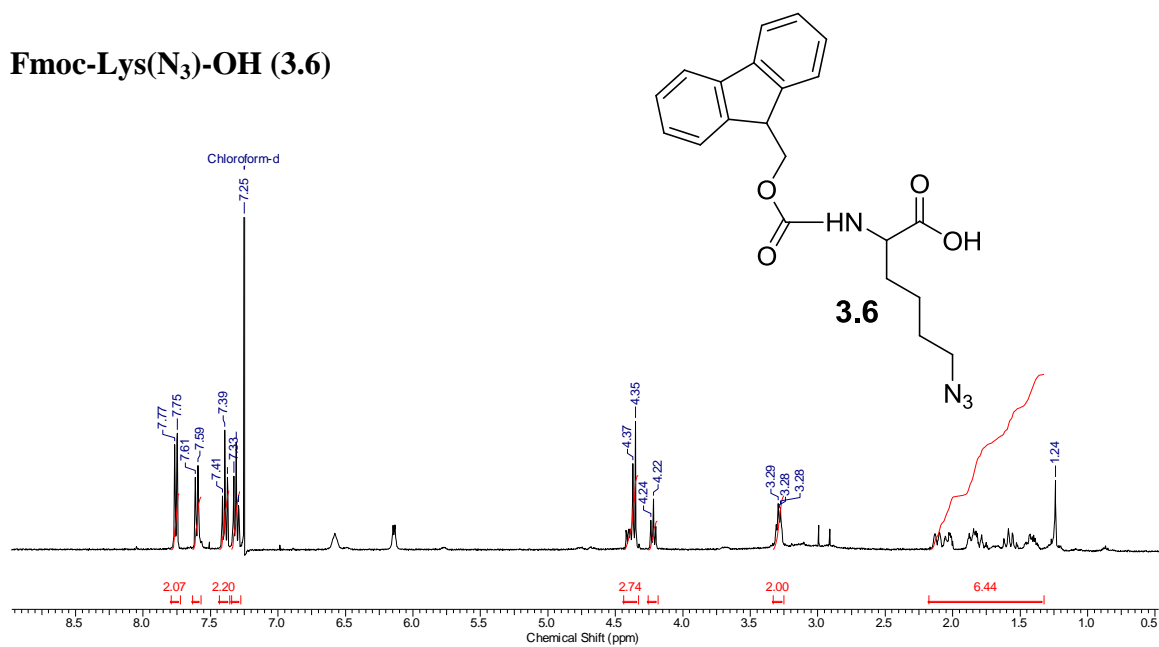
N-propargyl-pyridine-2-methylamine (3.1)**Figure A22:** ^1H NMR (400 MHz, CDCl_3) of **3.1****Figure A23:** ^{13}C NMR (100 MHz, CDCl_3) of **3.1**

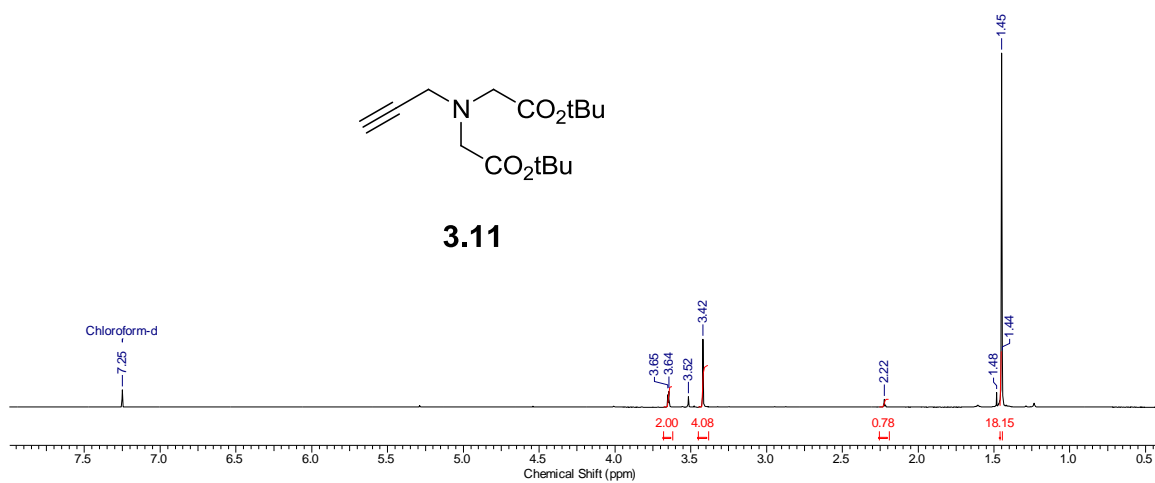
Ethyl-propargyl-pyridine-2-methylamino-acetate (3.2)**Figure A24:** ¹H NMR (400 MHz, CDCl₃) of **3.2****Figure A25:** ¹³C NMR (100 MHz, CDCl₃) of **3.2**

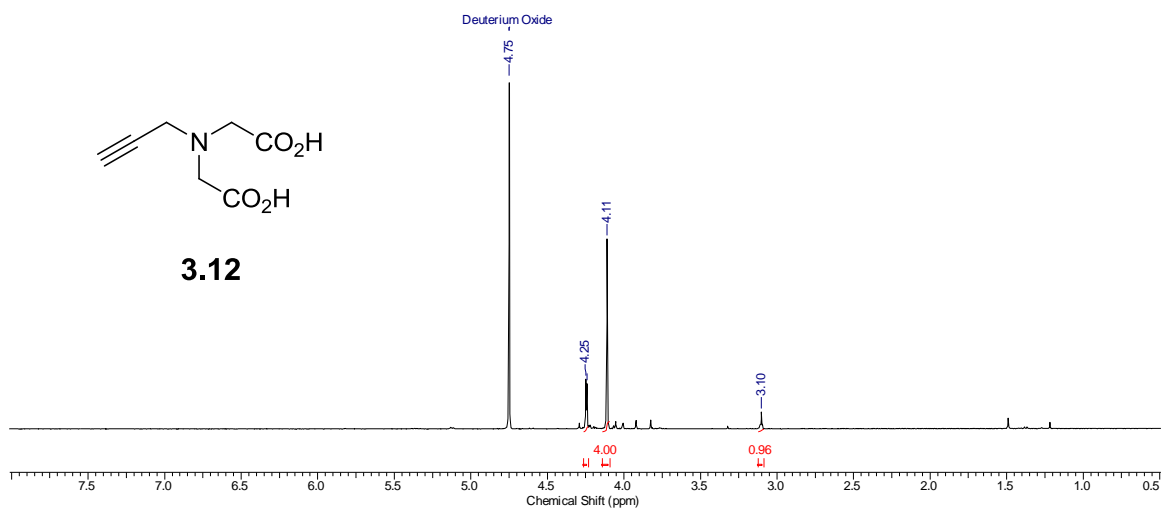
Propargyl-pyridine-2-methylamino-acetic acid (3.3)**Figure A26:** ^1H NMR (600 MHz, CDCl_3) of **3.3**

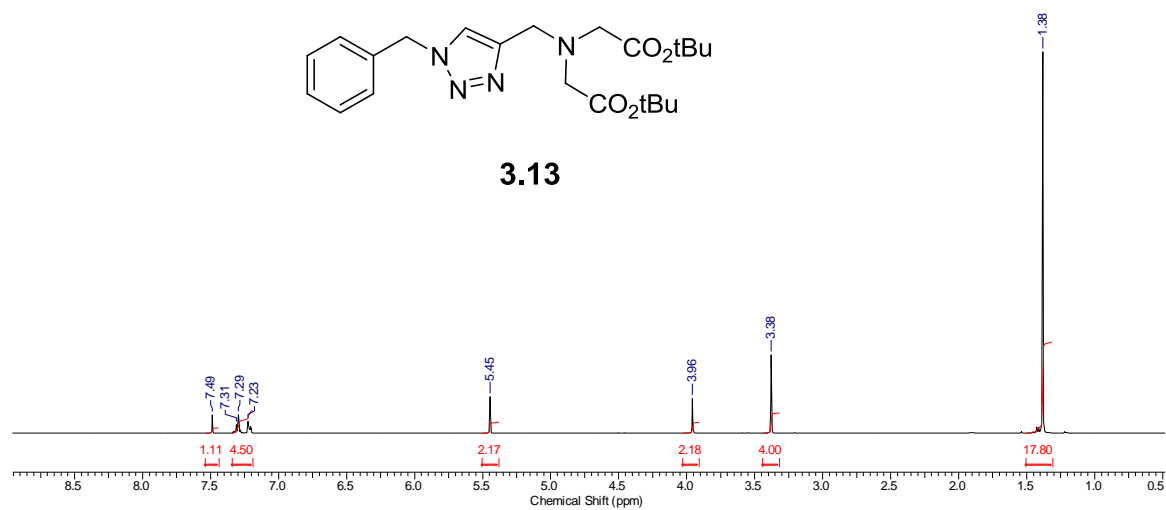
1-(benzyl)triazole-pyridine-2-methylamino-acetate (3.4)**Figure A27:** ¹H NMR (400 MHz, CDCl₃) of 3.4**Figure A28:** ¹³C NMR (100 MHz, CDCl₃) of 3.4

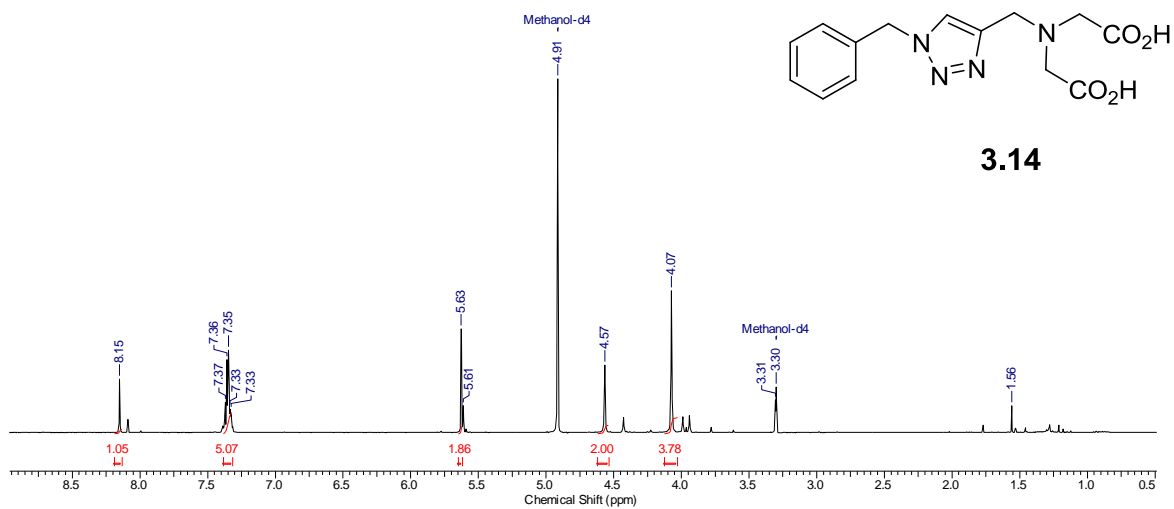
Rhenium(I) tricarbonyl-1-(benzyl)triazole-pyridine-2-methylamino-acetate (3.5)**Figure A29:** ¹H NMR (600 MHz, CDCl₃) of 3.5

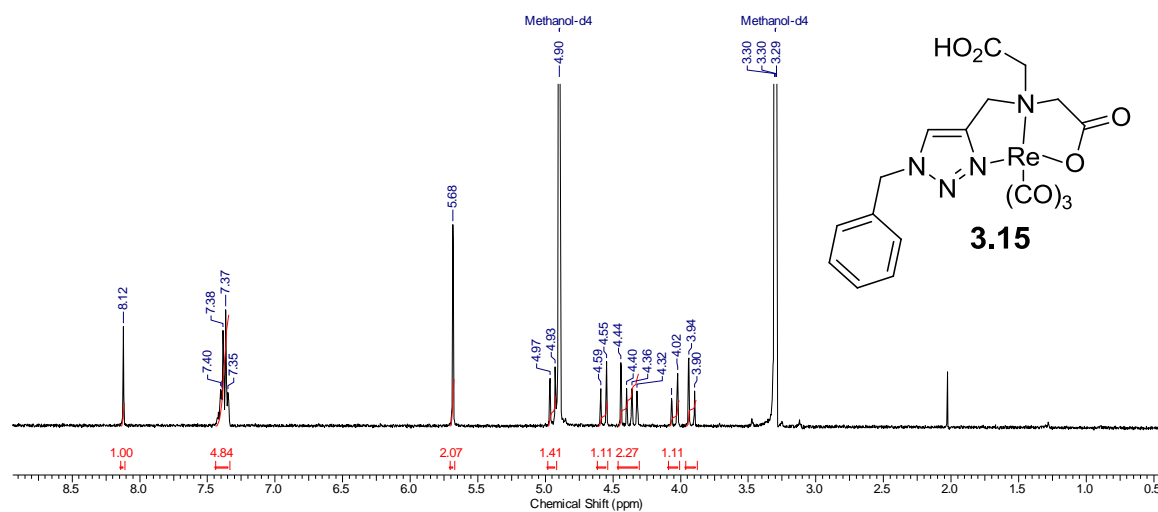
Fmoc-Lys(N₃)-OH (3.6)**Figure A30:** ¹H NMR (400 MHz, CDCl₃) of **3.6**

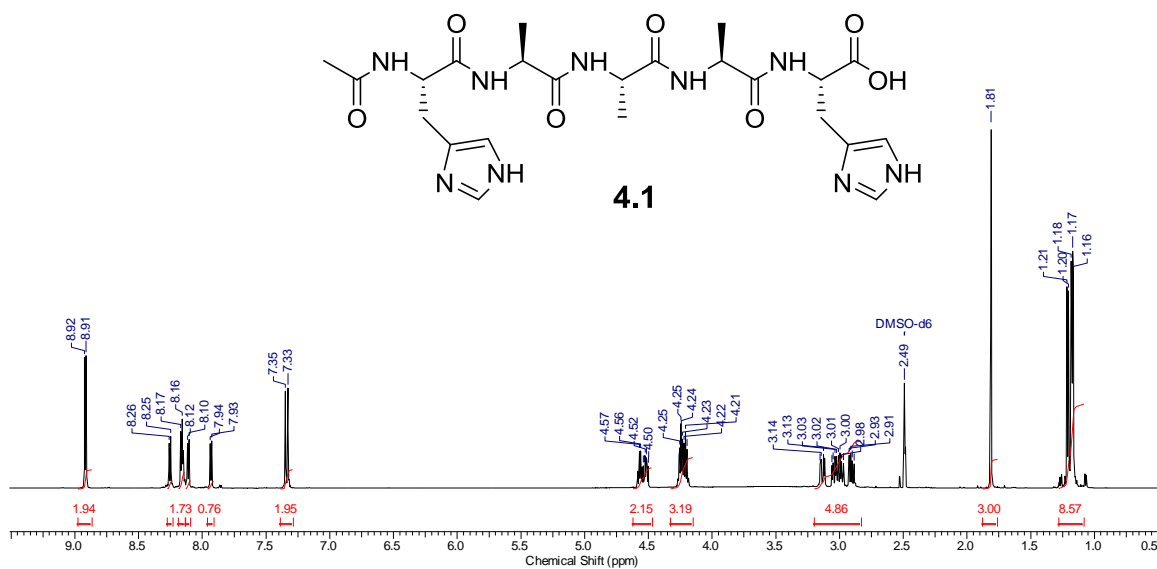
***tert*-butyl-propargyliminodiacetate (3.11)****Figure A31:** ¹H NMR (400 MHz, CDCl₃) of **3.11**

N-propargyliminodiacetic acid (3.12)**Figure A32:** ¹H NMR (400 MHz, D₂O) of **3.12**

1-(benzyl)triazole-propargyliminodiacetate (3.13)**Figure A33:** ¹H NMR (400 MHz, CDCl₃) of **3.13**

1-(benzyl)triazole-propargyliminodiacetic acid (3.14)**Figure A34:** ^1H NMR (400 MHz, MeOH-d_4) of **3.14**

Rhenium(I) tricarbonyl-1-(benzyl)triazole-propargyliminodiacetic acid (3.15)**Figure A35:** $^1\text{H NMR}$ (400 MHz, MeOH- d_4) of **3.15**

Ac-HAAA-H-OH (**4.1**)Figure A36: ^1H NMR (600 MHz, DMSO-d₆) of **4.1**

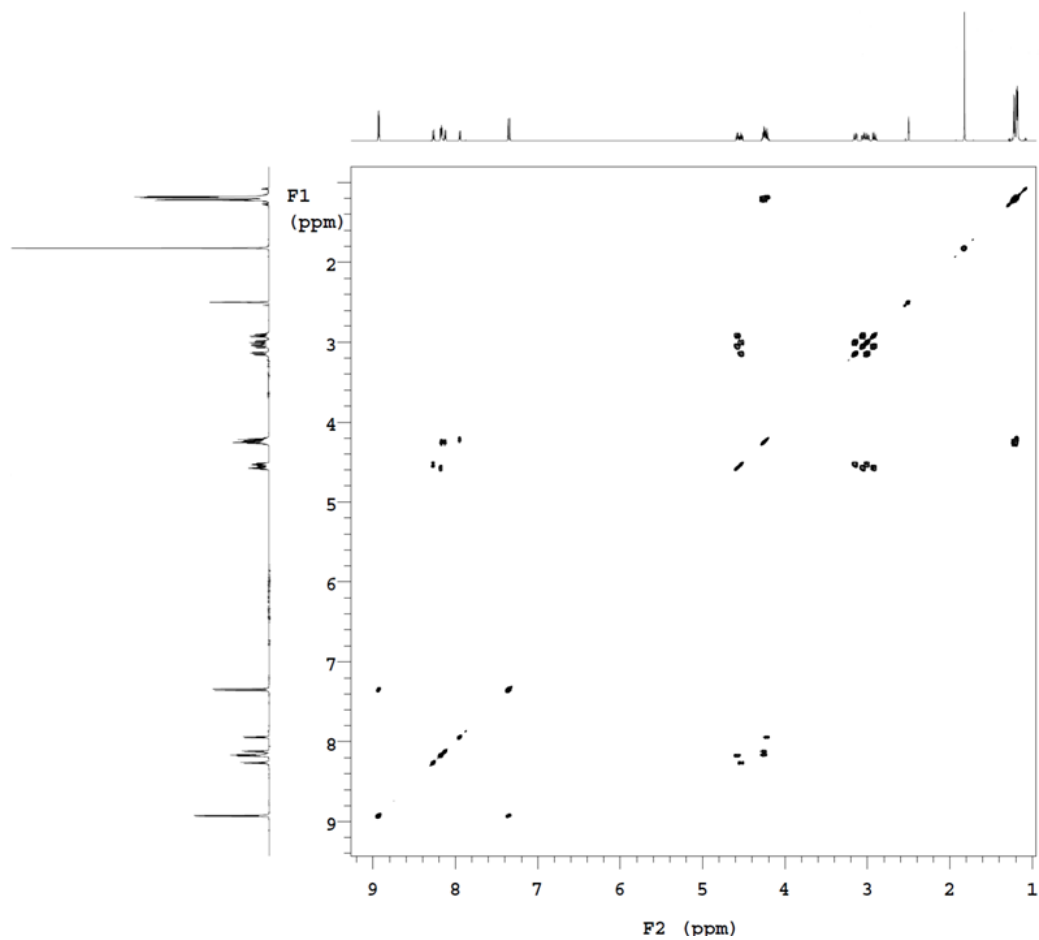


Figure A37: gCOSY spectrum (600 MHz, DMSO-d₆) of **4.1**

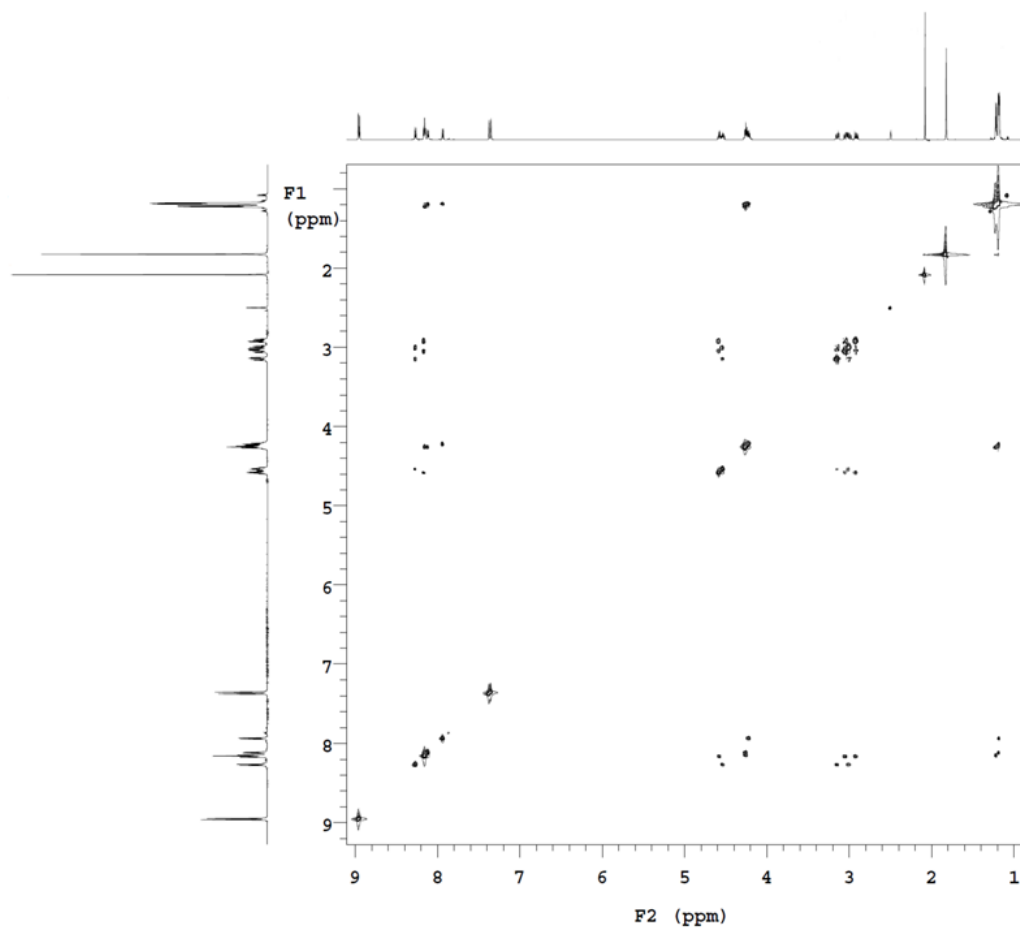
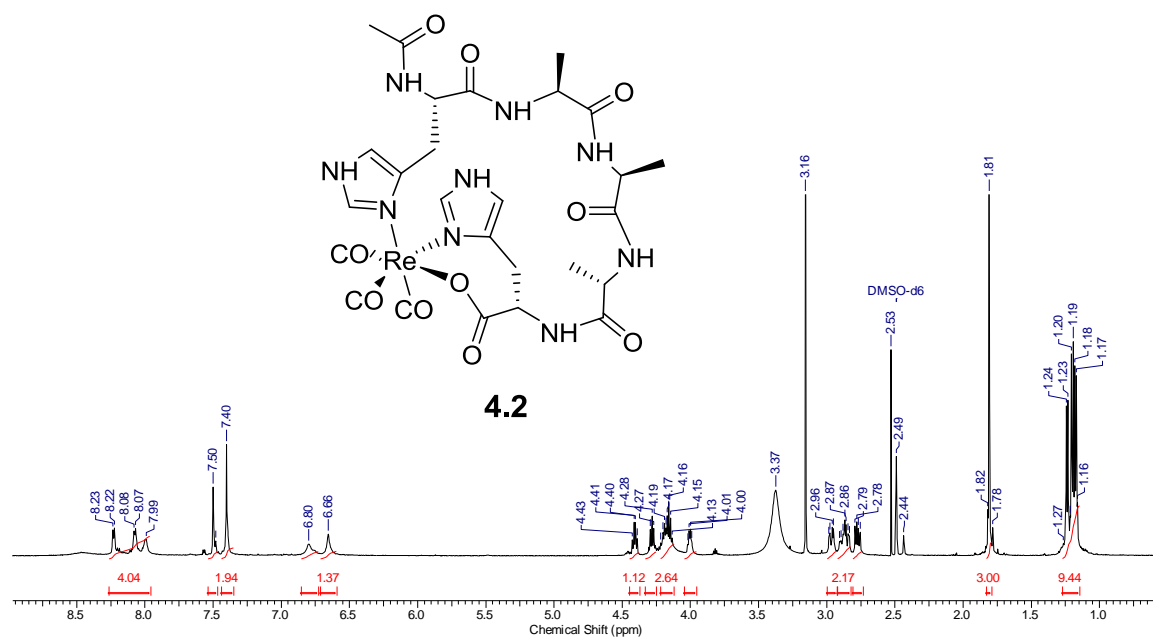


Figure A38: TOCSY spectrum (600 MHz, DMSO-d₆) of **4.1**

Re(CO)₃-Ac-HAAAHOH (4.2)**Figure A39:** ¹H NMR (600 MHz, DMSO-d₆) of 4.2

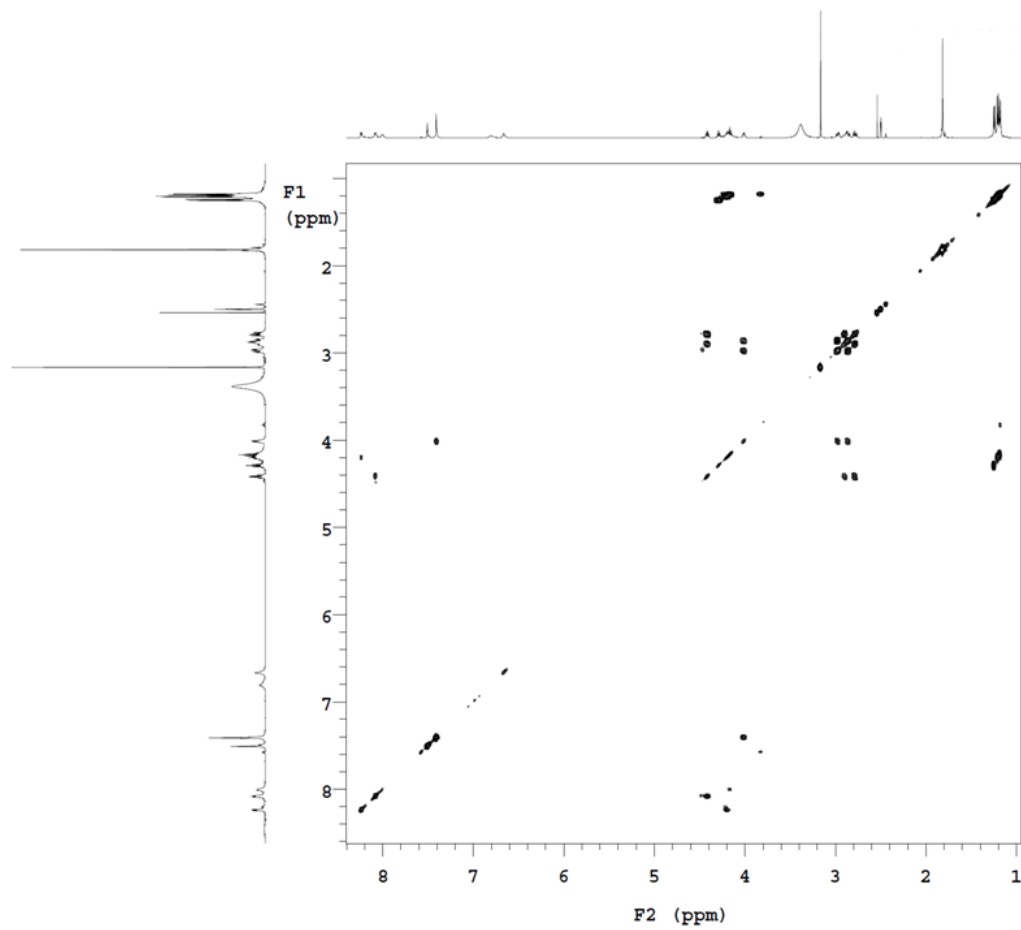


Figure A40: gCOSY spectrum (600 MHz, DMSO-d₆) of 4.2

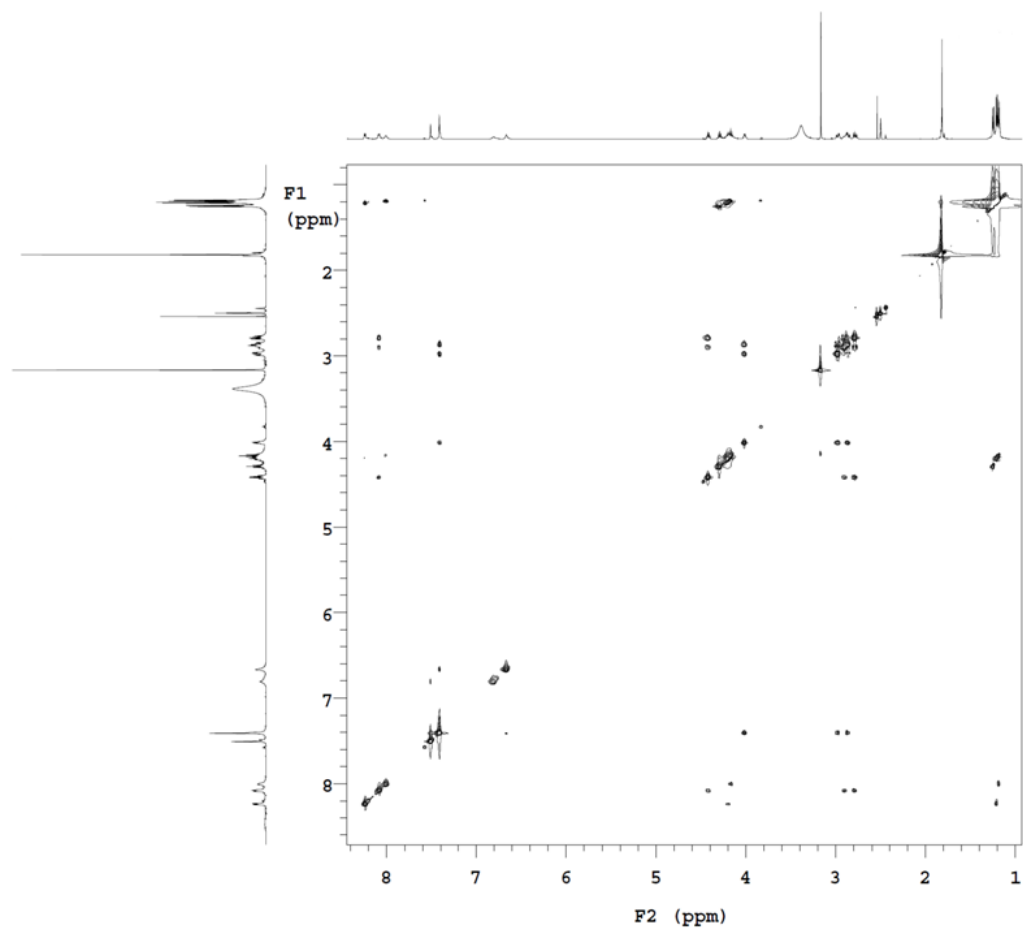


Figure A41: TOCSY spectrum (600 MHz, DMSO-d₆) of **4.2**

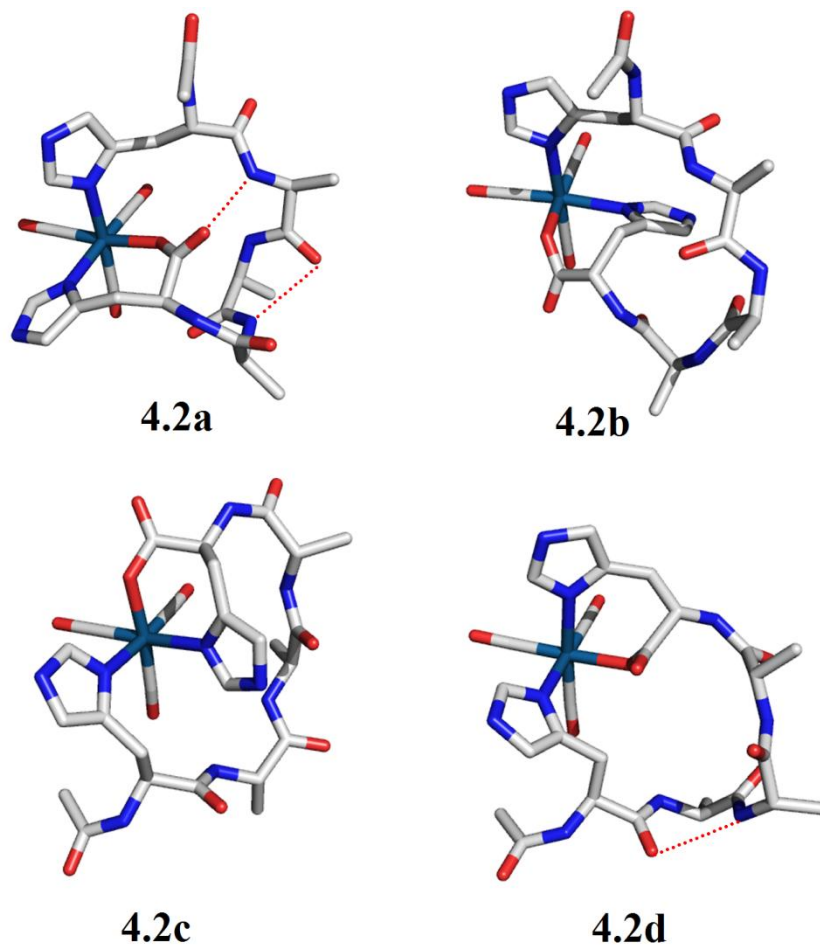


Figure A42: 3D structures showing intramolecular hydrogen bonding interactions (dashed red lines) of the four isomers of the proposed structure of cyclized peptide **4.2** where the imidazole-N1 of the N-terminal histidine is coordinated to the rhenium, with **4.2a** having the lowest energy

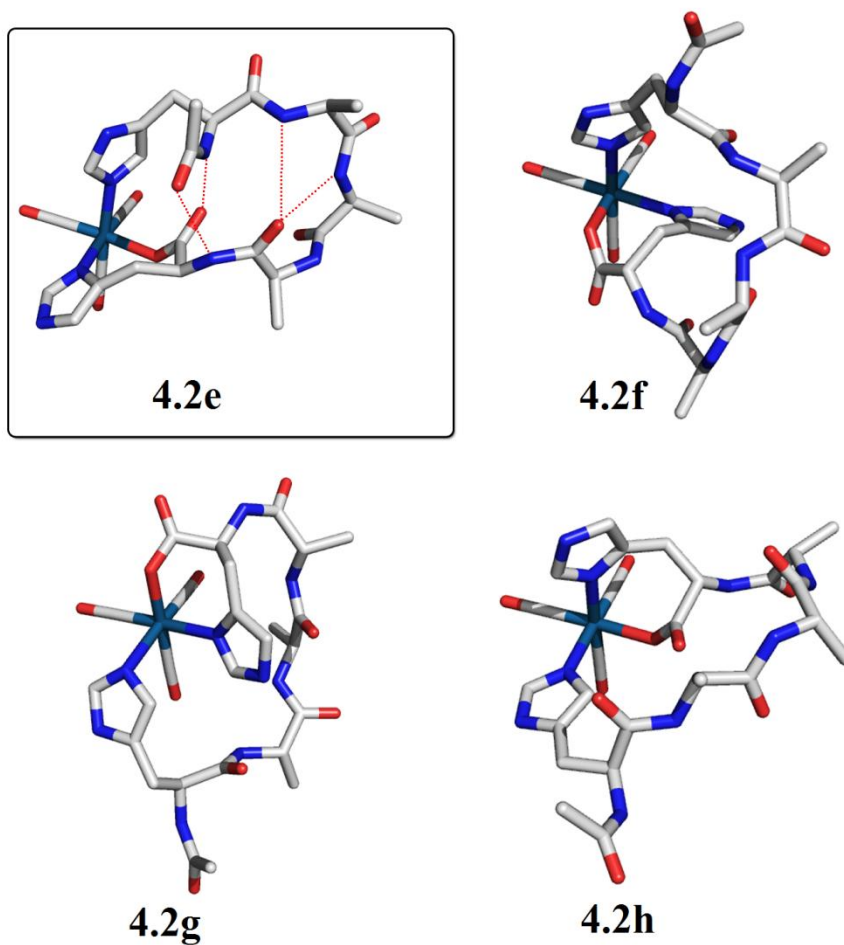


Figure A43: 3D structures showing intramolecular hydrogen bonding interactions (dashed red lines) of the four isomers of the proposed structure of cyclized peptide **4.2** where the imidazole-N3 of the N-terminal histidine is coordinated to the rhenium, with **4.2e** having the lowest energy and the same hydrogen bonding interactions as was seen in the VT NMR

Appendix B : Letter of Permission

RSC | Advancing the
Chemical Sciences

Royal Society of Chemistry
Thomas Graham House
Science Park
Milton Road
Cambridge
CB4 0WF

Tel: +44 (0)1223 420 066
Fax: +44 (0)1223 423 623
Email: contracts-copyright@rsc.org

www.rsc.org

Acknowledgements to be used by RSC authors

Authors of RSC books and journal articles can reproduce material (for example a figure) from the RSC publication in a non-RSC publication, including theses, without formally requesting permission providing that the correct acknowledgement is given to the RSC publication. This permission extends to reproduction of large portions of text or the whole article or book chapter when being reproduced in a thesis.

The acknowledgement to be used depends on the RSC publication in which the material was published and the form of the acknowledgements is as follows:

- For material being reproduced from an article in *New Journal of Chemistry* the acknowledgement should be in the form:
 - [Original citation] - Reproduced by permission of The Royal Society of Chemistry (RSC) on behalf of the Centre National de la Recherche Scientifique (CNRS) and the RSC
- For material being reproduced from an article *Photochemical & Photobiological Sciences* the acknowledgement should be in the form:
 - [Original citation] - Reproduced by permission of The Royal Society of Chemistry (RSC) on behalf of the European Society for Photobiology, the European Photochemistry Association, and RSC
- For material being reproduced from an article in *Physical Chemistry Chemical Physics* the acknowledgement should be in the form:
 - [Original citation] - Reproduced by permission of the PCCP Owner Societies
- For material reproduced from books and any other journal the acknowledgement should be in the form:
 - [Original citation] - Reproduced by permission of The Royal Society of Chemistry

The acknowledgement should also include a hyperlink to the article on the RSC website.

The form of the acknowledgement is also specified in the RSC agreement/licence signed by the corresponding author.

Except in cases of republication in a thesis, this express permission does not cover the reproduction of large portions of text from the RSC publication or reproduction of the whole article or book chapter.

A publisher of a non-RSC publication can use this document as proof that permission is granted to use the material in the non-RSC publication.

Curriculum Vitae

Name: Emily Simpson

Post-secondary Education and Degrees: The University of Western Ontario
London, Ontario, Canada
2005-2009 B.Sc.

The University of Western Ontario
London, Ontario, Canada
2009-2014 Ph.D.

Honours and Awards: Society of Radiopharmaceutical Sciences Bursary Award
Sept. 2010, Sept. 2011

UWO Division of Experimental Oncology Graduate Student Travel Award
Jan. 2011

Graduate Tuition Scholarship in Science
May 2009

Western Scholarship of Distinction
Sept. 2005

Related Work Experience: Teaching Assistant
The University of Western Ontario
Sept. 2009-Apr. 2014

Research Assistant
London Regional Cancer Program
Victoria Hospital
May – Aug. 2008

Publications:

Manuscripts

Simpson, E.J.; Ngo, B.; Hou, J.Q.; Luyt, L.G. *Cyclized Pentapeptides as [2+1] Chelation Systems for $^{99m}\text{Tc}/\text{Re}(\text{CO})_3$* . (In Preparation)

Simpson, E.J.; Gobbo, P.; Bononi, F.C.; Workentin, M.S.; Luyt, L.G. *Bombesin Functionalized Water-Soluble Gold Nanoparticles for Prostate Cancer Imaging*. (In Preparation)

Hickey, J.L.; Simpson, E.J.; Luyt, L.G. *Synthesis of Macrocyclic β -Sheet Scaffolds as Molecular Imaging Probes*. (Submitted to Chemistry – A European Journal)

Bruckman, M.A.; Jiang, K.; Simpson, E.J.; Randolph, L.N.; Luyt, L.G.; Yu, X.; Steinmetz, N.F. *Dual-modal magnetic resonance and fluorescence imaging of atherosclerotic plaques in vivo using VCAM-1 targeted tobacco mosaic virus*. *Nano Lett.*, **2014**, *14*, 1551-1558.

Cho, C.-F.; Sourabh, S.; Simpson, E.J.; Steinmetz, N.F.; Luyt, L.G. and Lewis, J.D. *Molecular Targeted Viral Nanoparticles as Tools for Imaging Cancer*. *Methods in Molecular Biology*, **2014**, in *Virus Hybrids as Nanomaterials*, Vol. 1108, pp 211-230.

Simpson, E.J.; Hickey, J.L.; Breadner, D.; Luyt, L.G. *Investigation of Isomer Formation Upon Coordination of Bifunctional Histidine Analogues with $^{99m}\text{Tc}/\text{Re}(\text{CO})_3$* . *Dalton Trans.*, **2012**, *41*, 2950-2958.

Simpson, E.J.; Breadner, D.; Hickey, J.L.; Luyt, L.G. *Isomers of the ($N^\alpha\text{His}$)Ac Chelator Upon Coordination of $^{99m}\text{Tc}/\text{Re}(\text{CO})_3$* . *Technetium and Other Radiometals in Chemistry and Medicine*, 117-118, Padova, Italy: SGEEditoriali, 2010.

Refereed abstracts

Simpson, E.J.; Hickey, J.L.; Luyt, L.G. September **2011**. *Click to Cyclize and Chelate*. 19th International Symposium on Radiopharmaceutical Sciences. Amsterdam, The Netherlands. *J. Labelled Compd. Radiopharm.* **2011**; *54*: S350 (Poster Presentation)

Simpson, E.J.; Breadner, D.; Hickey, J.L.; Luyt, L.G. September **2010**. *Isomers of the ($N^\alpha\text{His}$)Ac Chelator Upon Coordination of $^{99m}\text{Tc}/\text{Re}(\text{CO})_3$* . International Symposium on Technetium and Other Radiometals in Chemistry and Medicine. Bressanone, Italy. *Nucl. Med. Biol.* **2010**; *37*: 685 (Poster Presentation)

Hickey, J.L.; Simpson, E.J.; Luyt, L.G. July **2009**. *Technetium-99m Labelled Macrocyclic Peptides as Integrated Radiopharmaceuticals*. 18th International Symposium on Radiopharmaceutical Sciences. Edmonton, Alberta. *J. Labelled Compd. Radiopharm.* **2009**; *52*: S71(Oral Presentation)

Non-refereed abstracts

Bruckman, M.A.; Randolph, L.M.; VanMeter, A.; Jiang, K.; Simpson, E.J.; Luyt, L.G.; Yu, X.; Steinmetz, N.F. October **2014**. *Nanomanufacturing of Targeted Rod- and Spherical Shaped Viral Nanoparticle MRI Contrast Agents for in vivo Detection of Atherosclerotic Plaques in Mice*. Biomedical Engineering Society. San Antonio, Texas. (Poster Presentation)

Simpson, E.J.; Gobbo, P.; Bononi, F.; Workentin, M.S.; Luyt, L.G. June **2014**. *Bombesin Functionalized Water-Soluble Gold Nanoparticles for Prostate Cancer Imaging*. 97th Canadian Chemistry Conference and Exhibition. Vancouver, British Columbia. (Oral Presentation)

Gobbo, P.; Wang, R.; Simpson, E.J.; Nazemi, A.; Hudson, R.H.E.; Luyt, L.G.; Gillie, E.; Workentin, M.S. June **2014**. *Interfacial Strain-Promoted Alkyne-Azide Cycloaddition for the Creation of Gold Nanoparticle (AuNP) Bioconjugates and Hybrid Nanomaterials*. 97th Canadian Chemistry Conference and Exhibition. Vancouver, British Columbia. (Oral Presentation)

Randolph, L.M.; Bruckman, M.A.; Simpson, E.J.; Luyt, L.G.; Steinmetz, N.F. September **2013**. *Targeting Atherosclerotic Plaques in vivo Using Rod-shaped Tobacco Mosaic Virus*. Biomedical Engineering Society. Seattle, Washington. (Poster Presentation)

Bruckman, M.A.; Jiang, K.; Randolph, L.N.; Simpson, E.J.; Luyt, L.G.; Yu, X.; Steinmetz, N.F. September **2013**. *Distribution and Compatibility of VCAM-1 Targeted Rod-Shaped Viral Nanoparticles in an Atherosclerosis Mouse Model*. Biomedical Engineering Society. Seattle, Washington. (Poster Presentation)

Gobbo, P.; Milne, M.; Wang, R.; Simpson, E.J.; Luyt, L.G.; Hudson, R.; Workentin, M.S. May **2013**. *Clickable Gold Nanoparticles (AuNP) for Drug Delivery and Bioconjugation*. 96th Canadian Chemistry Conference and Exhibition. Quebec, Quebec. (Oral Presentation)

Hickey, J.L.; Simpson, E.J.; Luyt, L.G. June **2011**. *Synthesis of Macrocyclic β -sheet Mimics as Molecular Imaging Probes*. 94th Canadian Chemistry Conference and Exhibition. Montreal, Quebec. (Oral Presentation)

Simpson, E.J.; Luyt, L.G. June **2009**. *Studying the Formation of Isomers Upon Coordination of $Re(CO)_3^+$ with Histidine*. Oncology Research & Education Day. London, Ontario. (Poster Presentation)

Simpson, E.J.; Breadner, D.; Luyt, L.G. May **2009**. *Studying the Formation of Isomers Upon Coordination of $Re(CO)_3^+$ with Histidine*. 2nd Georgian Bay International Conference on Bioinorganic Chemistry. Parry Sound, Ontario. (Poster Presentation)

Simpson, E.J.; Luyt, L.G. March **2009**. *The Investigation of Isomer Formation for Histidine- $Re(CO)_3$ Containing Peptides*. 37th Southern Ontario Undergraduate Student Chemistry Conference. St. Catherines Ontario. (Oral Presentation)

Hickey, J.L.; Simpson, E.J.; Luyt, L.G. November **2008**. *The Synthesis of Metal Chelates for Use as Integrated Technetium-99m Peptidomimetics*. The 19th annual Quebec Ontario Minisymposium in Synthetic and Bioorganic Chemistry. Toronto, Ontario. (Poster Presentation)